Dissolved thorium, rare earth elements and neodymium isotopic composition in the Kerguelen Plateau: method development and application to quantify and trace lithogenic inputs

By Habacuc U. Pérez-Tribouillier, B. Ocean Sci., M. Sci. Geochemistry
Under the supervision of Zanna Chase, Taryn Noble, Ashley Townsend and Andrew Bowie

Submitted in partial fulfilment of the requirements for the degree of
Doctor of Philosophy
University of Tasmania October 2019

UNIVERSITY of TASMANIA

IMAS
INSTITUTE FOR MARINE & ANTARCTIC STUDIES

Declarations and statements

Declaration of originality

This thesis contains no material which has been accepted for a degree or diploma by the University or any other institution, except by way of background information and duly acknowledged in the thesis, and to the best of my knowledge and belief no material previously published or written by another person except where due acknowledgement is made in the text of the thesis, nor does the thesis contain any material that infringes copyright.

Authority of Access and statement regarding published work contained in the thesis

The publishers of the publication comprising Chapter 2 hold the copyright for that content, and access to the material should be sought from the respective journal. The remaining non published content of the thesis may be made available for loan and limited copying and communication in accordance with the Copyright Act 1968.

Statement of Co-Authorship

The following people and institutions contributed to the publication of work undertaken as part of this thesis:

1. Habacuc Perez-Tribouillier (candidate) – Institute for Marine and Antarctic Studies (IMAS), University of Tasmania, Hobart Australia; Antarctic Climate and Ecosystems Cooperative Research Centre (ACE
CRC), University of Tasmania, Hobart, Australia

2. Zanna Chase - Institute for Marine and Antarctic Studies (IMAS), University of Tasmania, Hobart, Australia.

3. Taryn L. Noble - Institute for Marine and Antarctic Studies (IMAS), University of Tasmania, Hobart, Australia.

4. Ashley T. Townsend - Central Science Laboratory (CSL), University of Tasmania, Hobart, Australia.

5. Andrew R. Bowie - Antarctic Climate and Ecosystems Cooperative Research Centre (ACE CRC), University of Tasmania, Hobart, Australia; Institute for Marine and Antarctic Studies (IMAS), University of Tasmania, Hobart, Australia.

6. Bruce L.A. Charlier - School of Geography, Environment and Earth Sciences, Victoria University of Wellington, Wellington, New Zealand

Author's contributions

Chapters 2, 3, and 4 of this thesis have been prepared as manuscripts for submission to peer-reviewed journals (Chapter 2 is already published). In all cases the design and implementation of the research, data analysis, interpretation of the results, and preparation of the manuscripts were the responsibility of the candidate but were carried out in consultation with supervisors and with the input of specialist contributors. These contributions are highlighted for each of these manuscripts below.

PAPER 1: Located in Chapter 2

Pérez-Tribouillier, H., Noble, T. L., Townsend, A. T., Bowie, A. R., & Chase, Z. (2019). Pre-concentration of thorium and neodymium isotopes using Nobias chelating resin: Method development and application to chromatographic separation. *Talanta*. https://doi.org/10.1016/j.talanta.2019.03.086

H. Perez-Tribouillier (first author): sample collection, sample processing and analysis, data analysis, first draft and subsequent modifications.
Z. Chase: sample collection, data analysis, manuscript writing
T.L. Noble: sample analysis, data analysis, manuscript writing
A.T. Townsend: sample analysis, data analysis, manuscript writing
A.R. Bowie: manuscript writing

PAPER 2: Located in Chapter 3

Quantifying lithogenic fluxes to the Kerguelen Plateau using long-lived thorium isotopes

H. Perez-Tribouillier (first author): sample collection, sample processing, sample analysis, data analysis, first draft and subsequent modifications.
Z. Chase: sample collection, data analysis, manuscript writing
T.L. Noble: sample analysis, data analysis, manuscript writing
A.T. Townsend: sample analysis, manuscript writing
A.R. Bowie: manuscript writing

PAPER 3: Located in Chapter 4

Sourcing lithogenic inputs to the Kerguelen Plateau using rare earth element concentrations and Nd isotopic composition

H. Perez-Tribouillier (first author): sample collection, sample processing, sample analysis, data analysis, first draft and subsequent modifications.
Z. Chase: sample collection, data analysis, manuscript writing
T.L. Noble: sample processing and analysis, data analysis, manuscript writing
A.T. Townsend: sample analysis, manuscript writing
A.R. Bowie: manuscript writing
B.L.A. Charlier: sample analysis

We, the undersigned, endorse the above stated contribution of work undertaken for each of the published (or submitted) peer-reviewed manuscripts contributing to this thesis:

Signed: _____ _____ _____

Habacuc Pérez-Tribouillier	Zanna Chase	Neil Holbrook
Candidate	Primary Supervisor	Head of School
Institute for marine and Antarctic studies	Institute for Marine and Antarctic Studies	Centre Head – Oceans & Cryosphere
University of Tasmania	University of Tasmania	University of Tasmania
Date: 2/10/2019	Date: 2/10/2019	Date: 4/10/2019

Acknowledgements

I want to start by thanking Zanna Chase for giving me the opportunity of doing this PhD. Thanks for all of your patience, motivation and support. I will be always amazed by how you always made time for all of your students despite all of your responsibilities. I feel like the door to your office was always open for us. You quick and accurate scientific thinking makes our life easier. You are really an example and an inspiration to me!

Taryn, thank you too for all of your support and motivation, you always kept encouraging me, especially when the method development got rough and the results were not the best. Thank you for all your precise and rigorous comments to my chapters, they were always very useful. Thanks too for almost forcing me to take breaks!

Ash, what would I do without your ICP-MS skills? Thank you for your involvement and commitment to my thesis. For keeping a contagious positive attitude even when the thorium measurements where still not the best. Thank you for your sharp comments to my manuscripts, they really made the difference.

I am grateful with Melanie Gault-Ringold, Kathrin Wüttig and Pam Quayle for their invaluable help and advice during the development of the second chapter.

I want to thank my parents and sister for their continuous support despite of being so far away. In particular my parents for the education they gave me! I also thank my beautiful partner Layla for her amazing support, especially in in these last months of my PhD (thanks for keeping me well fed). I am also incredibly grateful with Val and Brett Kitchener for almost adopting me, in these 4 years you became my Tasmanian family – you guys are an example of generosity and kindness. And Brett, mate, thanks for all that diving, you certainly contributed to help me stay a bit saner during all my PhD.

I also thank my crazy mates Ana, Fernando and Bruce for all those scientific and not so scientific conversations full of silliness! And to Cristina for being such an amazing lab-mate, thank you for making those long-hours in the lab funnier. To all the people that I met in IMAS, thank you so much!

Funding for this project was obtained through the following grants: Australian Research Council Discovery (DP150100345 and DP180102357), Australian Research Council LIEF (LF0989539), the Australian Antarctic Science Program (AAS4338) and the Australian

Research Council Special Research Initiative for Antarctic Gateway Partnership (Project ID SR140300001). The Ph.D. scholarship of H.P-T. was provided by the Mexican Council for Science and Technology (CONACYT, Scholarship No. 409833) in conjunction with the University of Tasmania.

Table of Contents

List of figures

List of tables

Abstract

Dissolved thorium, Rare Earth Elements and neodymium isotopic composition in the Kerguelen Plateau: method development and application to quantify and trace lithogenic inputs.

Ph.D. candidate: Habacuc Pérez-Tribouillier

The Southern Ocean (SO) is the largest high nutrient, low chlorophyll (HNLC) region in the global ocean, characterized by a minimum development of phytoplankton despite the abundance of macronutrients. The existence of such regions is caused by the absence of the bio-limiting trace element iron (Fe). In other ocean basins like the Atlantic and Pacific this limitation is overcome by the dissolution of aeolian dust. However, the SO is isolated from major dust sources. Here, the weathering and erosion of Subantarctic Islands, glacial run-off and resuspension of shelf-deposited sediments become the main source of lithogenic material. This lithogenic material naturally fertilizes surrounding waters with iron thus enabling the development of phytoplankton blooms, the largest of which occurs in the Kerguelen Plateau. The Kerguelen Plateau is the largest bathymetric barrier to the natural eastward flow of the Antarctic Circumpolar Current. Here, previous studies have demonstrated that the Heard and McDonald Islands located in the central part of the plateau and the Kerguelen Archipelago (northern part of the plateau) supply lithogenic material directly to the surface of the ocean. Additionally, the interaction between the ACC and the plateau causes dynamic conditions that can resuspend shelf-deposited sediments. These sediments release iron which can then be transported to the surface by vertical mixing or upwelling contributing with the natural fertilization over the plateau. The ACC can also transport Fe away from the plateau enabling the development of a plume with enhanced primary productivity that extends for several hundreds of kilometres east of the plateau. This bloom draws down atmospheric CO_2 into the surface of the ocean and because this is a region of formation of intermediate and deep waters, this CO_2 can potentially be incorporated into deeper layers of the ocean.

Understanding the conditions that drive these seasonal blooms is difficult first because of the remoteness of the SO. Iron also has a very complex oceanic biogeochemical cycle with several inputs and sinks. However, other trace elements like thorium (Th) and Rare Earth Elements (REE), which are not required by phytoplankton, can help trace lithogenic inputs, and represent a valuable toolbox for the study of ocean processes. Furthermore, Th and REE have a coherent chemical behaviour and constrained sources to the ocean. In the particular case of ^{232}Th and REE, their sources are the same as for Fe. This makes them suitable to trace iron inputs to the ocean. However, these elements and their isotopes are present in such low dissolved concentrations that rigorous analytical procedures are required in order to measure them in seawater.

In this thesis I aim to: (1) Develop a new technique to simultaneously pre-concentrate Th (^{232}Th, ^{230}Th) and neodymium (Nd) isotopes using the Nobias chelating resin. (2) Adapt an existing technique to measure dissolved REE in seawater using the same resin. (3) Apply the above-mentioned analytical techniques to increase the knowledge about the factors that

drive the seasonal phytoplankton bloom in the Kerguelen Plateau region. In particular, to better constrain the sources and pathways of iron in the plateau, and to provide a new estimate of the fluxes of lithogenic material using dissolved thorium data.

The results indicate that it is possible to accurately and precisely measure Th and Nd isotopes, as well as REE concentrations using the Nobias resin. This method drastically reduces sample processing time. The blank contribution of our techniques is comparable or less than previous studies. The analysis of different certified reference materials as well as intercalibration samples indicate an overall accuracy from both methods within 10% of the reported values and a long-term precision generally < 5%. We demonstrate that ^{230}Th can be used to provide a scavenging residence time based on its disequilibria from its parent nuclide ^{234}U. Following this approach, we calculate a residence time for the upper 500 m of the water column of ~ 260 days. We employ this residence time to calculate a dissolved ^{232}Th flux. Using the ^{232}Th concentration of the lithogenic material from the plateau and an estimated Th solubility of (1-20%) we obtain a dissolved lithogenic flux that ranges from 7 to 810 mg m^{-2} day^{-1}. This value is comparable to other studies in the Southern Ocean, and particularly similar to previous determinations of particulate fluxes in the Kerguelen Plateau using sediment traps (35-628 mg m^{-2} day^{-1}).

The REE and ε_{Nd} data confirm suggestions by previous studies that the predominant source of lithogenic material that fuels the bloom originates in the Heard and McDonald Islands, and surrounding shallow shelf. However, our results disagree about the relative importance to the region of material sourced from the Kerguelen archipelago. Europium and cerium anomalies, as well as the Nd/Yb normalized ratio and the ε_{Nd} of our data, together with data from previous studies clearly indicate that the Polar Front acts as an effective barrier to the dispersal of lithogenic material (and likely Fe) sourced from the Kerguelen archipelago.

This thesis has improved constraints on the sources of Fe that allow the development of primary productivity around the Kerguelen Plateau region. However, some uncertainties remain. A more detailed sampling of the area between Heard and McDonald Island and the Kerguelen Islands will help to completely constrain the factors that drive the bloom in the region. Our results also indicate the need for more detailed studies that establish the solubility of Th not only from material from our area of study but in general of the lithogenic-sourced particles in the ocean. Finally, the method development in this study also represents a breakthrough in the way Th and Nd isotopes can be pre-concentrated from seawater. In particular, this method has the potential to be applied at sea reducing the amount of sample that needs to be brought back to land and eliminating the need for sample storage and transport.

Chapter 1 - Introduction

The Southern Ocean (SO) is the largest high nutrient, low chlorophyll (HNLC) area of the global ocean. The HNLC regions are characterized by low primary productivity despite the abundance of macronutrients like nitrogen and phosphorus. The existence of HNLC areas is known to be caused by the absence of the bio-limiting or co-limiting element iron (Fe) (Martin, 1990; Moore et al., 2001; Boyd et al., 2007; Boyd et al., 2012). If Fe reaches HNLC areas, it is possible to overcome this condition. Most common sources of Fe to other ocean-basins are the deposition of aeolian dust (Jickells, 2005; Mahowald et al., 2009) and upwelling in equatorial regions (de Baar et al., 1995). However, the SO is located far away from any dust source. Here, the interaction of the Antarctic Circumpolar Current (ACC) with islands, shallow areas, icebergs and glaciers allows for Fe to be released and further transported (Blain et al., 2001; Moore and Abbott, 2002; Arrigo et al., 2008; Boyd et al., 2012). This Fe enables the development of several seasonal phytoplankton-blooms once the light is no longer a limiting factor. The largest SO phytoplankton bloom occurs above and around the Kerguelen Plateau (KP; Indian Sector of the Southern Ocean).

The Heard and McDonald Island Earth-Ocean-Biosphere Interaction Study (HEOBI), in which I participated during January and February of 2016, aimed to obtain a better characterization of the Fe sources in this region. For this thesis, long-lived Th isotopes (^{232}Th and ^{230}Th) were used to obtain an estimation of the budget of lithogenic material that naturally fertilizes the waters of the KP. The Nd isotopic composition (^{143}Nd/^{144}Nd) and rare eart elements (REE) concentrations were then used to better constrain its sources and pathways. In particular it was of interest to confirm the role of the Heard and McDonald Islands (HIMI) on the natural fertilization over the KP suggested by several authors (Park et

al., 2008b; Zhang et al., 2008; Grenier et al., 2018). Additionally, it was intended to increase the observations of Th and Nd isotopes in the SO, where very few observations exist, despite of being key-parameters of the international GEOTRACES program (Anderson et al., 2014; Schlitzer et al., 2018; Lam and Anderson, 2018).

Characterizing how Fe can naturally fertilize a large region is a challenging task: Fe is present in very low concentrations, it has multiple sources and sinks, interacts with the biota and its analysis is prone to contamination during sampling. However, Fe is supplied to the ocean mostly by the dissolution of crustal material, in the same way as many other trace elements. This property (same origin) allows for other elements to trace the Fe cycle in the ocean. Amongst these alternatives, aluminium and thorium (Th) have been used (Measures and Vink, 2000; Measures et al., 2005; Hsieh et al., 2011; Hayes et al., 2013a).

Thorium and REE have been previously applied in the KP (Zhang et al., 2008; Venchiarutti et al., 2008; Venchiarutti et al., 2011; Grenier et al., 2018), together with other chemical and physical parameters, satellite observations and modelling studies as part of the KEOPS 1 and KEOPS 2 voyages (Jouandet et al., 2008; Mongin et al., 2008; Park et al., 2008a; Park et al., 2008b; Savoye et al., 2008; Trull et al., 2008; Park et al., 2014; Bowie et al., 2015; Sanial et al., 2015, and references therein). Based on this data, the Kerguelen Archipelago (KA) and the HIMI were identified as the main source of lithogenic material to the region. The dissolution of this material releases Fe, thus naturally fertilizing the waters above the plateau. However, the relative contribution of both groups of islands is still not completely constrained, mainly because of the sparse spatial distribution of the sampling. In particular, the area surrounding HIMI remained almost unexplored. Additionally, there is the hypothesis that glaciers and hydrothermal activity in the region might interfere with the biogeochemical cycle of Fe (van der Merwe et al., 2019).

Th isotopes and REE represent a valuable “toolbox” for the study of the oceans (Jeandel and Derek, 2018; Lam and Anderson, 2018). They are affected by almost every process involved in the regulation of the biogeochemical cycles in the ocean. This means that they can be used as present and past tracers of such processes. In seawater Th and REE are present in such minuscule dissolved concentrations that their measurement requires clean and meticulous analytical techniques. Such low concentrations make necessary for the analytes to be pre-concentrated from seawater and then chromatographically separated. Commonly used pre-concentration techniques involve the use of Fe carrier solution to precipitate the target analytes (Anderson et al., 2012). This approach is well known to produce good quality results; however, it can be time consuming. Furthermore, this technique has remained almost unchanged during the last 40 years. I investigated the possibility of using the chelating resin Nobias as an alternative way to simultaneously pre-concentrate Th and Nd isotopes from a single seawater sample, and if it was possible to couple it to existing separation techniques (Chapter 2). Then, I applied these tracers to samples from the HIMI region to address the issues established in the previous paragraphs (Chapters 3 & 4).

The rest of this introductory chapter aims to provide an overview of the use of Th isotopes and REE in oceanographic studies. I discuss the fundamental physicochemical characteristics that allow these elements to track several oceanographic processes and provide a brief summary of their different applications, as well as the evolution of the analytical techniques to measure them in seawater. An introduction to the geography, geology and oceanographic setting of the KP is also provided.

1. Use of Th isotopes and REE in oceanography

1.1 Thorium isotopes

Since radioactivity was discovered in the last years of the XIX Century (Becquerel, 1896; Curie, 1898), it started to gain applications to study the Earth's history. It was found that the radioactive decay of thorium and uranium generated a series of isotopes of different elements. This succession of decay is known as the U and Th radioactive decay series. These series are composed of 8 core elements (U, Th, Pa, Ra, Rn, Po, Bi and Pb; Krishnaswami and Kirk Cochran, 2008). Due to their different chemical properties and half-lives, these isotopes fractionate among the members of the same decay chain resulting in radioactive disequilibrium. This disequilibrium provides information about the processes and timescales that produce them and is the key for their application in earth sciences. Amongst these radioactive isotopes (also known as radionuclides), several thorium isotopes have been applied by oceanographers to obtain different time-scale information about the particle dynamics in the ocean. These applications will be briefly discussed in the following section with an emphasis on the use of ^{232}Th and ^{230}Th. Finally, a time-evolution of the techniques and procedures to measure Th isotopes in seawater is provided.

Thorium is a chemical element from the actinide group with an atomic number of 90. Seven isotopes of Th naturally occur (^{227}Th, ^{228}Th, ^{229}Th, ^{230}Th, ^{231}Th, ^{232}Th and ^{234}Th). However, most of the Th is the primordial isotope ^{232}Th (99.98%, $t_{1/2}$=14.05x10^{9} years) and ^{230}Th (0.02%, $t_{1/2}$=75,400 years), the latter being contained mostly in the deep ocean. Despite their difference in concentration, all thorium isotopes predominantly exist in seawater in the oxidation state of 4+. This makes dissolved Th highly unstable, causing all isotopes to quickly hydrolyze after being introduced in the dissolved phase to seawater. This results in extremely insoluble chemical species, mostly $Th(OH)_4$ (Rutgers van der Loeff and Geibert, 2008).

The primordial nuclide ^{232}Th is found in the continental crust at an average concentration of 10.5 ppm (Rudnick and Gao, 2013). The dissolution of this crustal material is the main source of ^{232}Th to the ocean and produces dissolved concentrations that range from a few tens to a couple hundred pg kg^{-1}, being higher close to the source and decreasing towards the open ocean. The vertical distributions of ^{232}Th in the Atlantic and Pacific generally show higher concentrations in surface waters, reflecting continental, atmospheric and riverine inputs (Nozaki et al., 1987; Cochran et al., 1987). However, deviations from this pattern can be observed, with mid depth and even bottom water maxima in ^{232}Th. These variations are caused by additional sources of ^{232}Th other than the input through the ocean's surface, such as through lateral advection and nepheloid layers (Coppola et al., 2006; Hsieh et al., 2011; Okubo et al., 2012).

The isotopes ^{230}Th and ^{234}Th ($t_{1/2}$=24.1 days) share the characteristic of being supplied to the ocean almost entirely by the radioactive decay of their highly-soluble parent nuclides ^{234}U and ^{238}U respectively. The distribution of these uranium isotopes remains constant through the water column and is dependent on salinity (Chen et al., 1986; Owens et al., 2011). Due to its short half-life, ^{234}Th is generally found in equilibrium with its parent nuclide ^{238}U. However, in areas of high particle flux, a depletion of ^{234}Th from ^{238}U is observed (Figure 1; Bhat et al., 1968; Coale and Bruland, 1985; Rutgers van der Loeff and Geibert, 2008). Above the seafloor, ^{234}Th disequilibria from ^{238}U has been shown to result from extra scavenging due to an intense particle flux or a well-defined nepheloid layer (Amin et al., 1974; Bacon and Rutgers van der Loeff, 1989; Turnewitsch and Springer, 2001; Rutgers van der Loeff et al., 2002; Inthorn et al., 2006; Turnewitsch et al., 2008). Considering that all thorium isotopes behave in a similar way, this effect can also be expected with longer lived isotopes like ^{230}Th and ^{228}Th (Schmidt, 2006; Hsieh et al., 2011; Hayes et al., 2013b).

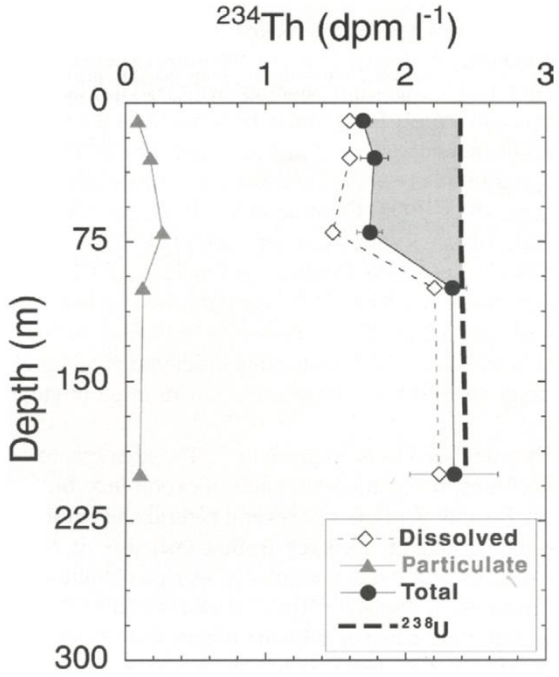

Figure 1-1. Disequilibrium between ^{234}Th (daughter) and ^{238}U (parent) in the surface of the ocean (taken from Rutgers van der Loeff and Geibert, 2008)

In many parts of the open ocean the distribution of ^{230}Th is controlled mainly by the process of reversible scavenging (Figure 2). The reversible-scavenging model involves a steady state and a continuous exchange of ^{230}Th between the dissolved and the particulate phase that causes a linear increase in the concentration with depth (Figure 2; Nozaki et al., 1981; Bacon and Anderson, 1982; Anderson et al., 1983b; Nozaki and Nakanishi, 1985; Roy-Barman et al., 1996). The steady state condition implies no lateral transport of ^{230}Th, meaning that it is all scavenged within the basin. A steady state condition does not apply for many parts of the ocean, in particular in the ocean margins. Here, the high particle load produced near the continents effectively scavenges laterally transported nuclides in a process known as boundary scavenging (Bacon et al., 1976; DeMaster, 1979; Nozaki and Horibe, 1983; Robert F. Anderson et al., 1983; Cochran et al., 1987; Roy-Barman et al., 2009). In some other areas, inter-basin mixing due to the advection of deep waters affects the distribution and flux of ^{230}Th in what is described as the scavenging-mixing model (Figure 2; Rutgers van der Loeff

and Berger, 1993; Kirk Cochran et al., 1995; Scholten et al., 1995; Moran et al., 1995; Moran et al., 1997; Vogler et al., 1998; Marchal et al., 2000; Moran et al., 2001; Okubo et al., 2012; Rempfer et al., 2017).

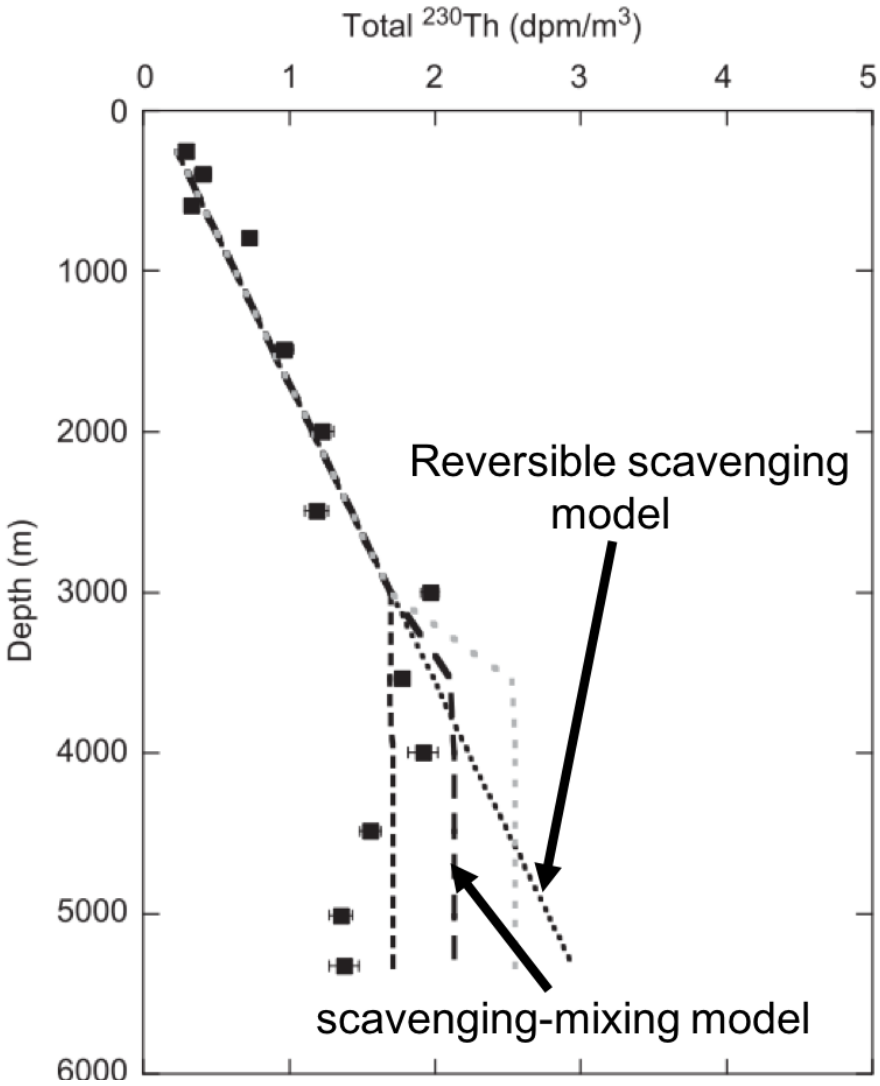

Figure 1-2. Comparison between the predictions in the ^{230}Th vertical distribution produced by the reversible scavenging model and different outcomes of the scavenging-mixing model (modified from Okubo et al., 2012).

Given the insoluble nature of Th isotopes, after production by radioactive decay, they are quickly subject to scavenging processes. However, their transfer from the dissolved pool to the particulate one is a complex process (Figure 3). The size and composition of the

particles plays a key role in the scavenging of thorium isotopes and it was found that most of the particle reactive radionuclides tend to be scavenged onto small particles, and then transported downwards by aggregation of these particles to larger ones (Bacon et al., 1985; Nozaki et al., 1987; Chase et al., 2002). At this point it is necessary to state that the term dissolved is only an operationally defined parameter. By convention, 0.45 μm is the threshold that separates the "dissolved" and "particulate" fractions. However not all the material that goes through this pore size can be considered to be fully dissolved. Honeyman and Santschi concluded that the aggregation of Th to filterable particles was a consequence of rapid absorption of Th species onto colloidal or sub-micron particles, followed by a gradual aggregation to filterable size particles by Brownian pumping. This process is still not completely constrained, and raises the question about the "truly" dissolved Th, as estimations of the amount of Th associated with the colloidal phase range from 0.04% to 80% (Baskaran et al., 1992; Moran and Buesseler, 1992; Guo et al., 1997; Gustafsson et al., 2000; Dai and Benitez-Nelson, 2001; Baskaran et al., 2003; Santschi et al., 2006).

Another scavenging mechanism is complexation. This process occurs when some cations in seawater (like Th^{4+}) interact with organic and inorganic ligands forming a larger unit with different chemical properties. This complexation process can also form at the surface of a particle, enhancing the direct transition between the dissolved and particulate phase (Hirose and Sugimura, 1993; Hirose, 1996). Thorium isotopes can also form complexes with strong organic ligands (Hirose and Tanoue, 1994). These complexes can keep Th in solution, however acid polysaccharides tend to aggregate and, depending on the intensity of the aggregation, they may be found in the colloidal or the particulate pool of seawater (Quigley et al., 2002). The effect of these organic ligands is most likely to affect Th isotopes in the surface of the ocean, i.e. ^{234}Th; due to their labile nature, organic ligands are not present in

deeper water and thus deep ^{230}Th speciation might be affected by processes that are still unknown (Alvarado Quiroz et al., 2006). All the mechanisms mentioned in this section have a fundamental role in the application of Th isotopes for particle dynamics studies in the ocean.

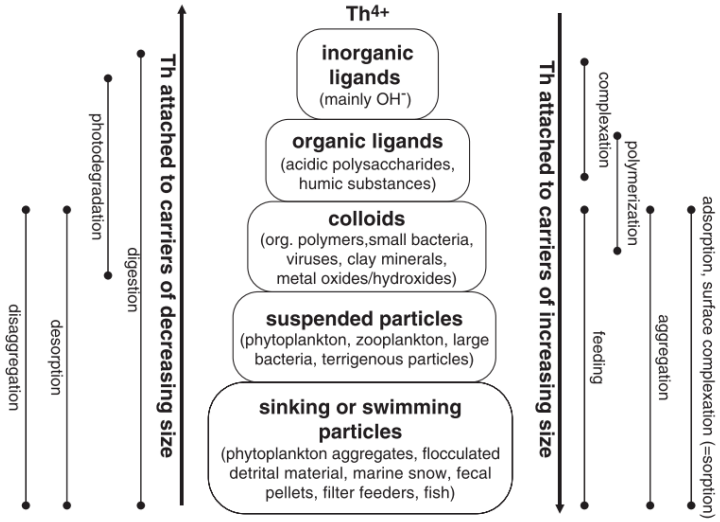

Figure 1-3. Mechanisms involved in the scavenging of Th isotopes (taken from Rutgers van der Loeff and Geibert, 2008).

1.1.2 Applications of thorium isotopes

Thorium isotopes have an amazing potential for the study of the ocean and throughout the years they have found several applications. Describing in detail all these applications is outside the scope of this chapter. In the following paragraphs I list these applications and provide references. Then I focus on the use of ^{232}Th and ^{230}Th to quantify lithogenic inputs, which is the way I apply ^{232}Th and ^{230}Th measurements in Chapter 3.

The reactivity of thorium isotopes and the fact that ^{228}Th, ^{230}Th and ^{234}Th are produced by in situ decay is the basis for their use as tracers of the particle dynamics in the ocean. The disequilibrium between daughter and parent nuclides provides a “chronometer” of the time required to remove Th isotopes from solution. Because ^{228}Th (1.9 years), ^{230}Th (75,400 years) and ^{234}Th (24.1 days) have different half-lives, it is possible to study particle related processes

at different time scales. This characteristic has been exploited in different applications including quantification of the export production (Bhat et al., 1968; Matsumoto, 1975; Coale and Bruland, 1985; Buesseler et al., 1992; Buesseler et al., 1995; Rutgers Van Der Loeff et al., 1997; Buesseler et al., 1998; Benitez-Nelson et al., 2001; Santschi et al., 2003; Benitez-Nelson and Moore, 2006; Thomalla et al., 2006; Jacquet et al., 2008; Savoye et al., 2008; Planchon et al., 2015; Pavia et al., 2019; and references threin), sediment trap calibration (Tsunogai et al., 1986; Buesseler et al., 1994; Buesseler et al., 2000; Scholten et al., 2001; Yu et al., 2001; Coppola et al., 2002; Gustafsson et al., 2004; Buesseler et al., 2007; Lalande et al., 2007; Lampitt et al., 2008), identification of nepheloid layers (Amin et al., 1974; McCave, 1986; Bacon and Rutgers van der Loeff, 1989; DeMaster et al., 1991; Rutgers van der Loeff and Boudreau, 1997; Turnewitsch and Springer, 2001; Rutgers van der Loeff et al., 2002; Venchiarutti et al., 2008), hydrothermal scavenging (Kadko, 1980; Shimmield and Price, 1988; Lalou et al., 1993; Kadko et al., 1994; Lopez et al., 2015; Lund et al., 2019; Pavia et al., 2019a), and paleoflux (also referred as ^{230}Th normalization; Bacon, 1984; Suman and Bacon, 1989; Francois et al., 1990; Francois et al., 1993; McManus et al., 1998; Henderson et al., 1999; Thomson et al., 1999; Francois, 2004; Lyle et al., 2005; Francois et al., 2007; Costa and McManus, 2017).

All the previously mentioned applications are based on the disequilibrium of thorium isotopes from their parent nuclides. However, they do not consider ^{232}Th, which provides a link with the lithogenic sources to the ocean as they represent their main source. Combining the ^{232}Th with ^{230}Th determinations has the advantage that, while ^{230}Th can provide a scavenging time, the ^{232}Th concentrations can be used to calculate a flux of this isotope to a particular water mass. This approach was originally applied in a similar way as the ^{230}Th normalization to reconstruct the history of accumulation of lithogenic material to the Pacific

sector of the SO (Chase et al., 2003) and the variability in the delivery of dust to the central equatorial Pacific Ocean (Anderson et al., 2006) and the Arabian Sea (Pourmand et al., 2004). A few years later the same approach was applied for the first time in seawater to quantify the flux of aeolian dust to the Atlantic (Hsieh et al., 2011; Deng et al., 2014) and North Pacific (Hayes et al., 2013a). For these studies, ^{230}Th was used to calculate a scavenging residence time, which was then used to calculate a flux of ^{232}Th. With knowledge about the Th content and solubility of the mineral dust, it was possible to produce estimations of the flux of ^{232}Th that generates the observed dissolved concentrations. In a similar way it is possible to calculate the flux of other trace elements based on their solubility relative to Th isotopes. This approach has potential for several applications in oceanography (Hayes et al., 2013b; Hayes et al., 2018). However it has several sources of uncertainty that require further investigation (Anderson et al., 2016), especially regarding the solubility of Th from lithogenic material and the effect of particle size and composition on the scavenging of thorium isotopes (Anderson et al., 2016). The Chapter 3 of this thesis is focused on applying this approach to a more coastal area like the Kerguelen Plateau.

1.1.3 Analytical determination of Th isotopes in seawater

Alpha particle spectrometry was the first technique that allowed the measurement of Th isotopes in seawater towards the end of the 1950s. Measurements were performed on 20 to 40 L of coastal and non-filtered seawater (Koczy et al., 1957; Sackett et al., 1958; Starik et al., 1959). The first measurement of truly open-ocean seawater was performed by Moore and Sackett using 220 L samples. These samples were centrifuged in order to remove at least the largest particles and then a ^{234}Th yield tracer was added. The isotopes of thorium were precipitated using a Fe carrier solution and then purified by a mixture of anion and cation exchange chromatography. Measurement was performed on the isotopes ^{228}Th, ^{230}Th and

^{232}Th on the α-spectrometer and the ^{234}Th tracer by β-particle spectrometry. Yields of this procedure ranged from 15-45%. This approach remained for the next twenty years (Nozaki et al., 1981; Nozaki and Nakanishi, 1985) until the use of in situ filtration onto MnO_2-impregnated filters to pre-concentrate Th isotopes started to be applied as well (Anderson et al., 1983a; 1983b; Nozaki and Horibe, 1983). Around the same time, the instrumental neutron analysis for the measurement of ^{230}Th (Greenberg and Kingston, 1983; Huh and Bacon, 1985) and ^{232}Th (Huh, 1987) was applied on small volume samples (< 500 mL), however it required a meticulous matrix removal and separation that involved coprecipitation, ion exchange chromatography and solvent extraction.

The development of mass spectrometry revolutionized the way Th isotopes were measured and quickly became the analytical technique of choice. It was first applied to measure Th and U in soils (Roshholt et al., 1966) , mollusk shells (Szabo and Rosholt, 1969), and lunar material collected during the Apollo voyages (Rosholt and Tatsumoto, 1970; Barnes et al., 1972). However, it was not until the second half of the 1980s that it was applied for the first time to measure total ^{232}Th, ^{238}U and ^{234}U concentrations in seawater (Chen et al., 1986). This technique allowed sample size to be reduced to 250-1000 mL. In a similar way as for the α-spectrometry, the samples were precipitated with an Fe carrier solution and chromatographically separated with an anion exchange resin, obtaining a chemical yield above 95 %.

With the development of more sophisticated mass spectrometers with potent detectors and improved software, most laboratories can reliably measure ^{230}Th and ^{232}Th using samples that range from 2 to 10 liters of seawater. Some of the thorium determinations are performed using the Thermal Ionization Mass Spectrometry (TIMS; Robinson et al., 2004; Andersson and Schöberg, 2012). Some other laboratories use either high resolution (Choi et

al., 2001; Shen et al., 2002; Hayes et al., 2015) or multi-collector (Thomas et al., 2006; Hayes et al., 2017) Inductively Coupled Plasma Mass Spectrometry (ICP-MS). Despite all these advances in spectrometry in the last two decades, sample pre-treatment has remained almost unchanged. In the next chapter of this thesis we present a new method to pre-concentrate ^{230}Th and ^{232}Th using the Nobias chelating resin (Pérez-Tribouillier et al., 2019).

1.2 Rare Earth Elements

The suite of rare earth elements is composed of 15 chemical elements with atomic masses that go from 57 through to 71. Due to the Oddo-Harkins effect, REE elements with an even atomic number are more abundant that the ones with an odd one. This is because of the variations in the binding energy of the nucleus as a function of neutron and proton number during the formation of the solar system (Dickin, 2018). This effect causes the REE to have a saw-like pattern, which can be minimized by "normalizing" the REE concentrations to a standard, being the Post Archean Australian Shale (PAAS) the most commonly used in oceanography (Elderfield et al., 1988). In seawater, REE exist predominantly in an oxidation state of 3+, which makes them have a very similar behavior. However, small differences cause them to fractionate, which can be used to provide information about processes in water-column. First, their stability constant increases as the atomic number of each REE increases. This makes light REE have an increased affinity to scavenging by particles relative to heavy REE. Cerium (Ce) can also exist in the insoluble oxidation state of 4+ (like Th isotopes). This causes Ce to hydrolyze and be incorporated into particles as CeO_2 (Elderfield and Greaves, 1981; de Baar et al., 1988; German et al., 1995). Both of these characteristics explain the typical PAAS-normalized REE pattern of REE in seawater (Figure 4), with a depletion of Ce with respect to their neighbors and an enrichment of the heavier REE. Under reducing conditions, Eu can also exist in the oxidation state of 2+, which makes it remain in solution. This causes

an enrichment of Eu in hydrothermal fluids (German et al., 1990; Olivarez and Owen, 1991). The speciation of REE in seawater is dominated by the complexation with carbonate ions (Elderfield et al., 1988; Jong Hyeon Lee and Byrne, 1993). The organic complexation of REE likely also plays a role in their speciation, because they have affinity for negatively charged sites on organic molecules (Byrne and Kim, 1990). However, more work is needed in this regard. Some studies have identified organic binding of REE in areas with high productivity (Haley et al., 2014; Grasse et al., 2017). Heavier REE also seem to have affinity to bacterial phosphate functional groups, and strong organic ligands (Takahashi et al., 2005; Takahashi et al., 2007; Ngwenya et al., 2009; Takahashi et al., 2010; Ngwenya et al., 2010). Uptake of REE by biogenic silica has also been suggested (Bertram and Elderfield, 1993; Akagi, 2013). All these complexation processes may be the cause of why the vertical distribution of REE in seawater shows a nutrient-like profile (Elderfield and Greaves, 1982; Elderfield et al., 1988; Schijf et al., 2015).

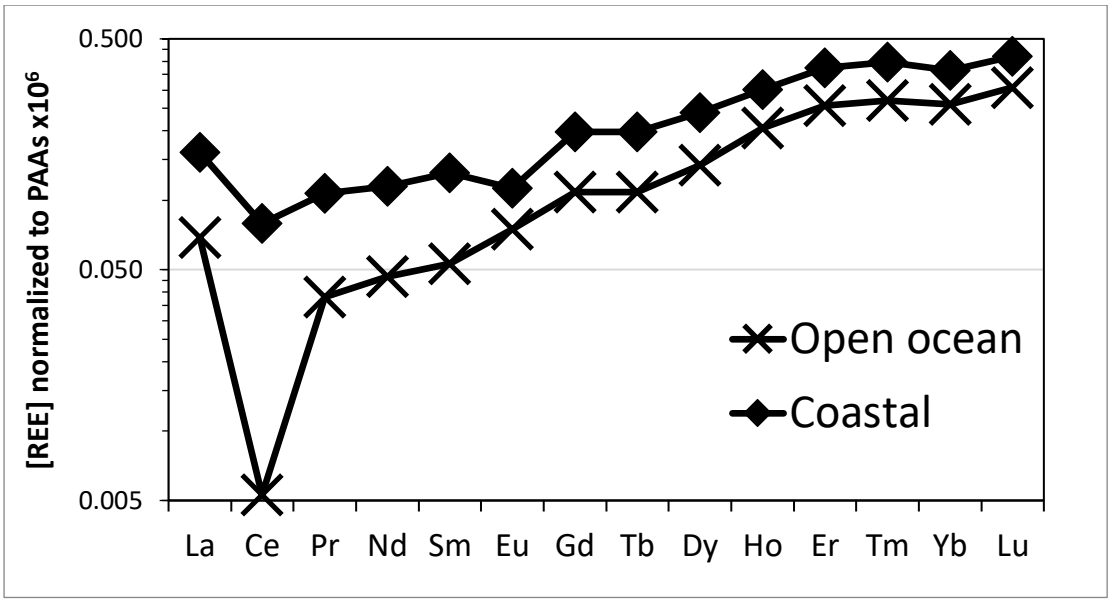

Figure 1-4. PAAS normalized patterns of REE in the surface waters (crosses) of the Southern Ocean compared to the surface next the Kerguelen Archipelago (diamonds; Grenier et al., 2018).

The continental crust is the main source of REE to the marine environment. The dissolution of sediment deposited in continental shelves and slopes dominates the REE cycle in the ocean, followed by aerosols and riverine input. Some REE are produced by radioactive decay. The ^{147}Sm isotope decays to the stable ^{143}Nd. Chemical fractionation during magma melting and the formation of continental crust produces a range of ^{147}Sm/^{144}Nd ratios, and hence different ^{143}Nd/^{144}Nd ratios in rocks and minerals as a function of age and the Sm/Nd ratio of the parent material (Lugmair, 1974; DePaolo and Wasserburg, 1976). However these changes are so small that the ^{143}Nd/^{144}Nd ratio is commonly normalized to the Chondritic Uniform Reservoir (^{143}Nd/^{144}Nd=0.512638) in order to be able to observe the changes in the Nd isotopic composition, and expressed as ε_{Nd} (DePaolo and Wasserburg, 1976; Equation 1). When these rocks and minerals enter into contact with seawater, their unique ^{143}Nd/^{144}Nd signature gets imprinted into that particular water mass and remains along its path through the ocean circulation cycle.

$$\varepsilon_{Nd} = \left[\frac{\left(\frac{^{143}Nd}{^{144}Nd}\right)_{sample}}{\left(\frac{^{143}Nd}{^{144}Nd}\right)_{CHUR}} - 1 \right] \times 10{,}000 \quad (Equation\ 1)$$

It is possible to use Nd isotopes as global circulation tracers because the oceanic residence time of Nd (~300 years) is shorter than the global oceanic mixing time (Tachikawa, 2003; Arsouze et al., 2007; Arsouze et al., 2009), and because they are not affected by biological fractionation. Intermediate and deep water masses therefore exhibit a quasi-conservative behaviour along their flow path through the global circulation (Frank, 2002; Goldstein and Hemming, 2003; Molina-Kescher et al., 2014). It is now known that the main source of Nd to the ocean are the different types of continental weathering and erosion and

exchange via the continental margins (Lacan and Jeandel, 2005). There are two main endmembers of the ε_{Nd} in the ocean: 1) water masses originating from regions where young mantle derived material is weathered, like in the Pacific Ocean, which exhibits more radiogenic values (ε_{Nd} = -2 to -4; Piepgras and Jacobsen, 1988; Amakawa et al., 2004; van de Flierdt et al., 2004); 2) water masses formed under the influence of older continental rock, like the NW Atlantic Ocean, carry less radiogenic values (ε_{Nd} = -13; Piepgras and Wasserburg, 1987; Rickli et al., 2009). However, the mechanisms involved in the transfer of the ε_{Nd} to seawater, their distribution and internal cycling are still not completely understood. This is further evidenced by the fact that there is a global decoupling between the observed Nd concentration and the ε_{Nd} in the water column (Goldstein and Hemming, 2003), which is commonly known as the "Nd-paradox". This can also be interpreted as a missing source of Nd to the ocean (Bertram and Elderfield, 1993; Jeandel et al., 1995; Flierdt et al., 2004). No matter the definition that is given to the Nd-paradox, data clearly point to additional sources, sinks and/or processes that play an important role in the global Nd cycle (Siddall et al., 2008). Considering additional sources, the role of hydrothermal activity has already been discarded as a significant contributor to the Nd budget due to immediate scavenging over the hydrothermal vents (Goldstein and O'Nions, 1981; German et al., 1990; Halliday et al., 1992). Additional sources could include interactions of river particles with seawater, input of volcanic ash, and near-bottom dissolution of deposited or resuspended sediments deposited on continental shelves and slopes, and submarine ground water discharges (Elderfield and Sholkovitz, 1987; Spivack and Wasserburg, 1988; Albarède et al., 1997; Johannesson and Burdige, 2007). More recent modelling and observational studies have found that near the continental margins, the Nd-paradox can be explained by a combination of lateral advection, vertical mixing and reversible scavenging (Siddall et al., 2008; Stichel et al., 2015), together

with the processes of boundary scavenging (Lacan and Jeandel, 2001; Lacan and Jeandel, 2005; Arsouze et al., 2007; Arsouze et al., 2009; Grenier et al., 2014)

1.2.2 Application of REE in oceanography

The REE distributions in the ocean are affected by almost every single process involved in the marine biogeochemical cycles. Therefore, measurements of REE concentration in seawater have been applied to trace different processes like the input of lithogenic material (e.g. Osborne et al., 2015; Molina-Kescher et al., 2018), hydrothermal activity (Klinkhammer et al., 1983; Olivarez and Owen, 1991; Cole et al., 2014), intensity of the biogeochemical cycling (Nozaki and Alibo, 2003; Hathorne et al., 2014; Zheng et al., 2016; Crocket et al., 2018), the redox state of seawater (de Baar et al., 1988; Byrne and Kim, 1990; German et al., 1995), amongst others.

Since the development of the techniques that have allowed the measurement of ε_{Nd} of seawater, REE concentrations began to be coupled with this parameter. This coupling allows a more complete "picture" of the different factors controlling the oceanic biogeochemical cycles, and their relation with the global climate on different time scales. Coupled with the global circulation tracer ε_{Nd}, the REE data provides insight into more local processes occurring in the water column. This approach has been used to characterize the past and current biogeochemical cycles of the different ocean basins (Piepgras and Jacobsen, 1992; Bertram and Elderfield, 1993; Scher and Martin, 2004; Pahnke et al., 2008; Carter et al., 2012; Grasse et al., 2012; Singh et al., 2012; Grenier et al., 2013; Garcia-Solsona et al., 2014; Molina-Kescher et al., 2014; Grasse et al., 2017; Haley et al., 2017; Grenier et al., 2018; and references therein).

1.2.3 Analytical determination of REE in seawater

The first determinations of REE in geological materials were performed by optical spectrography techniques (Minami, 1935a; Minami, 1935b; Goldschmidt, 1937), however the first measurements of REE in seawater were not reported until the 1960s (Balashov, 1961; Goldberg et al., 1963). The first seawater measurements were made by instrumental neutron activation analysis. This technique required extensive sample processing including irradiation, several precipitations with Fe carriers and different ion exchange columns (Mosen et al., 1961), in order to remove the background signal coming from the seawater matrix. Sample determination was performed in a low-level β counter. Instrumental neutron activation analysis remained as the most common way of measuring REE for the following decades (Høgdahl and Melsom, S.Bowen, 1968; Henderson and Pankhurst, 1984) until the appearance of mass spectrometry.

The development of mass spectrometry coupled with isotope dilution techniques quickly allowed for the REE determinations in seawater to gain in number and produced more accurate results (Palmer, 1983; Klinkhammer et al., 1983; De Baar et al., 1985; de Baar et al., 1988; Greaves et al., 1991). These methods comprised a pre-concentration with Fe carrier solution or by the use of chelating resins, separation of the REE from the seawater matrix using mixed/solvent ion exchange chromatography, and analysis using a mass spectrometer coupled to a single/multiple filament thermal ionization device (Schnetzler et al., 1967; Hooker et al., 1975). The introduction of the mass spectrometer also allowed the first measurements of the Nd isotopic composition (Piepgras et al., 1979; Piepgras and Wasserburg, 1980; Piepgras and Wasserburg, 1982; Piepgras and Wasserburg, 1983; Piepgras and Wasserburg, 1987). For these determinations, large volume samples - generally of 30 L - were required. The Nd isotopes were pre-concentrated by Fe precipitation and then the

water matrix was removed by a two-step ion exchange chromatography (Eugster et al., 1970; DePaolo and Wasserburg, 1976). The thermal ionization mass spectrometry and multi-collector inductively coupled mass spectrometry are nowadays the predominant techniques for the determination of the neodymium isotopic composition. The sample volume has been greatly reduced to less than 10 L (van de Flierdt et al., 2012). Samples are pre-concentrated by precipitation or by the use of chelating resins, then remaining cations are removed by cation exchange chromatography and Nd isotopes are separated from the rest of the REE with using extraction chromatographic procedures or α-HIBA chemistry (Choppin and Silva, 1956; Pin and Zalduegui, 1997; van de Flierdt et al., 2012; Pahnke et al., 2012).

2. Area of Study

2.1 Geographic setting, bathymetry and geology of the plateau

The Kerguelen plateau is located in the Indian Sector of the Southern Ocean (Figure 5), about ~3,500 km southwest of Perth, Australia and ~2,000 km north of Antarctica. It is a hotspot-based chain of islands that lies in a NNW-SSE trend for ~2,300 km long and ~600 km wide between 46°S and 64°S, forming a natural barrier for the flow of the Antarctic Circumpolar Current (ACC). Most of the plateau is situated 2 km above the surrounding abyssal plains floored by oceanic crust, except at the southern end where it is separated from the Antarctic mainland by the Princess Elizabeth Trough. It hosts two groups of islands, the KA and the volcanically-active HIMI. The bathymetrical features of the KP divide it in three regions (Figure 5): (1) The northern Kerguelen plateau is a well-defined, almost square shallow section of the plateau (<200 m) that includes the KA. It is limited to the north by the Kerguelen-Amsterdam passage (not shown) and to the south by the KA Trough. (2) The relatively shallow (<400 m) central KP includes HIMI and a series of seamounts and rises, referred as the HIMI shoal. It is defined by the 600 m isobath and limits to the south with the

Fawn Trough and to the east with the HIMI Trough that separates it from another seamount. (3) The deeper (1.5-2 km) southern Kerguelen plateau presents no outcrops, limited to the north by the Fawn Trough and to the south by the Princess Elizabeth Trough (not shown).

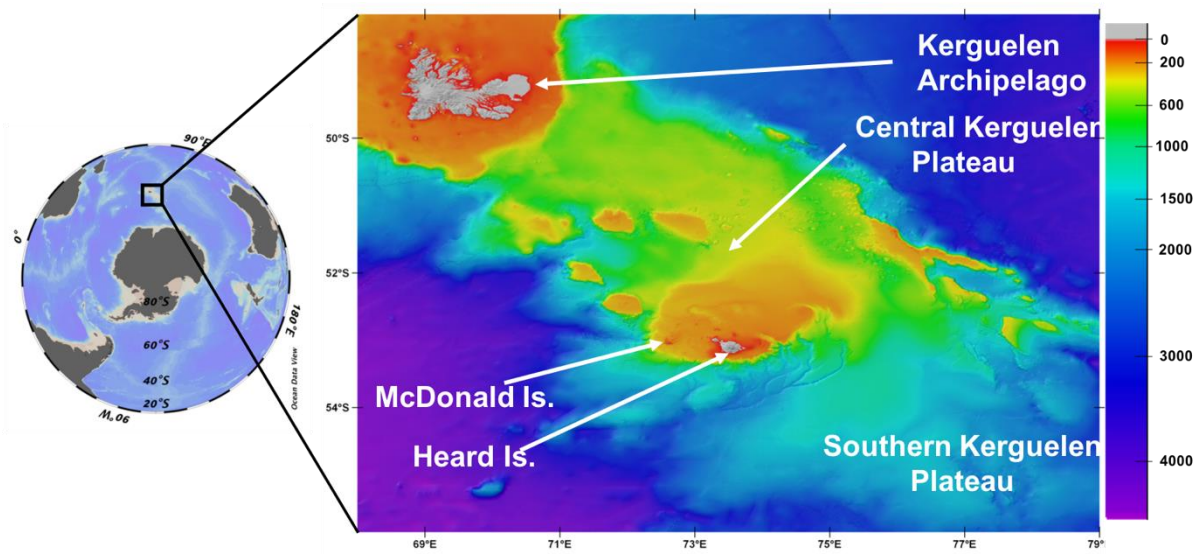

Figure 1-5. Bathymetrical features of the Kerguelen Plateau.

The Kerguelen Plateau is one of the two most voluminous Large Igneous Magmatic Provinces, together with the Ontgong Java in the Pacific (Frey et al., 2000). The Cretaceous Kerguelen Plateau represents voluminous volcanism associated with the arrival of the Kerguelen plume head below the young Indian Ocean lithosphere (Weis et al., 1992). Then, a rapid northward movement of the Indian plate over the plume formed a 5,000 km long hot spot track between ~82-38 Ma (Mahoney et al., 1983) . Around 40 Ma, the Southeast Indian Ridge intersected the plume's position; as this ridge migrated northeast relative to the plume, the magmatism of the hot spot became confined to the Antarctic plate. From this time onwards, the KA, HIMI and the NW-SW trending chain of submarine volcanoes (nowadays seamounts) were formed in the northern and central KP (Frey et al., 2000). More recent studies have determined, using radiometric dating, that magmatic rocks associated with the Kerguelen hot spot have ages that range from ~130 Ma to recent times (COFFIN, 2002; Bénard

et al., 2010). A geochemical contamination by continental material has been evidenced for all the studied magmatic rocks of the southern and central part of the Plateau. Only the basalts of the northern zone record the signature of ridge-derived magmas, suggesting that the South and Central Kerguelen Plateaus formed from the interaction between remnants of continental crust and the Kerguelen Plume, while the Northern KP was formed through interactions with the South East Indian Ridge (Bénard et al., 2010).

2.2 Circulation and hydrography of the Kerguelen Plateau

In the Southern Ocean, distinct water masses originating from different locations of the global ocean mix while circulating eastward around Antarctica, in what is known as the Antarctic Circumpolar Current (ACC). This region regulates the global climate because North Atlantic Deep Water upwells south of the ACC and transforms into the Antarctic Bottom Water and Antarctic Intermediate Water, exchanging heat and carbon along the way, and completing the southern-most component of the meridional overturning circulation (Park and Vivier, 2011).

The KP plateau represents a major topographic barrier for the flow of the ACC (Figure 6). About 75% of the total ACC flow (~140 Sv; 1 Sv = 10^6 m^3 s^{-1}) is deflected north of the KA through the Kerguelen-Amsterdam passage (Figure 6). The remaining transport (~50 Sv) still needs to pass between the Kerguelen islands and Antarctica (Park et al., 1991). The Fawn Trough Current constitutes a favoured passage for this remaining ACC component (Park and Gamberoni, 1997; McCartney and Donohue, 2007) with the strongest flow at the surface (0.6 m s^{-1}), decreasing towards 1000 m (0.3 m s^{-1}). A secondary eastward flow branch with a depth-averaged velocity of 0.2 m s^{-1} can also be found following the near-shore slope just south of HIMI. In the eastern flank of the plateau and south of the Fawn Trough Current the north-westward flowing Deep Western Boundary Current (DWBC) is highly barotropic and is mostly

confined within a narrow part of the continental slope (~75 km). This current transports around 36 Sv towards the plateau, which is then compensated by a poleward recirculation transport of 34 Sv (Park et al., 2008b). Finally, another important component of the eastward transport of the ACC that flows immediately south of the Kerguelen islands is the Polar Front. The location of the Polar Front has been debated in the past with an extreme discrepancy of over 10^{o} of latitude. However a recent study from Park et al.(2014) has validated the position of the PF to round the KA from the south and then turn northwards along the eastern escarpment of the northern KP (see Figure 6).

In the central part of the plateau the circulation is dominated mainly by the bathymetry. Calculated geostrophic currents indicated a dominant sluggish flow (3-5 m s^{-1}) with a general anticyclonic circulation that flows northwards east of HIMI roughly following the local bathymetry of the shallow platform (Park et al., 2008b). West of the HIMI the circulation is less defined, however it was proposed that this area holds a tentative topography-following southward circulation. In addition to horizontal transport,

Park et al.(2008a) identified activity of highly non-linear semidiurnal internal tides showing peak-to-peak isopycnal displacements of up to 80 m. The same authors estimated local vertical eddy diffusivities in the order of 4 x 10^{-4} m^2 s^{-1}. The vertical transport of water, together with the relatively slow circulation over the plateau, were identified as the main physical factors that enable the development of the seasonal bloom that occurs in the region (Park et al., 2008b).

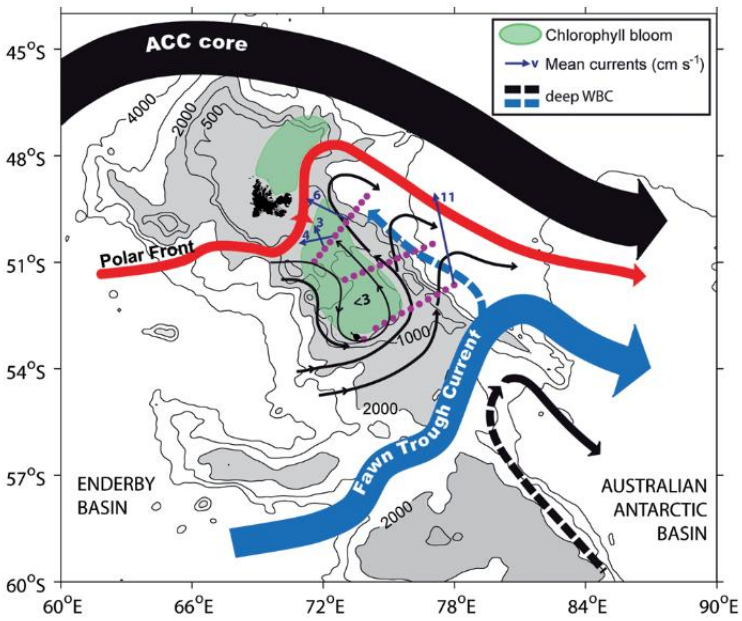

Figure 1-6. Predominant circulation pattern in the Kerguelen plateau (taken from Park et al., 2008b). The green colour represents areas where it is historically known for the bloom to appear in the region once the sun is no longer limiting in the austral summer. The red arrow represents the Polar Front.

References

Akagi T. (2013) Rare earth element (REE)-silicic acid complexes in seawater to explain the incorporation of REEs in opal and the "leftover" REEs in surface water: New interpretation of dissolved REE distribution profiles. *Geochim. Cosmochim. Acta* **113**, 174–192. Available at: http://dx.doi.org/10.1016/j.gca.2013.03.014.

Albarède F., Goldstein S. L. and Dautel D. (1997) The neodymium isotopic composition of manganese nodules from the Southern and Indian oceans, the global oceanic neodymium budget, and their bearing on deep ocean circulation. *Geochim. Cosmochim. Acta* **61**, 1277–1291. Available at: http://www.sciencedirect.com/science/article/pii/S0016703796004048 [Accessed December 22, 2015].

Alvarado Quiroz N. G., Hung C.-C. and Santschi P. H. (2006) Binding of thorium(IV) to carboxylate, phosphate and sulfate functional groups from marine exopolymeric substances (EPS). *Mar. Chem.* **100**, 337–353. Available at: https://linkinghub.elsevier.com/retrieve/pii/S0304420305002239.

Amakawa H., Nozaki Y., Alibo D. S., Zhang J., Fukugawa K. and Nagai H. (2004) Neodymium isotopic variations in Northwest Pacific waters. *Geochim. Cosmochim. Acta* **68**, 715–727. Available at: https://linkinghub.elsevier.com/retrieve/pii/S0016703703005015 [Accessed December 22, 2015].

Amin B. S., Krishnaswami S. and Somayajulu B. L. K. (1974) $^{234}Th/^{238}U$ activity ratios in Pacific Ocean bottom waters. *Earth Planet. Sci. Lett.* **21**, 342–344. Available at: https://linkinghub.elsevier.com/retrieve/pii/0012821X7490171X.

Anderson R. F. ., Mawji E., Cutter G. a. ., Measures C. I. and Jeandel C. (2014) GEOTRACES:

Changing the Way We Explore Ocean Chemistry. *Oceanography* **27**, 50–61. Available at: http://dx.doi.org/10.5670/oceanog.2014.07.

Anderson Robert F., Bacon M. P. and Brewer P. G. (1983) Removal of ^{230}Th and ^{231}Pa at ocean margins. *Earth Planet. Sci. Lett.* **66**, 73–90. Available at: https://linkinghub.elsevier.com/retrieve/pii/0012821X83901279.

Anderson R.F., Bacon M. P. and Brewer P. G. (1983) Removal of ^{230}Th and ^{231}Pa from the open ocean. *Earth Planet. Sci. Lett.* **62**, 7–23. Available at: https://linkinghub.elsevier.com/retrieve/pii/0012821X83900675 [Accessed July 5, 2016].

Anderson R. F., Cheng H., Edwards R. L., Landing W. M., Shelley R. U., Measures C. I., Lao Y., Ohnemus D. C., Fleisher M. Q., Hayes C. T., Moran S. B., Huang K.-F., Robinson L. F., Lam P. J., Kadko D., Lu Y. and Morton P. L. (2016) How well can we quantify dust deposition to the ocean? *Philos. Trans. R. Soc. A Math. Phys. Eng. Sci.* **374**, 20150285.

Anderson R. F., Fleisher M. Q. and Lao Y. (2006) Glacial–interglacial variability in the delivery of dust to the central equatorial Pacific Ocean. *Earth Planet. Sci. Lett.* **242**, 406–414. Available at: https://linkinghub.elsevier.com/retrieve/pii/S0012821X05008459 [Accessed July 27, 2016].

Anderson R. F., Fleisher M. Q., Robinson L. F., Edwards R. L., Hoff J. A., Moran S. B., van der Loeff M. R., Thomas A. L., Roy-Barman M. and Francois R. (2012) GEOTRACES intercalibration of 230Th, 232Th, 231Pa, and prospects for 10Be. *Limnol. Oceanogr. Methods* **10**, 179–213. Available at: http://doi.wiley.com/10.4319/lom.2012.10.179 [Accessed November 5, 2015].

Andersson P. S. and Schöberg H. (2012) Determination of ^{232}Th and ^{230}Th in seawater using a chemical separation procedure and thermal ionization mass spectrometry. *Limnol. Oceanogr. Methods* **10**, 296–303. Available at: http://doi.wiley.com/10.4319/lom.2012.10.296.

Arrigo K. R., van Dijken G. L. and Bushinsky S. (2008) Primary production in the Southern Ocean, 1997–2006. *J. Geophys. Res.* **113**, C08004. Available at: http://doi.wiley.com/10.1029/2007JC004578.

Arsouze T., Dutay J., Lacan F. and Jeandel C. (2009) Modeling the Nd Oceanic Cycle Using a Fully Prognostic Dynamical / Biogeochemical Coupled Model. *Assembly* **11**, 9279.

Arsouze T., Dutay J., Lacan F. and Jeandel C. (2007) Modeling the neodymium isotopic composition with a global ocean circulation model. *Chem. Geol.* **239**, 165–177. Available at: https://linkinghub.elsevier.com/retrieve/pii/S0009254106005353 [Accessed July 6, 2016].

De Baar H. J. W., Bacon M. P., Brewer P. G. and Bruland K. W. (1985) Rare earth elements in the Pacific and Atlantic Oceans. *Geochim. Cosmochim. Acta* **49**, 1943–1959. Available at: https://linkinghub.elsevier.com/retrieve/pii/0016703785900894 [Accessed December 22, 2015].

de Baar H. J. W., Bathmannt U., Smetacek V., Löscher B. M. and Veth C. (1995) Importance of iron for plankton blooms and carbon dioxide drawdown in the Southern Ocean. *Nature* **373**, 412–415.

de Baar H. J. W., German C. R., Elderfield H. and van Gaans P. (1988) Rare earth element distributions in anoxic waters of the Cariaco Trench. *Geochim. Cosmochim. Acta* **52**, 1203–1219. Available at: https://linkinghub.elsevier.com/retrieve/pii/001670378890275X.

Bacon M. P. (1984) Glacial to interglacial changes in carbonate and clay sedimentation in the

Atlantic Ocean estimated from 230Th measurements. *Chem. Geol.* **46**, 97–111. Available at: https://linkinghub.elsevier.com/retrieve/pii/0009254184901839 [Accessed May 15, 2016].

Bacon M. P. and Anderson R. F. (1982) Distribution of thorium isotopes between dissolved and particulate forms in the deep sea. *J. Geophys. Res.* **87**, 20–45. Available at: http://doi.wiley.com/10.1029/JC087iC03p02045.

Bacon M. P., Huh C.-A., Fleer A. P. and Deuser W. G. (1985) Seasonality in the flux of natural radionuclides and plutonium in the deep Sargasso Sea. *Deep Sea Res. Part A. Oceanogr. Res. Pap.* **32**, 273–286. Available at: https://linkinghub.elsevier.com/retrieve/pii/0198014985900792.

Bacon M. P. and Rutgers van der Loeff M. M. (1989) Removal of thorium-234 by scavenging in the bottom nepheloid layer of the ocean. *Earth Planet. Sci. Lett.* **92**, 157–164. Available at: https://linkinghub.elsevier.com/retrieve/pii/0012821X89900435.

Bacon M. P., Spencer D. W. and Brewer P. G. (1976) ^{210}Pb/^{226}Ra and ^{210}Po/^{210}Pb disequilibria in seawater and suspended particulate matter. *Earth Planet. Sci. Lett.* **32**, 277–296. Available at: https://linkinghub.elsevier.com/retrieve/pii/0012821X76900686.

Balashov Y. A. (1961) Distribution of the rare earths in the waters of the Indian Ocean. *Geochemistry, Transl. Geokhimiya* **9**, 877.

Barnes I. L., Carpenter B. S., Garner E. L., Gramlich J. W., Kuehner E. C., Machlan L. A., Maienthal E. J., Moody J. R., Moore L. J. and Murphy T. J. (1972) Isotopic abundance ratios and concentrations of selected elements in Apollo 14 samples. In *Lunar and Planetary Science Conference Proceedings* p. 1465.

Baskaran M., Santschi P. ., Benoit G. and Honeyman B. . (1992) Scavenging of thorium isotopes by colloids in seawater of the Gulf of Mexico. *Geochim. Cosmochim. Acta* **56**, 3375–3388. Available at: https://linkinghub.elsevier.com/retrieve/pii/001670379290385V.

Baskaran M., Swarzenski P. W. and Porcelli D. (2003) Role of colloidal material in the removal of ^{234}Th in the Canada basin of the Arctic Ocean. *Deep Sea Res. Part I Oceanogr. Res. Pap.* **50**, 1353–1373. Available at: https://linkinghub.elsevier.com/retrieve/pii/S0967063703001407.

Becquerel A. H. (1896) Sur les radiations invisibles émises par les corps phosphorescents. *CR Acad. Sci. Paris* **122**, 501.

Bénard F., Callot J.-P., Vially R., Schmitz J., Roest W., Patriat M. and Loubrieu B. (2010) The Kerguelen plateau: Records from a long-living/composite microcontinent. *Mar. Pet. Geol.* **27**, 633–649. Available at: https://linkinghub.elsevier.com/retrieve/pii/S0264817209001433.

Benitez-Nelson C., Buesseler K. O., Karl D. M. and Andrews J. (2001) A time-series study of particulate matter export in the North Pacific Subtropical Gyre based on ^{234}Th:^{238}U disequilibrium. *Deep Sea Res. Part I Oceanogr. Res. Pap.* **48**, 2595–2611. Available at: https://linkinghub.elsevier.com/retrieve/pii/S0967063701000322.

Benitez-Nelson C. R. and Moore W. S. (2006) Future applications of ^{234}Th in aquatic ecosystems. *Mar. Chem.* **100**, 163–165.

Bertram C. J. and Elderfield H. (1993) The geochemical balance of the rare earth elements and neodymium isotopes in the oceans. *Geochim. Cosmochim. Acta* **57**, 1957–1986. Available at: http://www.sciencedirect.com/science/article/pii/001670379390087D.

Bhat S. G., Krishnaswamy S., Lal D., Rama and Moore W. S. (1968) ^{234}Th/^{238}U ratios in the ocean. *Earth Planet. Sci. Lett.* **5**, 483–491. Available at:

https://linkinghub.elsevier.com/retrieve/pii/S0012821X68800834.
Blain S., Tréguer P., Belviso S., Bucciarelli E., Denis M., Desabre S., Fiala M., Martin Jézéquel V., Le Fèvre J., Mayzaud P., Marty J.-C. and Razouls S. (2001) A biogeochemical study of the island mass effect in the context of the iron hypothesis: Kerguelen Islands, Southern Ocean. *Deep Sea Res. Part I Oceanogr. Res. Pap.* **48**, 163–187. Available at: http://www.sciencedirect.com/science/article/pii/S0967063700000479.
Bowie A. R., van der Merwe P., Quéroué F., Trull T., Fourquez M., Planchon F., Sarthou G., Chever F., Townsend A. T., Obernosterer I., Sallée J.-B. and Blain S. (2015) Iron budgets for three distinct biogeochemical sites around the Kerguelen Archipelago (Southern Ocean) during the natural fertilisation study, KEOPS-2. *Biogeosciences* **12**, 4421–4445. Available at: https://www.biogeosciences.net/12/4421/2015/.
Boyd P. W., Arrigo K. R., Strzepek R. and van Dijken G. L. (2012) Mapping phytoplankton iron utilization: Insights into Southern Ocean supply mechanisms. *J. Geophys. Res. Ocean.* **117**, 1–18. Available at: http://doi.wiley.com/10.1029/2011JC007726.
Boyd P. W., Jickells T., Law C. S., Blain S., Boyle E. A., Buesseler K. O., Coale K. H., Cullen J. J., de Baar H. J. W., Follows M., Harvey M., Lancelot C., Levasseur M., Owens N. P. J., Pollard R., Rivkin R. B., Sarmiento J., Schoemann V., Smetacek V., Takeda S., Tsuda A., Turner S. and Watson A. J. (2007) Mesoscale Iron Enrichment Experiments 1993-2005: Synthesis and Future Directions. *Science (80-.).* **315**, 612–617. Available at: http://www.sciencemag.org/cgi/doi/10.1126/science.1131669.
Buesseler K., Ball L., Andrews J., Benitez-Nelson C., Belastock R., Chai F. and Chao Y. (1998) Upper ocean export of particulate organic carbon in the Arabian Sea derived from thorium-234. *Deep Sea Res. Part II Top. Stud. Oceanogr.* **45**, 2461–2487. Available at: https://linkinghub.elsevier.com/retrieve/pii/S0967064598800222.
Buesseler K. O., Andrews J. A., Hartman M. C., Belastock R. and Chai F. (1995) Regional estimates of the export flux of particulate organic carbon derived from thorium-234 during the JGOFS EqPac program. *Deep Sea Res. Part II Top. Stud. Oceanogr.* **42**, 777–804. Available at: https://linkinghub.elsevier.com/retrieve/pii/096706459500043P.
Buesseler K. O., Antia A. N., Chen M., Fowler S. W., Gardner W. D., Gustafsson O., Harada K., Michaels A. F., van der Loeff R. and Michiel S. (2007) Estimating upper ocean particle fluxes using sediment traps. *J. Mar. Res.* **65**, 345–416.
Buesseler K. O., Bacon M. P., Kirk Cochran J. and Livingston H. D. (1992) Carbon and nitrogen export during the JGOFS North Atlantic Bloom experiment estimated from ^{234}Th:^{238}U disequilibria. *Deep Sea Res. Part A. Oceanogr. Res. Pap.* **39**, 1115–1137. Available at: https://linkinghub.elsevier.com/retrieve/pii/0198014992900607.
Buesseler K. O., Michaels A. F., Siegel D. A. and Knap A. H. (1994) A three dimensional time-dependent approach to calibrating sediment trap fluxes. *Global Biogeochem. Cycles* **8**, 179–193. Available at: http://doi.wiley.com/10.1029/94GB00207.
Buesseler K. O., Steinberg D. K., Michaels A. F., Johnson R. J., Andrews J. E., Valdes J. R. and Price J. F. (2000) A comparison of the quantity and composition of material caught in a neutrally buoyant versus surface-tethered sediment trap. *Deep Sea Res. Part I Oceanogr. Res. Pap.* **47**, 277–294. Available at: https://linkinghub.elsevier.com/retrieve/pii/S0967063799000564.
Byrne R. H. and Kim K.-H. (1990) Rare earth element scavenging in seawater. *Geochim. Cosmochim. Acta* **54**, 2645–2656. Available at: https://linkinghub.elsevier.com/retrieve/pii/0016703790900023.
Carter P., Vance D., Hillenbrand C., Smith J. A. and Shoosmith D. R. (2012) The neodymium

isotopic composition of waters masses in the eastern Pacific sector of the Southern Ocean. *Geochim. Cosmochim. Acta* **79**, 41–59. Available at: https://linkinghub.elsevier.com/retrieve/pii/S0016703711007095 [Accessed December 22, 2015].

Chase Z., Anderson R. F., Fleisher M. Q. and Kubik P. W. (2003) Accumulation of biogenic and lithogenic material in the Pacific sector of the Southern Ocean during the past 40,000 years. *Deep Sea Res. Part II Top. Stud. Oceanogr.* **50**, 799–832. Available at: https://linkinghub.elsevier.com/retrieve/pii/S0967064502005957.

Chase Z., Anderson R. F., Fleisher M. Q. and Kubik P. W. (2002) The influence of particle composition and particle flux on scavenging of Th, Pa and Be in the ocean. *Earth Planet. Sci. Lett.* **204**, 215–229. Available at: https://linkinghub.elsevier.com/retrieve/pii/S0012821X02009846.

Chen J. H., Lawrence Edwards R. and Wasserburg G. J. (1986) 238U,234U and232Th in seawater. *Earth Planet. Sci. Lett.* **80**, 241–251. Available at: http://www.sciencedirect.com/science/article/pii/0012821X86901081.

Choi M., Francois R., Sims K., Bacon M. ., Brown-Leger S., Fleer A. ., Ball L., Schneider D. and Pichat S. (2001) Rapid determination of ^{230}Th and ^{231}Pa in seawater by desolvated micro-nebulization Inductively Coupled Plasma magnetic sector mass spectrometry. *Mar. Chem.* **76**, 99–112. Available at: https://linkinghub.elsevier.com/retrieve/pii/S0304420301000500.

Choppin G. R. and Silva R. J. (1956) Separation of the lanthanides by ion exchange with alpha-hydroxy isobutyric acid. *J. Inorg. Nucl. Chem.* **3**, 153–154.

Coale K. H. and Bruland K. W. (1985) 234 Th: 238 U disequilibria within the California Current1. *Limnol. Oceanogr.* **30**, 22–33. Available at: http://doi.wiley.com/10.4319/lo.1985.30.1.0022.

Cochran J. K., Livingston H. D., Hirschberg D. J. and Surprenant L. D. (1987) Natural and anthropogenic radionuclide distributions in the northwest Atlantic Ocean. *Earth Planet. Sci. Lett.* **84**, 135–152. Available at: https://linkinghub.elsevier.com/retrieve/pii/0012821X87900811.

COFFIN M. F. (2002) Kerguelen Hotspot Magma Output since 130 Ma. *J. Petrol.* **43**, 1121–1137. Available at: https://academic.oup.com/petrology/article-lookup/doi/10.1093/petrology/43.7.1121.

Cole C. S., James R. H., Connelly D. P. and Hathorne E. C. (2014) Rare earth elements as indicators of hydrothermal processes within the East Scotia subduction zone system. *Geochim. Cosmochim. Acta* **140**, 20–38. Available at: http://dx.doi.org/10.1016/j.gca.2014.05.018.

Coppola L., Roy-Barman M., Mulsow S., Povinec P. and Jeandel C. (2006) Thorium isotopes as tracers of particles dynamics and deep water circulation in the Indian sector of the Southern Ocean (ANTARES IV). *Mar. Chem.* **100**, 299–313. Available at: https://linkinghub.elsevier.com/retrieve/pii/S0304420305002203.

Coppola L., Roy-Barman M., Wassmann P., Mulsow S. and Jeandel C. (2002) Calibration of sediment traps and particulate organic carbon export using ^{234}Th in the Barents Sea. *Mar. Chem.* **80**, 11–26. Available at: https://linkinghub.elsevier.com/retrieve/pii/S0304420302000713.

Costa K. and McManus J. (2017) Efficacy of 230Th normalization in sediments from the Juan de Fuca Ridge, northeast Pacific Ocean. *Geochim. Cosmochim. Acta* **197**, 215–225. Available at: http://dx.doi.org/10.1016/j.gca.2016.10.034.

Crocket K. C., Hill E., Abell R. E., Johnson C., Gary S. F., Brand T. and Hathorne E. C. (2018) Rare Earth Element Distribution in the NE Atlantic: Evidence for Benthic Sources, Longevity of the Seawater Signal, and Biogeochemical Cycling. *Front. Mar. Sci.* **5**, 1–22. Available at: http://journal.frontiersin.org/article/10.3389/fmars.2018.00147/full.

Curie M. (1898) *Rayons émis par les composés de l'uranium et du thorium*., Gauthier-Villars.

Dai M. . and Benitez-Nelson C. . (2001) Colloidal organic carbon and ^{234}Th in the Gulf of Maine. *Mar. Chem.* **74**, 181–196. Available at: https://linkinghub.elsevier.com/retrieve/pii/S0304420301000123.

DeMaster D. J. (1979) *The marine budgets of silica and ^{32}Si*., Yale University.

DeMaster D. J., Brewster D. C., McKee B. A. and Nittrouer C. A. (1991) Rates of particle scavenging, sediment reworking, and longitudinal ripple formation at the HEBBLE site based on measurements of 234Th and 210Pb. *Mar. Geol.* **99**, 423–444. Available at: https://linkinghub.elsevier.com/retrieve/pii/0025322791900548.

Deng F., Thomas A. L., Rijkenberg M. J. A. and Henderson G. M. (2014) Controls on seawater ^{231}Pa, ^{230}Th and ^{232}Th concentrations along the flow paths of deep waters in the Southwest Atlantic. *Earth Planet. Sci. Lett.* **390**, 93–102. Available at: http://dx.doi.org/10.1016/j.epsl.2013.12.038.

DePaolo D. J. and Wasserburg G. J. (1976) Nd isotopic variations and petrogenetic models. *Geophys. Res. Lett.* **3**, 249–252. Available at: http://doi.wiley.com/10.1029/GL003i005p00249.

Dickin A. P. (2018) *Radiogenic isotope geology*., Cambridge university press.

Elderfield H. and Greaves M. J. (1981) Negative cerium anomalies in the rare earth element patterns of oceanic ferromanganese nodules. *Earth Planet. Sci. Lett.* **55**, 163–170. Available at: https://linkinghub.elsevier.com/retrieve/pii/0012821X81900959.

Elderfield H. and Greaves M. J. (1982) The rare earth elements in seawater. *Nature* **296**, 214–219. Available at: http://www.nature.com/articles/296214a0.

Elderfield H. and Sholkovitz E. R. (1987) Rare earth elements in the pore waters of reducing nearshore sediments. *Earth Planet. Sci. Lett.* **82**, 280–288. Available at: https://linkinghub.elsevier.com/retrieve/pii/0012821X87902020.

Elderfield H., Whitfield M., Burton J. D., Bacon M. P. and Liss P. S. (1988) The Oceanic Chemistry of the Rare-Earth Elements. *Philos. Trans. R. Soc. A Math. Phys. Eng. Sci.* **325**, 105–126. Available at: http://rsta.royalsocietypublishing.org/cgi/doi/10.1098/rsta.1988.0046.

Eugster O., Tera F., Burnett D. S. and Wasserburg G. J. (1970) Isotopic composition of gadolinium and neutron-capture effects in some meteorites. *J. Geophys. Res.* **75**, 2753–2768. Available at: http://doi.wiley.com/10.1029/JB075i014p02753.

Flierdt T. van de, Frank M., Lee D.-C., Halliday A. N., Reynolds B. C. and Hein J. R. (2004) New constraints on the sources and behavior of neodymium and hafnium in seawater from Pacific Ocean ferromanganese crusts. *Geochim. Cosmochim. Acta* **68**, 3827–3843. Available at: https://linkinghub.elsevier.com/retrieve/pii/S0016703704002315.

van de Flierdt T., Pahnke K., Amakawa H., Andersson P., Basak C., Coles B., Colin C., Crocket K., Frank M., Frank N., Goldstein S. L., Goswami V., Haley B. A., Hathorne E. C., Hemming S. R., Henderson G. M., Jeandel C., Jones K., Kreissig K., Lacan F., Lambelet M., Martin E. E., Newkirk D. R., Obata H., Pena L., Piotrowski A. M., Pradoux C., Scher H. D., Schöberg H., Singh S. K., Stichel T., Tazoe H., Vance D. and Yang J. (2012) GEOTRACES intercalibration of neodymium isotopes and rare earth element concentrations in seawater and suspended particles. Part 1: reproducibility of results

for the international intercomparison. *Limnol. Oceanogr. Methods* **10**, 234–251. Available at: http://onlinelibrary.wiley.com/doi/10.4319/lom.2012.10.234/full.

Francois R., Bacon M. P., Altabet M. A. and Labeyrie L. D. (1993) Glacial/interglacial changes in sediment rain rate in the SW Indian Sector of subantarctic Waters as recorded by ^{230}Th, ^{231}Pa, U, and δ^{15} N. *Paleoceanography* **8**, 611–629. Available at: http://doi.wiley.com/10.1029/93PA00784.

Francois R., Bacon M. P. and Suman D. O. (1990) Thorium 230 profiling in deep-sea sediments: High-resolution records of flux and dissolution of carbonate in the equatorial Atlantic during the last 24,000 years. *Paleoceanography* **5**, 761–787. Available at: http://onlinelibrary.wiley.com/doi/10.1029/PA005i005p00761/full [Accessed May 15, 2016].

Francois R., Frank M., Rutgers van der Loeff M., Bacon M. P., Geibert W., Kienast S., Anderson R. F., Bradtmiller L., Chase Z., Henderson G., Marcantonio F. and Allen S. E. (2007) Comment on "Do geochemical estimates of sediment focusing pass the sediment test in the equatorial Pacific?" by M. Lyle et al. *Paleoceanography* **22**, n/a-n/a. Available at: http://doi.wiley.com/10.1029/2005PA001235 [Accessed April 12, 2016].

Francois R., Frank M., Rutgers van der Loeff M. M. and Bacon M. P. (2004) Th normalization: An essential tool for interpreting sedimentary fluxes during the late Quaternary. *Paleoceanography* **19**, n/a-n/a. Available at: http://doi.wiley.com/10.1029/2003PA000939.

Frank M. (2002) Radiogenic isotopes: Tracers of past ocean circulation and erosional input. *Rev. Geophys.* **40**, 1001. Available at: http://doi.wiley.com/10.1029/2000RG000094.

Frey F. A., Coffin M. F., Wallace P. J., Weis D., Zhao X., Wise S. W., Wähnert V., Teagle D. A. H., Saccocia P. J., Reusch D. N., Pringle M. S., Nicolaysen K. E., Neal C. R., Müller R. D., Moore C. L., Mahoney J. J., Keszthelyi L., Inokuchi H., Duncan R. A., Delius H., Damuth J. E., Damasceno D., Coxall H. K., Borre M. K., Boehm F., Barling J., Arndt N. T. and Antretter M. (2000) Origin and evolution of a submarine large igneous province: the Kerguelen Plateau and Broken Ridge, southern Indian Ocean. *Earth Planet. Sci. Lett.* **176**, 73–89. Available at: https://linkinghub.elsevier.com/retrieve/pii/S0012821X99003155.

Garcia-Solsona E., Jeandel C., Labatut M., Lacan F., Vance D., Chavagnac V. and Pradoux C. (2014) Rare earth elements and Nd isotopes tracing water mass mixing and particle-seawater interactions in the SE Atlantic. *Geochim. Cosmochim. Acta* **125**, 351–372. Available at: http://dx.doi.org/10.1016/j.gca.2013.10.009.

German C. R., Klinkhammer G. P., Edmond J. M., Mura A. and Elderfield H. (1990) Hydrothermal scavenging of rare-earth elements in the ocean. *Nature* **345**, 516–518. Available at: http://www.nature.com/articles/345516a0.

German C. R., Masuzawa T., Greaves M. J., Elderfield H. and Edmond J. M. (1995) Dissolved rare earth elements in the Southern Ocean: Cerium oxidation and the influence of hydrography. *Geochim. Cosmochim. Acta* **59**, 1551–1558. Available at: https://linkinghub.elsevier.com/retrieve/pii/0016703795000614.

Goldberg E. D., Koide M., Schmitt R. A. and Smith R. H. (1963) Rare-Earth distributions in the marine environment. *J. Geophys. Res.* **68**, 4209–4217. Available at: http://doi.wiley.com/10.1029/JZ068i014p04209.

Goldschmidt V. M. (1937) The principles of distribution of chemical elements in minerals and rocks. The seventh Hugo Müller Lecture, delivered before the Chemical Society on

March 17th, 1937. *J. Chem. Soc.* **69**, 655–673. Available at: http://xlink.rsc.org/?DOI=JR9370000655.
Goldstein S. L. and Hemming S. R. (2003) Long-lived Isotopic Tracers in Oceanography, Paleoceanography, and Ice-sheet Dynamics. In *Treatise on Geochemistry* Elsevier. pp. 453–489. Available at: https://linkinghub.elsevier.com/retrieve/pii/B008043751606179X.
Goldstein S. L. and O'Nions R. K. (1981) Nd and Sr isotopic relationships in pelagic clays and ferromanganese deposits. *Nature* **292**, 324–327. Available at: http://www.nature.com/articles/292324a0.
Grasse P., Bosse L., Hathorne E. C., Böning P., Pahnke K. and Frank M. (2017) Short-term variability of dissolved rare earth elements and neodymium isotopes in the entire water column of the Panama Basin. *Earth Planet. Sci. Lett.* **475**, 242–253. Available at: http://dx.doi.org/10.1016/j.epsl.2017.07.022.
Grasse P., Stichel T., Stumpf R., Stramma L. and Frank M. (2012) The distribution of neodymium isotopes and concentrations in the Eastern Equatorial Pacific: Water mass advection versus particle exchange. *Earth Planet. Sci. Lett.* **353**–**354**, 198–207. Available at: http://linkinghub.elsevier.com/retrieve/pii/S0012821X12004438.
Greaves M. J., Rudnicki M. and Elderfield H. (1991) Rare earth elements in the Mediterranean Sea and mixing in the Mediterranean outflow. *Earth Planet. Sci. Lett.* **103**, 169–181. Available at: https://linkinghub.elsevier.com/retrieve/pii/0012821X9190158E.
Greenberg R. R. and Kingston H. M. (1983) Trace element analysis of natural water samples by neutron activation analysis with chelating resin. *Anal. Chem.* **55**, 1160–1165. Available at: https://pubs.acs.org/doi/abs/10.1021/ac00258a041.
Grenier M., Garcia-Solsona E., Lemaitre N., Trull T. W., Bouvier V., Nonnotte P., van Beek P., Souhaut M., Lacan F. and Jeandel C. (2018) Differentiating Lithogenic Supplies, Water Mass Transport, and Biological Processes On and Off the Kerguelen Plateau Using Rare Earth Element Concentrations and Neodymium Isotopic Compositions. *Front. Mar. Sci.* **5**. Available at: https://www.frontiersin.org/article/10.3389/fmars.2018.00426/full.
Grenier M., Jeandel C. and Cravatte S. (2014) From the subtropics to the equator in the Southwest Pacific: Continental material fluxes quantified using neodymium data along modeled thermocline water pathways. *J. Geophys. Res. Ocean.* **119**, 3948–3966. Available at: http://doi.wiley.com/10.1002/2013JC009670.
Grenier M., Jeandel C., Lacan F., Vance D., Venchiarutti C., Cros A. and Cravatte S. (2013) From the subtropics to the central equatorial Pacific Ocean: Neodymium isotopic composition and rare earth element concentration variations. *J. Geophys. Res. Ocean.* **118**, 592–618. Available at: http://doi.wiley.com/10.1029/2012JC008239.
Guo L., Santschi P. H. and Baskaran M. (1997) Interactions of thorium isotopes with colloidal organic matter in oceanic environments. *Colloids Surfaces A Physicochem. Eng. Asp.* **120**, 255–271. Available at: https://linkinghub.elsevier.com/retrieve/pii/S0927775796037235.
Gustafsson Ö., Andersson P., Roos P., Kukulska Z., Broman D., Larsson U., Hajdu S. and Ingri J. (2004) Evaluation of the collection efficiency of upper ocean sub-photic-layer sediment traps: a 24-month in situ calibration in the open Baltic Sea using ^{234}Th. *Limnol. Oceanogr. Methods* **2**, 62–74. Available at: http://doi.wiley.com/10.4319/lom.2004.2.62.
Gustafsson Ö., Düker A., Larsson J., Andersson P. and Ingri J. (2000) Functional separation of

colloids and gravitoids in surface waters based on differential settling velocity: Coupled cross-flow filtration-split flow thin-cell fractionation (CFF-SPLITT). *Limnol. Oceanogr.* **45**, 1731–1742. Available at: http://doi.wiley.com/10.4319/lo.2000.45.8.1731.

Haley B. A., Du J., Abbott A. N. and McManus J. (2017) The Impact of Benthic Processes on Rare Earth Element and Neodymium Isotope Distributions in the Oceans. *Front. Mar. Sci.* **4**, 1–12. Available at: http://journal.frontiersin.org/article/10.3389/fmars.2017.00426/full.

Haley B. A., Frank M., Hathorne E. and Pisias N. (2014) Biogeochemical implications from dissolved rare earth element and Nd isotope distributions in the Gulf of Alaska. *Geochim. Cosmochim. Acta* **126**, 455–474. Available at: http://dx.doi.org/10.1016/j.gca.2013.11.012.

Halliday A. N., Davidson J. P., Holden P., Owen R. M. and Olivarez A. M. (1992) Metalliferous sediments and the scavenging residence time of Nd near hydrothermal vents. *Geophys. Res. Lett.* **19**, 761–764. Available at: http://doi.wiley.com/10.1029/92GL00393.

Hathorne E. C., Stichel T., Brück B. and Frank M. (2014) Rare earth element distribution in the Atlantic sector of the Southern Ocean: The balance between particle scavenging and vertical supply. *Mar. Chem.* **177**, 157–171. Available at: http://dx.doi.org/10.1016/j.marchem.2015.03.011.

Hayes C. T., Anderson R. F., Fleisher M. Q., Serno S., Winckler G. and Gersonde R. (2013a) Quantifying lithogenic inputs to the North Pacific Ocean using the long-lived thorium isotopes. *Earth Planet. Sci. Lett.* **383**, 16–25. Available at: http://dx.doi.org/10.1016/j.epsl.2013.09.025.

Hayes C. T., Anderson R. F., Jaccard S. L., François R., Fleisher M. Q., Soon M. and Gersonde R. (2013b) A new perspective on boundary scavenging in the North Pacific Ocean. *Earth Planet. Sci. Lett.* **369**–**370**, 86–97. Available at: http://dx.doi.org/10.1016/j.epsl.2013.03.008.

Hayes C. T., Black E. E., Anderson R. F., Baskaran M., Buesseler K. O., Charette M. A., Cheng H., Cochran J. K., Edwards R. L., Fitzgerald P., Lam P. J., Lu Y., Morris S. O., Ohnemus D. C., Pavia F. J., Stewart G. and Tang Y. (2018) Flux of Particulate Elements in the North Atlantic Ocean Constrained by Multiple Radionuclides. *Global Biogeochem. Cycles* **32**, 1738–1758. Available at: https://onlinelibrary.wiley.com/doi/abs/10.1029/2018GB005994.

Hayes C. T., Fitzsimmons J. N., Boyle E. A., McGee D., Anderson R. F., Weisend R. and Morton P. L. (2015) Thorium isotopes tracing the iron cycle at the Hawaii Ocean Time-series Station ALOHA. *Geochim. Cosmochim. Acta* **169**, 1–16. Available at: http://dx.doi.org/10.1016/j.gca.2015.07.019.

Hayes C. T., Rosen J., McGee D. and Boyle E. A. (2017) Thorium distributions in high- and low-dust regions and the significance for iron supply. *Global Biogeochem. Cycles* **31**, 1–20. Available at: http://doi.wiley.com/10.1002/2016GB005511.

Henderson G. M., Heinze C., Anderson R. F. and Winguth A. M. E. (1999) Global distribution of the flux to ocean sediments constrained by GCM modelling. *Deep Sea Res. Part I Oceanogr. Res. Pap.* **46**, 1861–1893. Available at: https://linkinghub.elsevier.com/retrieve/pii/S0967063799000308.

Henderson P. and Pankhurst R. J. (1984) Analytical Chemistry. In pp. 467–499. Available at: https://linkinghub.elsevier.com/retrieve/pii/B9780444421487500186.

Hirose K. (1996) Determination of a strong organic ligand dissolved in seawater: Thorium-complexing capacity of oceanic dissolved organic matter. *J. Radioanal. Chem. Artic.*

204, 193–204.
Hirose K. and Sugimura Y. (1993) Chemical speciation of particulate ^{238}U, ^{239,240}Pu and Th isotopes in seawater. *Sci. Total Environ.* **130**–**131**, 517–524. Available at: https://linkinghub.elsevier.com/retrieve/pii/004896979390106G.
Hirose K. and Tanoue E. (1994) Thorium-particulate matter interaction. Thorium complexing capacity of oceanic particulate matter: Theory. *Geochim. Cosmochim. Acta* **58**, 1–7. Available at: https://linkinghub.elsevier.com/retrieve/pii/0016703794904413.
Høgdahl O. T. and Melsom, S.Bowen V. T. (1968) Neutron Activation Analysis of Lanthanide Elements in Sea Water. In pp. 308–325. Available at: https://pubs.acs.org/doi/abs/10.1021/ba-1968-0073.ch019.
Honeyman B. D. and Santschi P. H. (1989) A Brownian-pumping model for oceanic trace metal scavenging: Evidence from Th isotopes. *J. Mar. Res.* **47**, 951–992. Available at: http://openurl.ingenta.com/content/xref?genre=article&issn=0022-2402&volume=47&issue=4&spage=951.
Hooker P. J., O'Nions R. K. and Pankhurst R. J. (1975) Determination of rare-earth elements in USGS standard rocks by mixed-solvent ion exchange and mass-spectrometric isotope dilution. *Chem. Geol.* **16**, 189–196. Available at: https://linkinghub.elsevier.com/retrieve/pii/0009254175900273.
Hsieh Y., Henderson G. M. and Thomas A. L. (2011) Combining seawater ^{232}Th and ^{230}Th concentrations to determine dust fluxes to the surface ocean. *Earth Planet. Sci. Lett.* **312**, 280–290. Available at: http://dx.doi.org/10.1016/j.epsl.2011.10.022.
Huh C. (1987) Determination of thorium in seawater by neutron activation analysis and mass spectrometry. , 1–5.
Huh C. A. and Bacon M. P. (1985) Determination of thorium concentration in seawater by neutron activation analysis. *Anal. Chem.* **57**, 2138–2142. Available at: https://pubs.acs.org/doi/abs/10.1021/ac00288a030.
Inthorn M., Rutgers van der Loeff M. and Zabel M. (2006) A study of particle exchange at the sediment–water interface in the Benguela upwelling area based on ^{234}Th/^{238}U disequilibrium. *Deep Sea Res. Part I Oceanogr. Res. Pap.* **53**, 1742–1761. Available at: https://linkinghub.elsevier.com/retrieve/pii/S0967063706002196.
Jacquet S. H. M., Dehairs F., Savoye N., Obernosterer I., Christaki U., Monnin C. and Cardinal D. (2008) Mesopelagic organic carbon remineralization in the Kerguelen Plateau region tracked by biogenic particulate Ba. *Deep Sea Res. Part II Top. Stud. Oceanogr.* **55**, 868–879. Available at: http://www.sciencedirect.com/science/article/pii/S096706450800026X
Jeandel C., Bishop J. K. and Zindler A. (1995) Exchange of neodymium and its isotopes between seawater and small and large particles in the Sargasso Sea. *Geochim. Cosmochim. Acta* **59**, 535–547. Available at: https://linkinghub.elsevier.com/retrieve/pii/001670379400367U.
Jeandel C. and Derek V. (2018) New Tools, New Discoveries in Marine Geochemistry. *Elements* **14**, 379–384. Available at: https://pubs.geoscienceworld.org/msa/elements/article/14/6/379/567311/New-Tools-New-Discoveries-in-Marine-Geochemistry.
Jickells T. D. (2005) Global Iron Connections Between Desert Dust, Ocean Biogeochemistry, and Climate. *Science (80-.).* **308**, 67–71. Available at: http://www.sciencemag.org/cgi/doi/10.1126/science.1105959.
Johannesson K. H. and Burdige D. J. (2007) Balancing the global oceanic neodymium budget:

Evaluating the role of groundwater. *Earth Planet. Sci. Lett.* **253**, 129–142. Available at: https://linkinghub.elsevier.com/retrieve/pii/S0012821X06007436.

Jong Hyeon Lee and Byrne R. H. (1993) Complexation of trivalent rare earth elements (Ce, Eu, Gd, Tb, Yb) by carbonate ions. *Geochim. Cosmochim. Acta* **57**, 295–302. Available at: https://linkinghub.elsevier.com/retrieve/pii/001670379390432V.

Jouandet M. P., Blain S., Metzl N., Brunet C., Trull T. W. and Obernosterer I. (2008) A seasonal carbon budget for a naturally iron-fertilized bloom over the Kerguelen Plateau in the Southern Ocean. *Deep Sea Res. Part II Top. Stud. Oceanogr.* **55**, 856–867. Available at: http://www.sciencedirect.com/science/article/pii/S0967064508000209 [Accessed May 3, 2016].

Kadko D. (1980) A detailed study of unranium series nuclides at an abyssal hill near the East Pacific Rise at 8°45'N. *Earth Planet. Sci. Lett.* **51**, 115–131. Available at: file://localhost/Users/jescartin/WORK/Referencias/pdfs/Kadko1980.pdf.

Kadko D., Feely R. and Massoth G. (1994) Scavenging of ^{234}Th and phosphorus removal from the hydrothermal effluent plume over the North Cleft segment of the Juan de Fuca Ridge. *J. Geophys. Res. Solid Earth* **99**, 5017–5024. Available at: http://doi.wiley.com/10.1029/93JB02952.

Kirk Cochran J., Hirschberg D. J., Livingston H. D., Buesseler K. O. and Key R. M. (1995) Natural and anthropogenic radionuclide distributions in the Nansen Basin, Artic Ocean: Scavenging rates and circulation timescales. *Deep Sea Res. Part II Top. Stud. Oceanogr.* **42**, 1495–1517. Available at: https://linkinghub.elsevier.com/retrieve/pii/0967064595000518.

Klinkhammer G., Elderfield H. and Hudson A. (1983) Rare earth elements in seawater near hydrothermal vents. *Nature* **305**, 185–188. Available at: http://www.nature.com/articles/305185a0.

Koczy F. F., Picciotto E., Poulaert G. and Wilgain S. (1957) Mesure des isotopes du thorium dans l'eau de mer. *Geochim. Cosmochim. Acta* **11**, 103–129. Available at: http://www.sciencedirect.com/science/article/pii/001670375790008X.

Krishnaswami S. and Kirk Cochran J. (2008) Chapter 1 Introduction. In *Radioactivity in the Environment* pp. 1–10. Available at: https://linkinghub.elsevier.com/retrieve/pii/S1569486007000010.

Lacan F. and Jeandel C. (2005) Neodymium isotopes as a new tool for quantifying exchange fluxes at the continent–ocean interface. *Earth Planet. Sci. Lett.* **232**, 245–257. Available at: http://www.sciencedirect.com/science/article/pii/S0012821X05000233.

Lacan F. and Jeandel C. (2001) Tracing Papua New Guinea imprint on the central Equatorial Pacific Ocean using neodymium isotopic compositions and Rare Earth Element patterns. *Earth Planet. Sci. Lett.* **186**, 497–512. Available at: http://www.sciencedirect.com/science/article/pii/S0012821X01002631.

Lalande C., Lepore K., Cooper L. W., Grebmeier J. M. and Moran S. B. (2007) Export fluxes of particulate organic carbon in the Chukchi Sea: A comparative study using ^{234}Th/^{238}U disequilibria and drifting sediment traps. *Mar. Chem.* **103**, 185–196. Available at: https://linkinghub.elsevier.com/retrieve/pii/S0304420306001393.

Lalou C., Reyss J. and Brichet E. (1993) Actinide-series disequilibrium as a tool to establish the chronology of deep-sea hydrothermal activity. *Geochim. Cosmochim. Acta*. Available at: http://www.sciencedirect.com/science/article/pii/0016703793900596.

Lam P. J. and Anderson R. F. (2018) GEOTRACES: The Marine Biogeochemical Cycle of Trace Elements and Their Isotopes. *Elements* **14**, 377–378. Available at:

https://pubs.geoscienceworld.org/msa/elements/article/14/6/377/567309/GEOTRACES-The-Marine-Biogeochemical-Cycle-of-Trace.
Lampitt R. S., Boorman B., Brown L., Lucas M., Salter I., Sanders R., Saw K., Seeyave S., Thomalla S. J. and Turnewitsch R. (2008) Particle export from the euphotic zone: Estimates using a novel drifting sediment trap, ^{234}Th and new production. *Deep Sea Res. Part I Oceanogr. Res. Pap.* **55**, 1484–1502. Available at: https://linkinghub.elsevier.com/retrieve/pii/S0967063708001453.
Lopez G. I., Marcantonio F., Lyle M. and Lynch-Stieglitz J. (2015) Dissolved and particulate ^{230}Th–^{232}Th in the Central Equatorial Pacific Ocean: Evidence for far-field transport of the East Pacific Rise hydrothermal plume. *Earth Planet. Sci. Lett.* **431**, 87–95. Available at: https://linkinghub.elsevier.com/retrieve/pii/S0012821X15005865.
Lugmair G. W. (1974) Sm-Nd ages: a new dating method. *Meteoritics* **9**, 369.
Lund D. C., Pavia F. J., Seeley E. I., McCart S. E., Rafter P. A., Farley K. A., Asimow P. D. and Anderson R. F. (2019) Hydrothermal scavenging of ^{230}Th on the Southern East Pacific Rise during the last deglaciation. *Earth Planet. Sci. Lett.* **510**, 64–72. Available at: https://doi.org/10.1016/j.epsl.2018.12.037.
Lyle M., Mitchell N., Pisias N., Mix A., Martinez J. I. and Paytan A. (2005) Do geochemical estimates of sediment focusing pass the sediment test in the equatorial Pacific? *Paleoceanography* **20**, n/a-n/a. Available at: http://doi.wiley.com/10.1029/2004PA001019 [Accessed July 27, 2016].
Mahoney J. J., Macdougall J. D., Lugmair G. W. and Gopalan K. (1983) Kerguelen hotspot source for Rajmahal Traps and Ninetyeast Ridge? *Nature* **303**, 385–389. Available at: http://www.nature.com/articles/303385a0.
Mahowald N., Engelstaedter S. and Luo C. (2009) Atmospheric Iron Deposition: Global Distribution, Variability, and Human Perturbations*. *Annu. Rev.* Available at: http://www.annualreviews.org/doi/abs/10.1146/annurev.marine.010908.163727.
Marchal O., François R., Stocker T. F. and Joos F. (2000) Ocean thermohaline circulation and sedimentary ^{231}Pa/2^{30}Th ratio. *Paleoceanography* **15**, 625–641. Available at: http://onlinelibrary.wiley.com/doi/10.1029/2000PA000496/pdf [Accessed November 3, 2015].
Martin J. H. (1990) Glacial-interglacial CO 2 change: The Iron Hypothesis. *Paleoceanography* **5**, 1–13. Available at: http://doi.wiley.com/10.1029/PA005i001p00001.
Matsumoto E. (1975) 234Th□238U radioactive disequilibrium in the surface layer of the ocean. *Geochim. Cosmochim. Acta* **39**, 205–212. Available at: https://linkinghub.elsevier.com/retrieve/pii/0016703775901726.
McCartney M. S. and Donohue K. A. (2007) A deep cyclonic gyre in the Australian–Antarctic Basin. *Prog. Oceanogr.* **75**, 675–750. Available at: https://linkinghub.elsevier.com/retrieve/pii/S007966110700122X.
McCave I. N. (1986) Local and global aspects of the bottom nepheloid layers in the world ocean. *Netherlands J. Sea Res.* **20**, 167–181. Available at: https://linkinghub.elsevier.com/retrieve/pii/0077757986900402.
McManus J. F., Anderson R. F., Broecker W. S., Fleisher M. Q. and Higgins S. M. (1998) Radiometrically determined sedimentary fluxes in the sub-polar North Atlantic during the last 140,000 years. *Earth Planet. Sci. Lett.* **155**, 29–43. Available at: https://linkinghub.elsevier.com/retrieve/pii/S0012821X9700201X.
Measures C., Brown M. and Vink S. (2005) Dust deposition to the surface waters of the western and central North Pacific inferred from surface water dissolved aluminum

concentrations. *Geochemistry, Geophys.* Available at: http://onlinelibrary.wiley.com/doi/10.1029/2005GC000922/full.

Measures C. and Vink S. (2000) On the use of dissolved aluminum in surface waters to estimate dust deposition to the ocean. *Global Biogeochem. Cycles*. Available at: http://onlinelibrary.wiley.com/doi/10.1029/1999GB001188/full.

van der Merwe P., Wuttig K., Holmes T., Trull T. W., Chase Z., Townsend A. T., Goemann K. and Bowie A. R. (2019) High Lability Fe Particles Sourced From Glacial Erosion Can Meet Previously Unaccounted Biological Demand: Heard Island, Southern Ocean. *Front. Mar. Sci.* **6**, 1–20. Available at: https://www.frontiersin.org/article/10.3389/fmars.2019.00332/full.

Minami E. (1935a) *Gehalte an seltenen Erden in europäischen und japanischen Tonschiefern, von E. Minami...*, Weidmann.

Minami E. (1935b) *Selen-Gehalte von europäischen und japanischen Tonschiefern, von... E. Minami*., Weidmann.

Molina-Kescher M., Frank M. and Hathorne E. (2014) South Pacific dissolved Nd isotope compositions and rare earth element distributions: Water mass mixing versus biogeochemical cycling. *Geochim. Cosmochim. Acta* **127**, 171–189. Available at: http://dx.doi.org/10.1016/j.gca.2013.11.038.

Molina-Kescher M., Hathorne E. C., Osborne A. H., Behrens M. K., Kölling M., Pahnke K. and Frank M. (2018) The Influence of Basaltic Islands on the Oceanic REE Distribution: A Case Study From the Tropical South Pacific. *Front. Mar. Sci.* **5**. Available at: http://journal.frontiersin.org/article/10.3389/fmars.2018.00050/full.

Mongin M., Molina E. and Trull T. W. (2008) Seasonality and scale of the Kerguelen plateau phytoplankton bloom: A remote sensing and modeling analysis of the influence of natural iron fertilization in the Southern Ocean. *Deep Sea Res. Part II Top. Stud. Oceanogr.* **55**, 880–892. Available at: http://www.sciencedirect.com/science/article/pii/S0967064508000295 [Accessed May 3, 2016].

Moore J. K. and Abbott M. R. (2002) Surface chlorophyll concentrations in relation to the Antarctic Polar Front: seasonal and spatial patterns from satellite observations. *J. Mar. Syst.* **37**, 69–86. Available at: https://linkinghub.elsevier.com/retrieve/pii/S0924796302001963.

Moore J. K., Doney S. C., Glover D. M. and Fung I. Y. (2001) Iron cycling and nutrient-limitation patterns in surface waters of the World Ocean. *Deep Sea Res. Part II Top. Stud. Oceanogr.* **49**, 463–507. Available at: https://linkinghub.elsevier.com/retrieve/pii/S0967064501001096.

Moore W. S. and Sackett W. M. (1964) Uranium and thorium series inequilibrium in sea water. *J. Geophys. Res.* **69**, 5401–5405. Available at: http://www.agu.org/pubs/crossref/1964/JZ069i024p05401.shtml.

Moran S. B. and Buesseler K. O. (1992) Short residence time of colloids in the upper ocean estimated from 238U–234Th disequilibria. *Nature* **359**, 221–223. Available at: http://www.nature.com/articles/359221a0.

Moran S. B., Charette M. A., Hoff J. A., Edwards R. L. and Landing W. M. (1997) Distribution of ^{230}Th in the Labrador Sea and its relation to ventilation. *Earth Planet. Sci. Lett.* **150**, 151–160. Available at: https://linkinghub.elsevier.com/retrieve/pii/S0012821X97000812.

Moran S. B., Hoff J. A., Buesseler K. O. and Edwards R. L. (1995) High precision ^{230}Th and

^{232}Th in the Norwegian Sea and Denmark by thermal ionization mass spectrometry. *Geophys. Res. Lett.* **22**, 2589–2592. Available at: http://onlinelibrary.wiley.com/doi/10.1029/95GL02652/full [Accessed May 16, 2016].

Moran S. B., Shen C.-C., Weinstein S. E., Hettinger L. H., Hoff J. H., Edmonds H. N. and Edwards R. L. (2001) Constraints on deep water age and particle flux in the equatorial and South Atlantic Ocean based on seawater ^{231}Pa and ^{230}Th data. *Geophys. Res. Lett.* **28**, 3437–3440. Available at: http://doi.wiley.com/10.1029/2001GL013339.

Mosen A. W., Schmitt R. A. and Vasilevskis J. (1961) A procedure for the determination of the rare earth elements, lanthanum through lutetium, in chondritic, achondritic and iron meteorites by neutron-activation analysis. *Anal. Chim. Acta* **25**, 10–24. Available at: https://linkinghub.elsevier.com/retrieve/pii/S0003267001815117.

Ngwenya B. T., Magennis M., Olive V., Mosselmans J. F. W. and Ellam R. M. (2010) Discrete Site Surface Complexation Constants for Lanthanide Adsorption to Bacteria As Determined by Experiments and Linear Free Energy Relationships. *Environ. Sci. Technol.* **44**, 650–656. Available at: https://pubs.acs.org/doi/10.1021/es9014234.

Ngwenya B. T., Mosselmans J. F. W., Magennis M., Atkinson K. D., Tourney J., Olive V. and Ellam R. M. (2009) Macroscopic and spectroscopic analysis of lanthanide adsorption to bacterial cells. *Geochim. Cosmochim. Acta* **73**, 3134–3147. Available at: http://dx.doi.org/10.1016/j.gca.2009.03.018.

Nozaki Y. and Alibo D. S. (2003) Importance of vertical geochemical processes in controlling the oceanic profiles of dissolved rare earth elements in the northeastern Indian Ocean. *Earth Planet. Sci. Lett.* **205**, 155–172. Available at: https://linkinghub.elsevier.com/retrieve/pii/S0012821X02010270.

Nozaki Y. and Horibe Y. (1983) Alpha-emitting thorium isotopes in northwest Pacific deep waters. *Earth Planet. Sci. Lett.* **65**, 39–50. Available at: https://linkinghub.elsevier.com/retrieve/pii/0012821X83901887.

Nozaki Y., Horibe Y. and Tsubota H. (1981) The water column distributions of thorium isotopes in the western North Pacific. *Earth Planet. Sci. Lett.* **54**, 203–216. Available at: https://linkinghub.elsevier.com/retrieve/pii/0012821X81900042.

Nozaki Y. and Nakanishi T. (1985) ^{231}Pa and ^{230}Th profiles in the open ocean water column. *Deep Sea Res. Part A. Oceanogr. Res. Pap.* **32**, 1209–1220. Available at: http://www.sciencedirect.com/science/article/pii/0198014985900044.

Nozaki Y., Yang H.-S. and Yamada M. (1987) Scavenging of thorium in the ocean. *J. Geophys. Res.* **92**, 772. Available at: http://doi.wiley.com/10.1029/JC092iC01p00772.

Okubo A., Obata H., Gamo T. and Yamada M. (2012) ^{230}Th and ^{232}Th distributions in mid-latitudes of the North Pacific Ocean: Effect of bottom scavenging. *Earth Planet. Sci. Lett.* **339**–**340**, 139–150. Available at: http://dx.doi.org/10.1016/j.epsl.2012.05.012.

Olivarez A. M. and Owen R. M. (1991) The europium anomaly of seawater: implications for fluvial versus hydrothermal REE inputs to the oceans. *Chem. Geol.* **92**, 317–328. Available at: https://linkinghub.elsevier.com/retrieve/pii/0009254191900764.

Osborne A. H., Haley B. A., Hathorne E. C., Plancherel Y. and Frank M. (2015) Rare earth element distribution in Caribbean seawater: Continental inputs versus lateral transport of distinct REE compositions in subsurface water masses. *Mar. Chem.* **177**, 172–183. Available at: http://dx.doi.org/10.1016/j.marchem.2015.03.013.

Owens S. A., Buesseler K. O. and Sims K. W. W. (2011) Re-evaluating the ^{238}U-salinity relationship in seawater: Implications for the ^{238}U-^{234}Th disequilibrium method. *Mar. Chem.* **127**, 31–39. Available at: http://dx.doi.org/10.1016/j.marchem.2011.07.005.

Pahnke K., van de Flierdt T., Jones K. M., Lambelet M., Hemming S. R. and Goldstein S. L. (2012) GEOTRACES intercalibration of neodymium isotopes and rare earth element concentrations in seawater and suspended particles. Part 2: Systematic tests and baseline profiles. *Limnol. Oceanogr. Methods* **10**, 252–269. Available at: http://tube.m.aslo.net/lomethods/free/2012/0252.pdf [Accessed March 4, 2016].

Pahnke K., Goldstein S. L. and Hemming S. R. (2008) Abrupt changes in Antarctic Intermediate Water circulation over the past 25,000 years. *Nat. Geosci.* **1**, 870–874. Available at: http://www.nature.com/articles/ngeo360.

Palmer M. (1983) Rare earth elements and Nd and Sr isotopes in the Atlantic ocean.

Park Y.-H., Durand I., Kestenare E., Rougier G., Zhou M., D'Ovidio F., Cotté C. and Lee J.-H. (2014) Polar Front around the Kerguelen Islands: An up-to-date determination and associated circulation of surface/subsurface waters. *J. Geophys. Res. Ocean.* **119**, 6575–6592. Available at: http://doi.wiley.com/10.1002/2014JC010061.

Park Y.-H., Fuda J.-L., Durand I. and Naveira Garabato A. C. (2008a) Internal tides and vertical mixing over the Kerguelen Plateau. *Deep Sea Res. Part II Top. Stud. Oceanogr.* **55**, 582–593. Available at: http://www.sciencedirect.com/science/article/pii/S0967064508000118.

Park Y.-H. and Gamberoni L. (1997) Cross-frontal exchange of Antarctic Intermediate Water and Antarctic Bottom Water in the Crozet Basin. *Deep Sea Res. Part II Top. Stud. Oceanogr.* **44**, 963–986. Available at: https://linkinghub.elsevier.com/retrieve/pii/S0967064597000040.

Park Y.-H., Gambéroni L. and Charriaud E. (1991) Frontal structure and transport of the Antarctic Circumpolar Current in the south Indian Ocean sector, 40–80°E. *Mar. Chem.* **35**, 45–62. Available at: https://linkinghub.elsevier.com/retrieve/pii/S030442030990007X.

Park Y.-H., Roquet F., Durand I. and Fuda J.-L. (2008b) Large-scale circulation over and around the Northern Kerguelen Plateau. *Deep Sea Res. Part II Top. Stud. Oceanogr.* **55**, 566–581. Available at: http://www.sciencedirect.com/science/article/pii/S0967064508000106.

Park Y. and Vivier F. (2011) Circulation and hydrography over the Kerguelen Plateau. *Kerguelen Plateau Mar. Ecosyst. Fish.*, 43–55.

Pavia F. J., Anderson R. F., Black E. E., Kipp L. E., Vivancos S. M., Fleisher M. Q., Charette M. A., Sanial V., Moore W. S., Hult M., Lu Y., Cheng H., Zhang P. and Edwards R. L. (2019a) Timescales of hydrothermal scavenging in the South Pacific Ocean from ^{234}Th, ^{230}Th, and ^{228}Th. *Earth Planet. Sci. Lett.* **506**, 146–156. Available at: https://doi.org/10.1016/j.epsl.2018.10.038.

Pavia F. J., Anderson R. F., Lam P. J., Cael B. B., Vivancos S. M., Fleisher M. Q., Lu Y., Zhang P., Cheng H. and Edwards R. L. (2019b) Shallow particulate organic carbon regeneration in the South Pacific Ocean. *Proc. Natl. Acad. Sci.* **116**, 9753–9758. Available at: http://www.pnas.org/lookup/doi/10.1073/pnas.1901863116.

Pérez-Tribouillier H., Noble T. L., Townsend A. T., Bowie A. R. and Chase Z. (2019) Pre-concentration of thorium and neodymium isotopes using Nobias chelating resin: Method development and application to chromatographic separation. *Talanta* **202**, 600–609. Available at: https://doi.org/10.1016/j.talanta.2019.03.086.

Piepgras D. . and Wasserburg G. . (1987) Rare earth element transport in the western North Atlantic inferred from Nd isotopic observations. *Geochim. Cosmochim. Acta* **51**, 1257–1271. Available at: https://linkinghub.elsevier.com/retrieve/pii/0016703787902171.

Piepgras D. J. and Jacobsen S. B. (1992) The behavior of rare earth elements in seawater: Precise determination of variations in the North Pacific water column. *Geochim. Cosmochim. Acta* **56**, 1851–1862. Available at: https://linkinghub.elsevier.com/retrieve/pii/001670379290315A.

Piepgras D. J. and Jacobsen S. B. (1988) The isotopic composition of neodymium in the North Pacific. *Geochim. Cosmochim. Acta* **52**, 1373–1381. Available at: https://linkinghub.elsevier.com/retrieve/pii/0016703788902086 [Accessed July 28, 2016].

Piepgras D. J. and Wasserburg G. J. (1983) Influence of the Mediterranean Outflow on the isotopic composition of neodymium in waters of the North Atlantic. *J. Geophys. Res.* **88**, 5997. Available at: http://doi.wiley.com/10.1029/JC088iC10p05997.

Piepgras D. J. and Wasserburg G. J. (1982) Isotopic composition of neodymium in waters from the drake passage. *Science* **217**, 207–14. Available at: http://www.sciencemag.org/content/217/4556/207.short.

Piepgras D. J. and Wasserburg G. J. (1980) Neodymium isotopic variations in seawater. *Earth Planet. Sci. Lett.* **50**, 128–138. Available at: https://linkinghub.elsevier.com/retrieve/pii/0012821X80901247.

Piepgras D. J., Wasserburg G. J. and Dasch E. J. (1979) The isotopic composition of Nd in different ocean masses. *Earth Planet. Sci. Lett.* **45**, 223–236. Available at: https://linkinghub.elsevier.com/retrieve/pii/0012821X79901250.

Pin C. and Zalduegui J. S. (1997) Sequential separation of light rare-earth elements, thorium and uranium by miniaturized extraction chromatography: Application to isotopic analyses of silicate rocks. *Anal. Chim. Acta* **339**, 79–89. Available at: https://linkinghub.elsevier.com/retrieve/pii/S0003267096004990.

Planchon F., Ballas D., Cavagna A.-J., Bowie A. R., Davies D., Trull T., Laurenceau-Cornec E. C., Van Der Merwe P. and Dehairs F. (2015) Carbon export in the naturally iron-fertilized Kerguelen area of the Southern Ocean based on the ^{234}Th approach. *Biogeosciences* **12**, 3831–3848. Available at: https://www.biogeosciences.net/12/3831/2015/.

Pourmand A., Marcantonio F. and Schulz H. (2004) Variations in productivity and eolian fluxes in the northeastern Arabian Sea during the past 110 ka. *Earth Planet. Sci. Lett.* **221**, 39–54. Available at: https://linkinghub.elsevier.com/retrieve/pii/S0012821X04001098 [Accessed July 27, 2016].

Quigley M. S., Santschi P. H., Hung C.-C., Guo L. and Honeyman B. D. (2002) Importance of acid polysaccharides for ^{234}Th complexation to marine organic matter. *Limnol. Oceanogr.* **47**, 367–377. Available at: http://doi.wiley.com/10.4319/lo.2002.47.2.0367.

Rempfer J., Stocker T. F., Joos F., Lippold J. and Jaccard S. L. (2017) New insights into cycling of ^{231}Pa and ^{230}Th in the Atlantic Ocean. *Earth Planet. Sci. Lett.* **468**, 27–37. Available at: http://dx.doi.org/10.1016/j.epsl.2017.03.027.

Rickli J., Frank M. and Halliday A. N. (2009) The hafnium-neodymium isotopic composition of Atlantic seawater. *Earth Planet. Sci. Lett.* **280**, 118–127. Available at: http://dx.doi.org/10.1016/j.epsl.2009.01.026.

Robinson L. F., Belshaw N. S. and Henderson G. M. (2004) U and Th concentrations and isotope ratios in modern carbonates and waters from the Bahamas. *Geochim. Cosmochim. Acta* **68**, 1777–1789. Available at: https://linkinghub.elsevier.com/retrieve/pii/S0016703703007361.

Roshholt J. N., Doe B. R. and Tatsumoto M. (1966) Evolution of the isotopic composition of uranium and thorium in soil profiles. *Geol. Soc. Am. Bull.* **77**, 987–1004.

Rosholt J. N. and Tatsumoto M. (1970) Isotopic composition of uranium and thorium in Apollo 11 samples. *Geochim. Cosmochim. Acta Suppl.* **1**, 1499.

Roy-Barman M., Chen J. H., Wasserburg G. J. and Ocean E. (1996) ^{230}Th_^{232}Th systematics in the central Pacific The sources and the fates of thorium. *Earth Planet. Sci. Lett.* **139**, 351–363. Available at: http://ac.els-cdn.com/0012821X96000179/1-s2.0-0012821X96000179-main.pdf?_tid=d727d906-5006-11e7-9a21-00000aab0f6c&acdnat=1497337777_c0b320186973b7f8c1882f9dde0c8ac3.

Roy-Barman M., Lemaître C., Ayrault S., Jeandel C., Souhaut M. and Miquel J. C. (2009) The influence of particle composition on Thorium scavenging in the Mediterranean Sea. *Earth Planet. Sci. Lett.* **286**, 526–534. Available at: http://dx.doi.org/10.1016/j.epsl.2009.07.018.

Rudnick R. and Gao S. (2013) Composition of the Continental Crust. *Treatise Geochemistry Second Ed.* **4**, 1–51. Available at: http://dx.doi.org/10.1016/B978-0-08-095975-7.00301-6.

Rutgers van der Loeff M. M. and Berger G. W. (1993) Scavenging of ^{230}Th and ^{231}Pa near the antarctic polar front in the South Atlantic. *Deep Sea Res. Part I Oceanogr. Res. Pap.* **40**, 339–357. Available at: https://linkinghub.elsevier.com/retrieve/pii/096706379390007P.

Rutgers van der Loeff M. M. and Boudreau B. P. (1997) The effect of resuspension on chemical exchanges at the sediment-water interface in the deep sea — A modelling and natural radiotracer approach. *J. Mar. Syst.* **11**, 305–342. Available at: https://linkinghub.elsevier.com/retrieve/pii/S0924796396001285.

Rutgers Van Der Loeff M. M., Friedrich J. and Bathmann U. V (1997) Carbon export during the Spring Bloom at the Antarctic Polar Front, determined with the natural tracer ^{234}Th. *Deep Sea Res. Part II Top. Stud. Oceanogr.* **44**, 457–478. Available at: https://linkinghub.elsevier.com/retrieve/pii/S0967064596000677.

Rutgers van der Loeff M. M. and Geibert W. (2008) Chapter 7 U- and Th-Series Nuclides as Tracers of Particle Dynamics, Scavenging and Biogeochemical Cycles in the Oceans. *Radioact. Environ.* **13**, 227–268.

Rutgers van der Loeff M. M., Meyer R., Rudels B. and Rachor E. (2002) Resuspension and particle transport in the benthic nepheloid layer in and near Fram Strait in relation to faunal abundances and 234Th depletion. *Deep Sea Res. Part I Oceanogr. Res. Pap.* **49**, 1941–1958. Available at: https://linkinghub.elsevier.com/retrieve/pii/S0967063702001139.

Sackett W. M., Potratz H. A. and Goldberg E. D. (1958) Thorium Content of Ocean Water. *Science (80-.).* **128**, 204 LP – 205. Available at: http://science.sciencemag.org/content/128/3317/204.abstract.

Sanial V., van Beek P., Lansard B., Souhaut M., Kestenare E., D'Ovidio F., Zhou M. and Blain S. (2015) Use of Ra isotopes to deduce rapid transfer of sediment-derived inputs off Kerguelen. *Biogeosciences* **12**, 1415–1430. Available at: https://www.biogeosciences.net/12/1415/2015/.

Santschi P. H., Hung C.-C., Schultz G., Alvarado-Quiroz N., Guo L., Pinckney J. and Walsh I. (2003) Control of acid polysaccharide production and ^{234}Th and POC export fluxes by marine organisms. *Geophys. Res. Lett.* **30**, 2–5. Available at: http://doi.wiley.com/10.1029/2002GL016046.

Santschi P. H., Murray J. W., Baskaran M., Benitez-Nelson C. R., Guo L. D., Hung C.-C., Lamborg C., Moran S. B., Passow U. and Roy-Barman M. (2006) Thorium speciation in seawater. *Mar. Chem.* **100**, 250–268. Available at: https://linkinghub.elsevier.com/retrieve/pii/S0304420305002161.

Savoye N., Trull T. W., Jacquet S. H. M., Navez J. and Dehairs F. (2008) ^{234}Th-based export fluxes during a natural iron fertilization experiment in the Southern Ocean (KEOPS). *Deep Sea Res. Part II Top. Stud. Oceanogr.* **55**, 841–855. Available at: http://www.sciencedirect.com/science/article/pii/S0967064508000325.

Scher H. D. and Martin E. E. (2004) Circulation in the Southern Ocean during the Paleogene inferred from neodymium isotopes. *Earth Planet. Sci. Lett.* **228**, 391–405. Available at: https://linkinghub.elsevier.com/retrieve/pii/S0012821X04006193.

Schijf J., Christenson E. A. and Byrne R. H. (2015) YREE scavenging in seawater: A new look at an old model. *Mar. Chem.* **177**, 460–471. Available at: http://dx.doi.org/10.1016/j.marchem.2015.06.010.

Schlitzer R., Anderson R. F., Dodas E. M., Lohan M., Geibert W., Tagliabue A., Bowie A., Jeandel C., Maldonado M. T., Landing W. M., Cockwell D., Abadie C., Abouchami W., Achterberg E. P., Agather A., Aguliar-Islas A., van Aken H. M., Andersen M., Archer C., Auro M., de Baar H. J., Baars O., Baker A. R., Bakker K., Basak C., Baskaran M., Bates N. R., Bauch D., van Beek P., Behrens M. K., Black E., Bluhm K., Bopp L., Bouman H., Bowman K., Bown J., Boyd P., Boye M., Boyle E. A., Branellec P., Bridgestock L., Brissebrat G., Browning T., Bruland K. W., Brumsack H. J., Brzezinski M., Buck C. S., Buck K. N., Buesseler K., Bull A., Butler E., Cai P., Mor P. C., Cardinal D., Carlson C., Carrasco G., Casacuberta N., Casciotti K. L., Castrillejo M., Chamizo E., Chance R., Charette M. A., Chaves J. E., Cheng H., Chever F., Christl M., Church T. M., Closset I., Colman A., Conway T. M., Cossa D., Croot P., Cullen J. T., Cutter G. A., Daniels C., Dehairs F., Deng F., Dieu H. T., Duggan B., Dulaquais G., Dumousseaud C., Echegoyen-Sanz Y., Edwards R. L., Ellwood M., Fahrbach E., Fitzsimmons J. N., Russell Flegal A., Fleisher M. Q., van de Flierdt T., Frank M., Friedrich J., Fripiat F., Fröllje H., Galer S. J. G., Gamo T., Ganeshram R. S., Garcia-Orellana J., Garcia-Solsona E., Gault-Ringold M., George E., Gerringa L. J. A., Gilbert M., Godoy J. M., Goldstein S. L., Gonzalez S. R., Grissom K., Hammerschmidt C., Hartman A., Hassler C. S., Hathorne E. C., Hatta M., Hawco N., Hayes C. T., Heimbürger L. E., Helgoe J., Heller M., Henderson G. M., Henderson P. B., van Heuven S., Ho P., Horner T. J., Hsieh Y. Te, Huang K. F., Humphreys M. P., Isshiki K., Jacquot J. E., Janssen D. J., Jenkins W. J., John S., Jones E. M., Jones J. L., Kadko D. C., Kayser R., Kenna T. C., Khondoker R., Kim T., Kipp L., Klar J. K., Klunder M., Kretschmer S., Kumamoto Y., Laan P., Labatut M., Lacan F., Lam P. J., Lambelet M., Lamborg C. H., Le Moigne F. A. C., Le Roy E., Lechtenfeld O. J., Lee J. M., Lherminier P., Little S., López-Lora M., Lu Y., Masque P., Mawji E., Mcclain C. R., Measures C., Mehic S., Barraqueta J. L. M., van der Merwe P., Middag R., Mieruch S., Milne A., Minami T., Moffett J. W., Moncoiffe G., Moore W. S., Morris P. J., Morton P. L., Nakaguchi Y., Nakayama N., Niedermiller J., Nishioka J., Nishiuchi A., Noble A., Obata H., Ober S., Ohnemus D. C., van Ooijen J., O'Sullivan J., Owens S., Pahnke K., Paul M., Pavia F., Pena L. D., Peters B., Planchon F., Planquette H., Pradoux C., Puigcorbé V., Quay P., Queroue F., Radic A., Rauschenberg S., Rehkämper M., Rember R., Remenyi T., Resing J. A., Rickli J., Rigaud S., Rijkenberg M. J. A., Rintoul S., Robinson L. F., Roca-Martí M., Rodellas V., Roeske T., Rolison J. M., Rosenberg M., Roshan S., Rutgers van der Loeff M. M., Ryabenko E., Saito M. A., Salt L. A., Sanial V., Sarthou G., Schallenberg C., Schauer U., Scher H., Schlosser

C., Schnetger B., Scott P., Sedwick P. N., Semiletov I., Shelley R., Sherrell R. M., Shiller A. M., Sigman D. M., Singh S. K., Slagter H. A., Slater E., Smethie W. M., Snaith H., Sohrin Y., Sohst B., Sonke J. E., Speich S., Steinfeldt R., Stewart G., Stichel T., Stirling C. H., Stutsman J., Swarr G. J., Swift J. H., Thomas A., Thorne K., Till C. P., Till R., Townsend A. T., Townsend E., Tuerena R., Twining B. S., Vance D., Velazquez S., Venchiarutti C., Villa-Alfageme M., Vivancos S. M., Voelker A. H. L., Wake B., Warner M. J., Watson R., van Weerlee E., Alexandra Weigand M., Weinstein Y., Weiss D., Wisotzki A., Woodward E. M. S., Wu J., Wu Y., Wuttig K., Wyatt N., Xiang Y., Xie R. C., Xue Z., Yoshikawa H., Zhang J., Zhang P., Zhao Y., Zheng L., Zheng X. Y., Zieringer M., Zimmer L. A., Ziveri P., Zunino P. and Zurbrick C. (2018) The GEOTRACES Intermediate Data Product 2017. *Chem. Geol.* **493**, 210–223. Available at: https://doi.org/10.1016/j.chemgeo.2018.05.040.

Schmidt S. (2006) Impact of the Mediterranean Outflow Water on particle dynamics in intermediate waters of the Northeast Atlantic, as revealed by ^{234}Th and ^{228}Th. *Mar. Chem.* **100**, 289–298. Available at: https://linkinghub.elsevier.com/retrieve/pii/S0304420305002197.

Schnetzler C. C., Thomas H. H. and Philpotts J. A. (1967) Determination of rare earth elements in rocks and minerals by mass spectrometric, stable isotope dilution technique. *Anal. Chem.* **39**, 1888–1890. Available at: https://pubs.acs.org/doi/abs/10.1021/ac50157a073.

Scholten J. C., Fietzke J., Vogler S., Rutgers van der Loeff M. M., Mangini A., Koeve W., Waniek J., Stoffers P., Antia A. and Kuss J. (2001) Trapping efficiencies of sediment traps from the deep Eastern North Atlantic: *Deep Sea Res. Part II Top. Stud. Oceanogr.* **48**, 2383–2408. Available at: https://linkinghub.elsevier.com/retrieve/pii/S0967064500001764.

Scholten J. C., Rutgers van der Loeff M. M. and Michel A. (1995) Distribution of ^{230}Th and ^{231}Pa in the water column in relation to the ventilation of the deep Arctic basins. *Deep Sea Res. Part II Top. Stud. Oceanogr.* **42**, 1519–1531. Available at: https://linkinghub.elsevier.com/retrieve/pii/0967064595000526.

Shen C.-C., Lawrence Edwards R., Cheng H., Dorale J. A., Thomas R. B., Bradley Moran S., Weinstein S. E. and Edmonds H. N. (2002) Uranium and thorium isotopic and concentration measurements by magnetic sector inductively coupled plasma mass spectrometry. *Chem. Geol.* **185**, 165–178. Available at: http://www.sciencedirect.com/science/article/pii/S0009254101004041.

Shimmield G. B. and Price N. B. (1988) The scavenging of U, ^{230}Th and ^{231}Pa during pulsed hydrothermal activity at 20°S, East Pacific Rise. *Geochim. Cosmochim. Acta* **52**, 669–677. Available at: http://linkinghub.elsevier.com/retrieve/pii/0016703788903298 [Accessed July 26, 2016].

Siddall M., Khatiwala S., van de Flierdt T., Jones K., Goldstein S. L., Hemming S. and Anderson R. F. (2008) Towards explaining the Nd paradox using reversible scavenging in an ocean general circulation model. *Earth Planet. Sci. Lett.* **274**, 448–461. Available at: https://linkinghub.elsevier.com/retrieve/pii/S0012821X08004998.

Singh S. P., Singh S. K., Goswami V., Bhushan R. and Rai V. K. (2012) Spatial distribution of dissolved neodymium and ε Nd in the Bay of Bengal: Role of particulate matter and mixing of water masses. *Geochim. Cosmochim. Acta* **94**, 38–56. Available at: http://dx.doi.org/10.1016/j.gca.2012.07.017.

Spivack A. J. and Wasserburg G. . (1988) Neodymium isotopic composition of the Mediterranean outflow and the eastern North Atlantic. *Geochim. Cosmochim. Acta* **52**,

2767–2773. Available at: https://linkinghub.elsevier.com/retrieve/pii/0016703788901445 [Accessed July 28, 2016].

Starik I., F.K. L., Nikolayev D.S. Kolyadin L.B. Grashchenko L. and Kuznetzov Y.V. (1959) Concentration of thorium isotopes in the waters of the Black Sea. *Dokl. Akad. Nauk SSSR* **129**, 1041-1044 (AGU transl.).

Stichel T., Hartman A. E., Duggan B., Goldstein S. L., Scher H. and Pahnke K. (2015) Separating biogeochemical cycling of neodymium from water mass mixing in the Eastern North Atlantic. *Earth Planet. Sci. Lett.* **412**, 245–260. Available at: http://www.sciencedirect.com/science/article/pii/S0012821X14007614%5Cnhttp://dx.doi.org/10.1016/j.epsl.2014.12.008.

Suman D. O. and Bacon M. P. (1989) Variations in Holocene sedimentation in the North American Basin determined from 230Th measurements. *Deep Sea Res. Part A. Oceanogr. Res. Pap.* **36**, 869–878. Available at: https://linkinghub.elsevier.com/retrieve/pii/0198014989900332.

Szabo B. J. and Rosholt J. N. (1969) Uranium-series dating of Pleistocene molluscan shells from southern California-An open system model. *J. Geophys. Res.* **74**, 3253–3260. Available at: http://doi.wiley.com/10.1029/JB074i012p03253.

Tachikawa K. (2003) Neodymium budget in the modern ocean and paleo-oceanographic implications. *J. Geophys. Res.* **108**, 3254. Available at: http://doi.wiley.com/10.1029/1999JC000285 [Accessed August 6, 2015].

Takahashi Y., Châtellier X., Hattori K. H., Kato K. and Fortin D. (2005) Adsorption of rare earth elements onto bacterial cell walls and its implication for REE sorption onto natural microbial mats. *Chem. Geol.* **219**, 53–67. Available at: https://linkinghub.elsevier.com/retrieve/pii/S0009254105000926.

Takahashi Y., Hirata T., Shimizu H., Ozaki T. and Fortin D. (2007) A rare earth element signature of bacteria in natural waters? *Chem. Geol.* **244**, 569–583. Available at: https://linkinghub.elsevier.com/retrieve/pii/S0009254107003269.

Takahashi Y., Yamamoto M., Yamamoto Y. and Tanaka K. (2010) EXAFS study on the cause of enrichment of heavy REEs on bacterial cell surfaces. *Geochim. Cosmochim. Acta* **74**, 5443–5462. Available at: http://dx.doi.org/10.1016/j.gca.2010.07.001.

Thomalla S., Turnewitsch R., Lucas M. and Poulton A. (2006) Particulate organic carbon export from the North and South Atlantic gyres: The ^{234}Th/^{238}U disequilibrium approach. *Deep Sea Res. Part II Top. Stud. Oceanogr.* **53**, 1629–1648. Available at: https://linkinghub.elsevier.com/retrieve/pii/S0967064506001287.

Thomas A., Henderson G. and Robinson L. (2006) Interpretation of the ^{231}Pa/^{230}Th paleocirculation proxy: New water-column measurements from the southwest Indian Ocean. *Earth Planet. Sci. ….* Available at: http://www.sciencedirect.com/science/article/pii/S0012821X05008101.

Thomson J., Nixon S., Summerhayes C. P., Schönfeld J., Zahn R. and Grootes P. (1999) Implications for sedimentation changes on the Iberian margin over the last two glacial/interglacial transitions from (^{230}Thexcess) systematics. *Earth Planet. Sci. Lett.* **165**, 255–270. Available at: https://linkinghub.elsevier.com/retrieve/pii/S0012821X98002659.

Trull T. W., Davies D. and Casciotti K. (2008) Insights into nutrient assimilation and export in naturally iron-fertilized waters of the Southern Ocean from nitrogen, carbon and oxygen isotopes. *Deep Sea Res. Part II Top. Stud. Oceanogr.* **55**, 820–840. Available at:

http://www.sciencedirect.com/science/article/pii/S0967064508000271.
Tsunogai S., Taguchi K. and Harada K. (1986) Seasonal variation in the difference between observed and calculated particulate fluxes of Th-234 in Funka Bay, Japan. *J. Oceanogr. Soc. Japan* **42**, 91–98. Available at: http://link.springer.com/10.1007/BF02109095.
Turnewitsch R., Reyss J.-L., Nycander J., Waniek J. J. and Lampitt R. S. (2008) Internal tides and sediment dynamics in the deep sea—Evidence from radioactive $^{234}Th/^{238}U$ disequilibria. *Deep Sea Res. Part I Oceanogr. Res. Pap.* **55**, 1727–1747. Available at: https://linkinghub.elsevier.com/retrieve/pii/S096706370800160X.
Turnewitsch R. and Springer B. M. (2001) Do bottom mixed layers influence ^{234}Th dynamics in the abyssal near-bottom water column? *Deep Sea Res. Part I Oceanogr. Res. Pap.* **48**, 1279–1307. Available at: https://linkinghub.elsevier.com/retrieve/pii/S0967063700001047.
Venchiarutti C., Jeandel C. and Roy-Barman M. (2008) Particle dynamics study in the wake of Kerguelen Island using thorium isotopes. *Deep Sea Res. Part I Oceanogr. Res. Pap.* **55**, 1343–1363. Available at: http://www.sciencedirect.com/science/article/pii/S0967063708001180.
Venchiarutti C., van der Loeff M. R. and Stimac I. (2011) Scavenging of ^{231}Pa and thorium isotopes based on dissolved and size-fractionated particulate distributions at Drake Passage (ANTXXIV-3). *Deep. Res. Part II Top. Stud. Oceanogr.* **58**, 2767–2784. Available at: http://dx.doi.org/10.1016/j.dsr2.2010.10.040.
Vogler S., Scholten J., Rutgers van der Loeff, M. and Mangini, A. (1998) ^{230}Th in the eastern North Atlantic: the importance of water mass ventilation in the balance of ^{230}Th. *Earth Planet. Sci. Lett.* **156**, 61–74. Available at: https://linkinghub.elsevier.com/retrieve/pii/S0012821X98000119.
Weis D., White W. M., Frey F. A., Duncan R. A., Fisk M. R., Dehn J., Ludden J., Saunders A. and Storey M. (1992) The Influence of Mantle Plumes in Generation of Indian Oceanic Crust. In *Synthesis of Results from Scientific Drilling in the Indian Ocean* Geophysical Monograph Series. pp. 57–89. Available at: https://doi.org/10.1029/GM070p0057.
Yu E.-F., Francois R., Bacon M. ., Honjo S., Fleer A. ., Manganini S. ., Rutgers van der Loeff M. . and Ittekot V. (2001) Trapping efficiency of bottom-tethered sediment traps estimated from the intercepted fluxes of and. *Deep Sea Res. Part I Oceanogr. Res. Pap.* **48**, 865–889. Available at: https://linkinghub.elsevier.com/retrieve/pii/S0967063700000674.
Zhang Y., Lacan F. and Jeandel C. (2008) Dissolved rare earth elements tracing lithogenic inputs over the Kerguelen Plateau (Southern Ocean). *Deep Sea Res. Part II Top. Stud. Oceanogr.* **55**, 638–652. Available at: http://www.sciencedirect.com/science/article/pii/S0967064508000167.
Zheng X. Y., Plancherel Y., Saito M. A., Scott P. M. and Henderson G. M. (2016) Rare earth elements (REEs) in the tropical South Atlantic and quantitative deconvolution of their non-conservative behavior. *Geochim. Cosmochim. Acta* **177**, 217–237. Available at: http://dx.doi.org/10.1016/j.gca.2016.01.018.

Chapter 2 - Pre-concentration of thorium and neodymium isotopes using Nobias chelating resin: Method development and application to chromatographic separation.

This chapter was published as an article under the same title in the journal Talanta, by Elsevier, DOI: 10.1016/j.talanta.2019.03.086

1. Introduction

The isotopes of thorium (Th) and neodymium (Nd) are used to study a wide range of oceanic processes including vertical particle flux, circulation, productivity and many others (Nozaki et al., 1981; Anderson et al., 1983; Jeandel et al., 1998; Francois et al., 2004; Lacan and Jeandel, 2005; Arsouze et al., 2007; Hsieh et al., 2011). All Th isotopes have a stable oxidation state of IV (Santschi et al., 2006). Once in the dissolved fraction of seawater, Th will hydrolyse, adsorb onto settling particles and finally be incorporated into the sedimentary record (Moore and Sackett, 1964). Thorium isotopes provide information about biogeochemical cycles in the ocean because of their well constrained sources and particle reactivity (Krishnaswami and Cochran, 2011). ^{232}Th ($t_{1/2}$=1.4×10^{10} years) is a primordial isotope that is introduced to the ocean entirely by the dissolution of continental material (Brewer et al., 1980; Hayes et al., 2013). ^{230}Th ($t_{1/2}$=75,400 years) and ^{234}Th ($t_{1/2}$=24.1 days) are less abundant isotopes and are produced by the radioactive decay of ^{234}U and ^{238}U, respectively (Santschi et al., 2006). More recently, ^{232}Th and ^{230}Th have been used to track and quantify lithogenic fluxes of trace elements to the marine environment (Hsieh et al., 2011; Hayes et al., 2013; Hayes et al., 2017). In the case of Nd, three out of four of its most abundant isotopes originate from the decay of samarium (Sm) isotopes, with both parent and daughter elements existing in the III oxidation state. The long-lived ^{147}Sm ($t_{1/2}$=1.06 x 10^{11} years) and ^{148}Sm ($t_{1/2}$=7 x 10^{15} years) isotopes decay to the stable ^{143}Nd and to the long-lived ^{144}Nd ($t_{1/2}$=2.29 x 10^{15} years) respectively. Chemical fractionation during magma melting and the formation of continental crust produces a range of ^{147}Sm/^{144}Nd compositions, and hence different ^{143}Nd/^{144}Nd ratios in rocks and minerals as a function of age and

the Sm/Nd ratio (Goldstein and Hemming, 2003). The $^{143}Nd/^{144}Nd$ ratio in geological material is normally reported relative to the deviation from the Chondritic Uniform Reservoir (CHUR) and expressed in parts per ten thousand in what is known as epsilon notation (ε_{Nd}) (Jacobsen and Wasserburg, 1980). The ε_{Nd} of seawater has been recognised as a tracer of thermohaline circulation based on its distribution relative to oceanic temperature and salinity (Frank, 2002; Tachikawa et al., 2017). The unique ε_{Nd} signature imprinted on a water mass at the ocean margins traces the water mass source and mixing along the path of global ocean circulation (Piepgras et al., 1979; Piepgras and Wasserburg, 1980; Lacan et al., 2012). Nd isotopes are a quasi-conservative tracer of global oceanic circulation, however a complete understanding of the Nd biogeochemical cycle is still under development (Tachikawa, 2003; Lacan and Jeandel, 2005; Arsouze et al., 2009; Jeandel and Oelkers, 2015; Rousseau et al., 2015; van de Flierdt et al., 2016; Haley et al., 2017).

Both Th and Nd are nominated as key parameters in the GEOTRACES program (Anderson et al., 2014; Schlitzer et al., 2018), an international study of the biogeochemical cycles of trace elements and their isotopes in the oceans. Both Th and Nd isotopes have been the subject of intercalibration exercises to validate analyses from different laboratories (Anderson et al., 2012; van de Flierdt et al., 2012; Pahnke et al., 2012).Traditionally, Th and Nd isotopic systems in seawater have been studied separately. In recent years however, following the objective of the GEOTRACES programme, there has been a shift towards a multi-tracer approach (Jeandel and Derek, 2018; Hayes et al., 2018).

The first techniques to measure Th isotopes in seawater were developed during the second half of the 1950s and early 1960s (Koczy et al., 1957; Sackett et al., 1958; Moore and Sackett, 1964). Large volume samples (30–250 L) were typically pre-concentrated by co-precipitation by Fe-hydroxides (using a carrier solution containing $FeCl_3$) or by the in-situ extraction to MnO_2-impregnated absorbers. After chromatographic separation, Th content was measured by decay-

counting spectrometry. The development of mass spectrometry in the late 1970s allowed a reduction in sample size required for Th determinations by two orders of magnitude (Chen et al., 1986) and also enabled the first measurements of the Nd isotopic composition in seawater (Piepgras et al., 1979). Nowadays, Th and Nd isotopic measurements are performed by Thermal Ionization Mass Spectrometry (TIMS) (Jeandel, 1993; Robinson et al., 2004; Andersson and Schöberg, 2012) or Multi Collector Inductively Coupled Plasma Mass Spectrometry (MC-ICP-MS) (Thomas et al., 2006; van de Flierdt et al., 2012; Andersson and Schöberg, 2012). In addition to the previously mentioned techniques, single collector Sector Field ICP-MS (SF-ICP-MS) can also be used for Th determinations in some applications (Choi et al., 2001). The development of isotope dilution (ID) coupled with Mass Spectrometry (MS) has also contributed to the precise determination of Th and Nd isotopic abundances in geologic materials (Dietz et al., 1962). The ID method is referred to as an isotope internal standardization technique because an isotopic analogue (spike) is added at the beginning of the analytical procedure, reaching equilibrium with the analyte without losses or isotopic fractionation. This technique enables exact compensation to be made for any analyte loss at all stages of sample pre-treatment or analysis, as the concentration can be determined using the isotopic ratio between the spike and the analyte (Sargent et al., 2002). Despite all the above-mentioned improvements in inorganic MS and the continuous development of new instruments with more powerful detectors and software, as well as the implementation of modern sample introduction systems that help minimize spectral interferences, the pre-concentration and subsequent chromatographic separation of Th and Nd isotopes are unavoidable. These procedures have remained relatively unchanged over the last 60 years. Currently, most laboratories pre-concentrate 1-10 L samples using co-precipitation with Fe oxides, followed by purification using ion exchange chromatography (Anderson et al., 2012; Behrens et al., 2016). The simultaneous pre-concentration of both elements has been proposed (Jeandel and Venchiarutti, 2011; Andersson and Schöberg,

2012; Struve et al., 2016), however these methods still rely on co-precipitation for the initial pre-concentration step. This approach is time consuming, taking up to a week in some cases, with additional work required to purify the Fe carrier solution and to digest organic matter and amorphous silicon carried by the iron hydroxide (Anderson et al., 2012; Andersson and Schöberg, 2012; Auro et al., 2012).

In the last decade pre-concentration of trace elements with chelating resins has grown in popularity. C18 cartridges filled with a mixture of di(2-ethyl)hydrogen-phosphate and 2-ethylhexyldihydrogen-phosphate (HDEHP/H_2MEHP) have been used for Nd isotope analysis (Shabani et al., 1992; Jeandel et al., 1998). The Nobias® PA1L chelating resin (Hitachi Technologies, Japan) has also been employed for the pre-concentration of trace metals in seawater (Sohrin et al., 2008; Biller and Bruland, 2012; Middag et al., 2015), including the pre-concentration of ^{232}Th (Takata et al., 2011) and Rare Earth Elements (REE) (Persson et al., 2011; Hatje et al., 2014). However, the pre-concentration of ^{230}Th with this resin has not been reported.

In this study we investigate the use of the Nobias PA1L resin to simultaneously pre-concentrate dissolved Th and Nd isotopes from seawater. In particular, we investigate the optimal pH to simultaneously pre-concentrate both elements from a single seawater sample, and the coupling of this pre-concentration method with existing chromatographic techniques. We report the procedures followed to minimize blank contributions, together with a meticulous assessment of the accuracy and precision of the method to measure Th isotopes, and to a lesser extent Nd isotope. Finally, the validated method is applied to seawater samples collected from the Kerguelen Plateau (KP), located in the Indian-Ocean sector of the Southern Ocean.

2. Materials and methods

2.1 Materials and Reagents

All materials including sampling bottles, Teflon vessels, and filter capsules were cleaned following GEOTRACES protocols (Cutter et al., 2010). Ultra-high purity water (UPW, 18.2 MΩ cm^{-1}) was used to clean laboratory vessels and for reagent preparation. Concentrated CH_3COOH, HCl and HNO_3 were produced by distillation of analytical grade acids (Seastar Chemicals, Canada) in a DST-1000 purification system (Savillex, USA). HF, $HClO_4$ and NH_3 were Baseline® (Seastar Chemicals, Canada) ultra-high purity grade and used as received. A "stock" buffer solution of 2.5 M ammonium acetate was prepared by mixing 317 g of UPW, 74 g of 17 M CH_3COOH and 104 g of 11 M NH_3 solution. Elemental pre-concentration was performed using Nobias® PA1L (Hitachi Technologies, Japan) pre-packed cartridges containing 300 mg of resin. This resin consists of both ethylenediaminetriacetic and iminodiacetic acids immobilized into a hydrophilic methacrylate polymer (Sohrin et al., 2008). For the Th-separation (Figure 1) the anion exchange AG® 1-X8 (Bio-Rad, USA) resin was used, it is composed of strongly basic anion exchangers with quaternary ammonium functional groups attached to a styrene divinylbenzene copolymer lattice (100-200 mesh size). For the REE-purification (Figure 1) the AG® 50W-X8 (Bio-Rad, USA) resin was employed. This cation exchange resin contains sulfonic acid functional groups attached to a styrene divinylbenzene copolymer lattice (20-50 mesh size). For the Nd-separation (Figure 1) the extraction chromatography LN® (Eichrom Technologies, USA) resin was used, it is made of de(2-ethylexyl) orthophosphoric acid (HDEHP) on an inert polymeric support (particle size 50-100 μm).

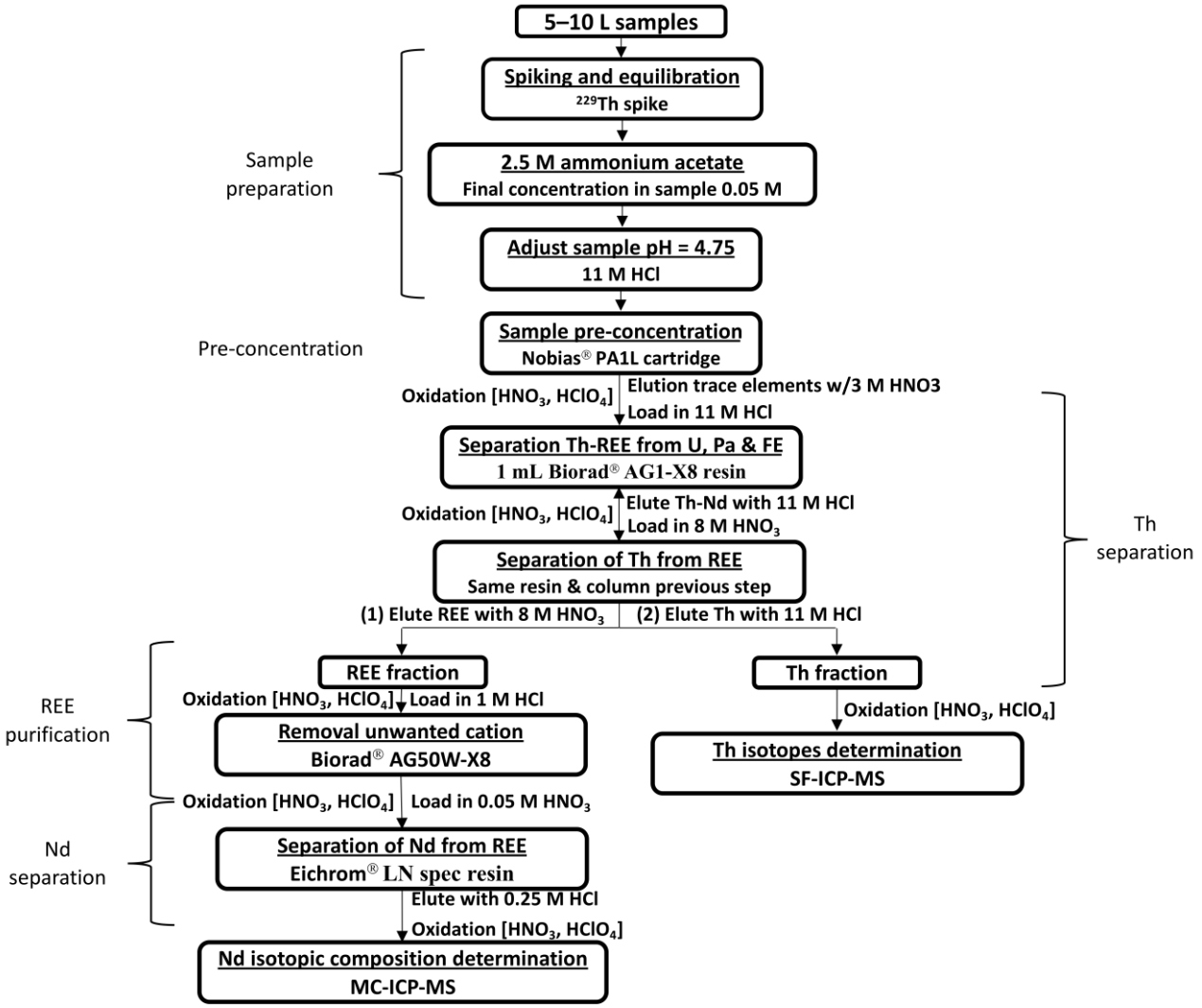

Figure 2-1. Optimised procedure for the determination of Th and Nd isotopes from a single seawater sample.

Enriched radioisotope standard solutions of ^{229}Th (NIST4328C, National Institute of Standards and Technology, USA) and ^{236}U (IRMM-3660a, Institute for Reference Materials and Measurements, European Union) were used for isotopic dilution analysis and elemental yield control. After the dilution of the original supplied ampules and determination by reverse isotopic dilution (RID) (Sargent et al., 2002) the resulting concentrations for ^{229}Th and ^{236}U were found to be 47.79±0.01 pg g^{-1} and 59.2±0.3 ng g^{-1}, respectively. A ^{150}Nd spike solution was obtained from the Australian National

University, a subsample sourced from the Charles Arm Laboratory (Wasserburg et al., 1981) (The California Institute of Technology, USA). The concentration of this solution was determined by RID to be 410 ng g^{-1}. This "stock" solution was further diluted to obtain a concentration of 100 ng g^{-1}, and was used to spike seawater samples.

Method accuracy was assessed using an intercalibrated reference seawater. This seawater sample (KN-193-6-Th-616) was collected at the Bermuda Atlantic Time series station in July 2008, at a depth of 2000 m, as part of the GEOTRACES intercalibration exercise focussing on Th, Pa and Be (Anderson et al., 2012) (herein referred to as BATS2000). This sample was divided in two sub-samples of 9 (BATS2000A) and 4.5 (BATS2000B) litres.

Long-term accuracy and precision were assessed using isotopic reference solutions. For Th isotopes repeated measurements of SW2010-1 and SW2010-2 solutions produced at the Lamont-Doherty Earth Observatory (LDEO) for the intercalibration of Th isotopes (Anderson et al., 2012) were carried out. There are no consensus values for the SW2010-1 and SW2010-2 solutions because the intercalibration is an ongoing process. Based on data generated by LDEO and the University of Minnesota, subsequent to the GEOTRACES intercalibration on Th (Anderson et al., 2012), and provided by R.F. Anderson we estimate an expected concentration of 983$\pm$15 pg g^{-1} (^{232}Th) and 247$\pm$4 fg kg^{-1} (^{230}Th) in the SW2010-1 solution. For the SW2010-2 solution, graphically extracted values from the images presented in the intercalibration (Anderson et al., 2012) indicate values of 53$\pm$2 (^{232}Th/^{229}Th), 0.01346$\pm$0.0005 (^{230}Th/^{229}Th) and 3973$\pm$184 (^{232}Th/^{230}Th). The JNdi-1 isotopic reference material (Tanaka et al., 2000) is a neodymium oxide (Nd_2O_3) sample, that was obtained upon request from the Geological Survey of Japan. An aliquot of the oxide was carefully weighed and then diluted with 2% HNO_3 to form a solution of ~100 ng kg^{-1} of Nd.

2.2 Seawater sampling

Samples were obtained as part of the Heard Earth-Ocean-Biosphere Interactions (HEOBI) voyage along the Kerguelen Plateau during January and February 2016 onboard the R/V Investigator (GEOTRACES process study GIpr05). For the method development, sub-surface large volume samples were collected using the ship's clean underway sampling system. The seawater (open ocean seawater collected in different locations off the plateau while the ship was in transit) was filtered directly from the tap through a 0.8/0.2 µm AcroPak® (PALL Corporation, USA) capsule filter into 30 L HDPE carboys and will be referred to as HEOBI Sub-surface Sample (HSs). Other samples were collected using a CTD rosette equipped with 12 L Niskin® bottles (General Oceanics, USA) and in the results and discussion we refer in particular to samples collected at station 18 (52°55'34.2"S 71°22'03.8"E, 2,725 m water depth), referred to as CTD18. Once on board, 5 – 10 L of seawater were filtered directly from the Niskin bottle, through a 0.8/0.2 µm capsule filter into pre-weighed 10 L cubitainers. On-board blanks (2 L) from the UPW system of the vessel where collected at every station. Samples were transferred to a laminar flow hood, in the wet lab of the ship, where 1 mL of 11M distilled HCl was added per litre of sample, resulting in a final pH value of ~ 1.7. Finally, sample containers were wrapped in plastic film, double bagged and stored for on-shore processing.

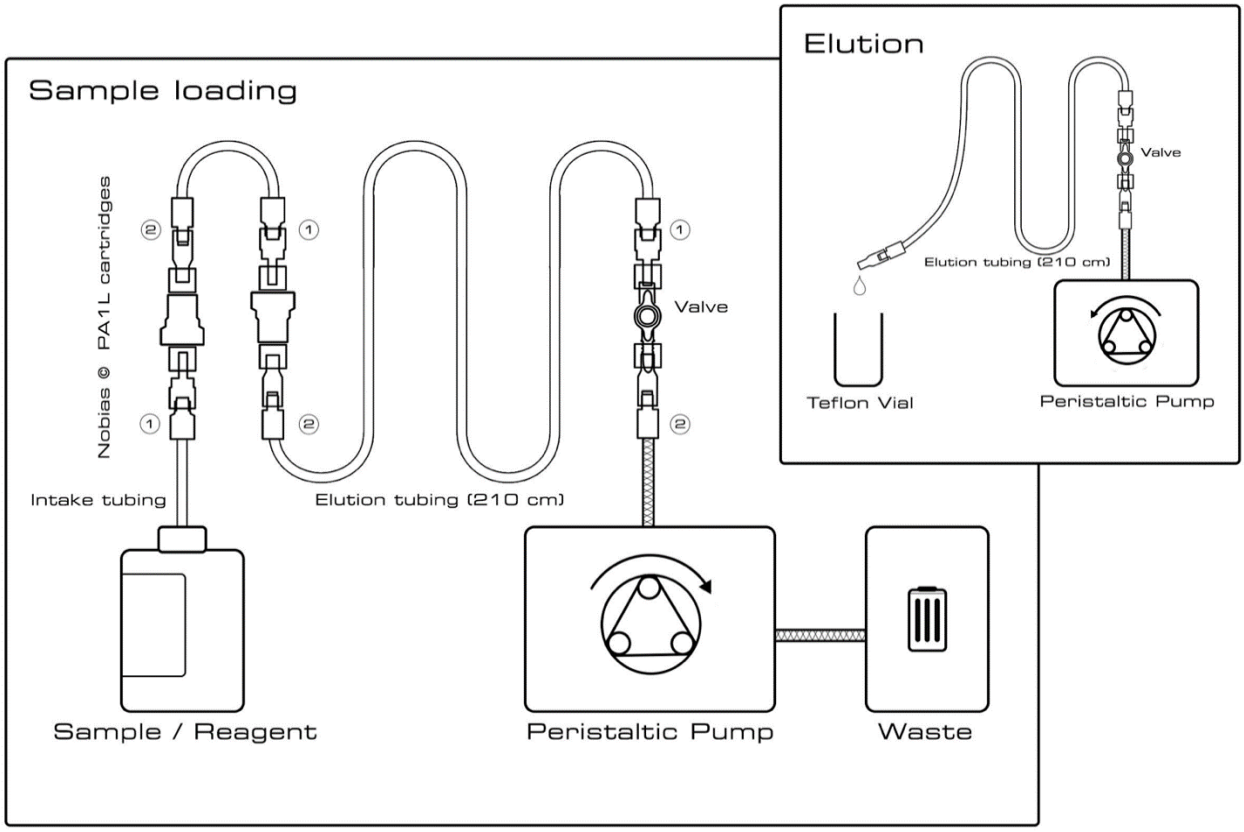

Figure 2-2. Manifold used for sample pre-concentration (not to scale). Only one of a total of six manifolds is shown. (1) ETFE/ Polypropylene 1/8" male luer lock to ¼-28 female adapter attached to the tubbing by an ETFE 1/8" flangeless nut and a Tefzel® 1/8 flangeless ferrule. (2) ETFE/ Polypropylene 1/8" female luer lock to ¼-28 female adapter attached to the tub- bing by an ETFE 1/8 flangeless nut and a Tefzel® 1/8 flangeless ferrule. Clear tubing represents the 1/8" Fluorinated Ethylene Propylene tubing, shaded tubing represents the Polyvinyl Chloride peristaltic pump tubing.

2.3 Pre-concentration procedure

For pre-concentration we used an array of 6 separate manifolds (Figure 2) which were all attached to an Ismatec® (Cole-Parmer GmbH, Germany) multiple-channel peristaltic pump with Ismatec® CA Cassettes, allowing the processing of six samples simultaneously. All tubing used to build the manifolds was 1/8" Fluorinated Ethylene Propylene (FEP, this type of tubing was selected for being translucent, corrosion resistant and relatively inexpensive) with the exception of the Polyvinyl chloride (PVC) peristaltic pump tubes. A sample/reagent intake probe (20 cm long) was attached to

the upper part of the cartridge. Approximately 210 cm of "elution tubing" (ET) containing the 5 mL of 3M HNO_3 used to elute metals from the column (from now on referred as E-HNO_3) was attached to the bottom of the cartridge. At the end of this tubing there is a Polyethylene (PE) one-way valve from which the PVC pump tubes attach. This valve avoids E-HNO_3 coming into contact with the PVC pump tubes during the elution process (they are not as resistant to corrosion as the FEP tubing) minimising any contributions to the procedure blank. For the processing of large volume samples, the manifolds were fitted with two Nobias PA1L cartridges in order to increase elemental recovery.

Prior to first use, each NOBIAS cartridge was cleaned with 5 mL of acetone at 1 mL min^{-1} to remove organic material and then the acetone was removed by rinsing with 30 mL of UPW (note that this was performed in a separate manifold for time saving purposes). Before processing samples, cartridges were cleaned with 3 cycles consisting of 30 mL of 3M HNO_3 and 30 mL of UPW (5 mL min^{-1}). Finally, cartridges were conditioned with 30 mL of 0.05M ammonia acetate solution.

Initial tests to determine the optimal pH for pre-concentration were conducted using small (125 mL) acidified aliquots of UPW and HSs samples. The tested pH values ranged from 3.5 to 5.5 (Figure 3). For these initial tests, aliquots were spiked with 25 pg ^{229}Th, 20 ng of ^{150}Nd and 0.5 ng of ^{236}U (only to seawater aliquots) and left to equilibrate for 24 hours. 2.5 M buffer solution was then added to a final concentration of 0.1 M before adjusting the pH using concentrated HCl. Immediately after, the sample was loaded onto the Nobias cartridge at a flow rate of 10 ml min^{-1}. Once the whole sample was passed through the cartridge, the resin was rinsed with 30 ml of UPW (5 mL min^{-1}). Next, a small bubble of air (2-3 cm long) was let into the manifold to separate the UPW from the E-HNO_3 used in the next step. Finally, Th and Nd isotopes (together with Pa, U and transition metals) were eluted from the resin using 5 mL of E-HNO_3 at 1 mL min^{-1}. When all E-HNO_3 had passed through the cartridges and was contained in the ET, the valve was closed and the manifolds were disconnected from the pump. Next, the cartridges were also disconnected, and one manifold at a time was

connected back to the pump. The flow direction of the pump was reversed and the E-HNO_3 collected into a clean Teflon vial. This procedure was repeated individually for all the 5 remaining manifolds (Figure 2).

The fully optimised method as applied to large volume samples, including those from the KP, involved some modifications to the procedure described above for 125 mL aliquots. First, 5 -10 L samples were weighed and amended with 29 M HF to achieve a final concentration of 1 mM. HF was used to keep the Th isotopes in solution during sample preconcentration (see Analysis of large volume samples). Second, samples were spiked with 1 pg of ^{229}Th per kg of seawater, and left to equilibrate for at least 72 hrs. On the day of pre-concentration, 2.5 M ammonia acetate was added to the sample to achieve a final concentration of 0.05 M (~100 g for a 5 L sample). Immediately after, the pH was adjusted to a value of 4.75 with concentrated HCl. Samples were then passed through the conditioned Nobias PA1L cartridges at a flow rate of 15 mL min^{-1}. The elution of the samples was performed in the same way described above.

Ultra-pure water blanks (2 L) were spiked with 4 pg of ^{229}Th and 5 ng of ^{150}Nd. Quality assurance was assessed by adding either the SW2010-1 or SW2010-2 reference material to 2.5 L of UPW. Both blanks and standard solutions were then treated and analysed in the same way as samples.

2.4 Separation chemistry

After pre-concentration, separation of Th from Nd and further elemental purification was necessary (Figure 1). Here we largely followed published protocols for separation of Th and Nd isotopes (Pin and Zalduegui, 1997; Anderson et al., 2012; Auro et al., 2012; Struve et al., 2016). An important point of difference, however, was the addition of an oxidation step after each column separation, including after the Nobias separation and previous to ICP-MS determination. The leaching of organic compounds from chromatographic resins has been previously identified as a possible

cause of elemental loss in subsequent separation steps (Auro et al., 2012; Struve et al., 2016) and has also been shown to produce isotopic shifts during analysis with ICP-MS techniques (Gault-Ringold and Stirling, 2012). To decompose any organics that may have leached from any of the resins used in this study, a strong oxidation was performed. This involved the addition of 0.5 mL of concentrated HNO_3 and 100 µL of concentrated $HCLO_4$ to all elution fractions, followed by heating (200 ^oC) to a very small drop inside a $HClO_4$ approved laminar flow hood. Samples were then converted into required forms depending on the stage of the chromatographic procedure (Figure 1).

The objective of the first stage of the chromatographic separation (from now on referred as "Th-separation", Figure 1) was to purify Th isotopes by separating them from the REE, Pa, U, Fe and other transition metals. Our initial tests to perform this procedure were based on the protocols described by Auro et al.(2012) with the only difference that we used AG® 1-X8 (Bio-Rad, USA) anion exchange resin instead of the suggested Eichrom® 1-X8. However, during the process of our investigation and mostly with the intention of reducing ^{232}Th blank contribution (see control of blank levels) our final procedure closely followed the protocols described in detail by the GEOTRACES intercalibration for Th and Pa isotopes (Anderson et al., 2012). Amongst measures implemented to help reduce blanks was a bulk cleaning of the resin. For this, ~ 20 g of the resin were placed in a clean PE container (50 mL capacity) with 6 M HCl added. A lid was placed on the container and then it was gently shaken for 10 mins using a mixer tube rotary rotisserie. After this, the 6 M HCl was decanted and the same procedure was repeated with UPW. This cycle was repeated three times in order to remove as much ^{232}Th as possible.

The objective of the second stage of the chromatographic separation (from now on REE-purification, Figure 1) was to strip the REE fraction from remaining traces of barium (Ba), strontium (Sr) and other seawater matrix cations to avoid interferences during mass spectrometric analysis. This was performed using AG® 50W-X8 (Bio-Rad, USA) resin following the procedure described by

Struve et al. (Struve et al., 2016). The goal of the third and final stage was to separate Nd isotopes from the rest of the Light Rare Earth Elements (LREE) in particular Pr and Sm. The procedure was based on the methodology reported by Pin and Zalduegui (1997) using LN resin (Eichrom, USA). Each column containing the LN resin was previously calibrated to identify the right elution scheme to isolate Nd isotopes.

2.5 Analysis

Following final oxidation, Th fractions were dissolved in 0.6 mL of 2% HNO_3 + 0.3% HF prior to analysis on an Element 2 SF-ICP-MS (Thermo Fisher Scientific, Germany). In order to minimise overlapping hydride formation and increase instrument sensitivity, sample introduction was via an Aridius® II (CETAC Technologies, USA) desolvating nebulizer (DSN). At the beginning of every measurement session the instrument was carefully tuned using a natural U solution (nominal concentration 100 pg g^{-1}, resultant U signal of ~1 x 10^6 cps). Analog/counting correction was evaluated at the beginning and throughout every analytical session in order to ensure equivalent detector response irrespective of analyte intensity with detector mode. This approach allowed the measurement of all Th isotopes in a single run: masses 229, 230 and half masses in-between were evaluated using counting detector mode, while abundant mass 232 was quantified with the detector in analog mode. Tailing correction due to high ^{232}Th abundance in samples can be large when analysing soils, particles and sediments. However, in seawater these corrections are less significant (Choi et al., 2001). The tailing correction on ^{230}Th under our analytical conditions was typically less than 0.1 % of the total ^{232}Th peak. After each Th measurement a washing period of 5 min was performed to reduce sample memory effects. Mass fractionation corrections were calculated using the exponential law for every analytical session using the CRM145B U isotopic reference material (New Brunswick Laboratory, USA) ($^{238}U/^{235}U$ = 137.88). The 2% HNO_3 + 0.3% HF solution used to redissolve samples was repeatedly analysed as an instrument blank. ^{232}Th and ^{230}Th concentrations

were determined using ID equations (Sargent et al., 2002). Instrument error for ^{232}Th was always below 3 %. For ^{230}Th it was normally less than 7 %.

Results reported in the effects of pH and matrix removal section were measured in the SF-ICP-MS directly after pre-concentration. Uranium and Th were determined from E-HNO_3 using the DSN (same analytical parameters described above). An aliquot (1 mL) of the E-HNO_3 was taken and analysed in the SF-ICP-MS without the DSN to obtain the Nd concentration. Recoveries for each element where then calculated using an external calibration.

Nd fractions were analysed using SF-ICP-MS to obtain a semi-quantitative estimation of the Nd content. Samples were matched in concentration and standard bracketed using JNdi-1 and measured using a Neptune Plus MC-ICP-MS (Thermo Fisher Scientific, Bremen, Germany) at School of Earth Sciences, Australian National University, Canberra. The measured ^{143}Nd/^{144}Nd ratios were corrected for machine induced mass fractionation (exponential law) using the ^{146}Nd/^{144}Nd value of 0.7219, and normalised to the accepted standard JNdi-1 ^{143}Nd/^{144}Nd value of 0.512115. The external reproducibility was calculated from JNdi-1 standards, and ranged from 0.36 to 1 epsilon Nd units for standards with a concentration of 20 and 10 ppb respectively.

3. Results and discussion

Results are presented and discussed in this manuscript in a way that reflects the chronological evolution of our investigation. First, we determined the effect of pH on the collection of Th and Nd from small samples (125 mL), using the Nobias resin. Once we knew the optimal pH to pre-concentrate samples, focus shifted to reducing blank levels, especially for ^{232}Th. Next, an assessment of accuracy and precision was undertaken through analysis of different standard solutions. Finally, the developed method was used to process and analyse larger volume samples, including samples collected from the KP.

3.1 Effects of pH and matrix removal

Sample pH has an important effect on elemental yields when using the Nobias resin to pre-concentrate Th, Nd and other trace elements from seawater (Sohrin et al., 2008; Persson et al., 2011; Takata et al., 2011; Quéroué et al., 2014). Initial tests to find the optimal pH for simultaneous pre-concentration of Th and Nd were carried out on small volume samples (125 mL). Straight after pre-concentration the contents of ^{229}Th, ^{150}Nd and ^{236}U were determined using SF-ICP-MS, with no further separation. Thorium and Nd showed similar trends in recovery as a function of pH in UPW and seawater. In both matrixes, Nd yield was lower at pH 3.5, tending to increase towards 100% at pH 5.5 (Figure 3). Thorium recovery is less sensitive to pH, however the lowest yield was still obtained at pH 3.5 and increases towards higher pH, reaching 95 and 100 % in UPW and seawater, respectively, at pH 5.5 (Figure 3). These results are in accordance with previous studies that used the Nobias resin to pre-concentrate Nd from UPW (Sohrin et al., 2008) and seawater (Persson et al., 2011; Hatje et al., 2014), and for Th in UPW (Sohrin et al., 2008). However, they differ from results obtained by Takata et al.(2011), who described a method to determine ^{232}Th concentrations from 200 mL samples of seawater. These authors found that the optimal pH to collect Th isotopes using Nobias resin occurred between pH values of 2-3, with yield decreasing towards pH of 6. We do not fully understand the reason for this difference, however, we suspect that it may be because in (Takata et al., 2011) ammonium acetate was not added in all the samples to determine optimal pH for pre-concentration (at different values), not for all samples as considered here. The buffer solution not only helps to keep the pH constant while performing pre-concentration, but also appears to increase the affinity of Th and Nd isotopes to the Nobias resin. Pre-concentrating samples without adding the ammonium acetate solution produced a decrease in Th and Nd recoveries of at least 20%, as observed too for Nd isotopes by Persson et al.(2011). The addition of HF prior to Nobias pre-concentration, suggested by Middag et al.(2015), also increases Th elemental recovery (See “analysis

of large volume samples" section below). In summary, Th and Nd isotopes were found to be pre-concentrated using the Nobias resin with an efficiency above 90 % in the pH range 4.5 to 5.5.

The determination of U isotopes was not an objective of our study however, it is important to know if there is U present in the E-HNO_3 because ^{234}U will decay into ^{230}Th over time. The recovery of U increases from 24 % at pH = 3.5 to 79 % at pH = 5.5 (Figure 3b). Therefore, the best approach is to perform the chromatographic separation straight after the pre-concentration in order to remove U isotopes from the Th fraction. Where a long delay between preconcentration and separation is anticipated (> 1 year, as could be the case if the pre-concentration is conducted in the field), it is advisable to spike samples with ^{236}U before pre-concentration, so that the U recovery can be accurately quantified for the purposes of in-growth correction.

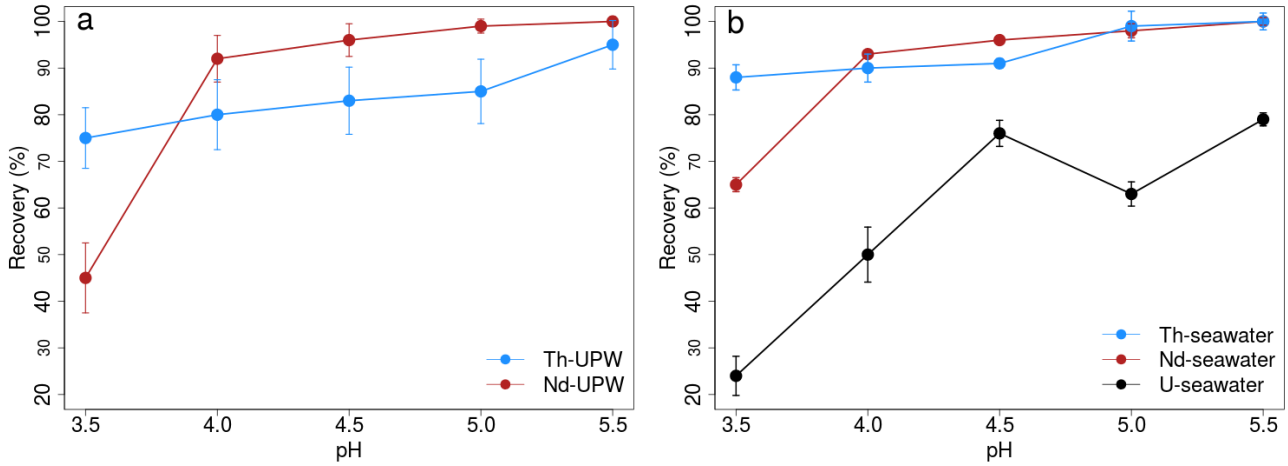

Figure 2-3. Recovery of Th, Nd and U after Nobias pre-concentration in (a) UPW and (b) seawater, as a function of sample pH. Error bars represent the standard deviation of triplicate measurements. (b) shows the recovery of Th, Nd and U in seawater when HF is added to the sample to a final concentration of 1mM previous to pre-concentration.

The Nobias resin is able to remove elements of the alkaline and alkali-earth groups at acidic and neutral pH values (Sohrin et al., 2008). We determined the concentration of some of the major components of the seawater matrix in the E-HNO_3 straight after elemental pre-concentration.

Remaining concentrations of sodium (Na) in samples were below $5x10^{-6}$ ng kg^{-1} after elution from the Nobias resin. Considering magnesium (Mg), calcium (Ca) and strontium (Sr), their concentrations were under $1x10^{-6}$ ng kg^{-1}. Barium (Ba) removal by the Nobias resin is of importance to minimise possible isobaric interference of BaO formed during plasma analysis, known to overlap with Nd isotopes (Dulski, 1994). Ba concentrations were below 4 pg kg^{-1}. Compared to typical seawater concentrations (Bernat et al., 1972; Millero, 2013), this indicates a removal efficiency of > 99 % for these major seawater ions.

3.2 Control of blank level

Contamination during sample collection, processing and analysis is always possible when measuring trace element concentrations in seawater. Of all the isotopes targeted in this study, ^{232}Th poses the highest risk of contamination. Using the Nobias resin to pre-concentrate Th and Nd isotopes has the advantage over traditional co-precipitation methods in that no Fe carrier solution needs to be added. This is a time-saving feature which also eliminates an additional contaminating source. However, reducing blank levels for ^{232}Th requires careful attention and sytematic testing.

As reported in earlier studies (Andersson and Schöberg, 2012; Auro et al., 2012), the BioRad AG1-X8 resin used for Th separation here proved to be a large source of ^{232}Th contamination (Figure 4). Our initial “Th separation” procedures were based on the protocol proposed by (Auro et al., 2012) and produced full procedural blanks as high as 160 pg (Figure 4) for a 10 L sample. This amount of ^{232}Th can easily be found in seawater (Krishnaswami and Cochran, 2011) and therefore the blank needed to be reduced. Andersson et al. (Andersson and Schöberg, 2012) showed that a “bulk” cleaning of the resin can help to mitigate this issue. After applying the “bulk” cleaning described in the methods section we were able to reduce the blank to ~ 40 pg of ^{232}Th (Figure 4). Although lower, this concentration still suggested improvement was necessary.

Accordingly, the amount of AG1-X8 resin was reduced from 5 mL to 2 mL. This reduced the ^{232}Th blank to ~ 20 pg (Figure 4), with no impact on Th or Nd recovery. We then started to recycle the columns and resin used for Th separation, so no extra ^{232}Th was released through the use of new resin. First attempts to do so rendered low yields for Th which were caused by interference of organics that were being retained by the pre-filter (Eichrom, USA) resin. This resin was removed from the procedure and instead strong oxidation of the sample was performed before re-loading samples onto the resin, in a similar manner as described by Anderson et al. (Anderson et al., 2012). This, together with the further reduction of the used amount of resin to 1 mL and the transfer of our procedure to a lab under ISO-5 conditions, resulted in consistent blanks below 10 pg of ^{232}Th for 10 L of sample (Figure 4).

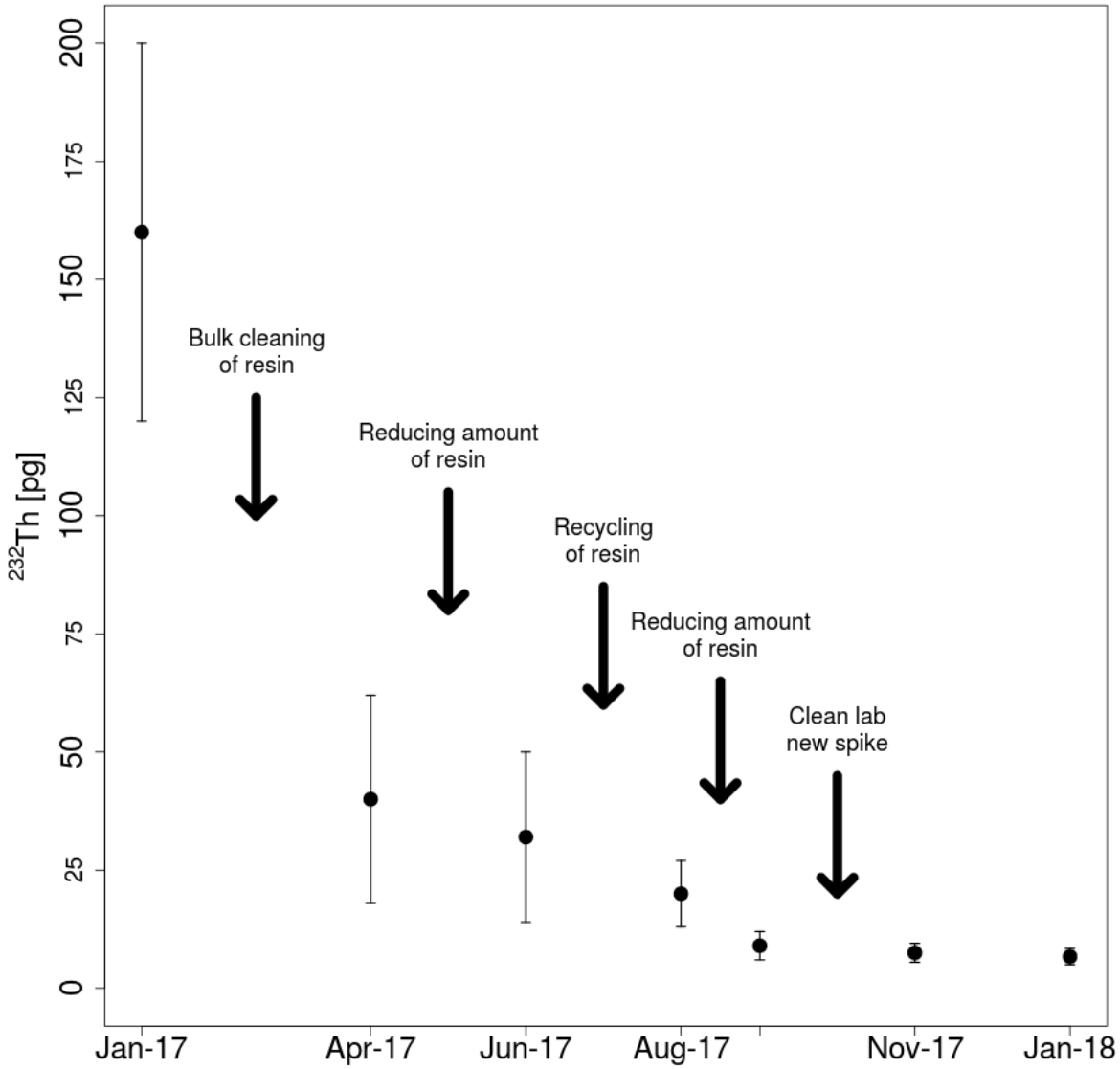

Figure 2-4. Evolution of ^{232}Th blank levels over a period of a year during method development.

^{232}Th eluted from the Nobias and AG1-X8 resins, as well as in the ammonia acetate buffer solution was analysed. Table 1 shows that, after eliminating ^{232}Th contamination from the AG1-X8 through bulk cleaning, the buffer solution becomes the largest source of ^{232}Th. If blanks levels need to be further reduced, the buffer solution can be passed through a clean Nobias cartridge.

Reagent/resin	^{232}Th (pg)	S.D. (pg)	n
NOBIAS	1.3	1	6
Ammonium acetate	4.9	1.5	3
AG1-X8	1	0.6	10
Total	7.2		

Table 2-1. ^{232}Th blank contribution from the resins and ammonium acetate buffer solution used in this study. Reported ^{232}Th is found in the elution fractions collected from the resins (no sample added) and in 200 g of the buffer solution.

The shipboard milli-Q blanks collected during the HEOBI expedition (n = 10) contained 2 to 17 pg ($\bar{x}$ = 8.5) ^{232}Th. This amount of ^{232}Th is comparable with levels found in our reagents and resins (Table 1). This is a good indication that no significant ^{232}Th blank contamination occurred during the sampling process. Because ^{232}Th represents 99.98% of all Th in nature, the risk of ^{230}Th contamination during sample separation and handling is quite low. Blank levels for ^{230}Th (n=10) were measured between 0.1 and 1.8 fg ($\bar{x}$ = 0.9 fg) for a 10 L sample, equivalent to 0.5-6 % of the ^{230}Th signal expected for seawater samples (depending on depth) (Krishnaswami and Cochran, 2011). Measured ^{232}Th and ^{230}Th blanks were comparable to those found in previous studies (Choi et al., 2001; Anderson et al., 2012; Hayes et al., 2013). The procedural blank for Nd was determined as 63 $\pm$ 20 pg (n = 3), which is also comparable to other studies presented in the GEOTRACES intercalibration for Nd and REE (van de Flierdt et al., 2012).

3.3 Quality assurance

The accuracy of our method for Th was first tested using SW2010-1 synthetic reference solution (see materials and methods). Early measurements of ^{232}Th were slightly higher (~1025 pg g^{-1}) than the expected value of 983$\pm$15 pg g^{-1} (Figure 5a, black symbols). We believe the SW2010-1 solution may have been contaminated when it was handled in a laboratory where sediment digestions were also being performed. After obtaining (i) a new SW2010-1 solution, (ii) a new ^{229}Th

spike, and (iii) moving our procedure inside a trace metal grade laboratory (ISO 5), the ^{232}Th concentrations dropped to an average of 974 ± 5 pg g^{-1}, n=5 (Figure 5a, green symbols). This represents ~ 1 % error of the expected value. Despite ^{232}Th contamination, ^{230}Th concentrations across both SW2010-1 solutions showed an average value of 249 ± 1.8 fg g^{-1} (n=9, Figure 5b). Again, this value agrees within 1 % of the expected value of 247 ± 3 fg g^{-1}(Anderson et al., 2012). This confirms that contamination of ^{230}Th is much less likely.

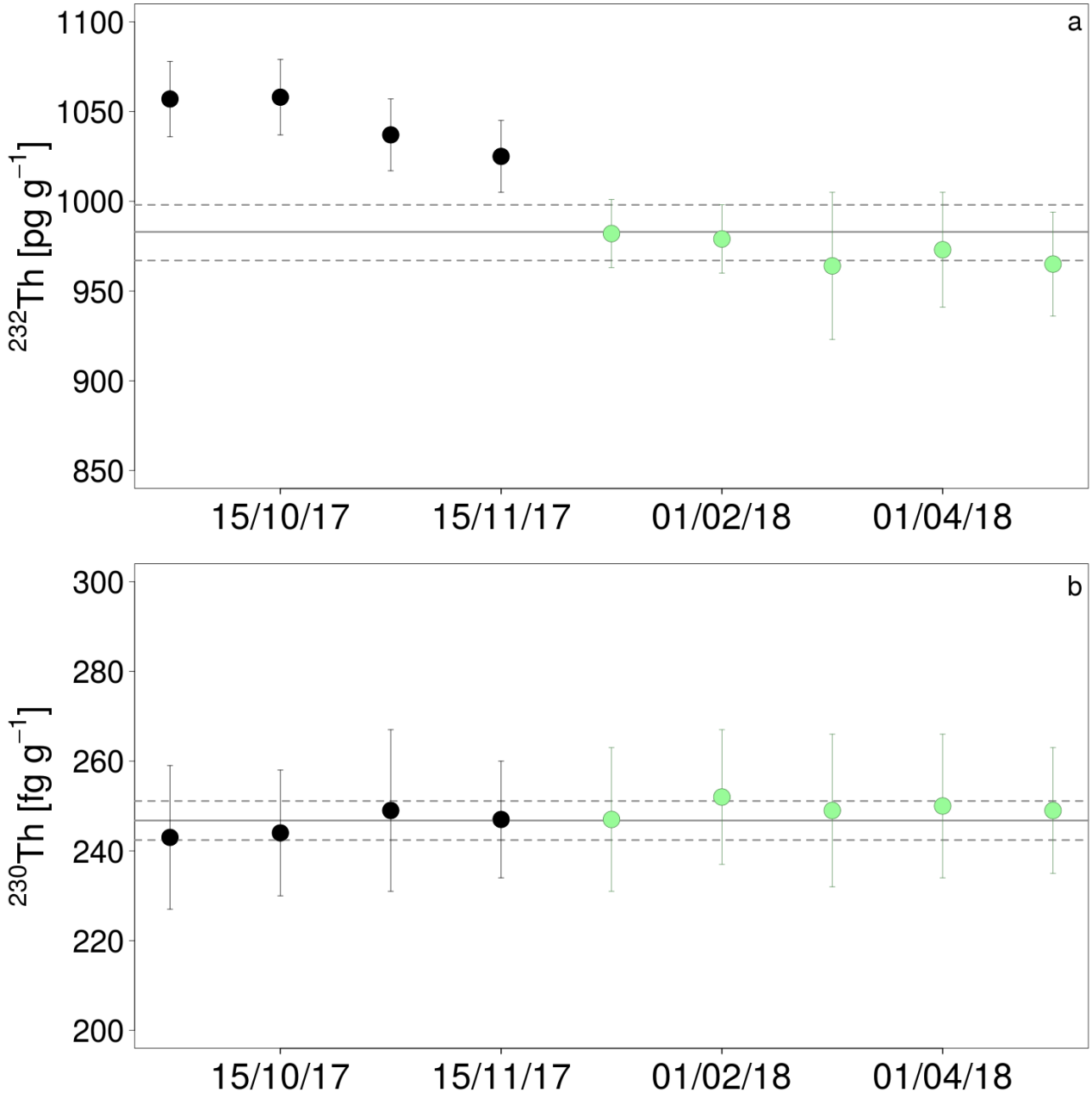

Figure 2-5. ^{232}Th (a) and ^{230}Th (b) concentrations measured in SW2010-1 reference material. Black circles (old bottle) are for a SW2010-1 solution that was obtained in 2014 and was handled in a laboratory where sediments were being digested. Green circles represent data obtained for a new bottle of SW2010-1 solution received in 2018. Solid line represents the average and dashed lines the standard deviation of the values obtained from 2 labs that participated in the GEOTRACES intercalibration for Th and Pa (Anderson et al., 2012)(see Section 2.1 Materials and reagents). Error bars are 1σ of the uncertainty associated with measured ^{229}Th/^{232}Th or ^{229}Th/^{230}Th ratios and with the ^{229}Th concentration of the spike. (For interpretation of the references to colour in this figure legend, the reader

Accuracy was also evaluated through analysis of both BATS2000 samples. The Bermuda Atlantic Timeseries Study (BATS) station has been used as a reference to intercalibrate key parameters of the GEOTRACES programme, including the intercalibrations for Th, Pa and Nd. Table 2 shows the ^{232}Th, ^{230}Th and ε_{Nd} values after applying the full procedure described in Figure 1. Obtained concentrations for ^{232}Th are within < 1 % of the intercalibration value while those for ^{230}Th are within 4 % (Anderson et al., 2012). Similarly, Nd isotopic composition obtained in this study for sample BATS2000A was ε_{Nd} =13.05±0.30, which agrees within 1 % of the reported value of 13.14±0.57 ε_{Nd} units (van de Flierdt et al., 2012).

	^{232}Th [dpm m^{-3}]	^{230}Th [dpm m^{-3}]	ε_{Nd}
BATS2000A	0.013 ± 3x10^{-4}	0.44 ± 0.02	13.05±0.3
BATS2000B	0.013 ± 5x10^{-4}	0.43 ± 0.05	-
Intercalibration value	0.013 ± 0.005	0.42 ± 0.14	13.14±0.57

Table 2-2. Determinations of ^{232}Th, ^{230}Th and ε_{Nd} in BATS2000A and BATS2000B samples. The error on Th measurements is 1σ uncertainty of the instrument and the ^{229}Th spike. For Nd determination it represents 1σ of the external error determined by multiple measurements of the JNd$_i$-1 reference solution. The reported intercalibration value for Th was graphically extracted from the data

presented in (Anderson et al., 2012). For Nd it represents the average obtained by all the participating laboratories (van de Flierdt et al., 2012).

The accuracy and reproducibility of the procedure was assessed by analysing SW2010-2 during the processing of samples from the Kerguelen Plateau over a 7-month period (Figure 6). For every batch of 11 samples, at least one sample containing 0.5 mL of the SW2010-2 reference solution dissolved in 2.5 L of UPW was processed and analysed in the same manner as the samples. The average values (n = 6) for $^{232}Th/^{230}Th$, $^{232}Th/^{229}Th$ and $^{230}Th/^{229}Th$ isotopic ratios were 3890±35, 53.1±0.4 and 0.0136±0.0001 respectively. These ratios agree within 2 % of reported values (Anderson et al., 2012) and indicate an excellent reproducibility over a period of 7 months (Figure 6).

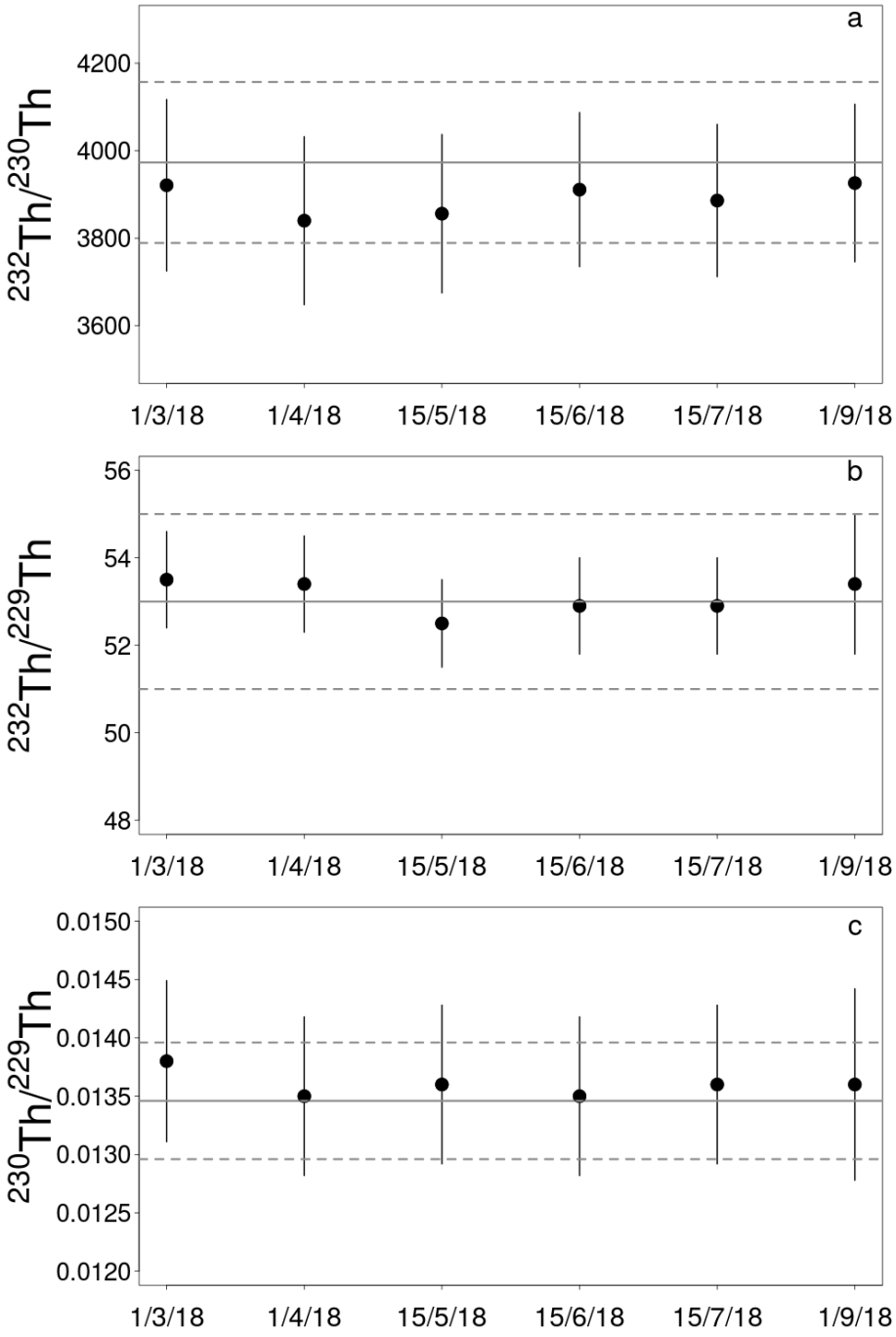

Figure 2-6. Measured Th isotope ratios in SW2010-2 reference solution. Shown are results for 6 separate analyses performed over 7-month period. Solid grey line represents the average value and the dashed grey lines represent 1 standard deviation of the values reported by participating laboratories in the intercalibration (Anderson et al., 2012). Error bars on measurements are 1σ of the instrument error.

3.4 Analysis of large volume seawater samples

The pre-concentration of larger volume seawater samples (>5 L) proved to not be a straightforward scaling up of our method developed for the processing of smaller samples, especially for the analysis of Th isotopes. Initial tests indicated that pre-concentrating samples at a pH = 5 would produce recoveries for both Th and Nd close to 100 % (considering that the efficiency of the Th-separation is close to 100 %). However, the first batch of 10 L aliquots from the HSs sample at pH = 5 produced Th yields of only 75 $\pm$ 9 %. We suspect the loss of Th occurred during the ~12 hours after pH adjustment while the sample was pumped through the Nobias cartridge. During this period of time at elevated pH, Th isotopes may form complexes with organic and inorganic colloids, precipitate as hydroxides or adsorb to the container walls (Santschi et al., 2006; Takata et al., 2011; Middag et al., 2015). Reducing the pre-concentration pH to values of 4, 4.25 or 4.5 did not improve Th yields. The addition of HF acid (final concentration 1 mM) prior to pre-concentration, as suggested by Middag et al.(2015), was effective at increasing Th recovery at pH 5. The formation of Th-fluoride complexes prevents Th from hydrolysing and is also thought to help increase the lability of metal-water complexes, which increases the chance of the resin to form a complex with the analyte (Middag et al., 2015). The Nd yield in large samples was not found to be affected by adsorption to container walls, or by the complexation to organic and inorganic colloids. This is attributed to the less particle reactive nature of Nd compared to Th.

3.5 Application of the method to samples from Kerguelen Plateau

For the analysis of samples collected from the KP region preconcentration of samples was performed using a pH of 4.75. After applying chromatographic separation, average Th yield of 82±7 % was obtained across the 57 analysed samples, with volumes ranging from 5 to 10 L. Some samples had recoveries as high as 95% while other samples exhibited recoveries as low as 50 %. We are unable to fully explain the reason for these differences. However, we noticed that most of the low-yield

samples were collected in the upper layers of the water column close to Heard and McDonald Islands. In these areas the concentration of organic substances in samples can be higher. Previous studies have shown that oxidizing the samples with UV-light prior to pre-concentration helps to release elements like Co and Cu from organic-bound to a more labile forms [50,59,67]. Applying a UV pre-treatment to the samples for Th and Nd pre-concentration could potentially increase the elemental recovery of these samples. Reducing the sample pH for the pre-concentration could also potentially increase the Th yield. However, both hypotheses need to be investigated further.

Now, we present a short analysis of the oceanographic conditions controlling Th and Nd profiles at station CTD18 from the HEOBI voyage. This station is located on the western flank of the plateau, in a low energy gyre of the Antarctic Circumpolar Current, where water circulation is relatively calm (Park et al., 1998b; Park et al., 1998a; Park et al., 2008). At this station, ^{230}Th concentrations show a constant increase with depth (Figure 7, blue line), typical of oceanic settings. In such environments, ^{230}Th concentrations are controlled mainly by the process of reversible scavenging between dissolved and particulate phases (Nozaki et al., 1981; Bacon and Anderson, 1982; Anderson et al., 1983; Roy-Barman et al., 1996). Observed behaviour and very similar ^{230}Th concentrations were reported for KERFIX station (Venchiarutti et al., 2008) (Figure 7, dashed lines), located ~300 km north-east of the CTD18 station. At CTD18 sub-surface maximum of ^{232}Th and a rapid decrease in concentration towards the surface indicate strong scavenging in the upper 100 m. At depths below, concentrations were influenced by reverse scavenging (Figure 7, red line).

The dissolved Nd isotopic profile at station CTD18 shows a typical composition for the Southern Ocean (Stichel et al., 2012). The upper 1000 m show variation in the ε_{Nd} from -8.1 to -8.8 $\pm$ 0.5, while deeper samples (> 1000 m) showed less radiogenic Nd isotopic values (Figure 7, black line).

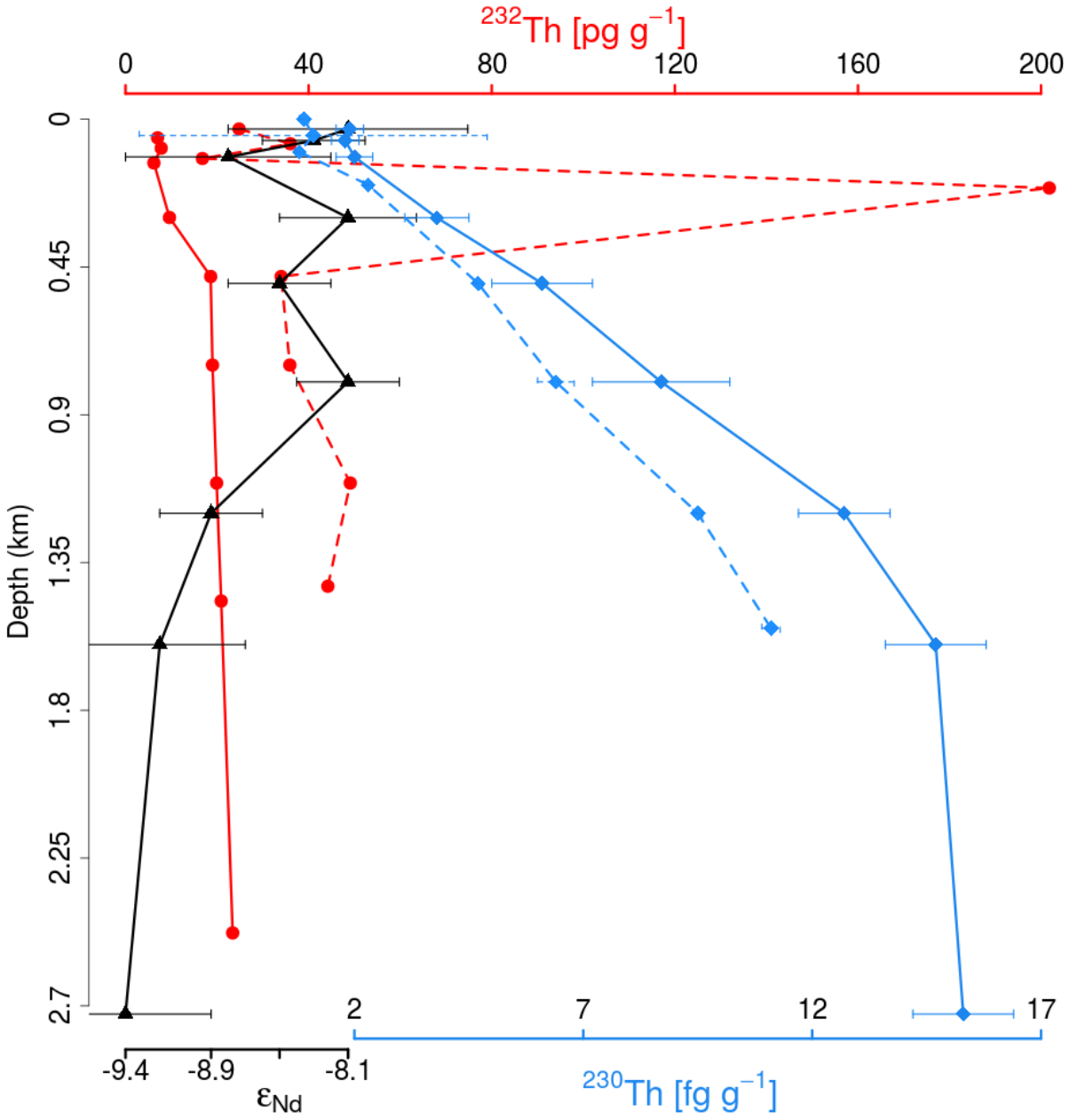

Figure 2-7. ^{232}Th (red), ^{230}Th (blue) and ε_{Nd} (black) in CTD 18. Dashed lines represent data published by Venchiarutti et al. (Venchiarutti et al., 2008) at the Kerfix station. Error bars on thorium measurements are 1σ of the instrument error and spike uncertainty. Error bars in ε_{Nd} represent 1σ of the external error determined by multiple measurements of the JNd$_i$-1 reference solution.

3.6 Future work and considerations

The Nd separation procedure can likely be simplified by removing the Biorad AG50W-X8 resin step. Indeed, when REE were preconcentrated form seawater using C18 cartdridges (van de Flierdt

et al., 2012; Stichel et al., 2015), Nd isotopes were separated from other REE without an additional matrix removal step. Likewise, as the Nobias resin removes 99.9 % of the seawater matrix it is very likely that further REE-purification using the Biorad AG50W-X8 resin described in this study may not be necessary. However this needs further investigation. The addition of ^{150}Nd as a Nd recovery monitor during sample preparation may be advantageous and will be included in future samples analyzed by the authors. The analysis of Pa and U can also be accomplished with this methodology with the addition of the proper isotopically enriched spikes (^{233}Pa and ^{236}U).

One of the motivations for this study was to produce a method for the pre-concentration of Th and Nd that could be applied on-board research vessels. This would offer the advantage of drastically reducing the size of the sample that needs to be brought back to land (from liters to just 5 mL of E-HNO3), eliminating the need for storage space. Furthermore, the sample would be ready for chromatographic separation immediately following strong oxidation in home laboratories, reducing the time from sample collection to publication.

4. Conclusion

The Nobias resin can quantitatively pre-concentrate Th and Nd isotopes in seawater samples at a working pH ranging from 4.5 to 5.5 following ammonia acetate buffer solution and HF addition. Sample pre-concentration procedures were then successfully coupled with known chromatographic separation techniques. The full procedure produced low blank levels (< 10 pg of ^{232}Th) comparable with previous studies, and excellent accuracy (typically within $\pm$1% of reported values) and reproducibility. The analysis of samples collected from the Kerguelen Plateau showed that our method can be successfully applied to large volume samples and indicates oceanographic consistence compared to previous studies in that region. However, the nature of the sample was found to play an important role in the efficiency of the Nobias resin to collect Th and Nd. The tested method reduces sample handling, minimises potential contamination sources, and is a time-saving

option compared to the commonly used iron co-precipitation approach. In particular a 10 L sample can be processed overnight (compared with up to a week for Fe co-precipitation) while the use of the Nobias resin avoids the need to use Fe-carrier (which requires meticulous cleaning for blank reduction). The simplicity of the proposed pre-concentration process makes it ideal for application during sampling campaigns at sea.

References

Anderson R. F. ., Mawji E., Cutter G. a. ., Measures C. I. and Jeandel C. (2014) GEOTRACES: Changing the Way We Explore Ocean Chemistry. *Oceanography* **27**, 50–61. Available at: http://dx.doi.org/10.5670/oceanog.2014.07.

Anderson R. F., Bacon M. P. and Brewer P. G. (1983) Removal of 230Th and 231Pa from the open ocean. *Earth Planet. Sci. Lett.* **62**, 7–23. Available at: https://linkinghub.elsevier.com/retrieve/pii/0012821X83900675.

Anderson R. F., Fleisher M. Q., Robinson L. F., Edwards R. L., Hoff J. A., Moran S. B., van der Loeff M. R., Thomas A. L., Roy-Barman M. and Francois R. (2012) GEOTRACES intercalibration of 230Th, 232Th, 231Pa, and prospects for 10Be. *Limnol. Oceanogr. Methods* **10**, 179–213. Available at: http://doi.wiley.com/10.4319/lom.2012.10.179.

Andersson P. S. and Schöberg H. (2012) Determination of 232Th and 230Th in seawater using a chemical separation procedure and thermal ionization mass spectrometry. *Limnol. Oceanogr. Methods* **10**, 296–303. Available at: http://doi.wiley.com/10.4319/lom.2012.10.296.

Arsouze T., Dutay J., Lacan F. and Jeandel C. (2009) Modeling the Nd Oceanic Cycle Using a Fully Prognostic Dynamical / Biogeochemical Coupled Model. *Assembly* **11**, 9279.

Arsouze T., Dutay J., Lacan F. and Jeandel C. (2007) Modeling the neodymium isotopic composition with a global ocean circulation model. *Chem. Geol.* **239**, 165–177. Available at: https://linkinghub.elsevier.com/retrieve/pii/S0009254106005353.

Auro M. E., Robinson L. F., Burke A., Bradtmiller L. I., Fleisher M. Q. and Anderson R. F. (2012) Improvements to 232-thorium, 230-thorium, and 231-protactinium analysis in seawater arising from GEOTRACES intercalibration. *Limnol. Oceanogr. Methods* **10**, 464–474. Available at: http://doi.wiley.com/10.4319/lom.2012.10.464.

Bacon M. P. and Anderson R. F. (1982) Distribution of thorium isotopes between dissolved and particulate forms in the deep sea. *J. Geophys. Res.* **87**, 20–45. Available at: http://doi.wiley.com/10.1029/JC087iC03p02045.

Behrens M. K., Muratli J., Pradoux C., Wu Y., Böning P., Brumsack H. J., Goldstein S. L., Haley B., Jeandel C., Paffrath R., Pena L. D., Schnetger B. and Pahnke K. (2016) Rapid and precise analysis of rare earth elements in small volumes of seawater - Method and intercomparison. *Mar. Chem.* **186**, 110–120. Available at: http://dx.doi.org/10.1016/j.marchem.2016.08.006.

Bernat M., Church T. and Allegre C. J. (1972) Barium and strontium concentrations in Pacific and Mediterranean sea water profiles by direct isotope dilution mass spectrometry. *Earth Planet. Sci. Lett.* **16**, 75–80. Available at: https://linkinghub.elsevier.com/retrieve/pii/0012821X72902385.

Biller D. V and Bruland K. W. (2012) Analysis of Mn , Fe , Co , Ni , Cu , Zn , Cd , and Pb in seawater using the Nobias-chelate PA1 resin and magnetic sector inductively coupled plasma mass

spectrometry (ICP-MS). *Mar. Chem.* **130**–**131**, 12–20. Available at: http://dx.doi.org/10.1016/j.marchem.2011.12.001.

Brewer P. G., Nozaki Y., Spencer D. W. and Fleer A. P. (1980) Sediment trap experiments in the deep North Atlantic: isotopic and elemental fluxes. *J. Mar. Res.* **38**, 703–728.

Chen J. H., Lawrence Edwards R. and Wasserburg G. J. (1986) 238U,234U and232Th in seawater. *Earth Planet. Sci. Lett.* **80**, 241–251. Available at: http://www.sciencedirect.com/science/article/pii/0012821X86901081.

Choi M., Francois R., Sims K., Bacon M. ., Brown-Leger S., Fleer A. ., Ball L., Schneider D. and Pichat S. (2001) Rapid determination of 230Th and 231Pa in seawater by desolvated micro-nebulization Inductively Coupled Plasma magnetic sector mass spectrometry. *Mar. Chem.* **76**, 99–112. Available at: https://linkinghub.elsevier.com/retrieve/pii/S0304420301000500.

Cutter G., Andersson P., Codispoti L., Croot P., François R., Lohan M. C., Obata H. and Rutgers v. d. Loeff M. (2010) Sampling and Sample-handling Protocols for GEOTRACES Cruises. Available at: http://epic.awi.de/34484/1/Cookbook.pdf.

Dietz L. A., Paghugki C. F. and Land G. A. (1962) Internal Standard Technique for Precise Isotopic Abundance Measurments in Thermal Ionization Mass Spectrometry. *Anal. Chem.* **34**, 709–710. Available at: https://pubs.acs.org/doi/abs/10.1021/ac60186a001.

Dulski P. (1994) Interferences of oxide, hydroxide and chloride analyte species in the determination of rare earth elements in geological samples by inductively coupled plasma-mass spectrometry. *Fresenius. J. Anal. Chem.* **350**, 194–203. Available at: http://link.springer.com/10.1007/BF00322470.

van de Flierdt T., Griffiths A. M., Lambelet M., Little S. H., Stichel T. and Wilson D. J. (2016) Neodymium in the oceans: a global database, a regional comparison and implications for palaeoceanographic research. *Philos. Trans. R. Soc. A Math. Phys. Eng. Sci.* **374**, 20150293. Available at: https://royalsocietypublishing.org/doi/10.1098/rsta.2015.0293.

van de Flierdt T., Pahnke K., Amakawa H., Andersson P., Basak C., Coles B., Colin C., Crocket K., Frank M., Frank N., Goldstein S. L., Goswami V., Haley B. A., Hathorne E. C., Hemming S. R., Henderson G. M., Jeandel C., Jones K., Kreissig K., Lacan F., Lambelet M., Martin E. E., Newkirk D. R., Obata H., Pena L., Piotrowski A. M., Pradoux C., Scher H. D., Schöberg H., Singh S. K., Stichel T., Tazoe H., Vance D. and Yang J. (2012) GEOTRACES intercalibration of neodymium isotopes and rare earth element concentrations in seawater and suspended particles. Part 1: reproducibility of results for the international intercomparison. *Limnol. Oceanogr. Methods* **10**, 234–251. Available at: http://onlinelibrary.wiley.com/doi/10.4319/lom.2012.10.234/full.

Francois R., Frank M., Rutgers van der Loeff M. M. and Bacon M. P. (2004) 230 Th normalization: An essential tool for interpreting sedimentary fluxes during the late Quaternary. *Paleoceanography* **19**, n/a-n/a. Available at: http://doi.wiley.com/10.1029/2003PA000939.

Frank M. (2002) Radiogenic isotopes: Tracers of past ocean circulation and erosional input. *Rev. Geophys.* **40**, 1001. Available at: http://doi.wiley.com/10.1029/2000RG000094.

Gault-Ringold M. and Stirling C. H. (2012) Anomalous isotopic shifts associated with organic resin residues during cadmium isotopic analysis by double spike MC-ICPMS. *J. Anal. At. Spectrom.* **27**, 449. Available at: http://xlink.rsc.org/?DOI=c2ja10360e.

Goldstein S. L. and Hemming S. R. (2003) Long-lived Isotopic Tracers in Oceanography, Paleoceanography, and Ice-sheet Dynamics. In *Treatise on Geochemistry* Elsevier. pp. 453–489. Available at: https://linkinghub.elsevier.com/retrieve/pii/B008043751606179X.

Haley B. A., Du J., Abbott A. N. and McManus J. (2017) The Impact of Benthic Processes on Rare Earth Element and Neodymium Isotope Distributions in the Oceans. *Front. Mar. Sci.* **4**, 1–12. Available at: http://journal.frontiersin.org/article/10.3389/fmars.2017.00426/full.

Hatje V., Bruland K. W. and Flegal a. R. (2014) Determination of rare earth elements after pre-concentration using NOBIAS-chelate PA-1® resin: Method development and application in the San Francisco Bay. *Mar. Chem.* **160**, 34–41. Available at: http://dx.doi.org/10.1016/j.marchem.2014.01.006.

Hayes C. T., Anderson R. F., Fleisher M. Q., Serno S., Winckler G. and Gersonde R. (2013) Quantifying lithogenic inputs to the North Pacific Ocean using the long-lived thorium isotopes. *Earth Planet. Sci. Lett.* **383**, 16–25. Available at: http://dx.doi.org/10.1016/j.epsl.2013.09.025.

Hayes C. T., Black E. E., Anderson R. F., Baskaran M., Buesseler K. O., Charette M. A., Cheng H., Cochran J. K., Edwards R. L., Fitzgerald P., Lam P. J., Lu Y., Morris S. O., Ohnemus D. C., Pavia F. J., Stewart G. and Tang Y. (2018) Flux of Particulate Elements in the North Atlantic Ocean Constrained by Multiple Radionuclides. *Global Biogeochem. Cycles* **32**, 1738–1758. Available at: https://onlinelibrary.wiley.com/doi/abs/10.1029/2018GB005994.

Hayes C. T., Rosen J., McGee D. and Boyle E. A. (2017) Thorium distributions in high- and low-dust regions and the significance for iron supply. *Global Biogeochem. Cycles* **31**, 1–20. Available at: http://doi.wiley.com/10.1002/2016GB005511.

Hsieh Y., Henderson G. and Thomas A. (2011) Combining seawater 232Th and 230Th concentrations to determine dust fluxes to the surface ocean. *Earth Planet. Sci. Lett.* **312**, 280–290. Available at: http://linkinghub.elsevier.com/retrieve/pii/S0012821X11006170.

Jacobsen S. B. and Wasserburg G. J. (1980) Sm-Nd isotopic evolution of chondrites. *Earth Planet. Sci. Lett.* **50**, 139–155. Available at: https://linkinghub.elsevier.com/retrieve/pii/0012821X80901259.

Jeandel C. (1993) Concentration and isotopic composition of Nd in the South Atlantic Ocean. *Earth Planet. Sci. Lett.* **117**, 581–591. Available at: http://www.sciencedirect.com/science/article/pii/0012821X9390104H.

Jeandel C. and Derek V. (2018) New Tools, New Discoveries in Marine Geochemistry. *Elements* **14**, 379–384. Available at: https://pubs.geoscienceworld.org/msa/elements/article/14/6/379/567311/New-Tools-New-Discoveries-in-Marine-Geochemistry.

Jeandel C. and Oelkers E. H. (2015) The influence of terrigenous particulate material dissolution on ocean chemistry and global element cycles. *Chem. Geol.* **395**, 50–66. Available at: http://dx.doi.org/10.1016/j.chemgeo.2014.12.001.

Jeandel C., Thouron D. and Fieux M. (1998) Concentrations and isotopic compositions of neodymium in the eastern Indian Ocean and Indonesian straits. *Geochim. Cosmochim. Acta* **62**, 2597–2607. Available at: http://www.sciencedirect.com/science/article/pii/S0016703798001690.

Jeandel C. and Venchiarutti C. (2011) Single column sequential extraction of Ra, Nd, Th, Pa and U from a natural sample. *Geostand. …*. Available at: http://onlinelibrary.wiley.com/doi/10.1111/j.1751-908X.2010.00087.x/full.

Koczy F. F., Picciotto E., Poulaert G. and Wilgain S. (1957) Mesure des isotopes du thorium dans l'eau de mer. *Geochim. Cosmochim. Acta* **11**, 103–129. Available at: http://www.sciencedirect.com/science/article/pii/001670375790008X.

Krishnaswami S. and Cochran J. K. (2011) *U-Th series nuclides in aquatic systems*., Elsevier.

Lacan F. and Jeandel C. (2005) Neodymium isotopes as a new tool for quantifying exchange fluxes at the continent–ocean interface. *Earth Planet. Sci. Lett.* **232**, 245–257. Available at: http://www.sciencedirect.com/science/article/pii/S0012821X05000233.

Lacan F., Tachikawa K. and Jeandel C. (2012) Neodymium isotopic composition of the oceans: A compilation of seawater data. *Chem. Geol.* **300**–**301**, 177–184. Available at:

http://dx.doi.org/10.1016/j.chemgeo.2012.01.019.
Middag R., Séférian R., Conway T. M., John S. G., Bruland K. W. and de Baar H. J. W. (2015) Intercomparison of dissolved trace elements at the Bermuda Atlantic Time Series station. *Mar. Chem.* **177**, 476–489. Available at: http://dx.doi.org/10.1016/j.marchem.2015.06.014.
Millero F. J. (2013) Chemical Oceanography, Fourth Edition. , 591. Available at: https://books.google.com/books?id=w780s8h_qrkC&pgis=1.
Moore W. S. and Sackett W. M. (1964) Uranium and thorium series inequilibrium in sea water. *J. Geophys. Res.* **69**, 5401–5405. Available at: http://www.agu.org/pubs/crossref/1964/JZ069i024p05401.shtml.
Nozaki Y., Horibe Y. and Tsubota H. (1981) The water column distributions of thorium isotopes in the western North Pacific. *Earth Planet. Sci. Lett.* **54**, 203–216. Available at: https://linkinghub.elsevier.com/retrieve/pii/0012821X81900042.
Pahnke K., van de Flierdt T., Jones K. M., Lambelet M., Hemming S. R. and Goldstein S. L. (2012) GEOTRACES intercalibration of neodymium isotopes and rare earth element concentrations in seawater and suspended particles. Part 2: Systematic tests and baseline profiles. *Limnol. Oceanogr. Methods* **10**, 252–269. Available at: http://doi.wiley.com/10.4319/lom.2012.10.252.
Park Y.-H., Charriaud E. and Fieux M. (1998a) Thermohaline structure of the Antarctic Surface Water/Winter Water in the Indian sector of the Southern Ocean. *J. Mar. Syst.* **17**, 5–23. Available at: https://linkinghub.elsevier.com/retrieve/pii/S0924796398000268.
Park Y.-H., Charriaud E., Pino D. R. and Jeandel C. (1998b) Seasonal and interannual variability of the mixed layer properties and steric height at station KERFIX, southwest of Kerguelen. *J. Mar. Syst.* **17**, 571–586. Available at: https://linkinghub.elsevier.com/retrieve/pii/S0924796398000657.
Park Y.-H., Fuda J.-L., Durand I. and Naveira Garabato A. C. (2008) Internal tides and vertical mixing over the Kerguelen Plateau. *Deep Sea Res. Part II Top. Stud. Oceanogr.* **55**, 582–593. Available at: http://www.sciencedirect.com/science/article/pii/S0967064508000118.
Persson P., Andersson P. and Zhang J. (2011) Determination of Nd isotopes in water: a chemical separation technique for extracting Nd from seawater using a chelating resin. *Anal. …* **83**, 1336–1341. Available at: http://pubs.acs.org/doi/abs/10.1021/ac102559k.
Piepgras D. J. and Wasserburg G. J. (1980) Neodymium isotopic variations in seawater. *Earth Planet. Sci. Lett.* **50**, 128–138. Available at: https://linkinghub.elsevier.com/retrieve/pii/0012821X80901247.
Piepgras D. J., Wasserburg G. J. and Dasch E. J. (1979) The isotopic composition of Nd in different ocean masses. *Earth Planet. Sci. Lett.* **45**, 223–236. Available at: https://linkinghub.elsevier.com/retrieve/pii/0012821X79901250.
Pin C. and Zalduegui J. S. (1997) Sequential separation of light rare-earth elements, thorium and uranium by miniaturized extraction chromatography: Application to isotopic analyses of silicate rocks. *Anal. Chim. Acta* **339**, 79–89. Available at: https://linkinghub.elsevier.com/retrieve/pii/S0003267096004990.
Quéroué F., Townsend A., van der Merwe P., Lannuzel D., Sarthou G., Bucciarelli E. and Bowie A. (2014) Advances in the offline trace metal extraction of Mn, Co, Ni, Cu, Cd, and Pb from open ocean seawater samples with determination by sector field ICP-MS analysis. *Anal. Methods* **6**, 2837–2847. Available at: http://xlink.rsc.org/?DOI=C3AY41312H.
Robinson L. F., Belshaw N. S. and Henderson G. M. (2004) U and Th concentrations and isotope ratios in modern carbonates and waters from the Bahamas. *Geochim. Cosmochim. Acta* **68**, 1777–1789. Available at: https://linkinghub.elsevier.com/retrieve/pii/S0016703703007361.
Rousseau T. C. C., Sonke J. E., Chmeleff J., van Beek P., Souhaut M., Boaventura G., Seyler P. and

Jeandel C. (2015) Rapid neodymium release to marine waters from lithogenic sediments in the Amazon estuary. *Nat. Commun.* **6**, 7592. Available at: http://www.nature.com/articles/ncomms8592.

Roy-Barman M., Chen J. H., Wasserburg G. J. and Ocean E. (1996) 230Th_ 232 Th systematics in the central Pacific The sources and the fates of thorium. *Earth Planet. Sci. Lett.* **139**, 351–363. Available at: http://ac.els-cdn.com/0012821X96000179/1-s2.0-0012821X96000179-main.pdf?_tid=d727d906-5006-11e7-9a21-00000aab0f6c&acdnat=1497337777_c0b320186973b7f8c1882f9dde0c8ac3.

Sackett W. M., Potratz H. A. and Goldberg E. D. (1958) Thorium Content of Ocean Water. *Science (80-.).* **128**, 204 LP – 205. Available at: http://science.sciencemag.org/content/128/3317/204.abstract.

Santschi P. H., Murray J. W., Baskaran M., Benitez-Nelson C. R., Guo L. D., Hung C.-C., Lamborg C., Moran S. B., Passow U. and Roy-Barman M. (2006) Thorium speciation in seawater. *Mar. Chem.* **100**, 250–268. Available at: https://linkinghub.elsevier.com/retrieve/pii/S0304420305002161.

Sargent M., Harte R. and Harrington C. (2002) Guidelines for achieving high accuracy in isotope dilution mass spectrometry (IDMS). Available at: https://books.google.com/books?hl=es&lr=&id=9wwLS5pcD9sC&oi=fnd&pg=PA1&dq=guidelines+for+achieving+high+accuracy+in+isotope+dilution&ots=TI80X664yI&sig=-NVdYoYJtnc_SarNw4UVRm1L2jo [Accessed June 23, 2017].

Schlitzer R., Anderson R. F., Dodas E. M., Lohan M., Geibert W., Tagliabue A., Bowie A., Jeandel C., Maldonado M. T., Landing W. M., Cockwell D., Abadie C., Abouchami W., Achterberg E. P., Agather A., Aguliar-Islas A., van Aken H. M., Andersen M., Archer C., Auro M., de Baar H. J., Baars O., Baker A. R., Bakker K., Basak C., Baskaran M., Bates N. R., Bauch D., van Beek P., Behrens M. K., Black E., Bluhm K., Bopp L., Bouman H., Bowman K., Bown J., Boyd P., Boye M., Boyle E. A., Branellec P., Bridgestock L., Brissebrat G., Browning T., Bruland K. W., Brumsack H. J., Brzezinski M., Buck C. S., Buck K. N., Buesseler K., Bull A., Butler E., Cai P., Mor P. C., Cardinal D., Carlson C., Carrasco G., Casacuberta N., Casciotti K. L., Castrillejo M., Chamizo E., Chance R., Charette M. A., Chaves J. E., Cheng H., Chever F., Christl M., Church T. M., Closset I., Colman A., Conway T. M., Cossa D., Croot P., Cullen J. T., Cutter G. A., Daniels C., Dehairs F., Deng F., Dieu H. T., Duggan B., Dulaquais G., Dumousseaud C., Echegoyen-Sanz Y., Edwards R. L., Ellwood M., Fahrbach E., Fitzsimmons J. N., Russell Flegal A., Fleisher M. Q., van de Flierdt T., Frank M., Friedrich J., Fripiat F., Fröllje H., Galer S. J. G., Gamo T., Ganeshram R. S., Garcia-Orellana J., Garcia-Solsona E., Gault-Ringold M., George E., Gerringa L. J. A., Gilbert M., Godoy J. M., Goldstein S. L., Gonzalez S. R., Grissom K., Hammerschmidt C., Hartman A., Hassler C. S., Hathorne E. C., Hatta M., Hawco N., Hayes C. T., Heimbürger L. E., Helgoe J., Heller M., Henderson G. M., Henderson P. B., van Heuven S., Ho P., Horner T. J., Hsieh Y. Te, Huang K. F., Humphreys M. P., Isshiki K., Jacquot J. E., Janssen D. J., Jenkins W. J., John S., Jones E. M., Jones J. L., Kadko D. C., Kayser R., Kenna T. C., Khondoker R., Kim T., Kipp L., Klar J. K., Klunder M., Kretschmer S., Kumamoto Y., Laan P., Labatut M., Lacan F., Lam P. J., Lambelet M., Lamborg C. H., Le Moigne F. A. C., Le Roy E., Lechtenfeld O. J., Lee J. M., Lherminier P., Little S., López-Lora M., Lu Y., Masque P., Mawji E., Mcclain C. R., Measures C., Mehic S., Barraqueta J. L. M., van der Merwe P., Middag R., Mieruch S., Milne A., Minami T., Moffett J. W., Moncoiffe G., Moore W. S., Morris P. J., Morton P. L., Nakaguchi Y., Nakayama N., Niedermiller J., Nishioka J., Nishiuchi A., Noble A., Obata H., Ober S., Ohnemus D. C., van Ooijen J., O'Sullivan J., Owens S., Pahnke K., Paul M., Pavia F., Pena L. D., Peters B., Planchon F., Planquette H., Pradoux C., Puigcorbé V., Quay P., Queroue F., Radic A., Rauschenberg S., Rehkämper M., Rember R.,

Remenyi T., Resing J. A., Rickli J., Rigaud S., Rijkenberg M. J. A., Rintoul S., Robinson L. F., Roca-Martí M., Rodellas V., Roeske T., Rolison J. M., Rosenberg M., Roshan S., Rutgers van der Loeff M. M., Ryabenko E., Saito M. A., Salt L. A., Sanial V., Sarthou G., Schallenberg C., Schauer U., Scher H., Schlosser C., Schnetger B., Scott P., Sedwick P. N., Semiletov I., Shelley R., Sherrell R. M., Shiller A. M., Sigman D. M., Singh S. K., Slagter H. A., Slater E., Smethie W. M., Snaith H., Sohrin Y., Sohst B., Sonke J. E., Speich S., Steinfeldt R., Stewart G., Stichel T., Stirling C. H., Stutsman J., Swarr G. J., Swift J. H., Thomas A., Thorne K., Till C. P., Till R., Townsend A. T., Townsend E., Tuerena R., Twining B. S., Vance D., Velazquez S., Venchiarutti C., Villa-Alfageme M., Vivancos S. M., Voelker A. H. L., Wake B., Warner M. J., Watson R., van Weerlee E., Alexandra Weigand M., Weinstein Y., Weiss D., Wisotzki A., Woodward E. M. S., Wu J., Wu Y., Wuttig K., Wyatt N., Xiang Y., Xie R. C., Xue Z., Yoshikawa H., Zhang J., Zhang P., Zhao Y., Zheng L., Zheng X. Y., Zieringer M., Zimmer L. A., Ziveri P., Zunino P. and Zurbrick C. (2018) The GEOTRACES Intermediate Data Product 2017. *Chem. Geol.* **493**, 210–223. Available at: https://doi.org/10.1016/j.chemgeo.2018.05.040.

Shabani M. B., Akagi T. and Masuda A. (1992) Preconcentration of trace rare-earth elements in seawater by complexation with bis(2-ethylhexyl) hydrogen phosphate and 2-ethylhexyl dihydrogen phosphate adsorbed on a C18 cartridge and determination by inductively coupled plasma mass spectrometry. *Anal. Chem.* **64**, 737–743. Available at: https://pubs.acs.org/doi/abs/10.1021/ac00031a008.

Sohrin Y., Urushihara S. and Nakatsuka S. (2008) Multielemental determination of GEOTRACES key trace metals in seawater by ICPMS after preconcentration using an ethylenediaminetriacetic acid chelating resin. *Anal. …*. Available at: http://pubs.acs.org/doi/abs/10.1021/ac800500f.

Stichel T., Frank M., Rickli J. and Haley B. A. (2012) The hafnium and neodymium isotope composition of seawater in the Atlantic sector of the Southern Ocean. *Earth Planet. Sci. Lett.* **317**–**318**, 282–294. Available at: http://dx.doi.org/10.1016/j.epsl.2011.11.025.

Stichel T., Hartman A. E., Duggan B., Goldstein S. L., Scher H. and Pahnke K. (2015) Separating biogeochemical cycling of neodymium from water mass mixing in the Eastern North Atlantic. *Earth Planet. Sci. Lett.* **412**, 245–260. Available at: http://www.sciencedirect.com/science/article/pii/S0012821X14007614%5Cnhttp://dx.doi.org/10.1016/j.epsl.2014.12.008.

Struve T., van de Flierdt T., Robinson L. F., Bradtmiller L. I., Hines S. K., Adkins J. F., Lambelet M., Crocket K. C., Kreissig K., Coles B. and Auro M. E. (2016) Neodymium isotope analyses after combined extraction of actinide and lanthanide elements from seawater and deep-sea coral aragonite. *Geochemistry, Geophys. Geosystems* **17**, 232–240. Available at: http://doi.wiley.com/10.1002/2015GC006130 [Accessed December 13, 2016].

Tachikawa K. (2003) Neodymium budget in the modern ocean and paleo-oceanographic implications. *J. Geophys. Res.* **108**, 3254. Available at: http://doi.wiley.com/10.1029/1999JC000285.

Tachikawa K., Arsouze T., Bayon G., Bory A., Colin C., Dutay J. C., Frank N., Giraud X., Gourlan A. T., Jeandel C., Lacan F., Meynadier L., Montagna P., Piotrowski A. M., Plancherel Y., Pucéat E., Roy-Barman M. and Waelbroeck C. (2017) The large-scale evolution of neodymium isotopic composition in the global modern and Holocene ocean revealed from seawater and archive data. *Chem. Geol.* **457**, 131–148. Available at: http://dx.doi.org/10.1016/j.chemgeo.2017.03.018.

Takata H., Zheng J., Tagami K., Aono T. and Uchida S. (2011) Determination of 232Th in seawater by ICP-MS after preconcentration and separation using a chelating resin. *Talanta* **85**, 1772–7. Available at: http://www.sciencedirect.com/science/article/pii/S0039914011005789.

Tanaka T., Togashi S., Kamioka H., Amakawa H., Kagami H., Hamamoto T., Yuhara M., Orihashi Y., Yoneda S., Shimizu H., Kunimaru T., Takahashi K., Yanagi T., Nakano T., Fujimaki H., Shinjo R., Asahara Y., Tanimizu M. and Dragusanu C. (2000) JNdi-1: a neodymium isotopic reference in consistency with LaJolla neodymium. *Chem. Geol.* **168**, 279–281. Available at: https://linkinghub.elsevier.com/retrieve/pii/S0009254100001984.

Thomas A., Henderson G. and Robinson L. (2006) Interpretation of the 231 Pa/230 Th paleocirculation proxy: New water-column measurements from the southwest Indian Ocean. *Earth Planet. Sci. ….* Available at: http://www.sciencedirect.com/science/article/pii/S0012821X05008101.

Venchiarutti C., Jeandel C. and Roy-Barman M. (2008) Particle dynamics study in the wake of Kerguelen Island using thorium isotopes. *Deep Sea Res. Part I Oceanogr. Res. Pap.* **55**, 1343–1363. Available at: http://www.sciencedirect.com/science/article/pii/S0967063708001180.

Wasserburg G. J., Jacobsen S., DePaolo D. J., McCulloch M. T. and Wen T. (1981) Precise determination of ratios Sm and Nd isotopic abundances in standard solutions. *Geochim. Cosmochim. Acta* **45**, 2311–2323. Available at: papers2://publication/uuid/9687D48D-6F02-4C2C-8E61-16031CC2907B.

Wuttig K., Townsend A. T., Merwe P. van der, Gault-Ringold M., Holmes T., Schallenberg C., Latour P., Tonnard M., Rijkenberg M. J. A., Lannuzel D. and Bowie A. R. (2019) Critical evaluation of a seaFAST system for the analysis of trace metals in marine samples. *Talanta* **197**, 653–668. Available at: https://doi.org/10.1016/j.talanta.2019.01.047.

Chapter 3 - Quantifying lithogenic fluxes to the Kerguelen Plateau using long-lived thorium isotopes

1. Introduction

The different isotopes of thorium (Th) provide important information about a variety of processes that occur in the oceans. In seawater, all Th isotopes have a stable oxidation state of IV, making them highly particle reactive (Santschi et al., 2006). Thorium isotopes also have very well constrained and limited sources to the marine environment. The very-long lived primordial isotope ^{232}Th ($t_{1/2}$=1.4×10^{10} years) represents ~99.98 % of all natural thorium and it is supplied to the ocean exclusively by the dissolution of continental material transported to the ocean by rivers and wind (Krishnaswami and Cochran, 2011). The next most abundant thorium isotope is ^{230}Th ($t_{1/2}$=75,400 years). It is supplied to the ocean almost entirely by the decay of the highly soluble ^{234}U, and removed at an almost constant rate to the sediments by interaction with particles (Anderson et al., 1983). This makes ^{230}Th one of the most versatile tools in particle flux studies in the ocean and applied to marine sediments. (Francois et al.,

1990; Francois et al., 2004; Costa and McManus, 2017; Luo, 2017). In the last decade, the ^{232}Th-^{230}Th system has gained popularity as a tracer to quantify lithogenic sources of trace elements to the marine environment (Hsieh et al., 2011; Hayes et al., 2013; Deng et al., 2014). The long-lived Th isotopes can be used to track and quantify the input of lithogenic material to the ocean because ^{232}Th acts as the tracer of the lithogenic input, while ^{230}Th provides a residence time with respect to scavenging that is assessed through its disequilibria from its soluble parent nuclide ^{234}U (Broecker et al., 1973). Finally, with knowledge about the composition and solubility of the lithogenic material, it is possible to estimate the input of lithogenic particles and the fluxes of trace elements originating from the same material (Hsieh et al., 2011; Hayes et al., 2018).

Trace elements (TE) are important because they act as limiting factors for the development of phytoplankton in the photic layer. In particular, the absence of bio-available iron (Fe) has been recognized to be the main cause of low productivity in areas of the ocean's surface with abundant macronutrients like nitrogen and phosphorus (known as high nutrient, low chlorophyll or HNLC; Martin, 1990; Boyd et al., 2007). The HNLC areas occupy around one third of the world's oceans, and mainly receive Fe through the dissolution of aeolian dust (Jickells, 2005). The Southern Ocean (SO) is the largest of these HNLC regions. Away from the influence of dust plumes, islands and shallow continental shelves become a natural source of iron to the surface of the ocean enabling the proliferation of phytoplanktonic blooms (Blain et al., 2001; Tyrrell et al., 2005; Tagliabue et al., 2009; Tagliabue et al., 2014), and hence influence the oceanic carbon cycle and the sequestration of CO_2 from the atmosphere (Fung et al., 2000; Sarthou et al., 2007; Mahowald et al., 2009; Boyd and Ellwood, 2010).

The Kerguelen Plateau (KP) area hosts the largest phytoplankton bloom of the SO. It appears in the austral spring after photosynthesis is no longer light-limited, and can extend

for more than 45,000 km^2 (Blain et al., 2007). A series of voyages carried out during the summer of 2005 and spring of 2011 (KEOPS 1 & 2) significantly increased our understanding of the biogeochemistry of the region, including studies about the effect of the natural Fe fertilization on the carbon budget of the region (Blain et al., 2007; Blain et al., 2008b; Blain et al., 2008a; Jacquet et al., 2008; Jouandet et al., 2008; Mosseri et al., 2008; Sarthou et al., 2008), remote-sensing and modelling of the bloom (Bopp et al., 2008; Mongin et al., 2008), and detailed descriptions of the region's physical oceanography (Figure 1; Park et al., 2008a; Park et al., 2008b; Park et al., 2014). Particle dynamics (Venchiarutti et al., 2008; Venchiarutti et al., 2011b) and carbon fluxes (Savoye et al., 2008; Planchon et al., 2015) were studied through the analysis of thorium isotopes in the dissolved and particulate phases of seawater. Conditions favouring phytoplankton development were also investigated through data analysis from bio-profilers deployed during the KEOPS 2 voyage (Grenier et al., 2015). Other work focused on constraining the origin of the lithogenic material that provides Fe to sustain the phytoplankton bloom (van Beek et al., 2008; Zhang et al., 2008; van der Merwe et al., 2015; Grenier et al., 2018). The dominant source of iron was found to be the dissolution of sediments deposited on the plateau and transported to the surface by vertical mixing (Zhou et al., 2014), and the lateral transport of lithogenic material supplied by the Kerguelen and Heard Islands (van Beek et al., 2008; van der Merwe et al., 2015; Sanial et al., 2015). It was found that the bloom persisted even with Fe concentrations close to values known to be metabolically limiting for phytoplankton, highlighting the importance of efficient Fe recycling in the mixed layer, as well as of other sources of Fe to the region like Heard and McDonald Islands (HIMI) in the central part of the plateau (Bown et al., 2012; Bowie et al., 2015).

The Heard and McDonald Earth-Ocean-Biosphere Interactions study (HEOBI; GEOTRACES process study GIpr05) conducted in the summer of 2016 focused on sampling the central part

of the KP around HIMI. The main objectives of this voyage were to increase the knowledge on the contribution of HIMI and surrounding shallow areas to the biogeochemical cycle of Fe in the region. Special attention was paid to the role of particles originating from the islands as well as any possible hydrothermal contribution to the Fe inventory. Results from this expedition noted the importance of HIMI on the iron availability that influences the drawdown of nutrients above the plateau (Holmes et al., 2019) and also confirmed that glacial erosion can meet the previously unaccounted biological demand (van der Merwe et al., 2019). The aim of this work was to apply the method developed in the previous chapter to measure dissolved ^{232}Th and ^{230}Th concentration in samples from the HEOBI voyage. This data was used to provide an estimation of the budget of the lithogenic material released from the plateau and the associated fluxes of Fe and other TE.

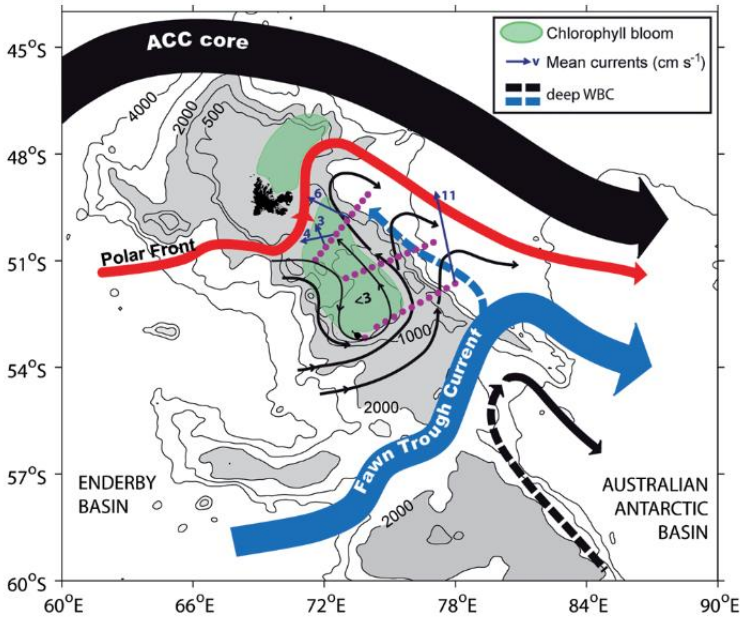

Figure 3-1. Predominant circulation pattern in the Kerguelen plateau (taken from Park et al., 2008b). The green colour represents areas where it is historically known for the bloom to appear in the region once the sun is no longer limiting in the austral spring.

2. Materials and methods

2.1 Sampling

Seawater samples were collected along the Kerguelen plateau during the HEOBI voyage during January and February 2016 onboard the R/V Investigator (Figure 2). All sampling was performed following the protocols described in the GEOTRACES intercalibration for Th and Pa isotopes (Anderson et al., 2012). Samples ranging from 5 to 10 litres were collected directly from Niskin bottles mounted on a standard CTD and filtered through a 0.8/0.2 µm AcroPak® capsule filters into 10 L pre-weighted cubitainers. Samples were then acidified with 1 mL of 11 M distilled acid per litre of sample obtaining a final pH value ~1.7. In order to determine procedural blank concentrations, 2 L of Ultra-high purity water (UPW) were collected from the onboard system and acidified in the same way as the samples. In total, 75 samples from 10 different locations (Figure 3) were analysed. Two stations (18 and 25) were sampled on the western flank of the plateau and were suggested as reference stations because of the water column characteristics at sampling time. A series of samples were collected within 1 km of Heard (30 & 31) and McDonald (22 & 34) islands in order to establish a Th signal from the islands. Station 16 was collected right in the middle of the plateau and is part of a transect that includes stations 6, 9 and 12, which were collected to sample the transition from the plateau (~450 m depth) to open water (3600 m depth) sub-Antarctic conditions.

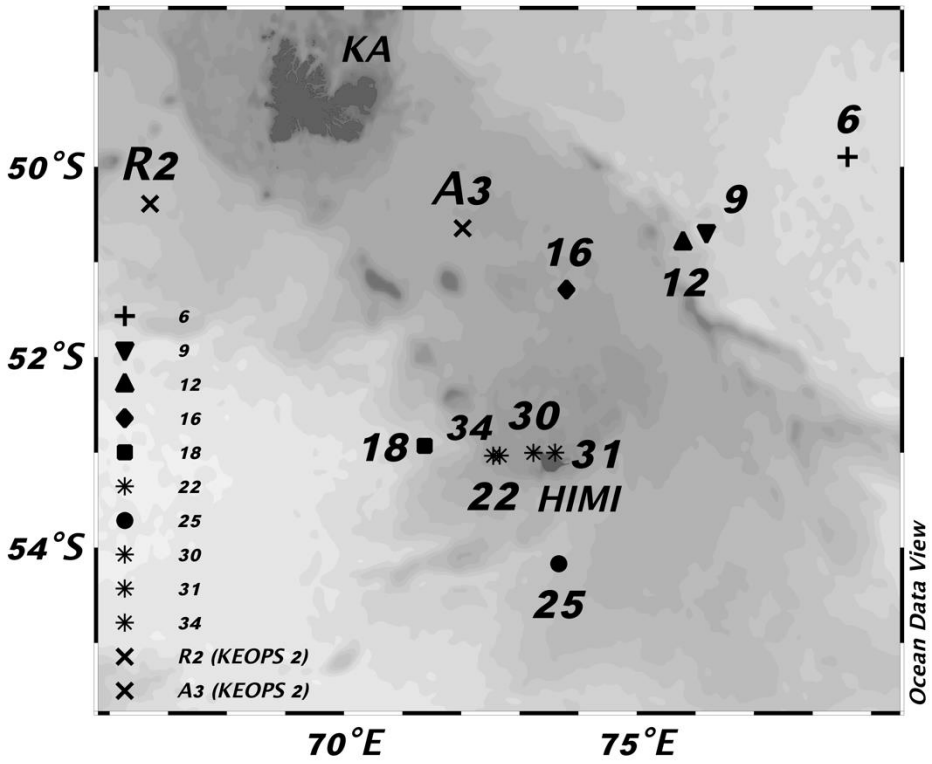

Figure 3-2. Location of the stations sampled for Th isotopes during the HEOBI voyage (January and February 2016). Included are also Stations R2 and A3 from the KEOPS 2 voyage where ^{234}Th was sampled during October and November 2011.

2.2 Pre-concentration and column chemistry

The pre-concentration and chromatographic separation applied in this study are part of a technique developed to simultaneously determine thorium and neodymium isotopes from a single seawater sample, fully detailed in Pérez-Tribouillier et al.(2019 ;see Chapter 2). Briefly, samples were spiked with 1 pg of ^{229}Th per kg of seawater and amended with ~200 µL of concentrated HF acid. Samples were left to equilibrate for at least 48 hours. After this period, 2.5 M ammonium acetate buffer solution was added until a final concentration of 0.05 M. The pH was then adjusted to 4.75 with concentrated HCl acid. Immediately after, samples were pumped through an array of two Nobias PA1L cartridges. Once all sample went through

the cartridges, remaining salts were washed off the resin with UPW. Finally, thorium and other trace elements were eluted with 5 mL of 3 M HNO_3.

After pre-concentration, samples were oxidized with 0.5 mL of a mixture of concentrated HNO_3 and $HClO_4$ acids (4:1) at 200 ^oC in order to remove any organic substances. Thorium isotopes were chromatographically separated and purified using 1 mL Bio-Rad AG1-X8 anion exchange resin (Anderson et al., 2012). Samples were transformed to the hydrochloric form and loaded onto the pre-conditioned resin in order to retain transition metals as well as uranium and protactinium isotopes. The samples were oxidized again and transformed into 8 M nitric form and loaded onto the same resin (pre-conditioned with 8 M HNO_3) in order to separate the rare earth elements. Thorium isotopes were finally eluted from the resin with 11 M HCl, oxidized and redissolved in 0.6 mL of 2% HNO_3 + 0.3% HF in preparation for analysis. Sample processing occurred in batches consisting of 10 seawater samples, a 2.5 L UPW procedure blank (spiked with ^{229}Th) and the intercalibrated reference material SW2010-2 (Anderson et al., 2012). An aliquot of this reference material was diluted in 2.5 L of UPW. Both the blank and the reference material were processed in the same way as the samples, including pre-concentration and column chemistry.

2.3 Sector field inductively coupled plasma mass spectrometry (SF-ICP-MS) analysis

The measurement of Th isotopes was performed on an Element 2 SF-ICP-MS at the Central Science Laboratory of the University of Tasmania, with sample introduction via an Aridius II desolvating nebulizer to minimize oxide formation. Isotopes with masses 229 and 230 were evaluated using counting detector mode while the more abundant mass 232 was assessed in analog detecting mode. Tailing contribution of ^{232}Th on ^{230}Th was found to be less than 0.1% of the ^{232}Th signal and considered neglectable. A maximum of 12 samples were analysed during each session, with a wash period of 5 min between samples in order to

minimize memory effects. Mass fractionation corrections were calculated using the exponential law for every analytical session with the CRM145B U isotopic reference material (New Brunswick Laboratory, USA) ($^{238}U/^{235}U$=137.88). The 2% HNO_3 + 0.3% HF solution used to re-dissolve samples was repeatedly analysed as an instrument blank. Working parameters for our instrument can be found in table 1.

Instrument	Operating Conditions
Equipment	
Nebuliser	PFA 200 µL/min; self-aspirating
CETAC Aridius 2	Sweep gas: 4.5-5 L/min; Nitrogen gas: 5-8 mL/min
Spray chamber	Heated PFA chamber
Sampler and skimmer cones	Nickel
Parameters	
ICP Torch gas flows (L/min)	0.9/0.75/15 (nebuliser/auxiliary/cooling)
RF Power (W)	~ 1250
Detection mode	229, 230: Counting; 232: Analog

Table 3-1. Operational conditions for the SF-ICP-MS during the analysis of HEOBI Th samples.

2.4 Blanks and quality control

In order to reduce blank contribution all sample processing was performed inside a ducted laminar-flow hood inside an ISO-5 environment. The procedural blank values ranged from 2-17 pg and 0.2-1.8 fg for ^{232}Th and ^{230}Th, respectively. The reproducibility of the intercalibrated reference material SW2010-2 remained within 5% of the reported values during a period of 7 months indicating good accuracy and precision (see Pérez-Tribouillier et al., 2019b).

2.5 Data treatment

The ^{232}Th and ^{230}Th signals were corrected for instrument blank and mass bias. Additionally, an average procedural blank, based on the blank determinations from all stations was also subtracted. For ^{230}Th, this signal represented less than 5 % of the total signal,

however it increased towards 10% for shallower samples. For ^{232}Th, the blank contribution was generally less than 3 %. ^{232}Th and ^{230}Th concentrations were obtained by applying the isotope dilution equations (Sargent et al., 2002). The measured ^{230}Th concentrations were corrected for ingrowth due to decay of ^{234}U during the storage period. The ingrowth was calculated based on the ^{238}U concentration of each sample using the relation ^{238}U (ng g-^{1}± 0.061) = 0.100 × Salinity-0.326 (Owens et al., 2011) and considering a λ^{234} of 2.8263×10^{-6} yr^{-1} and a sample storage time of 2 years (Eq. 1).

$$^{230}Th_{IG} = {}^{234}U \times \left(1 - e^{(\lambda \times \text{years})}\right) (Eq. 1)$$

The contribution of lithogenic ^{230}Th was also corrected using the measured ^{232}Th concentration of each sample and a ^{230}Th/^{232}Th for the lithogenic material of 4.0X10^{-6} mol/mol (Roy-Barman et al., 2009; Eq. 2). The ingrowth correction varies from 5 to 50 % and is higher towards the surface of each station because of the lower ^{230}Th concentrations. The contribution of lithogenic material is much smaller, being less than 2% for most of the samples.

$$^{230}Th_{xs} = {}^{230}Th_{IG\ CORR} - {}^{232}Th_{measured} \times \left[{}^{230}Th/{}^{232}Th\right]_{litho} (Eq. 2)$$

The corrected ingrowth and lithogenic corrected $^{230}Th_{xs}$ concentrations were used to obtain a residence time for thorium as shown in equation 3 (Hayes et al., 2013):

$$Residence\ time\ (\tau_{Th}) = \frac{\int_0^z dissolved\ {}^{230}Th_{xs}\ activity\ dz}{\int_0^z {}^{234}U activity \times \lambda_{230}\ dz} (Eq. 3)$$

where the dissolved ^{230}Th activity is the measured concentration converted into dpm terms, the ^{234}U activity was obtained from the salinity, and λ_{230} (9.2x10^{-6} year^{-1}) is the radioactive decay rate of ^{230}Th. This obtained Th-residence time was then used to calculate a dissolved ^{232}Th flux by dividing the depth-integrated ^{232}Th inventory by the residence time (eq. 4):

$$Dissolved\ ^{232}Th\ flux = \frac{\int_0^z dissolved\ ^{232}Th\ activity\ dz}{\tau_{Th}\ (dz)}\ (Eq. 4)$$

The dissolved ^{232}Th flux was then used to estimate a particulate lithogenic flux considering the content of ^{232}Th in the lithogenic material around the Kerguelen Plateau (5.3 ppm; Duncan et al., 2016) and the solubility of ^{232}Th as shown in equation 5.

$$Lithogenic\ flux\ (z) = \frac{Dissolved\ ^{232}Th\ flux\ (z)}{[Th]_{Kerg}\ \times\ S_{Th}}\ (Eq. 5)$$

Subsequently, with knowledge about the composition and solubility of metals relative to ^{232}Th, it is possible to produce an estimation of dissolved metal fluxes originating from the dissolution of lithogenic particles as follows:

$$Dissolved\ metal\ flux = \left[\frac{metal}{^{232}Th}\right]_{Kerg} \times \left(\frac{S_{metal}}{S_{Th}}\right) \times Dissolved\ ^{232}Th\ flux \text{ (Eq. 6)}$$

3. Results

3.1 Water mass distribution during the HEOBI voyage

The temperature-salinity diagram (Figure 3) indicates that the samples from stations located near HIMI (stations 22,30,31 and 34) have salinities below 34 psu and temperature above 2 °C that are consistent with the properties of the Antarctic Surface Water (AASW). Similar temperature-salinity properties are found for the surface waters at the other stations, except at Station 6. At this station, above 75 m the water temperature is greater than 4.5 °C and density below 26.75. These properties might indicate the presence of the Polar Front Surface Water (PFSW; Park et al., 2014). Below the mixed layer, Stations 9, 16, 18 and 25 exhibit a subsurface temperature minimum (< 2 °C) and fresher water (<34.2) than deeper layers. These characteristics match the definition of Winter Water reported in the Kerguelen Plateau and centred at ~200 m depth (Park et al., 2008b). Below 300 m, there is a transition

to the UCDW associated with a temperature maximum of ~2.5 °C and an oxygen minimum (180 μmol L^{-1}). A deep salinity maximum confirms the presence of Lower Circumpolar Deep Water (LCDW). Below 2,600 m, Stations 6, 9 and 18 properties indicate the presence of Antarctic Bottom Water (AABW). with low temperature and salinity but with a higher oxygen content towards the bottom (Park et al., 2008b). This water-column composition is typical of the austral summer (Park et al., 1998) and is consistent with the findings of other studies (Park et al., 2008b; Park and Vivier, 2011; Park et al., 2014; Holmes et al., 2019) . Conductivity, temperature, depth and other water column properties can be found in Australian Marine National Facility data access portal (http://www.marlin.csiro.au/geonetwork/srv/eng/search#!6ba5a0ce-b87a-4bda-b16c-3527279c3bca).

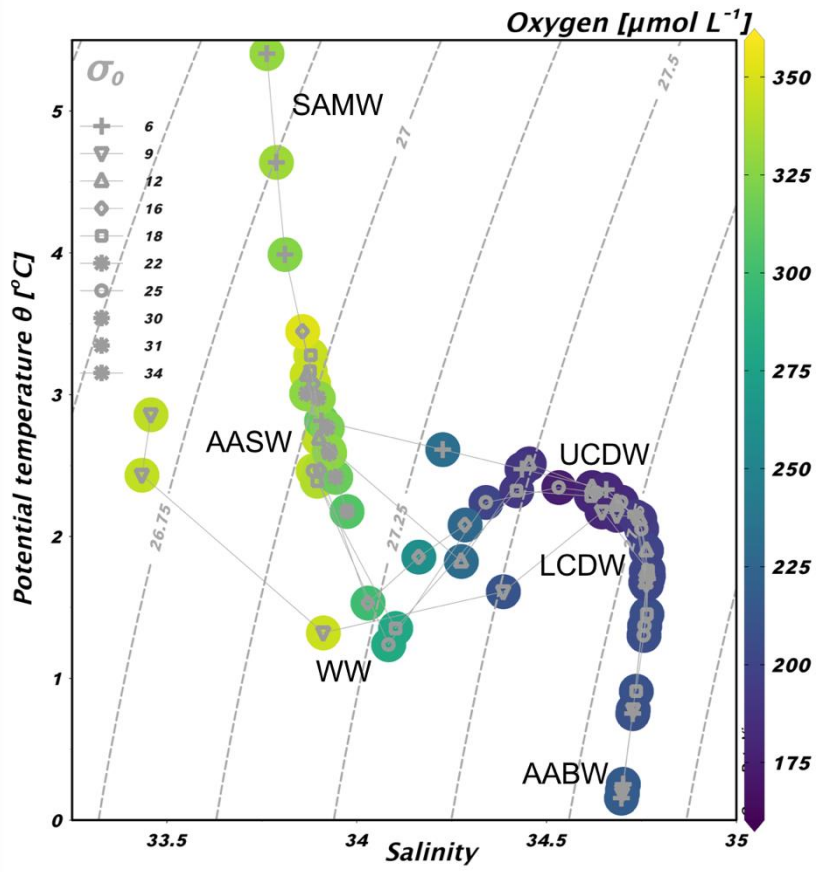

Figure 3-3. Temperature-salinity diagram for the samples collected during the HEOBI voyage.

3.2 ^{232}Th and ^{230}Th concentrations

3.2.1 Plateau and off-plateau stations

$^{230}Th_{xs}$ concentrations in the samples range from 0.7 fg kg^{-1} (CTD18, 60 m) to 18.2 fg kg^{-1} (CTD6, 3579 m). These values are similar to other parts of the SO including the Weddell Sea (Rutgers van der Loeff and Berger, 1993), the Drake Passage (Venchiarutti et al., 2011a), the Crozet Basin (Coppola et al., 2006) and particularly similar to a previous study in the Kerguelen plateau (Venchiarutti et al., 2008).

All profiles indicate a roughly linear increase of $^{230}Th_{xs}$ concentrations with depth (Figure 4). This is more evident in the upper 600 m of the water column. Below that depth, Stations 9 and 25 and 12 (to a lesser extent) indicate some concave features. By contrast, Stations 6 and 18 show a depletion of $^{230}Th_{xs}$ towards the bottom. Similar mixed features in the $^{230}Th_{xs}$ concentration profiles have been observed in other oceanic settings in the Southern Atlantic (Moran et al., 2002; Deng et al., 2014), the Arctic (Trimble et al., 2004; Grenier et al., 2019), and along the path of the ACC (Rutgers van der Loeff and Berger, 1993; Venchiarutti et al., 2011a), including the Kerguelen plateau (Venchiarutti et al., 2008).

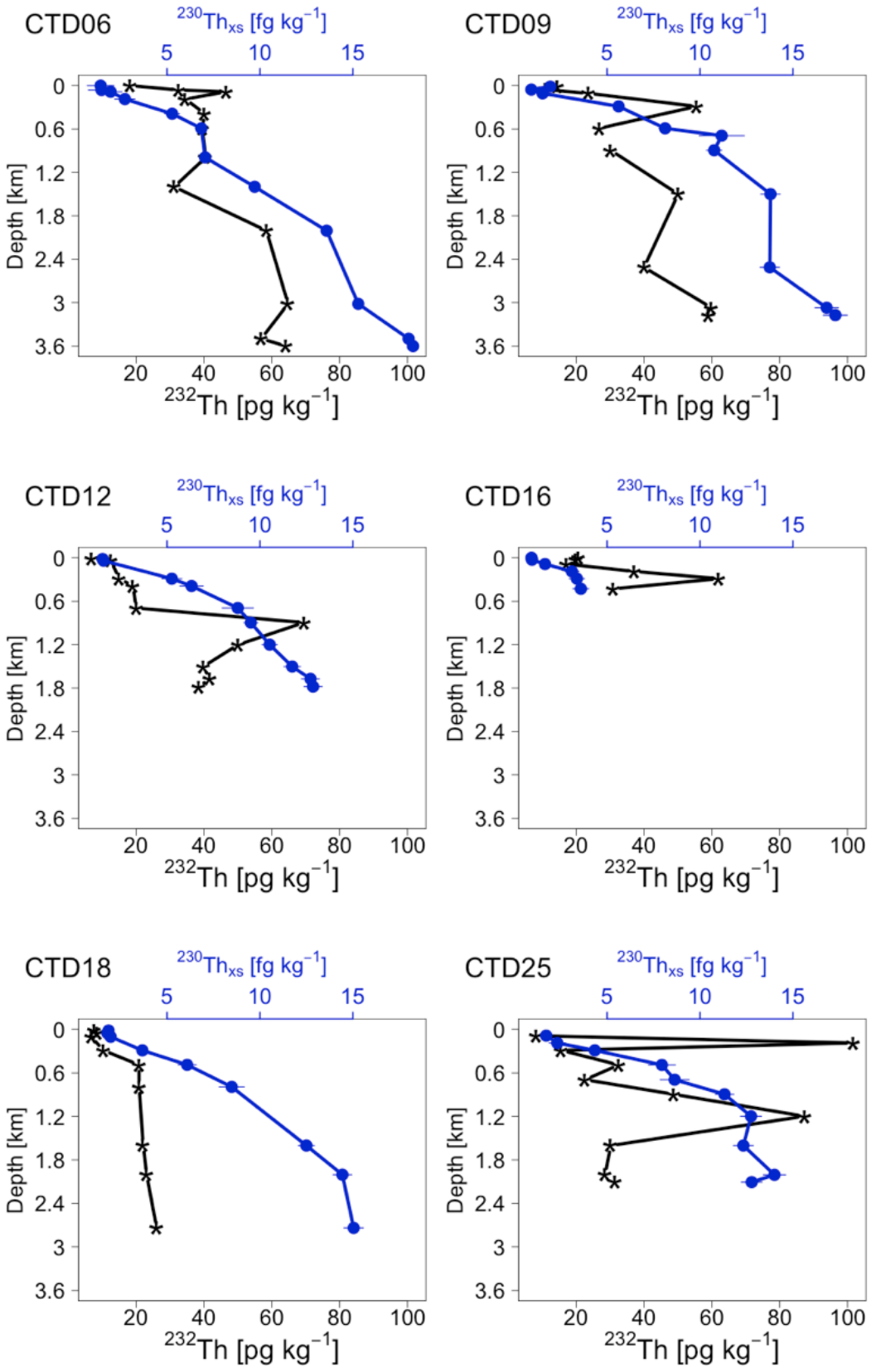
CTD06
CTD09
CTD12
CTD16
CTD18
CTD25
$^{230}Th_{xs}$ [fg kg^{-1}]
5
10
15
Depth [km]
0
0.6
1.2
1.8
2.4
3
3.6
20
40
60
80
100
^{232}Th [pg kg^{-1}]

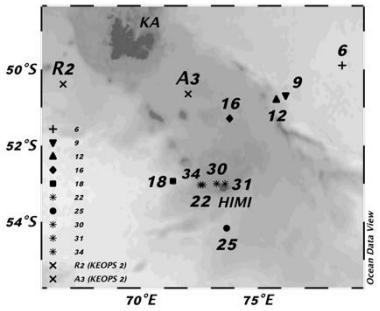

Figure 3-4. ^{232}Th (stars) and $^{230}Th_{xs}$ (circles) concentrations of the vertical profiles for the HEOBI non-coastal stations. Note that the deepest sample of each profile was collected ~10 m above the bottom.

The dissolved ^{232}Th concentrations range from 6.9 pg kg^{-1} (CTD12, 30 m) to 101 pg kg^{-1} (CTD25, 200m). Most of our data is within the same order of magnitude of previous ^{232}Th concentrations reported in the plateau by Venchiarutti et al., 2008. However, in this study they report several samples with high concentration that in some cases are as much as 4.5 times higher (450 pg kg^{-1}) the values found in our samples near HIMI.

With exception of Station 18 and 12, all profiles show a subsurface maximum in the ^{232}Th concentration. Below 600 m, ^{232}Th concentrations generally increase with depth, however some spikes stand out in most of the stations (Figure 4). Particularly, Station 25 shows two prominent peaks at 200 m (100 pg kg^{-1}) and 1200 m (87 pg kg^{-1}). Such concentrations could very easily be a result of contamination during sampling or analysis. However blank contribution at that station remained low. Therefore, and because of the higher concentrations previously reported for the plateau we cannot rule out those measurements. However, these concentrations need to be treated with discretion and will not be discussed in detail in the following sections.

3.2.2 Near-island shallow stations

The samples collected close to Heard (Stations 30, 31) and McDonald (Stations 22, 34) Islands (Figure 2) presented a fully-mixed water column with ^{232}Th and ^{230}Th concentrations that seem to be quite uniform regardless of the location and depth (Table 2). The mean ^{232}Th concentration of these samples is 87.5 $\pm$ 13 pg kg^{-1} (1-σ). This range of concentrations is amongst the highest of our data set and can be compared with ^{232}Th concentrations (84 – 273 pg kg^{-1}) found near Heard Island during the KEOPS 1 expedition (Venchiarutti et al., 2008). The mean $^{230}Th_{XS}$ concentration of these samples is 2.7 $\pm$ 1.2 fg kg^{-1} (1-σ). These concentrations are higher than the ones reported in the previously mentioned study around HIMI (0.5-1.35 fg kg^{-1}). In particular the ^{230}Th concentration of Sample 30 at 75 m (5.5 fg kg^{-1}) is unusually high for that depth.

Station	Depth [m]	^{232}Th [pg kg^{-1}]	1-σ [pg]	$^{230}Th_{xs}$ [fg kg-1]	1-σ [fg]	$^{232}Th/^{230}Th$
34	50.0	96.6	1.9	2.8	0.3	28,695 ± 1545
34	80.0	94.3	1.9	4.1	0.4	25,278 ± 1361
34	122.0	81.5	1.6	3.9	0.2	32,600 ± 1756
31	45.0	81.3	1.6	3.5	0.2	16,938 ± 912
30	88.0	59.8	1.2	2.5	0.2	16,162 ± 918
30	75.0	88.8	1.8	5.5	0.4	12,870 ± 731
22	151.0	100.8	2.0	2.3	0.2	27,243 ± 1853
22	190.0	96.8	1.9	2.5	0.2	24,821 ± 1688

Table 3-2. ^{232}Th, $^{230}Th_{xs}$ and $^{232}Th/^{230}Th$ ratio in the near-island stations 22, 30, 31 and 34.

3.4 $^{232}Th/^{230}Th$ ratios

The highest $^{232}Th/^{230}Th$ ratios are found near HIMI (Table 2), with a maximum value of 32,600 found at Station 34 at 122 m depth, and the lowest a value of 1,735 at reference Station 18 at 2,200 m depth. The water column profile of the ratios shows an enrichment of ^{232}Th above 600 m (σ_θ ~ 27.7 kg m^{-3}; Figure 5), with the exception of Station 18 that exhibits an almost uniform ratio with depth. Below 600 m, Stations 6 and 9 also indicate a uniform $^{232}Th/^{230}Th$ ratio.

Additionally, Stations 12 and 25 also exhibit ^{232}Th enrichments at 900 and 1,200 m respectively.

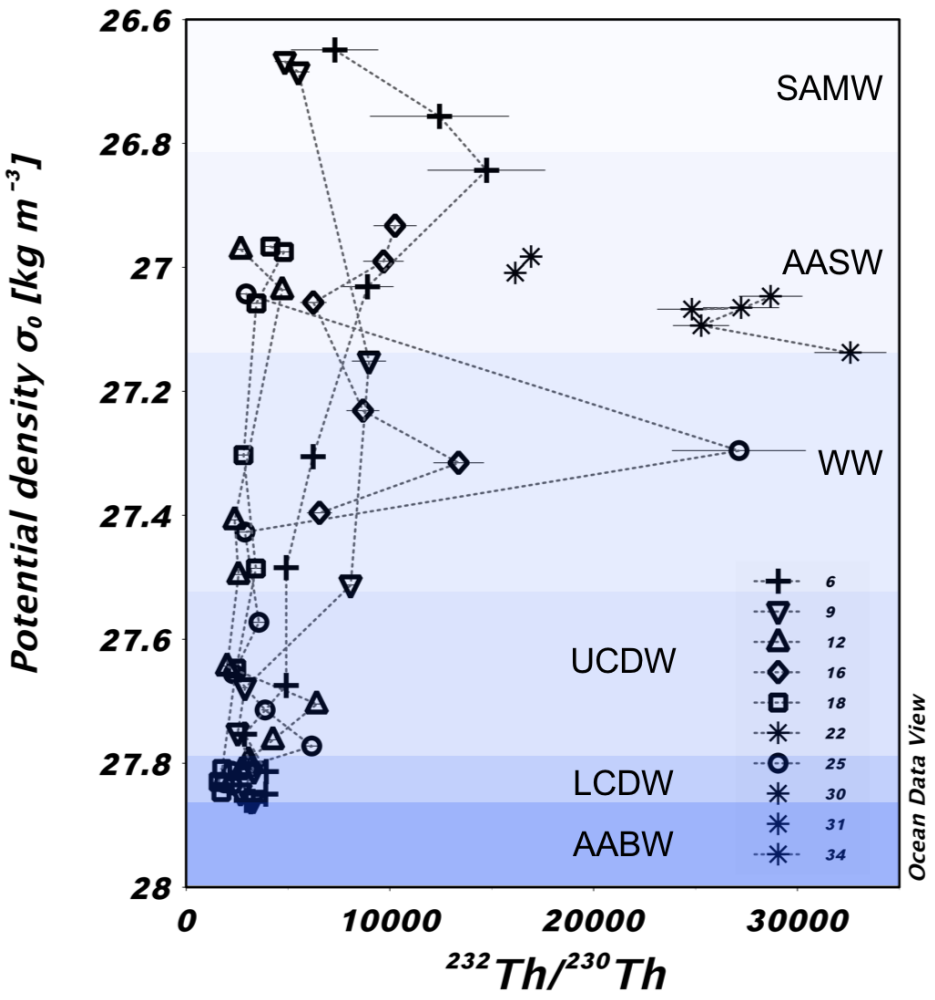

Figure 3-5. ^{232}Th/^{230}Th atom ratio plotted against potential density for the HEOBI samples. Different background shading indicates the different water masses sampled during the HEOBI voyage. Standard error of many of the samples is smaller than the symbol. Note that the bottom sample of each station was collected ~10 m above the seafloor.

4. Discussion

4.1 ^{232}Th enrichments above the plateau and the contribution from hydrology

Lithogenic material from the plateau allows the development of productivity once the light is no longer limiting in the region. Supplied by the direct weathering and erosion of the islands, glacial run-off and resuspension of shelf-deposited sediments, this material releases

Th isotopes, Fe and other trace elements (Figure 6). Because ^{232}Th is released to the ocean only by the dissolution of this type of material, it can be used to track this supply.

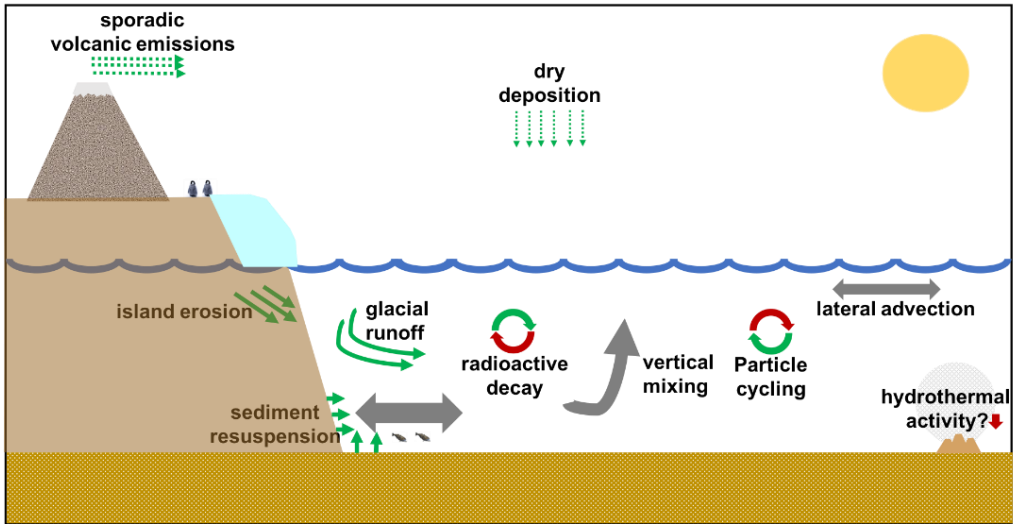

Figure 3-6. Possible sources (green arrows), sinks (red arrows) and transport vectors (grey arrows) of thorium isotopes and other trace elements to the waters of the Kerguelen Plateau.

Without the influence of the plateau, it would be expected for the $^{232}Th/^{230}Th$ ratio to remain constant throughout the water column. Such a behaviour can be seen in Station 18 (Figure 5, squares) where the ratio remains fairly uniform (2910 ± 1100). Such a pattern is caused because in this station the ^{232}Th and ^{230}Th concentrations are controlled almost entirely by the adsorption/desorption into particles. This process, known as reversible scavenging, dominates in oceanic environments (Anderson et al., 1983; Nozaki and Nakanishi, 1985). These characteristics allow us to establish Station 18 as a reference of oceanic conditions. By contrast, the rest of the stations show -at different extents- ^{232}Th enrichments in the top 500 m of the water column. These enrichments "fingerprint" the supplies of lithogenic material from the Kerguelen Plateau to the AASW, WW and the top layers of the UCDW (Figure 5). As expected, this imprint is more intense in the near-island Stations 22,30,31 and 34 because there is a direct and constant inputs of lithogenic material,

generating much higher $^{232}Th/^{230}Th$ ratios. Once this material enters the ocean, it releases dissolved ^{232}Th, Fe and other trace elements. These dissolved elements as well as some lithogenic particles can be transported away from the islands by the local circulation, enabling a downstream development of the productivity. In fact, the historical positions of both branches of the bloom that occur in the KP (Figure 1, green areas) match the topography-following circulation (constrained by the PF) in the northern and central parts of the plateau respectively.

Considering $^{232}Th/^{230}Th$ as a fingerprint of lithogenic inputs and that most of the lithogenic material is supplied to the surface, we would expect a gradient in surface spatial distribution of the $^{232}Th/^{230}Th$, being higher near the source and decreasing as the signal is transported away due to mixing. Unfortunately, our Th data over the plateau has not enough spatial distribution to accurately track the possible pathways of the surface/subsurface circulation. However, some pattern does exist in the $^{232}Th/^{230}Th$ distribution that seems to confirm the importance of the HIMI in the natural fertilization of the waters north of these islands (Figure 7; van Beek et al., 2008; Zhang et al., 2008; Grenier et al., 2018; Holmes et al., 2019; van der Merwe et al., 2019). The $^{232}Th/^{230}Th$ ratio near HIMI is the highest for the surface of our dataset (22,259 ± 6600, n=8). In the middle of the plateau at Station 16 this value decreases to 10,262 ± 1042. Considering the northwards predominant circulation in this part of the plateau (Figure 2, Park et al., 2008b), this lower $^{232}Th/^{230}Th$ value could be very well attributed to a dilution of the HIMI signal. This hypothesis is supported by the low $^{232}Th/^{230}Th$ ratio (4141 ± 341) found upstream at Station 18. This station is located right before the circulation turns west towards HIMI and, at this point, seawater has not received any contribution from the lithogenic material from the plateau. After the current passes next to HIMI and travels north towards Station 16 at a speed of 2.6 km day^{-1}, some component turns

east and reaches station 9 where the value has decreased to 4853 ± 500. Enrichment at station 12 is even smaller (2,683 ± 240). A possible explanation for this anomalously low ^{232}Th concentration might be that it is flushed away by the western boundary current that flows along the eastern flank of the plateau (Figure 1). The surface enrichment at Station 6 (7,300 ± 200) is higher than at Station 9, even though this station is further away from the plateau. In this region however, the circulation from the central Kerguelen Plateau converges with the flow of the Polar Front, probably causing an increase in the surface ^{232}Th/^{230}Th ratio. A more detailed sampling above the central part of the plateau, especially between HIMI and Station 16 would have been useful to better constrain the circulation over the plateau using only the ^{232}Th/^{230}Th signal. However, in the next chapter of this thesis we use Rare Earth Element concentrations and Nd isotopic composition to further investigate this.

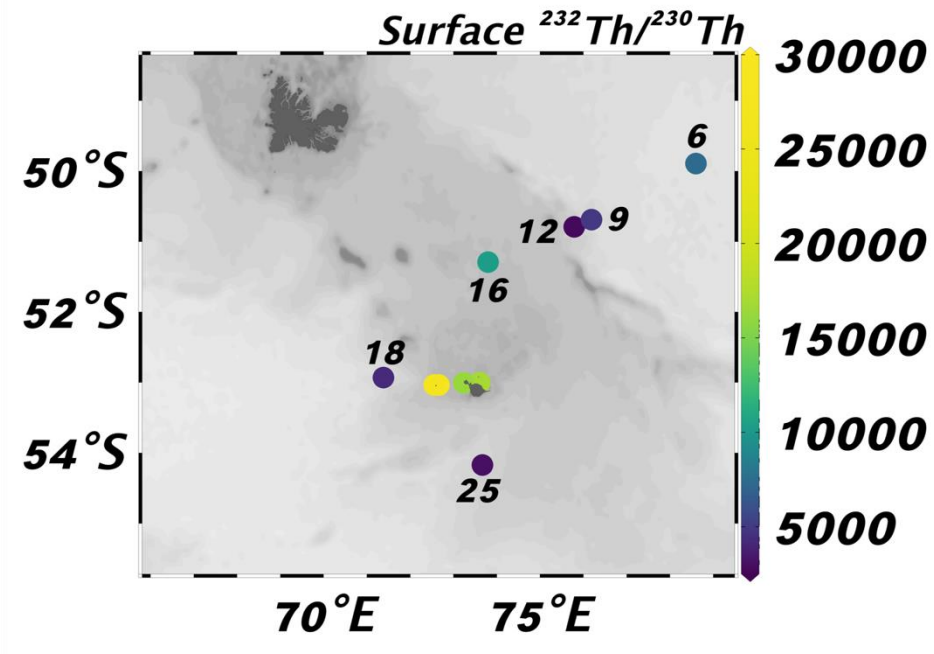

Figure 3-7. Spatial distribution of the surface ^{232}Th/^{230}Th atom ratio over the plateau.

4.2 Th-scavenging removal residence time in surface waters of the Kerguelen Plateau

The calculation of ^{232}Th fluxes requires information about its removal rate from the dissolved fraction of seawater. This residence time can be obtained from the less abundant

isotopes ^{228}Th, ^{230}Th and ^{234}Th and the disequilibria from their parent nuclides. In fact, the short lived ^{234}Th isotope ($t_{1/2}$=24.1 days) is routinely used to estimate the export of Particulate Organic Carbon (POC) from the surface of the ocean (Buesseler et al., 1992; Cochran et al., 2000). Using ^{230}Th to calculate surface residence times has also been applied (Hsieh et al., 2011; Hayes et al., 2013; Deng et al., 2014). However, these studies have shown that ^{230}Th derived residence time (230_{RT}) can be affected by upwelling and vertical mixing of "pre-formed" ^{230}Th and probably by the particle size fractionation (Coppola et al., 2006), although more studies concerning this latter point are needed.

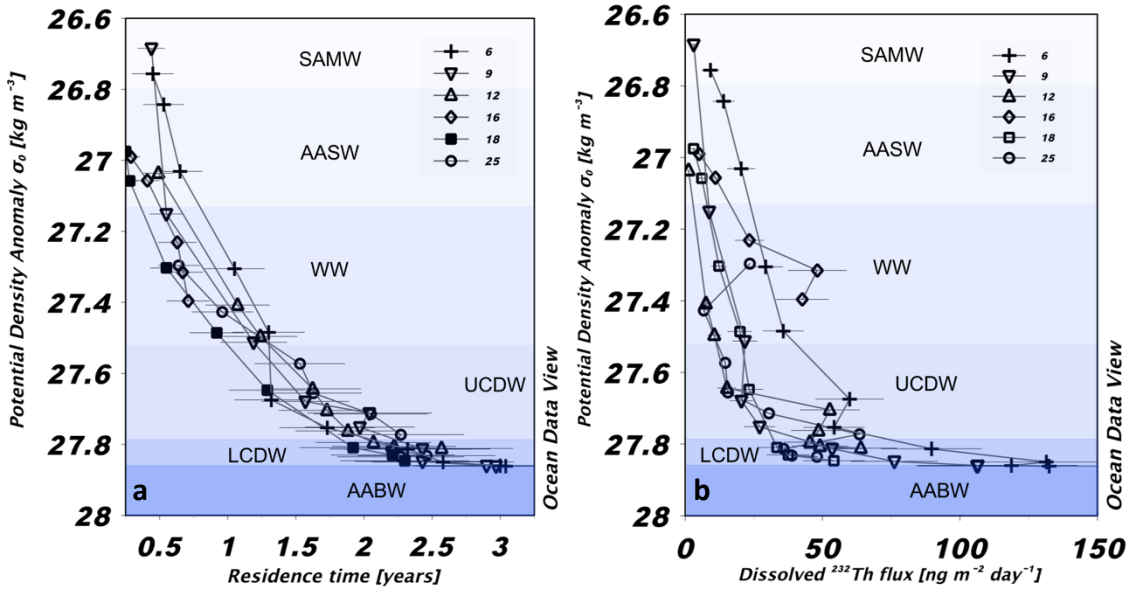

Figure 3-8. Estimated scavenging residence time (a) and ^{232}Th flux (b) for the HEOBI stations. Error was propagated considering all the parameters used for the calculation and represent around 25%. Note that the deepest samples of each station were collected ~10 m above the bottom.

The 230_{RT} increases gradually with depth reflecting the long-term process of ^{230}Th adsorption and desorption from particles through its path down the water column (Figure 8a; Nozaki et al., 1981; Anderson et al., 1983). In particular, 230_{RT} for the top 300 m is less than a

year in all stations (Figure 8). The value at 430 m in Station 16 is slightly lower (0.7 years) due to enhanced scavenging of ^{230}Th by sediments resuspended from the bottom. The mixed layer 230_{RT} (Table 3) in Station 12 is higher than the rest of the stations very likely because of the influence by the Fawn Through Current that brings higher concentrations of "pre-formed" ^{230}Th from deeper depths, thereby increasing the residence time.

Station (ML depth)	ML residence time (years)	500 m residence time (years)	ML diss. ^{232}Th flux [ng m^{-2} day^{-1}]	500 m dissolved ^{232}Th flux [ng m^{-2} day^{-1}]
6 (110 m)	0.53 ± 0.15	1.17 ± 0.22	14 ± 4	33 ± 6
9 (154 m)	0.55 ± 0.12	1.42 ± 0.26	9 ± 2	21 ± 5
12 (189 m)	1.07 ± 0.23	1.46 ± 0.31	8 ± 2	12 ± 3
16 (181 m)	0.63 ± 0.14	0.71* ± 0.16	23 ± 5	43 ± 9
18 (282 m)	0.55 ± 0.12	0.92 ± 0.20	12 ± 3	20 ± 5
25 (202 m)	0.64 ± 0.15	1.53 ± 0.33	24 ± 5	15 ± 3

Table 3-3. 230_{RT} and ^{232}Th fluxes at the mixed layer depth and 500 m during the HEOBI voyage. $^{*}230_{RT}$ for Station 16 was calculated at 430 m. Error has been propagated considering all variables used for the calculation of the residence time and ^{232}Th flux. If a measurement was not available at the ML depth or at 500 meters, the ^{230}Th concentration was calculated using a lineal interpolation between the closest samples.

These mixed layer 230_{RT} values are comparable to the ones found in the North Pacific (0.7-1.2 years; Hayes et al., 2013), but shorter compared to data obtained in the Atlantic Ocean (1.2-2.5 years; Hsieh et al., 2011; Deng et al., 2014). This difference is expected because the stations from the mentioned studies in the Atlantic were collected in a more oceanic environment, away from direct sources of particles other than the deposition of aeolian dust. By contrast, the sampled areas of the North Pacific and the KP are closer to lithogenic sources. This causes a larger supply of particles to the surface that increases scavenging rates, subsequently shortening 230_{RT}. At 500 m however the 230_{RT} for the KP is considerably shorter than in the Pacific at the same depth (3.3-6.4 years; Hayes et al., 2013) and in the Atlantic at

250 m (3.5-6.4 years; Deng et al., 2014). This difference can be explained because of the shallow bathymetry over the plateau (< 500 m) and its interaction with the ACC that generates a dynamic coastal environment and a continuous load of particles, even at 500 m, which increases scavenging rates thus shortening the residence time.

Using ^{230}Th to obtain scavenging removal rate has so far not been applied in coastal environments, which prevents a direct comparison of our results. In order to compensate this lack of information, equation 3 was applied to ^{234}Th data generated during the KEOPS 2 voyage (Table 4; Planchon et al., 2015). Although the samples were not collected the same year or at the exact same location, we consider that both datasets were collected close enough and during the same season, legitimizing the comparison (Figure 2). Both reference stations are located on the western flank of the plateau, in an area of relatively calm dynamics. The on-plateau stations are located over the central KP in the area where the seasonal phytoplanktonic bloom occurs north of HIMI.

	^{234}Th residence time (days)		^{230}Th residence time (days)	
	Reference (R-2)	Plateau (A-3)	Reference (18)	Plateau (16)
100 m	60 ± 20	30 ± 10	102 ± 37	150 ± 26
400 m	61 ± 19	31 ± 8	266 ± 40	259 ± 33

Table 3-4. Residence time obtained using ^{230}Th and ^{234}Th data at a reference and a plateau station during the KEOPS 2 and HEOBI voyage.

It is clear that the 230_{RT} is longer than ^{234}Th derived residence time (234_{RT}) in both settings and this difference increases with depth (Table 4). The residence time at 100 m in the reference stations is ~100 days for 230_{RT}, which is slightly higher than 60 days calculated for 234_{RT}. Over the plateau 230_{RT} (150 days) is 5 times longer than 234_{RT} (30 days). At 400 m the difference becomes more evident being 230_{RT} around 4 and 8 times longer in the reference

and plateau stations respectively. As stated before, towards the surface this discrepancy could be the effect of vertical mixing of ^{230}Th. To constrain the extent of vertical mixing, we have calculated a dissolved ^{230}Th concentration gradient through the mixed layer and multiplied by the vertical mixing coefficients for the plateau (K_v=26 m^2 day^{-1}) and reference station (K_v=9 m^2 day^{-1}) reported in Rosso et al. (2014) and Bowie et al. (2015). Additionally, an upwelling flux was calculated by multiplying the ^{230}Th concentration at the base of the mixed layer by the upwelling velocities at the two different locations (reference=0.13 m day^{-1}; plateau=0.5 m day^{-1}; Rosso et al., 2014; Bowie et al., 2015). Together, vertical mixing and upwelling supply an amount of ^{230}Th equivalent to 15% to 30% of the production rate of ^{230}Th in the mixed layer, which could lead to an overestimation of 230_{RT} by a factor of 1.1 to 1.3. Therefore, vertical transport can explain the difference between 230_{RT} and 234_{RT} in the surface of the reference station. However, it is not enough to account for the 5 times longer 230_{RT} over the plateau's mixed layer. With our data we cannot completely explain this difference. Coppola et al.(2006) found that in the Indian Sector of the Southern Ocean (just north of the KP), ^{234}Th preferentially adsorbs into larger particles while ^{230}Th seems to have more affinity to smaller-size particles. A higher particle flux and a potentially larger proportion of large-size particles over the plateau would remove ^{234}Th more efficiently from solution hence producing shorter residence time. This could be an explanation for the different residence times obtained with ^{234}Th and ^{230}Th, respectively. However, it is not expected for different isotopes of such a heavy element to present significant differences in their chemical behaviour. We are more inclined to believe that the residence time difference is due to the distinct timescales over which the two isotopes integrate. These findings however, suggest the need of more studies that confirm that there is no effect from the particle size composition on the scavenging of thorium isotopes.

With depth 230_{RT} increases even more because the longer half-life of ^{230}Th allows it to accumulate, while ^{234}Th decays away, causing an increase in the ^{230}Th/^{234}Th ratio and therefore 230_{RT} is much larger deeper in the water column. Results from this section indicate that ^{230}Th can be used to estimate scavenging removal rates even in coastal environments like the Kerguelen plateau. Results also confirm that while 234_{RT} might be more appropriate to estimate surface removal rates, 230_{RT} provides a better representation of dissolved/particulate interactions over an integrated depth interval which is likely to be more similar to ^{232}Th residence time.

4.3 Thorium-derived lithogenic fluxes from the Kerguelen Plateau

To obtain an estimation of the flux of lithogenic material with dissolved thorium-isotopes data, it is necessary to convert ^{232}Th concentrations into a dissolved flux using the residence time calculated in the previous section, based on the assumption that ^{232}Th and ^{230}Th are similarly scavenged by the particles. For this, dissolved ^{232}Th concentrations were integrated from the surface to sample depth and divided by the corresponding 230_{RT} (Figure 8; Eq. 4). As a starting point to quantify the lithogenic flux from all the sources over the plateau, we calculated dissolved ^{232}Th fluxes for the mixed layer at each station and compared them with values obtained at 500 m to cover the subsurface peaks of ^{232}Th concentration. At all stations except 25, the dissolved ^{232}Th flux increases with depth at almost the same rate as the increase of the 230_{RT} (Table 3). This is an indication that the ^{232}Th inventory increases with a deeper integration depth as expected due to a decrease in the removal rate (Hayes et al., 2013). An overestimation of the mixed layer 230_{RT} due to upward transport of ^{230}Th can also produce an apparent increase of the ^{232}Th flux with depth. Applying the same approach to quantify the vertical transport as in the previous section, shows that 230_{RT} can be overestimated as much as by a factor of 1.4. This amount cannot fully explain the difference

in the ^{232}Th flux at 500m compared to the ML because it will still be an increase in the ^{232}Th flux with depth. In a similar way, lateral advection can produce an overestimation of ^{232}Th flux. Considering the results discussed in the first section of the discussion it is obvious that there is ^{232}Th being laterally transported at some extent to all stations. However, this ^{232}Th is very likely to be originated in the plateau and therefore we don't consider it to be an overestimation as it is just another local lithogenic source, and we are interested in quantifying all the sources of ^{232}Th originated from the KP.

The 230_{RT} in the mixed layer represents the short-term mixture of the different lithogenic sources. Integrating the flux of ^{232}Th to 500 m additionally captures the exchanges of ^{232}Th between the dissolved and particulate phases as it sinks down the water column. In Station 16 the 230_{RT} at 500 m also account for possible contributions from the dissolution of bottom sediments. Therefore, we select a 500 m depth to better represent a net input of material originating from the plateau.

The ^{232}Th fluxes (Figure 8b) can now be converted to lithogenic-material fluxes with the proper knowledge about the composition of the material and its solubility (Eq. 5). In other words, this flux of lithogenic material gives information about the amount of material required to sustain the calculated dissolved ^{232}Th fluxes and therefore measured concentrations of ^{232}Th. Previous studies dedicated to quantifying the input of dust to the ocean have used the average ^{232}Th concentrations of the upper continental crust, which can range from 10.5 ppm to 14.6 ppm (Taylor and McLennan, 1985; Rudnick and Gao, 2013; Serno et al., 2014). Volcanic material, however, is known to have lower ^{232}Th concentrations. As the KP is a volcanic province we use the average concentration of ^{232}Th in rocks collected around the Kerguelen Plateau (5.4 $\pm$ 1.5 ppm; Duncan et al., 2016; J. Fox 2019, personal communication).

The largest source of uncertainty in the calculation of lithogenic fluxes is the solubility of ^{232}Th from particles, which is a highly unconstrained parameter, especially for volcanic-derived material. From the few studies that report the ^{232}Th solubility in marine particles, highly variable values were found ranging from 1-23 % depending on the particle size and depth (Arraes-Mescoff et al., 2001; Roy-Barman et al., 2002). Experiments to constrain the solubility from sediments and particles from the Kerguelen Plateau are on their way, however for this manuscript we have no other option than to use the above-mentioned solubility range.

Area of Study	Lithogenic flux [mg m^{-2} day^{-1}]
HEOBI Th derived flux (S_{Th}=1%)[a]	144 - 810
HEOBI Th derived flux (S_{Th}=20%)[b]	7 - 39
Kerguelen Plateau (KEOPS 2, Bowie et al., 2015)	35 - 628
Ross Sea (Chiarini et al., 2019)	26.5 - 148
Southern Ocean, along 170W (Honjo et al., 2000)	0.14 - 2
Bransfield Straight (Wefer et al., 1987)	8.4 - 777

Table 3-5. Fluxes of lithogenic material for the top 500 m of the water column in different areas of the Southern Ocean. First two rows show fluxes obtained based on thorium long-lived isotopes considering a Th concentration in lithogenic material of 5.3 ppm and solubility of [a]1% and [b]20%. The rest of the columns show data obtained with sediment traps by other studies.

When using a Th solubility of 1 % we obtain fluxes of lithogenic material that range from 144 – 810 mg m^{-2} day^{-1} in the top 500 m of the water column, while the values range from 7-39 mg m^{-2} day^{-1} when using a Th solubility from particles of 20% (Table 5). The dissolved thorium estimated lithogenic fluxes are much higher than the values reported in a transect along the Southwest sector of the Pacific Ocean (Honjo et al., 2000). This difference is consistent with the oceanic setting of the Pacific Ocean stations at 170W, away from any

lithogenic source. Our calculated lithogenic fluxes are however comparable to fluxes obtained from sediment traps in more "coastal" parts of the Southern Ocean like the Ross Sea (Chiarini et al., 2019) and the Bransfield Straight (Wefer et al., 1988). Furthermore, all of our Th-derived lithogenic fluxes fall within the range reported over the KP using drifting sediment traps (Table 5; Bowie et al., 2015). These results confirm that the Th solubility is a highly variable parameter and that more studies are needed for this investigation. Despite of this, lithogenic material flux calculation using thorium isotopes for coastal areas seems to be promising and once the Th solubility in the plateau is better constrained, it is expected to produce values closer to reality.

4.4 Quantification of metal fluxes to the plateau

In a similar way as in the previous section, ^{232}Th fluxes can be used to estimate fluxes of Fe and other trace elements from lithogenic material. For this, information about the metal concentration in lithogenic particles and its solubility relative to that of ^{232}Th is required (Eq. 3). The solubility of trace elements in lithogenic particles is again a highly unconstrained parameter, moreover, data on the solubility of trace elements with respect of thorium has so far not been reported. However, it has been suggested that relatively insoluble elements (like Th and Fe) tend to present a similar solubility over a longer period of time (Hayes et al., 2013). Considering that the residence time at 500 m depth is around a year, we can expect that the relative solubility of Fe and Th at this depth should be close to one. Making this assumption and considering the Fe/^{232}Th ratio of lithogenic material of the KP (21,195 g g^{-1}, Duncan et al., 2016; J. Fox 2019, personal communication), we obtain Fe fluxes that range from 716 - 2,220 nmol m^{-2} day^{-1}. These values are within the same order of magnitude and range of dissolved Fe fluxes obtained through the use of drifting sediment traps in the KP, which range between 188 and 3,722 nmol m^{-2} day^{-1} (Bowie et al., 2015). This confirms that thorium isotopes can

not only be used to estimate metal fluxes from the dissolution of mineral dust (Hsieh et al., 2011; Hayes et al., 2013; Deng et al., 2014) but also from the dissolution of lithogenic material originating from and transported through coastal areas, as long as the oceanographic conditions are well constrained.

5. Conclusion

The spatial distribution of ^{232}Th concentrations in the surface of the plateau clearly indicates that Heard and McDonald Islands contribute with the supply of lithogenic material that fuels the phytoplankton bloom in the Central Kerguelen Plateau during the summer. We applied long-lived thorium isotopes to produce an estimation of the fluxes of lithogenic material and Fe from the Kerguelen Plateau. We demonstrate the potential of long-lived thorium isotopes to produce this type of information not only from the dissolution of aeolian dust to the open ocean like other studies have proved but also from the input of lithogenic sources to coastal areas. The similarity of our results with the ones obtained by the use of sediment traps in the Southern Ocean suggests that measuring thorium isotopes can be an alternative to obtain this type of information when there is no time for the deployment of sediment traps. However, some limitations arise due to the lack of information about the Th solubility from continental-originated material, and from other trace elements (including Fe) in relation with Th solubility, as well as from the effect of particle size in the speciation of thorium. Systematic studies about characterizing the dissolution of particles of different origin and composition will allow to improve the results produced by this technique.

References

Anderson R. F., Bacon M. P. and Brewer P. G. (1983) Removal of 230Th and 231Pa from the open ocean. *Earth Planet. Sci. Lett.* **62**, 7–23. Available at: https://linkinghub.elsevier.com/retrieve/pii/0012821X83900675.

Anderson R. F., Fleisher M. Q., Robinson L. F., Edwards R. L., Hoff J. A., Moran S. B., van der Loeff M. R., Thomas A. L., Roy-Barman M. and Francois R. (2012) GEOTRACES intercalibration of ^{230}Th, ^{232}Th, ^{231}Pa, and prospects for ^{10}Be. *Limnol. Oceanogr. Methods* **10**, 179–213. Available at: http://doi.wiley.com/10.4319/lom.2012.10.179.

Arraes-Mescoff R., Roy-Barman M., Coppola L., Souhaut M., Tachikawa K., Jeandel C., Sempéré R. and Yoro C. (2001) The behavior of Al, Mn, Ba, Sr, REE and Th isotopes during in vitro degradation of large marine particles. *Mar. Chem.* **73**, 1–19. Available at: https://linkinghub.elsevier.com/retrieve/pii/S0304420300000657.

van Beek P., Bourquin M., Reyss J.-L., Souhaut M., Charette M. A. and Jeandel C. (2008) Radium isotopes to investigate the water mass pathways on the Kerguelen Plateau (Southern Ocean). *Deep Sea Res. Part II Top. Stud. Oceanogr.* **55**, 622–637. Available at: http://www.sciencedirect.com/science/article/pii/S0967064508000155.

Blain S., Quéguiner B., Armand L., Belviso S., Bombled B., Bopp L., Bowie A., Brunet C., Brussaard C., Carlotti F., Christaki U., Corbière A., Durand I., Ebersbach F., Fuda J.-L., Garcia N., Gerringa L., Griffiths B., Guigue C., Guillerm C., Jacquet S., Jeandel C., Laan P., Lefèvre D., Lo Monaco C., Malits A., Mosseri J., Obernosterer I., Park Y.-H., Picheral M., Pondaven P., Remenyi T., Sandroni V., Sarthou G., Savoye N., Scouarnec L., Souhaut M., Thuiller D., Timmermans K., Trull T., Uitz J., van Beek P., Veldhuis M., Vincent D., Viollier E., Vong L. and Wagener T. (2007) Effect of natural iron fertilization on carbon sequestration in the Southern Ocean. *Nature* **446**, 1070–1074. Available at: http://www.nature.com/articles/nature05700.

Blain S., Quéguiner B. and Trull T. (2008a) The natural iron fertilization experiment KEOPS (KErguelen Ocean and Plateau compared Study): An overview. *Deep Sea Res. Part II Top. Stud. Oceanogr.* **55**, 559–565. Available at: http://www.sciencedirect.com/science/article/pii/S096706450800009X.

Blain S., Sarthou G. and Laan P. (2008b) Distribution of dissolved iron during the natural iron-fertilization experiment KEOPS (Kerguelen Plateau, Southern Ocean). *Deep Sea Res. Part II Top. Stud. Oceanogr.* **55**, 594–605. Available at: http://www.sciencedirect.com/science/article/pii/S096706450800012X.

Blain S., Tréguer P., Belviso S., Bucciarelli E., Denis M., Desabre S., Fiala M., Martin Jézéquel V., Le Fèvre J., Mayzaud P., Marty J.-C. and Razouls S. (2001) A biogeochemical study of the island mass effect in the context of the iron hypothesis: Kerguelen Islands, Southern Ocean. *Deep Sea Res. Part I Oceanogr. Res. Pap.* **48**, 163–187. Available at: http://www.sciencedirect.com/science/article/pii/S0967063700000479.

Bopp L., Aumont O., Belviso S. and Blain S. (2008) Modelling the effect of iron fertilization on dimethylsulphide emissions in the Southern Ocean. *Deep Sea Res. Part II Top. Stud. Oceanogr.* **55**, 901–912. Available at: http://www.sciencedirect.com/science/article/pii/S0967064508000337.

Bowie A. R., van der Merwe P., Quéroué F., Trull T., Fourquez M., Planchon F., Sarthou G., Chever F., Townsend A. T., Obernosterer I., Sallée J.-B. and Blain S. (2015) Iron budgets

for three distinct biogeochemical sites around the Kerguelen Archipelago (Southern Ocean) during the natural fertilisation study, KEOPS-2. *Biogeosciences* **12**, 4421–4445. Available at: https://www.biogeosciences.net/12/4421/2015/.

Bown J., Boye M., Laan P., Bowie A. R., Park Y.-H., Jeandel C. and Nelson D. M. (2012) Imprint of a dissolved cobalt basaltic source on the Kerguelen Plateau. *Biogeosciences* **9**, 5279–5290. Available at: https://www.biogeosciences.net/9/5279/2012/.

Boyd P. W. and Ellwood M. J. (2010) The biogeochemical cycle of iron in the ocean. *Nat. Geosci.* **3**, 675–682. Available at: http://dx.doi.org/10.1038/ngeo964.

Boyd P. W., Jickells T., Law C. S., Blain S., Boyle E. A., Buesseler K. O., Coale K. H., Cullen J. J., de Baar H. J. W., Follows M., Harvey M., Lancelot C., Levasseur M., Owens N. P. J., Pollard R., Rivkin R. B., Sarmiento J., Schoemann V., Smetacek V., Takeda S., Tsuda A., Turner S. and Watson A. J. (2007) Mesoscale Iron Enrichment Experiments 1993-2005: Synthesis and Future Directions. *Science (80-.).* **315**, 612–617. Available at: http://www.sciencemag.org/cgi/doi/10.1126/science.1131669.

Broecker W. S., Kaufman A. and Trier R. M. (1973) The residence time of thorium in surface sea water and its implications regarding the rate of reactive pollutants. *Earth Planet. Sci. Lett.* **20**, 35–44. Available at: https://linkinghub.elsevier.com/retrieve/pii/0012821X73901374.

Buesseler K. O., Bacon M. P., Kirk Cochran J. and Livingston H. D. (1992) Carbon and nitrogen export during the JGOFS North Atlantic Bloom experiment estimated from ^{234}Th:^{238}U disequilibria. *Deep Sea Res. Part A. Oceanogr. Res. Pap.* **39**, 1115–1137. Available at: https://linkinghub.elsevier.com/retrieve/pii/0198014992900607.

Chiarini F., Ravaioli M. and Capotondi L. (2019) Interannual variability of vertical particle fluxes in the Ross Sea (Antarctica). *Nat. Conserv.* **34**, 417–440. Available at: https://natureconservation.pensoft.net/article/30732/.

Cochran J. K., Buesseler K. O., Bacon M. P., Wang H. W., Hirschberg D. J., Ball L., Andrews J., Crossin G. and Fleer A. (2000) Short-lived thorium isotopes as indicators of POC export and particle cycling in the Ross Sea, Southern Ocean. *Deep Sea Res. Part II Top. Stud. Oceanogr.* **47**, 3451–3490. Available at: https://linkinghub.elsevier.com/retrieve/pii/S0967064500000758.

Coppola L., Roy-Barman M., Mulsow S., Povinec P. and Jeandel C. (2006) Thorium isotopes as tracers of particles dynamics and deep water circulation in the Indian sector of the Southern Ocean (ANTARES IV). *Mar. Chem.* **100**, 299–313. Available at: https://linkinghub.elsevier.com/retrieve/pii/S0304420305002203.

Costa K. and McManus J. (2017) Efficacy of 230Th normalization in sediments from the Juan de Fuca Ridge, northeast Pacific Ocean. *Geochim. Cosmochim. Acta* **197**, 215–225. Available at: http://dx.doi.org/10.1016/j.gca.2016.10.034.

Deng F., Thomas A. L., Rijkenberg M. J. A. and Henderson G. M. (2014) Controls on seawater ^{231}Pa, ^{230}Th and ^{232}Th concentrations along the flow paths of deep waters in the Southwest Atlantic. *Earth Planet. Sci. Lett.* **390**, 93–102. Available at: http://dx.doi.org/10.1016/j.epsl.2013.12.038.

Duncan R. A., Falloon T. J., Quilty P. G. and Coffin M. F. (2016) Widespread Neogene volcanism on Central Kerguelen Plateau, Southern Indian Ocean. *Aust. J. Earth Sci.* **63**, 379–392. Available at: https://doi.org/10.1080/08120099.2016.1221857.

Francois R., Bacon M. P. and Suman D. O. (1990) Thorium 230 profiling in deep-sea sediments: High-resolution records of flux and dissolution of carbonate in the equatorial Atlantic during the last 24,000 years. *Paleoceanography* **5**, 761–787.

Available at: http://onlinelibrary.wiley.com/doi/10.1029/PA005i005p00761/full.
Francois R., Frank M., Rutgers van der Loeff M. M. and Bacon M. P. (2004) ^{230}Th normalization: An essential tool for interpreting sedimentary fluxes during the late Quaternary. *Paleoceanography* **19**, n/a-n/a. Available at: http://doi.wiley.com/10.1029/2003PA000939.
Fung I. Y., Meyn S. K., Tegen I., Doney S. C., John J. G. and Bishop J. K. B. (2000) Iron supply and demand in the upper ocean. *Global Biogeochem. Cycles* **14**, 281–295. Available at: http://doi.wiley.com/10.1029/1999GB900059.
Grenier M., François R., Soon M., Rutgers van der Loeff M., Yu X., Valk O., Not C., Moran S. B., Edwards R. L., Lu Y., Lepore K. and Allen S. E. (2019) Changes in Circulation and Particle Scavenging in the Amerasian Basin of the Arctic Ocean over the Last Three Decades Inferred from the Water Column Distribution of Geochemical Tracers. *J. Geophys. Res. Ocean.*, 2019JC015265. Available at: https://onlinelibrary.wiley.com/doi/abs/10.1029/2019JC015265.
Grenier M., Garcia-Solsona E., Lemaitre N., Trull T. W., Bouvier V., Nonnotte P., van Beek P., Souhaut M., Lacan F. and Jeandel C. (2018) Differentiating Lithogenic Supplies, Water Mass Transport, and Biological Processes On and Off the Kerguelen Plateau Using Rare Earth Element Concentrations and Neodymium Isotopic Compositions. *Front. Mar. Sci.* **5**. Available at: https://www.frontiersin.org/article/10.3389/fmars.2018.00426/full.
Grenier M., Della Penna A. and Trull T. W. (2015) Autonomous profiling float observations of the high-biomass plume downstream of the Kerguelen Plateau in the Southern Ocean. *Biogeosciences* **12**, 2707–2735. Available at: https://www.biogeosciences.net/12/2707/2015/.
Hayes C. T., Anderson R. F., Fleisher M. Q., Serno S., Winckler G. and Gersonde R. (2013) Quantifying lithogenic inputs to the North Pacific Ocean using the long-lived thorium isotopes. *Earth Planet. Sci. Lett.* **383**, 16–25. Available at: http://dx.doi.org/10.1016/j.epsl.2013.09.025.
Hayes C. T., Black E. E., Anderson R. F., Baskaran M., Buesseler K. O., Charette M. A., Cheng H., Cochran J. K., Edwards R. L., Fitzgerald P., Lam P. J., Lu Y., Morris S. O., Ohnemus D. C., Pavia F. J., Stewart G. and Tang Y. (2018) Flux of Particulate Elements in the North Atlantic Ocean Constrained by Multiple Radionuclides. *Global Biogeochem. Cycles* **32**, 1738–1758. Available at: https://onlinelibrary.wiley.com/doi/abs/10.1029/2018GB005994.
Holmes T. M., Wuttig K., Chase Z., van der Merwe P., Townsend A. T., Schallenberg C., Tonnard M. and Bowie A. R. (2019) Iron availability influences nutrient drawdown in the Heard and McDonald Islands region, Southern Ocean. *Mar. Chem.* **211**, 1–14. Available at: https://doi.org/10.1016/j.marchem.2019.03.002.
Honjo S., Francois R., Manganini S., Dymond J. and Collier R. (2000) Particle fluxes to the interior of the Southern Ocean in the Western Pacific sector along 170°W. *Deep Sea Res. Part II Top. Stud. Oceanogr.* **47**, 3521–3548. Available at: https://linkinghub.elsevier.com/retrieve/pii/S0967064500000771.
Hsieh Y., Henderson G. M. and Thomas A. L. (2011) Combining seawater ^{232}Th and ^{230}Th concentrations to determine dust fluxes to the surface ocean. *Earth Planet. Sci. Lett.* **312**, 280–290. Available at: http://dx.doi.org/10.1016/j.epsl.2011.10.022.
Jacquet S. H. M., Dehairs F., Savoye N., Obernosterer I., Christaki U., Monnin C. and Cardinal D. (2008) Mesopelagic organic carbon remineralization in the Kerguelen Plateau region tracked by biogenic particulate Ba. *Deep Sea Res. Part II Top. Stud. Oceanogr.* **55**, 868–

879. Available at: http://www.sciencedirect.com/science/article/pii/S096706450800026X.
Jickells T. D. (2005) Global Iron Connections Between Desert Dust, Ocean Biogeochemistry, and Climate. *Science (80-.).* **308**, 67–71. Available at: http://www.sciencemag.org/cgi/doi/10.1126/science.1105959.
Jouandet M. P., Blain S., Metzl N., Brunet C., Trull T. W. and Obernosterer I. (2008) A seasonal carbon budget for a naturally iron-fertilized bloom over the Kerguelen Plateau in the Southern Ocean. *Deep Sea Res. Part II Top. Stud. Oceanogr.* **55**, 856–867. Available at: http://www.sciencedirect.com/science/article/pii/S0967064508000209.
Krishnaswami S. and Cochran J. K. (2011) *U-Th series nuclides in aquatic systems*., Elsevier.
Luo Y. (2017) Reinterpretation of oceanic 230 Th profiles based on decadal export. *Sci. Rep.*, 1–12. Available at: http://dx.doi.org/10.1038/s41598-017-00604-y.
Mahowald N., Engelstaedter S. and Luo C. (2009) Atmospheric Iron Deposition: Global Distribution, Variability, and Human Perturbations*. *Annu. Rev.* Available at: http://www.annualreviews.org/doi/abs/10.1146/annurev.marine.010908.163727.
Martin J. H. (1990) Glacial-interglacial CO 2 change: The Iron Hypothesis. *Paleoceanography* **5**, 1–13. Available at: http://doi.wiley.com/10.1029/PA005i001p00001.
van der Merwe P., Bowie A. R., Quéroué F., Armand L., Blain S., Chever F., Davies D., Dehairs F., Planchon F., Sarthou G., Townsend A. T. and Trull T. W. (2015) Sourcing the iron in the naturally fertilised bloom around the Kerguelen Plateau: particulate trace metal dynamics. *Biogeosciences* **12**, 739–755. Available at: https://www.biogeosciences.net/12/739/2015/.
van der Merwe P., Wuttig K., Holmes T., Trull T. W., Chase Z., Townsend A. T., Goemann K. and Bowie A. R. (2019) High Lability Fe Particles Sourced From Glacial Erosion Can Meet Previously Unaccounted Biological Demand: Heard Island, Southern Ocean. *Front. Mar. Sci.* **6**, 1–20. Available at: https://www.frontiersin.org/article/10.3389/fmars.2019.00332/full.
Mongin M., Molina E. and Trull T. W. (2008) Seasonality and scale of the Kerguelen plateau phytoplankton bloom: A remote sensing and modeling analysis of the influence of natural iron fertilization in the Southern Ocean. *Deep Sea Res. Part II Top. Stud. Oceanogr.* **55**, 880–892. Available at: http://www.sciencedirect.com/science/article/pii/S0967064508000295.
Moran S. B., Shen C.-C., Edmonds H. N., Weinstein S. E., Smith J. N. and Edwards R. L. (2002) Dissolved and particulate ^{231}Pa and ^{230}Th in the Atlantic Ocean: constraints on intermediate/deep water age, boundary scavenging, and ^{231}Pa/^{230}Th fractionation. *Earth Planet. Sci. Lett.* **203**, 999–1014. Available at: https://linkinghub.elsevier.com/retrieve/pii/S0012821X02009287.
Mosseri J., Quéguiner B., Armand L. and Cornet-Barthaux V. (2008) Impact of iron on silicon utilization by diatoms in the Southern Ocean: A case study of Si/N cycle decoupling in a naturally iron-enriched area. *Deep Sea Res. Part II Top. Stud. Oceanogr.* **55**, 801–819. Available at: http://www.sciencedirect.com/science/article/pii/S0967064508000301.
Nozaki Y., Horibe Y. and Tsubota H. (1981) The water column distributions of thorium isotopes in the western North Pacific. *Earth Planet. Sci. Lett.* **54**, 203–216. Available at: https://linkinghub.elsevier.com/retrieve/pii/0012821X81900042.
Nozaki Y. and Nakanishi T. (1985) ^{231}Pa and ^{230}Th profiles in the open ocean water column. *Deep Sea Res. Part A. Oceanogr. Res. Pap.* **32**, 1209–1220. Available at: http://www.sciencedirect.com/science/article/pii/0198014985900044.

Owens S. A., Buesseler K. O. and Sims K. W. W. (2011) Re-evaluating the ^{238}U-salinity relationship in seawater: Implications for the ^{238}U-^{234}Th disequilibrium method. *Mar. Chem.* **127**, 31–39. Available at: http://dx.doi.org/10.1016/j.marchem.2011.07.005.

Park Y.-H., Charriaud E. and Fieux M. (1998) Thermohaline structure of the Antarctic Surface Water/Winter Water in the Indian sector of the Southern Ocean. *J. Mar. Syst.* **17**, 5–23. Available at: https://linkinghub.elsevier.com/retrieve/pii/S0924796398000268.

Park Y.-H., Durand I., Kestenare E., Rougier G., Zhou M., D'Ovidio F., Cotté C. and Lee J.-H. (2014) Polar Front around the Kerguelen Islands: An up-to-date determination and associated circulation of surface/subsurface waters. *J. Geophys. Res. Ocean.* **119**, 6575–6592. Available at: http://doi.wiley.com/10.1002/2014JC010061.

Park Y.-H., Fuda J.-L., Durand I. and Naveira Garabato A. C. (2008a) Internal tides and vertical mixing over the Kerguelen Plateau. *Deep Sea Res. Part II Top. Stud. Oceanogr.* **55**, 582–593. Available at: http://www.sciencedirect.com/science/article/pii/S0967064508000118.

Park Y.-H., Roquet F., Durand I. and Fuda J.-L. (2008b) Large-scale circulation over and around the Northern Kerguelen Plateau. *Deep Sea Res. Part II Top. Stud. Oceanogr.* **55**, 566–581. Available at: http://www.sciencedirect.com/science/article/pii/S0967064508000106.

Park Y. and Vivier F. (2011) Circulation and hydrography over the Kerguelen Plateau. *Kerguelen Plateau Mar. Ecosyst. Fish.*, 43–55.

Pérez-Tribouillier H., Noble T. L., Townsend A. T., Bowie A. R. and Chase Z. (2019) Pre-concentration of thorium and neodymium isotopes using Nobias chelating resin: Method development and application to chromatographic separation. *Talanta* **202**, 600–609. Available at: https://doi.org/10.1016/j.talanta.2019.03.086.

Planchon F., Ballas D., Cavagna A.-J., Bowie A. R., Davies D., Trull T., Laurenceau-Cornec E. C., Van Der Merwe P. and Dehairs F. (2015) Carbon export in the naturally iron-fertilized Kerguelen area of the Southern Ocean based on the ^{234}Th approach. *Biogeosciences* **12**, 3831–3848. Available at: https://www.biogeosciences.net/12/3831/2015/.

Rosso I., Hogg A. M. C., Strutton P. G., Kiss A. E., Matear R., Klocker A. and van Sebille E. (2014) Vertical transport in the ocean due to sub-mesoscale structures: Impacts in the Kerguelen region. *Ocean Model.* **80**, 10–23. Available at: http://dx.doi.org/10.1016/j.ocemod.2014.05.001.

Roy-Barman M., Coppola L. and Souhaut M. (2002) Thorium isotopes in the western Mediterranean Sea: an insight into the marine particle dynamics. *Earth Planet. Sci. Lett.* **196**, 161–174. Available at: https://linkinghub.elsevier.com/retrieve/pii/S0012821X01006069.

Roy-Barman M., Lemaître C., Ayrault S., Jeandel C., Souhaut M. and Miquel J. C. (2009) The influence of particle composition on Thorium scavenging in the Mediterranean Sea. *Earth Planet. Sci. Lett.* **286**, 526–534. Available at: http://dx.doi.org/10.1016/j.epsl.2009.07.018.

Rudnick R. and Gao S. (2013) Composition of the Continental Crust. *Treatise Geochemistry Second Ed.* **4**, 1–51. Available at: http://dx.doi.org/10.1016/B978-0-08-095975-7.00301-6.

Rutgers van der Loeff M. M. and Berger G. W. (1993) Scavenging of ^{230}Th and ^{231}Pa near the antarctic polar front in the South Atlantic. *Deep Sea Res. Part I Oceanogr. Res. Pap.* **40**, 339–357. Available at:

https://linkinghub.elsevier.com/retrieve/pii/096706379390007P.
Sanial V., van Beek P., Lansard B., Souhaut M., Kestenare E., D'Ovidio F., Zhou M. and Blain S. (2015) Use of Ra isotopes to deduce rapid transfer of sediment-derived inputs off Kerguelen. *Biogeosciences* **12**, 1415–1430. Available at: https://www.biogeosciences.net/12/1415/2015/.
Santschi P. H., Murray J. W., Baskaran M., Benitez-Nelson C. R., Guo L. D., Hung C.-C., Lamborg C., Moran S. B., Passow U. and Roy-Barman M. (2006) Thorium speciation in seawater. *Mar. Chem.* **100**, 250–268. Available at: https://linkinghub.elsevier.com/retrieve/pii/S0304420305002161.
Sargent M., Harte R. and Harrington C. (2002) Guidelines for achieving high accuracy in isotope dilution mass spectrometry (IDMS). Available at: https://books.google.com/books?hl=es&lr=&id=9wwLS5pcD9sC&oi=fnd&pg=PA1&dq=guidelines+for+achieving+high+accuracy+in+isotope+dilution&ots=TI80X664yI&sig=-NVdYoYJtnc_SarNw4UVRm1L2jo.
Sarthou G., Baker A. R., Kramer J., Laan P., Laës A., Ussher S., Achterberg E. P., de Baar H. J. W., Timmermans K. R. and Blain S. (2007) Influence of atmospheric inputs on the iron distribution in the subtropical North-East Atlantic Ocean. *Mar. Chem.* **104**, 186–202. Available at: https://linkinghub.elsevier.com/retrieve/pii/S0304420306001885.
Sarthou G., Vincent D., Christaki U., Obernosterer I., Timmermans K. R. and Brussaard C. P. D. (2008) The fate of biogenic iron during a phytoplankton bloom induced by natural fertilisation: Impact of copepod grazing. *Deep Sea Res. Part II Top. Stud. Oceanogr.* **55**, 734–751. Available at: http://www.sciencedirect.com/science/article/pii/S0967064508000234.
Savoye N., Trull T. W., Jacquet S. H. M., Navez J. and Dehairs F. (2008) ^{234}Th-based export fluxes during a natural iron fertilization experiment in the Southern Ocean (KEOPS). *Deep Sea Res. Part II Top. Stud. Oceanogr.* **55**, 841–855. Available at: http://www.sciencedirect.com/science/article/pii/S0967064508000325.
Serno S., Winckler G., Anderson R. F., Hayes C. T., McGee D., Machalett B., Ren H., Straub S. M., Gersonde R. and Haug G. H. (2014) Eolian dust input to the Subarctic North Pacific. *Earth Planet. Sci. Lett.* **387**, 252–263. Available at: http://dx.doi.org/10.1016/j.epsl.2013.11.008.
Tagliabue A., Bopp L. and Aumont O. (2009) Evaluating the importance of atmospheric and sedimentary iron sources to Southern Ocean biogeochemistry. *Geophys. Res. Lett.* **36**, L13601. Available at: http://doi.wiley.com/10.1029/2009GL038914.
Tagliabue A., Sallée J.-B., Bowie A. R., Lévy M., Swart S. and Boyd P. W. (2014) Surface-water iron supplies in the Southern Ocean sustained by deep winter mixing. *Nat. Geosci.* **7**, 314–320. Available at: http://www.nature.com/articles/ngeo2101.
Taylor S. R. and McLennan S. M. (1985) The continental crust: its composition and evolution.
Trimble S. M., Baskaran M. and Porcelli D. (2004) Scavenging of thorium isotopes in the Canada Basin of the Arctic Ocean☆. *Earth Planet. Sci. Lett.* **222**, 915–932. Available at: https://linkinghub.elsevier.com/retrieve/pii/S0012821X04002110.
Tyrrell T., Merico A., Waniek J. J., Wong C. S., Metzl N. and Whitney F. (2005) Effect of seafloor depth on phytoplankton blooms in high-nitrate, low-chlorophyll (HNLC) regions. *J. Geophys. Res. Biogeosciences* **110**, n/a-n/a. Available at: http://doi.wiley.com/10.1029/2005JG000041.
Venchiarutti C., Jeandel C. and Roy-Barman M. (2008) Particle dynamics study in the wake of Kerguelen Island using thorium isotopes. *Deep Sea Res. Part I Oceanogr. Res. Pap.* **55**,

1343–1363. Available at: http://www.sciencedirect.com/science/article/pii/S0967063708001180.

Venchiarutti C., van der Loeff M. R. and Stimac I. (2011a) Scavenging of ^{231}Pa and thorium isotopes based on dissolved and size-fractionated particulate distributions at Drake Passage (ANTXXIV-3). *Deep. Res. Part II Top. Stud. Oceanogr.* **58**, 2767–2784. Available at: http://dx.doi.org/10.1016/j.dsr2.2010.10.040.

Venchiarutti C., Loeff M. R. Van Der and Stimac I. (2011b) Deep-Sea Research II Scavenging of ^{231}Pa and thorium isotopes based on dissolved and size-fractionated particulate distributions at Drake Passage (ANTXXIV-3). *Deep. Res. Part II* **58**, 2767–2784. Available at: http://dx.doi.org/10.1016/j.dsr2.2010.10.040.

Wefer G., Fischer G., Füetterer D. and Gersonde R. (1988) Seasonal particle flux in the Bransfield Strait, Antartica. *Deep Sea Res. Part A. Oceanogr. Res. Pap.* **35**, 891–898. Available at: https://linkinghub.elsevier.com/retrieve/pii/0198014988900660.

Zhang Y., Lacan F. and Jeandel C. (2008) Dissolved rare earth elements tracing lithogenic inputs over the Kerguelen Plateau (Southern Ocean). *Deep Sea Res. Part II Top. Stud. Oceanogr.* **55**, 638–652. Available at: http://www.sciencedirect.com/science/article/pii/S0967064508000167.

Zhou M., Zhu Y., D'Ovidio F., Park Y.-H., Durand I., Kestenare E., Sanial V., Van-Beek P., Queguiner B., Carlotti F. and Blain S. (2014) Surface currents and upwelling in Kerguelen Plateau regions. *Biogeosciences Discuss.* **11**, 6845–6876. Available at: https://www.biogeosciences-discuss.net/11/6845/2014/.

Chapter 4 - Sourcing lithogenic inputs to the Kerguelen Plateau using rare earth element concentrations and Nd isotopic composition

1. Introduction

The rare earth elements (REE) are a group of chemical elements that provide valuable information about several processes that occur in the ocean. The main source of REE to the ocean is the dissolution of sediments on the continental shelves and slopes (Jeandel et al., 1998; Lacan and Jeandel, 2005; Arsouze et al., 2007). The flux from dissolved river loads and the dissolution of aerosols also contribute to the REE global budget (Tachikawa et al., 1999; Barroux et al., 2006). All REE are chemically similar, with a predominant oxidation state of 3+ under normal oceanic conditions, which makes them behave in a similar way (Elderfield and Greaves, 1982). However, subtle changes in their chemical characteristics lead to a relative fractionation of the REE content in seawater. This fractionation happens mainly because of two factors: differences in scavenging sensitivity, and differences in redox sensitivity.

Systematic changes in the ionic radii occur as the atomic number increases. These changes produce an ordered variation in the complexation and surface adsorption stability constants of the REE. This property is reflected in the REE speciation in seawater, which is dominated by carbonate complexation (Cantrell and Byrne, 1987). REE complexation by seawater carbonate ligands increases with increasing atomic number. Therefore, the number of free ions decreases with increasing atomic number, which makes heavy REE less susceptible to adsorption onto particles (Elderfield and Greaves, 1982). This results in the typical dissolved REE seawater pattern to have a higher abundance of heavier REE and a relative depletion of lighter REE due to their increased susceptibility to be scavenged (Turekian, 1977; Elderfield et al., 1988).

The other cause of REE fractionation is the redox state of seawater, as cerium (Ce) and europium (Eu) can also exist as 4+ and 2+ oxidation states, respectively (Michard et al., 1983; Sholkovitz et al., 1994). Under normal oxidative conditions of seawater, Ce will tend to exist in the 4+ oxidation state, causing it to quickly precipitate as CeO_2 into authigenic mineral phases (Elderfield and Greaves, 1981; Elderfield et al., 1988). This causes most seawater to have a Ce depletion in relation to its neighbor elements. In comparison, under reducing

conditions Eu will adopt a predominant oxidation state of 2+, which leads Eu to stay preferably in a dissolved state. Hydrothermal fluids are typically enriched in Eu close to the vents, however this Eu gets quickly scavenged from seawater, enriching surrounding sediments (Olivarez and Owen, 1991). These above mentioned characteristics make the REE group a powerful tool, which can be used to track lithogenic sources of trace elements (Sholkovitz et al., 1999). They also provide important information about the redox conditions of seawater and the scavenging intensity in the upper layer of the ocean (Elderfield et al., 1988; German et al., 1995). Additionally, with the increase in the use of REE for industrial and medical applications, REE are being introduced to the ocean by human activity. Near highly developed coastal regions, like California, China and the Baltic Sea, gadolinium can be used as a tracer of human activity (Kulaksız and Bau, 2007; Hatje et al., 2014).

Some REE are produced by radioactive decay. The long-lived ^{147}Sm ($t_{1/2}=1.06\times10^{11}$ years) and ^{148}Sm ($t_{1/2}=7\times10^{15}$ years) isotopes decay to the stable ^{143}Nd and to the long-lived ^{144}Nd ($t_{1/2}=2.29\times10^{15}$ years), respectively. However, ^{148}Sm has such a long half-life that it is not capable of producing measurable variations in ^{144}Nd abundance over cosmological intervals (10^{10} years; Dickin, 2018). By contrast, chemical fractionation during magma melting and the formation of continental crust produces a range of $^{147}Sm/^{144}Nd$ ratios, and hence different $^{143}Nd/^{144}Nd$ ratios in rocks and minerals as a function of age and the Sm/Nd ratio of the parent material (Lugmair, 1974; DePaolo and Wasserburg, 1976). When these rocks and minerals enter into contact with seawater, their unique $^{143}Nd/^{144}Nd$ signature gets imprinted into that particular water mass and remains along its path through the ocean circulation cycle, making it a quasi-conservative tracer of the global oceanic circulation (Piepgras et al., 1979; Goldstein and Hemming, 2003). However, in more coastal environments (like the KP), the $^{143}Nd/^{144}Nd$ of seawater is prone to no longer be conservative. The particulate/dissolved exchange that occurs along the continental margins can modify the Nd isotopic composition of a particular water mass. This process, known as boundary exchange, can act as a sink or a source (or both) of trace elements and, hence, has an important role in the control of the biogeochemical cycles in these areas (Lacan and Jeandel, 2005).

The lithogenic material that supplies REE to the ocean is also essential for phytoplankton growth in certain regions of the ocean where despite the abundance of nutrients the primary productivity remains low despite the abundance of nutrients. These areas, commonly known as high nutrient, low chlorophyll regions (HNLC), occupy about one

third of the ocean's surface and are caused by the absence of the bio-limiting micro-nutrient iron (Fe; Martin, 1990b; Martin, 1990a; Boyd et al., 2007). When Fe reaches HNLC areas it enables the proliferation of phytoplankton blooms, which have the potential to drive atmospheric CO_2 into deeper layers of the ocean (de Baar et al., 1995).

In most HNLC areas, Fe is supplied by the dissolution of mineral dust originating from deserts and transported to the ocean by the wind (Jickells, 2005). In the Equatorial Pacific, Fe is also upwelled to the surface of the ocean (Coale et al., 1996). The Southern Ocean (SO) - which is the largest HNLC area- is located far away from any dust source. Here the natural fertilization of Fe occurs thanks to the dissolution of lithogenic particles sourced from bathymetric features like islands, rises and seamounts, enabling the proliferation of seasonal phytoplankton blooms (Blain et al., 2001; Tagliabue et al., 2014). The bloom occurring over and downstream the Kerguelen Plateau (KP; South of the Indian Ocean) is the largest in the SO. Because of their similar continental origin, REE distributions in the KP have been used to track the origin of the Fe supplying the bloom in the region (Zhang et al., 2008; Grenier et al., 2018). The KEOPS 1 study identified Heard and McDonald Islands (HIMI) as the potential sources of lithogenic material (Zhang et al., 2008). Results from an expedition to the northern part of the plateau (KEOPS 2) showed that the Kerguelen Archipelago (KA) plays an important role in the fertilization of the area north of the Polar Front (Grenier et al., 2018). Results from KEOPS 2 also suggested that lithogenic material from the KA can actively cross the PF in a southwards direction and contribute with the bloom towards the central part of the plateau (Sanial et al., 2015). More recently, the Heard and McDonald Earth Ocean Biosphere Interaction Study (HEOBI), undertaken in the austral summer of 2016, confirmed that the drawdown of nutrients in the region north of this group of islands was largely due to the supply of Fe (Holmes et al., 2019). In particular, the importance of high lability Fe particles sourced from glacial runoff from Heard Island was highlighted (van der Merwe et al., 2019).

This chapter is aimed to further constrain the sources and pathways of lithogenic material to the plateau using dissolved REE concentrations and Nd isotopic compositions measured in the waters flowing around HIMI and over the central part of the plateau. Nd isotopic composition measurements will add to a limited body of values and increase our understanding of the Southern Ocean, in particular the intermediate-depth water masses around the Kerguelen Plateau.

2. Materials and methods

2.1 Sampling

Samples were collected as part of the HEOBI study over and around the central Kerguelen Plateau in January and February 2016. Procedures for the collection of the samples have been fully explained in the previous two chapters. Briefly, seawater was filtered directly from Niskin bottles mounted on a CTD through an 0.8/0.2 µm AcroPak® (PALL Corporation, USA) clean capsule filter into 10 L clean cubitainers. On-board blanks (2 L) from the ultra-high purity water (UPW) system of the vessel were also collected at every station. Both samples and blanks were acidified with 1 mL of concentrated HCl per liter of sample. Samples were packed and stored for land-based analysis. Once in the laboratory a 250 mL aliquot was taken for REE analysis and stored in a clean HDPE bottle (Station 25 was not sampled for REE analysis). The rest of the sample was used for the simultaneous determination of ^{232}Th, ^{230}Th and ε_{Nd} (Chapter 2).

A total of 15 surface sediment samples (Figure 1) were collected using either a sediment dredge or Smith McIntyre grab. Once on board, all organisms were manually removed from the main sample and then subsamples of the bulk sediments were placed in a plastic bag and immediately stored in the freezer (-20 °C).

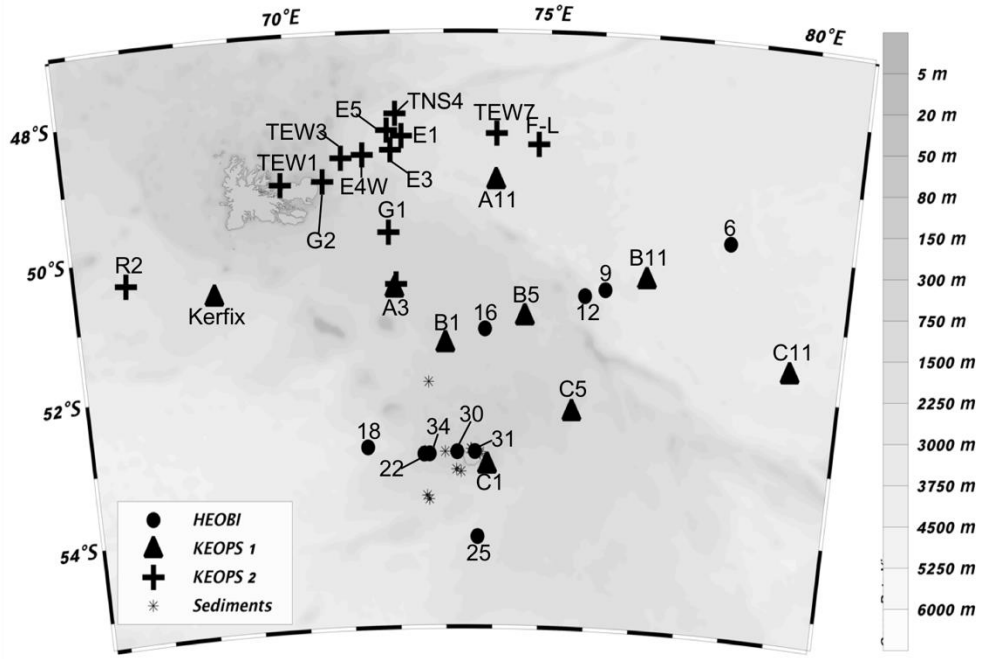

Figure 4-1. Location of stations where REE determinations were made for the KEOPS 1 (triangles; Zhang et al., 2008), and KEOPS 2 (crosses; Grenier et al., 2018) voyages and this study (circles).

2.2 Reagents and materials

All laboratory materials used in this study were meticulously cleaned following GEOTRACES protocols (Cutter et al., 2010). For the cleaning of the materials as well as for reagent preparation, ultra-high purity water (UPW, 18.2 $M\Omega cm^{-1}$) was employed. High purity HNO_3, HCl and CH_3COOH were produced by the distillation of analytical grade acids (Seastar Chemicals, Canada) in a DST-100 acid cleaning system (Savillex, USA). Additionally, HF, $HClO_4$ and HNO_3 were Baseline (Seastar Chemicals, Canada) ultra-high purity acids and used as received by the supplier.

A "stock" 2.5 M ammonium acetate buffer solution was prepared by mixing 317 g of UPW, 74 g of 17 M CH_3COOH and 104 g of 11 M NH_3 solution. This stock solution was employed in both procedures to pre-concentrate REE and Nd-isotopes, respectively. In the case of the REE procedure this solution was passed through a clean Nobias cartridge in order to decrease its contribution to the procedural blank.

For the REE method calibration a multi-element MISA-5 (Brand, Place, Country) standard containing all REE was used. The original solution with a concentration of 100 ppm was serially diluted to obtain a working solution with a REE concentration of 1 ppb. Additionally, for extra sample yield control a ^{150}Nd spike solution was added to the seawater samples. This spike was obtained from the Australian National University and was an aliquot of the original solution produced in the Charles Arm Laboratory from the California Institute of Technology (Wasserburg et al., 1981).

The quality assurance for our REE procedure was controlled by analyzing the GEOTRACES intercalibration sample BATS15 (van de Flierdt et al., 2012). For the Nd isotopic composition quality assurance, the BATS2000 GEOTRACES intercalibration material (Anderson et al., 2012) and the JNdi-1 neodymium isotopic composition CRM (Tanaka et al., 2000) were employed.

2.3 Rare Earth Element determination

Because of the picomolar levels of REE in seawater it is necessary to pre-concentrate samples in order to obtain measurable amounts of REE. For this purpose, we applied a modification of the procedure reported by Hatje et al.(2014) using the Nobias resin. Amongst the modifications, we used a different manifold array, based on the ones reported earlier by

Pérez-Tribouillier et al.(2019). We also used commercially available pre-packed NOBIAS cartridges of the resin instead of hand packed ones.

Based on previous studies, the Nobias resin can produce yields close to 100% for all REE at a pH close to 5 (Hatje et al., 2014). This suggests that REE concentrations can be determined by a simple external calibration. To obtain a calibration curve that is representative of the seawater matrix, we produced a "REE-free" seawater by passing surface water collected in the Southern Ocean through a clean Nobias cartridge several times until most of the REE were stripped off. Seawater calibration samples were prepared with 60 mL aliquots of "REE-free" seawater amended with different amounts of the multi-element MISA-5 standard solution to produce different concentrations (from now referred to as SW-calibrations; 0.2, 1.8, 3.5, 5 pg g^{-1}). The resulting solutions were processed in accordance to the procedure described in the following section. The efficiency of our method is described in the results section. It was evaluated by comparing the signal obtained from the analysis of the SW-calibrations (after dilution factor correction) to the signal produced by the direct measurement of a calibration curve with the same concentrations and no sample treatment (multi-REE solution was diluted in 3 M HNO_3 and immediately analysed using SF-ICP-MS). Additionally, the recovery was also assessed by adding ^{150}Nd tracer to our samples.

2.3.1 Pre-concentration

An aliquot of 60 mL (from the previously described 250 mL aliquot) of acidified seawater was poured into clean and pre-weighed polypropylene containers. Samples were spiked with 50 pg of ^{150}Nd and left to equilibrate for at least 24 hours. Prior to the pre-concentration, 2 mL of 2.5 M ammonium acetate solution were added and the pH was adjusted to a value of 4.75 using ~100 µL of concentrated HCl. The pH of the samples was checked and then immediately pumped through the cartridges at a flow rate of 0.5 ml min^{-1}. After all the sample volume passed through the cartridges, the sea salts were removed by rinsing with 5 mL of UPW at the same flow rate. Finally, REE were eluted from the cartridges using 3.5 mL of 3 M HNO_3 at a flow rate of 0.4 mL min^{-1} into clean 5 mL polypropylene vials. At this stage samples were ready to be measured using SF-ICP-MS.

2.3.2 Quality assurance and blank contribution

At least one blank and a reference material were analyzed with each batch of samples. The blank contribution was assessed through multiple analysis of procedural blanks with UPW as well as measurements of the REE-free seawater used for the external calibration. The signals of the procedural blanks were subtracted from all samples, while the signal of the latter was subtracted from the calibration curve samples. The quality control of our method was achieved by the analysis of the BATS15 intercalibrated sample (van de Flierdt et al., 2012).

2.3.3 Analysis

An Element 2 SF-ICP-MS (Thermo Fisher Scientific, Germany) was used for this study. The operational conditions are presented in Table 1. In order to minimise overlapping oxide/hydride formations and increase instrument sensitivity, samples were introduced via an Aridius® II (CETAC Technologies, USA) desolvating nebulizer. At the beginning of every measurement session, the instrument was carefully tuned to minimized oxide formations by separately analysing four mono-element solutions of Ba, Ce, Pr and Nd (50 pg g^{-1}). Polyatomic interferences ratio of $^{138}Ba^{16}O$, $^{140}Ce^{16}O$, $^{141}Pr^{16}O$ and $^{146}Nd^{16}O$ were less than 0.1%, 0.06%, 0.03% and 0.06%, respectively, through all of our measuring sessions. The isotopes ^{139}La, ^{140}Ce, ^{141}Pr, ^{146}Nd, ^{150}Nd, ^{147}Sm, ^{153}Eu, ^{157}Gd, ^{159}Tb, ^{163}Dy, ^{165}Ho, ^{166}Er, ^{169}Tm, ^{172}Yb, ^{175}Lu were selected by considering individual isotopic abundances and potential isobaric and polyatomic interferences (Robinson et al., 1999). After each REE measurement a short wash of 1-2 min was performed with 10% HNO_3 solution. A multi-element standard solution containing 5 ppt of all the elements analysed in 3 M HNO_3 was passed after every 5-10 samples on the ICP-MS as a quality control check in order to follow and correct for instrument drift. The instrument blank for the ICP-MS was estimated by running 3 M HNO_3 solution (the same solution used for the elution) after every 5-10 samples. The average signal of the instrument blank was subtracted from all samples, standards and procedural blanks.

Instrument	Operating Conditions
Equipment	
Nebuliser	PFA 200 µL/min; self-aspirating
CETAC Aridus 2	Sweep gas: 4.5-5 L/min; Nitrogen gas: 5-8 mL/min
Spray chamber	Heated PFA chamber
Sampler and skimmer cones	Nickel
Parameters	
ICP Torch gas flows (L/min)	0.9/0.75/15 (nebuliser/auxiliary/cooling)
RF Power (W)	1350
Detection mode	Counting
Sample time (s)	0.005 for ^{139}La, ^{140}Ce, ^{141}Pr, ^{146}Nd
	0.01 for ^{147}Sm, ^{153}Eu, ^{157}Gd, ^{159}Tb, ^{163}Dy, ^{165}Ho, ^{166}Er, ^{169}Tm, ^{172}Yb, ^{175}Lu
Mass window	80
Samples/peak	40
Resolution	Low

Table 4-1. Common conditions of operation for the SF-ICP-MS during the different REE measuring sessions.

2.3.4 Data treatment

The REE patterns presented in the results and discussion section were obtained by normalizing the sample's REE concentration to the REE content of the Post-Archean Australian Sedimentary rocks (Taylor and McLennan, 1985; Pourmand et al., 2004). These PAAS normalized values were then used to calculate the Ce (Bolhar et al., 2004; Eq. 2) and Eu (Bau et al., 1996; Eq. 3) anomalies as well as the Nd/Yb normalized ratio (Grenier et al., 2018; Eq. 3)

$$\frac{Ce}{Ce^*} = \frac{[Ce]_n}{2[Pr]_n - [Nd]_n} \ (Eq.1) \quad \frac{Eu}{Eu^*} = \frac{4\,[Eu]_n}{3\,[Sm]_n + [Dy]_n} \ (Eq.2) \quad \left({}^{Nd}/_{Yb}\right)_n = \frac{Nd_n}{Yb_n} \ (Eq.3)$$

2.4 Nd isotopic composition determination

2.4.1 Pre-concentration

The pre-concentration and chromatographic separation of Nd isotopes has been described in full detail in the second chapter (Pérez-Tribouillier et al., 2019). It is part of a simultaneous procedure to pre-concentrate and separate Th and Nd isotopes from the same seawater sample. It was performed using an array of two pre-packed Nobias PA1L cartridges.

On the day of pre-concentration, the samples were supplied with enough 2.5 M ammonium acetate buffer solution to obtain a concentration in the samples of 0.05 M. Immediately after, 0.5 mL of concentrated HCl was added to achieve a final pH of ~4.75. After checking the pH value, the samples were passed through the cartridges using a peristaltic pump and an array of six manifolds as described in Pérez-Tribouillier et al.(2019). After all the volume of the sample passed through the resin, salts were removed with 25 mL of UPW. Finally, targeted analytes were eluted using 5 mL of 3 M HNO_3.

2.4.2 Nd isotopes chromatographic separation

After pre-concentration and between every chromatographic step the samples were strongly oxidized with a mixture of 0.4 mL concentrated HNO_3 and 0.1 mL of $HClO_4$ at 220 ^{o}C. This oxidation step was carried out with the objective of removing any organic substance that may have been leached from the chromatographic resin, as organics can interfere with the efficiency of the subsequent chromatographic step as well as produce interference during measurement (Gault-Ringold and Stirling, 2012).

After the first oxidation was performed, the samples were diluted in 1 mL of concentrated HCl and loaded onto 0.5 mL of BioRad AG1-X8 anion exchange resin (pre-cleaned and conditioned). The aim of this first loading was to separate Th and the REE from U, Pa and transition metals including Fe. Afterwards the same resin was cleaned and conditioned in 8 M HNO_3. The samples were also dissolved in 1 mL of 8M HNO_3 (after oxidation) and loaded onto the resin. This step is performed to separate the REE from Th isotopes (which remain in the resin).

For the next chromatographic column, 1.4 mL the BioRad AG50W-X8 cation exchange resin was employed (Struve et al., 2016). It is used to remove any remaining cations in the sample. After oxidation, the samples were redissolved in 1 mL of 1 M HCl and loaded onto a

cleaned and conditioned column. The cations were then removed with 6 mL of 3 M HCl and the REE were finally eluted with 5 mL of 6 M HCl. The final chromatographic step was to isolate Nd isotopes from the rest of the REE, and was performed using pre-calibrated columns containing Eichrom LN separation chromatography resin (Pin and Zalduegui, 1997). Samples were loaded in 0.125 mL of 0.225 M HCl and washed with ~20 mL of the same acid. Afterward Nd was collected with 5 mL of the diluted HCl acid. This fraction was oxidized one final time prior to determination by MC-ICP-MS or TIMS.

2.4.3 ε_{Nd} determination

In the early stages of this thesis it was planned that the Nd isotopic composition from the HEOBI samples would be measured using Multi Collector ICP-MS at the Australian National University. This was undertaken for the ε_{Nd} determination of samples from Station 18 (see Chapter 2). However, results from this station indicated that the Nd concentration of some samples were too low and the analytical errors were relatively high. Therefore, it was decided that further samples would be analysed by Thermal Ionization Mass Spectrometry (TIMS).

Neodymium Isotope ratio measurements were carried out on a Thermo-Finnegan Triton TIMS instrument at Victoria University of Wellington. Samples were dissolved in 1 µl of 0.01 M H_3PO_4 and loaded onto the evaporation side of outgassed zone-refined double rhenium filament assemblies. The measurement protocol consisted of a static measurement involving five Faraday cups collecting masses 144, 145, 146, 147 and 150 with ^{145}Nd as the axial mass. All Faraday cups were connected to 10^{13} Ω feedback resistors to optimise the measurement of small ion beams (generally 100-200 mV on mass ^{145}Nd). Measured $^{143}Nd/^{144}Nd$ ratios were corrected for Sm interference using $^{144}Sm/^{147}Sm = 0.20667$, and for instrumental fractionation to $^{146}Nd/^{144}Nd = 0.7219$ using the exponential law. Isotope ratios were collected over 18 blocks consisting of 10 ratios each with an 8.389 s integration time. A 400 s baseline was measured prior to analysis during filament warm up with the analyser valve closed. Repeated analysis of 5 ng loads of the JNdi standard yielded $^{143}Nd/^{144}Nd = 0.512108 \pm 0.00002$ (45.5 ppm 2SD; n = 14).

2.4.4 Data treatment

Differences in the $^{143}Nd/^{144}Nd$ ratio of samples) are so small that it is necessary to present data using ε_{Nd} notation (Eq. 4; DePaolo and Wasserburg, 1976). This notation normalizes the $^{143}Nd/^{144}Nd$ ratio of the samples to that of the Chondritic Uniform Reservoir (0.512638, CHUR; Jacobsen and Wasserburg, 1980).

$$\varepsilon_{Nd} = \left[\frac{\left(\frac{^{143}Nd}{^{144}Nd}\right)_{sample}}{\left(\frac{^{143}Nd}{^{144}Nd}\right)_{CHUR}} - 1 \right] \times 10{,}000 \quad (Eq. 4)$$

2.5 Sediment digestion

The sediments collected around HIMI were of black gravelly nature, consistent with volcanic material. Digestion was performed following the protocols described in Durand et al.(2016). A Milestone Ethos EZ laboratory microwave oven with SK-12 (medium pressure) rotor (Shelton, CT, USA) was used for digestions with a maximum power, temperature and pressure of 1500 W, 300°C and 35 bar, respectively. The sequence for acid digestion was as follows: temperature ramping over 10 min to 180°C, stabilisation at this temperature for 40 min, before final increase to 200°C over 4 min. The reaction vessel was held at this temperature for 20 min. Applied microwave power was adjusted automatically by the unit to perform the sequence described above.

Two hundred milligrams of crushed and dried sediment were placed in the microwave vessels. In a fume hood, 4 mL of concentrated HCl was added and the beakers were placed on a hotplate at 150°C for 2 h to allow CO_2 to be released. The vessels were left to cool for 1 h with lids on. Ten millilitres of concentrated HNO_3 and 2 mL of concentrated HF were then added and the microwave digestion procedure described above was applied. The vessels were allowed to cool for up to 1 h with the fan of the microwave turned on to accelerate cooling. Each solution was carefully transferred into a clean 30 mL Teflon beaker. The microwave vessels and their lids were rinsed two times with 1 mL of concentrated HNO_3 to collect as much of the digested sediments as possible. The solutions were then heated on a hotplate at 105°C and taken to incipient dryness. Afterwards the samples were diluted and subject to a chromatographic separation using the TRU-spec resin in order to remove unwanted cations (Crocket et al., 2014). A 1 mL aliquot of the resulting solution was taken

and analysed on the SF-ICP-MS in order to obtain REE concentration in the samples. The remaining solution was subject to the Nd purification scheme using the LN resin (Pin and Zalduegui, 1997).

3. Results

3.1 REE method development

In this section we present the results of our adaptation of the method described by Hatje et al., (2014) to measure dissolved REE concentrations in seawater. The main difference with our methodology is we use pre-packed Nobias cartridges with a different amount of resin. Therefore, we present the results of the investigations to obtain the right volume to effectively elute most of the REE from our larger cartridges. Then we present the calibration process of these cartridges to obtain REE concentrations. Next we report the blank levels, detection limits, accuracy and precision obtained by our method. Finally, REE profiles in HEOBI samples are presented.

3.1.1 Optimal elution volume

The main difference of our proposed method with the one reported by Hatje et al.(2014) are the cartridges that contain the Nobias resin. In previous work, cartridges were hand-packed with 27 μL of Nobias PA1 resin. For our work we used pre-packed Nobias PA1L cartridges with a capacity of ~300 μL. Therefore, our first objective was to establish the optimal concentration and volume of the E-HNO_3 required to elute most of the REE from our particular cartridges. To test this, we designed a simple experiment where a known concentration of REE was loaded onto the cartridges and then REE were eluted using 2.4 mL of 1.5 M and 3M HNO_3 acid in increments of 0.6 mL (Figure 2). Using 2.4 mL of 1.5 M HNO_3 was not enough to quantitatively recover all the REE, and the HREE showed recoveries of less than 80 %. Using 3 M HNO_3 resulted in recovery levels above 93% for all the REE. Therefore, the latter more efficient elution scheme was selected for our larger volume cartridges.

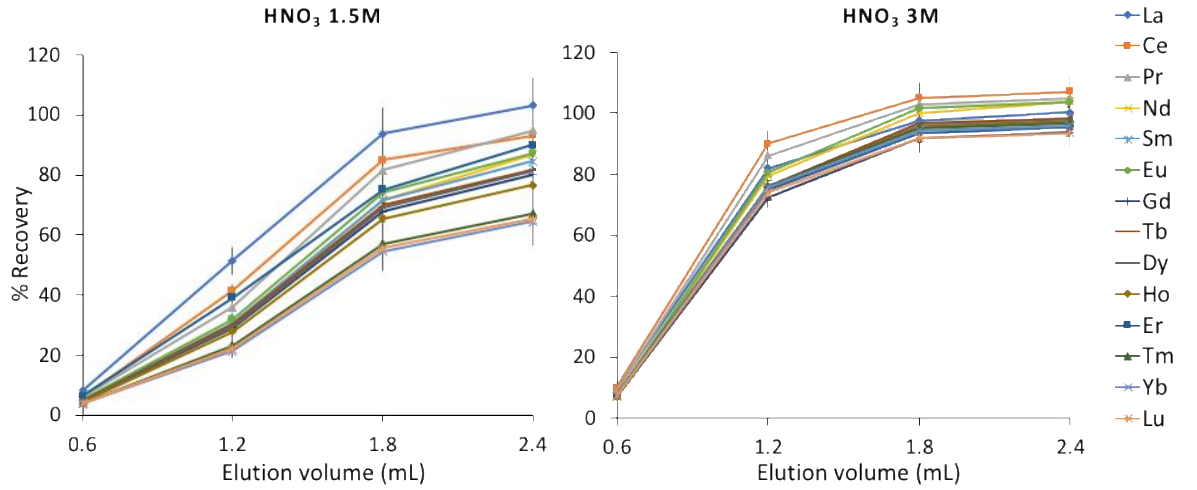

Figure 4-2. The effect of different E-HNO3 concentration and volume on the recovery of REE in UPW from the Nobias PA1L pre-packed cartridges. The values shown are the average of three different measurements and the error bars represent the standard deviation of these measurements.

3.1.2 External calibrations

The excellent yield showed by the Nobias resin to pre-concentrate REE allows for their concentrations to be determined without the needing to apply isotope dilution techniques (Hatje et al., 2014). In the previous section we showed that using the pre-packed cartridges can produce REE yield above 93 % for all REE. However, we wanted to make sure that the same recovery levels could also be achieved with a seawater matrix. For this, we followed the same approach suggested by Hatje et al.(2014). Aliquots (60 mL) of the "REE-free" seawater described in the methods section were spiked with the REE standard solution (MISA-5 standard) in order to obtain different concentrations (0.2-5 ppt). These aliquots were pre-concentrated onto a Nobias cartridge and after elution in 3 M HNO_3, were analyzed using SF-ICP-MS. After correction for dilution factor, obtained signals (Figure 3, orange symbols) were compared with the signal produced by the analysis of the REE standards at the same concentrations as the above-mentioned aliquots, but without any pre-concentration step (just dissolved in 3M HNO_3 and introduced into the instrument).

The results indicate that all the REE, with the exception of lanthanum, can be quantitatively recovered following our proposed procedure. As in the previous section, the REE recovery of the pre-packed Nobias cartridges is above 93 % in a seawater matrix. Excluding La, the difference between the on-column calibrations and the external standards

remained below 7% for all the REE over all concentrations, with the exception of Ce that showed a difference of 16% at 5 pg g^{-1}. The on-column calibrations showed a good linearity with a correlation coefficient above 95% (Figure 3). The calibration curve for La is not presented because it showed what appears to be contamination issues throughout all of our experiments which prevented us from obtaining a linear calibration. Confirmation that La signals were not being compromised through additional overlapping BaH formation was obtained through repetitive analysis of mono-element Ba solutions. BaH formation rate was quantified as < 0.05% under typical working conditions. The anomalous La calibration curve could also be caused by the presence of Ba in the "REE-free" seawater used for the calibrations. The relative abundance of ^{138}Ba could be contributing with tailing to the much less abundant ^{139}La. However, this theory was discarded after analyzing the REE elution fractions and finding no significant Ba amount. In addition, the analysis of the intercalibration material BATS15 showed anomalous La concentrations that confirm a potential La contamination (see blanks section).

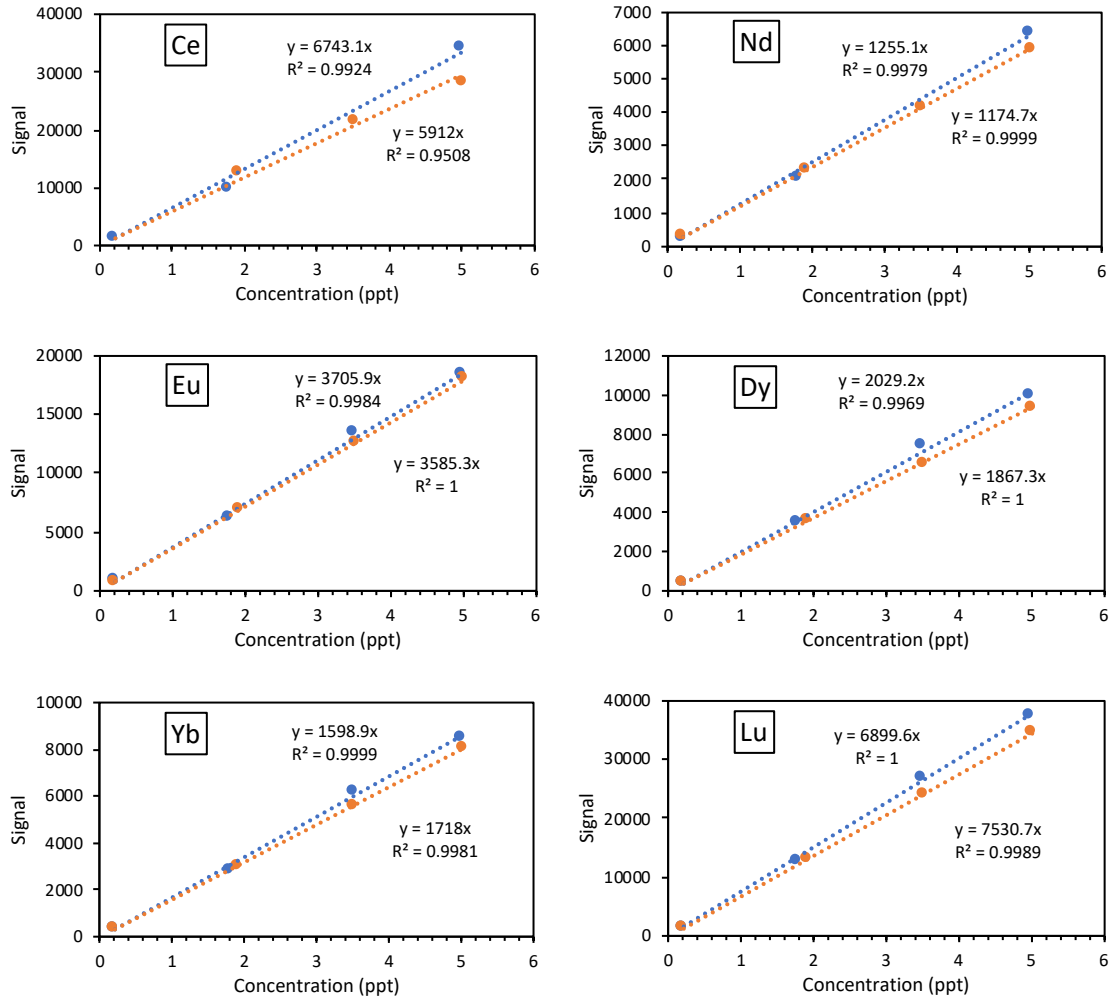

Figure 4-3. External calibration curves for REE spiked seawater eluted from Nobias cartridges (orange dots) compared to an external calibration (blue dots) for selected REE dissolved in 3M HNO3. For the sake of simplicity, we do not present the graphs for every REE.

3.1.3 Blank levels and detection limit

The REE blank contributions of our method are within the reported values in previous studies (Zheng et al., 2015; Behrens et al., 2016), with the exception of lanthanum, cerium and neodymium. In addition to the calibration problems stated in the previous section, the La blank is about 20 times larger than in the mentioned studies. Therefore, we have no other option to explain these anomalous La levels other than blank contribution. Although experiments are on their way to identify this source, at the moment of writing this thesis we do not know exactly where this La is coming from. The Ce and Nd blanks are 4 and 10 times larger respectively than previous studies. However, they only represent less than 5 % of the concentration found in the BATS15 reference material. The blank contribution for the rest of the REE is less than 2 % of the signal associated with the same reference material.

Element	Average Blank (pmol/kg)	Detection Limit (pmol/kg)
La	2	1.6
Ce	**0.870**	**0.042**
Pr	0.080	0.275
Nd	**0.600**	**0.517**
Sm	0.007	0.008
Eu	**0.002**	**0.002**
Gd	0.010	0.020
Tb	**0.001**	**0.002**
Dy	0.020	0.050
Ho	**0.001**	**0.002**
Er	0.005	0.007
Tm	**0.001**	**0.001**
Yb	0.002	0.004
Lu	**0.001**	**0.001**

Table 4-2. Average procedural blanks during REE determination from HEOBI samples (n = 8). The detection limit is reported, equals to three times the standard deviation of the total procedural blanks.

3.1.4 Quality assurance

The repeated analysis of the BATS15 intercalibration standard indicates a good overall accuracy for our method within 5% of agreed values (van de Flierdt et al., 2012; Behrens et al., 2018) for all the REE with the exception of La that is almost twice the consensus value. As reported in the previous sections there is an issue in the determination of La with our method that we have not fully resolved. The long-term precision (3 months, 7 ICP-MS sessions) of the analysis of the BATS15 material during the study is better than 10 % for all the REE with the exception of Ce and Lu, that showed values of 15% and 12%, respectively. These results indicate that our method can effectively be used to measure REE concentrations (excepting La) from seawater samples.

BATS 15m

	La	Ce	Pr	Nd	Sm	Eu	Gd	Tb	Dy	Ho	Er	Tm	Yb	Lu
Average of this study (n=5)	27.1	12.5	3.30	14.17	3.27	0.89	4.72	0.79	5.68	1.48	4.72	0.66	4.19	0.65
2σ SD (pmol/kg)	8.9	1.8	0.3	0.7	0.1	0.05	0.4	0.05	0.4	0.1	0.4	0.1	0.4	0.1
2σ RSD%	33	15	9	5	4	6	7	7	7	9	9	10	9	12
GEOTRACES intercalibration value	14.7	12.0	3.12	14.10	3.21	0.89	4.83	0.79	5.90	1.49	4.80	0.70	4.16	0.67
2σ SD (pmol/kg)	2.2	2.7	0.4	1.2	0.4	0.1	0.6	0.1	0.5	0.1	0.4	0.1	0.5	0.1
2σ RSD%	15	23	12	9	11	12	11	11	9	9	9	9	12	14
Behrens et al. Value (n=5)	14.1	11.9	3.3	14	3.2	0.86	4.84	0.81	5.91	1.45	4.83	0.69	4.24	0.69
2σ SD (pmol/kg)	1.2	1.3	0.2	0.4	0.1	0.02	0.25	0.01	0.2	0.04	0.1	0.02	0.1	0.01
2σ RSD%	9	11	8	3	2	2	5	1	4	3	2	2	3	1

Table 4-3 REE concentrations in the GEOTRACES BATS15 intercalibration sample compared to previously reported values.

For the quality control of the ε_{Nd} measurements, a 2.5 L aliquot of MQW containing ~50 ng JNdi-1 reference material was processed for every batch of 11 samples. The resulting solution was processed as described in Chapter 2, including pre-concentration, anion and cation exchange chromatography, and finally the Nd isotopes were isolated using the LN resin. The procedural ~50 ng JNdi-1 standards analyzed by TIMS (Figure 4, grey diamonds 2SD, 39 ppm) are within the external reproducibility of the instrument (Figure 4, grey shading

2SD; 43 ppm on 5 ng), and within the analytical error to the value reported by Tanaka et al.(2000) of 0.512115 ± 14 ppm (Figure 4, black circle).

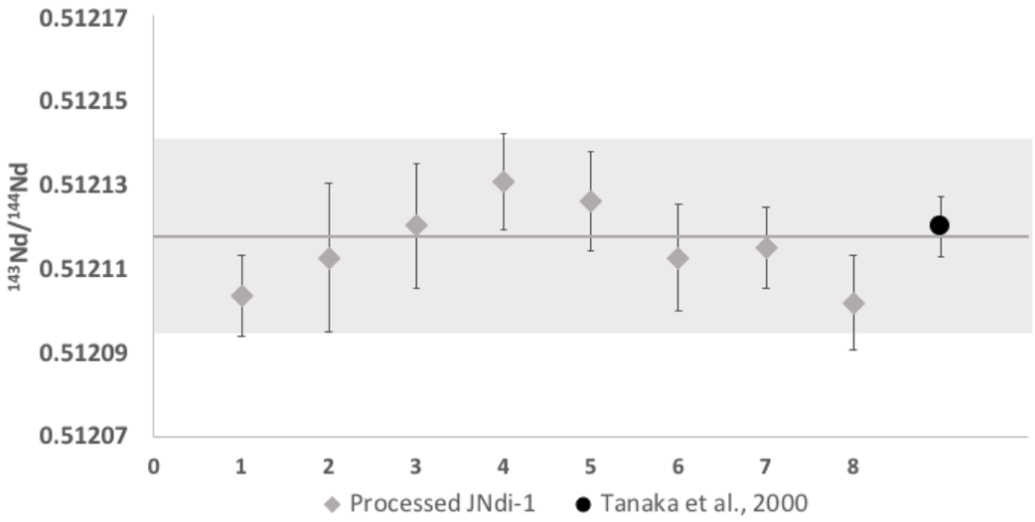

Figure 4-4. Corrected $^{143}Nd/^{144}Nd$ values (grey diamonds) for the JNdi-1 quality control samples containing ~50 ng of Nd, within the analytical uncertainty of the JNdi-1 reference value (Tanaka et al., 2000; black circle). The grey shading represents the instrument external reproducibility (2SD; 43 ppm on 5 ng) of 14 measurements of the JNdi-1 (5 ng) performed through the different measuring sessions in the TIMS.

3.2 Rare Earth Element profiles

For the presentation of the REE concentration results, we separate deep from shallow stations. Amongst the deep sites, Station 18 is located on the western flank of the plateau and was considered as the reference station of the last chapter. Stations 9 and 12 are located on the eastern slope of the plateau and Station 6 is located 400 km east of the Kerguelen Plateau, just south of the Polar Front. The REE concentration depth profiles for these stations are plotted together in the same figure to make it easier to identify trends in their behavior (Figure 5). Individual REE concentrations of the coastal stations 22,30,31, and 34 are plotted together with Station 16, which is located in the middle of the central part of the KP.

The REE concentrations in the deep stations indicate a typical nutrient-like behavior for the open ocean with low concentrations towards the surface that gradually increase with depth (Elderfield and Greaves, 1982; De Baar et al., 1985; Elderfield et al., 1988). The only element that does not follow this trend is Ce, which presents relatively high concentrations

in the surface of Stations 6 and 9. Below 300 m Ce concentrations are lower, and the variability in Ce concentration is largely within the analytical uncertainty of our method. An outstanding feature of the deep stations is that station 18, which was considered as a reference station for other parameters such as Th (previous chapter) and Fe (Holmes et al., 2019) does not seem to apply for the REE. The concentration profiles clearly indicate that Station 6 has the lowest concentrations and less variable profile. Furthermore, the REE concentrations increase towards the bottom of Station 18, probably influenced by the addition of REE by dissolution of bottom sediments.

The REE concentrations in all shallow stations (16, 22, 30, 31 and 34) are higher than in all deep stations at the same depth range (Figure 5). Furthermore, the REE concentrations measured around HIMI are the highest of our data set in the surface portion of the water column. At Station 16, located in the central part of the Plateau, the concentration profiles of the REE from Ce to Tb indicate a surface maximum which quickly decreases into a subsurface minimum value. This pattern is more evident toward the lightest REE and decreases as the atomic number increases. For the rest of the "heavier" REE this characteristic disappears and values simply increase with depth. This behavior clearly reflects that heavier REE are less likely to be scavenged by particles (Elderfield et al., 1988).

The REE concentrations in both the deep and shallow stations are within the range of values reported by previous studies in the Kerguelen Plateau (Zhang et al., 2008; Grenier et al., 2018), in the South Atlantic (Garcia-Solsona et al., 2014) and in other parts of the Southern Ocean (German et al., 1995; Hathorne et al., 2014).

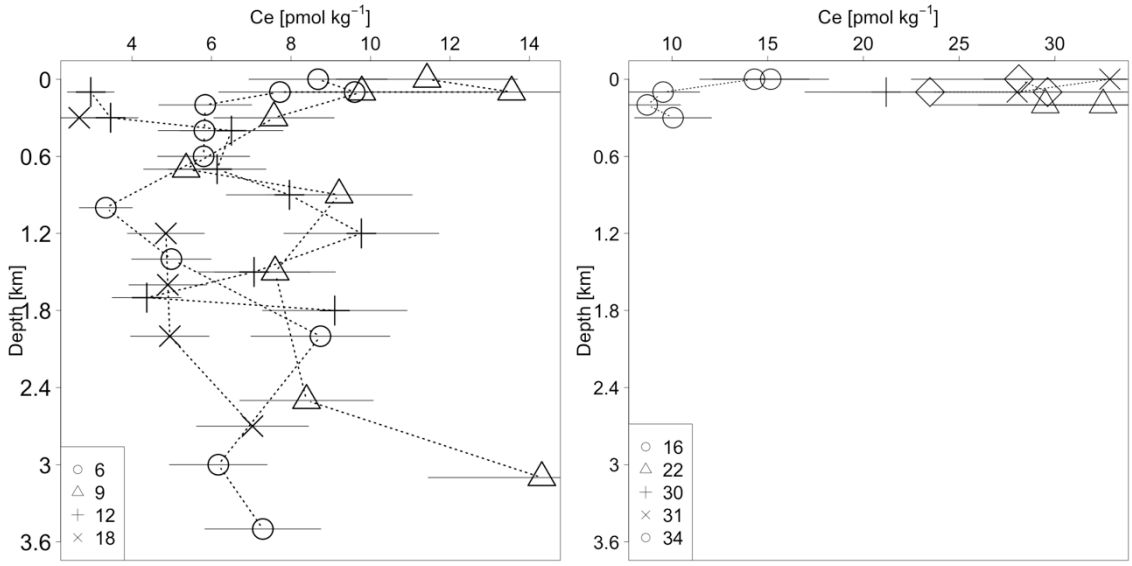

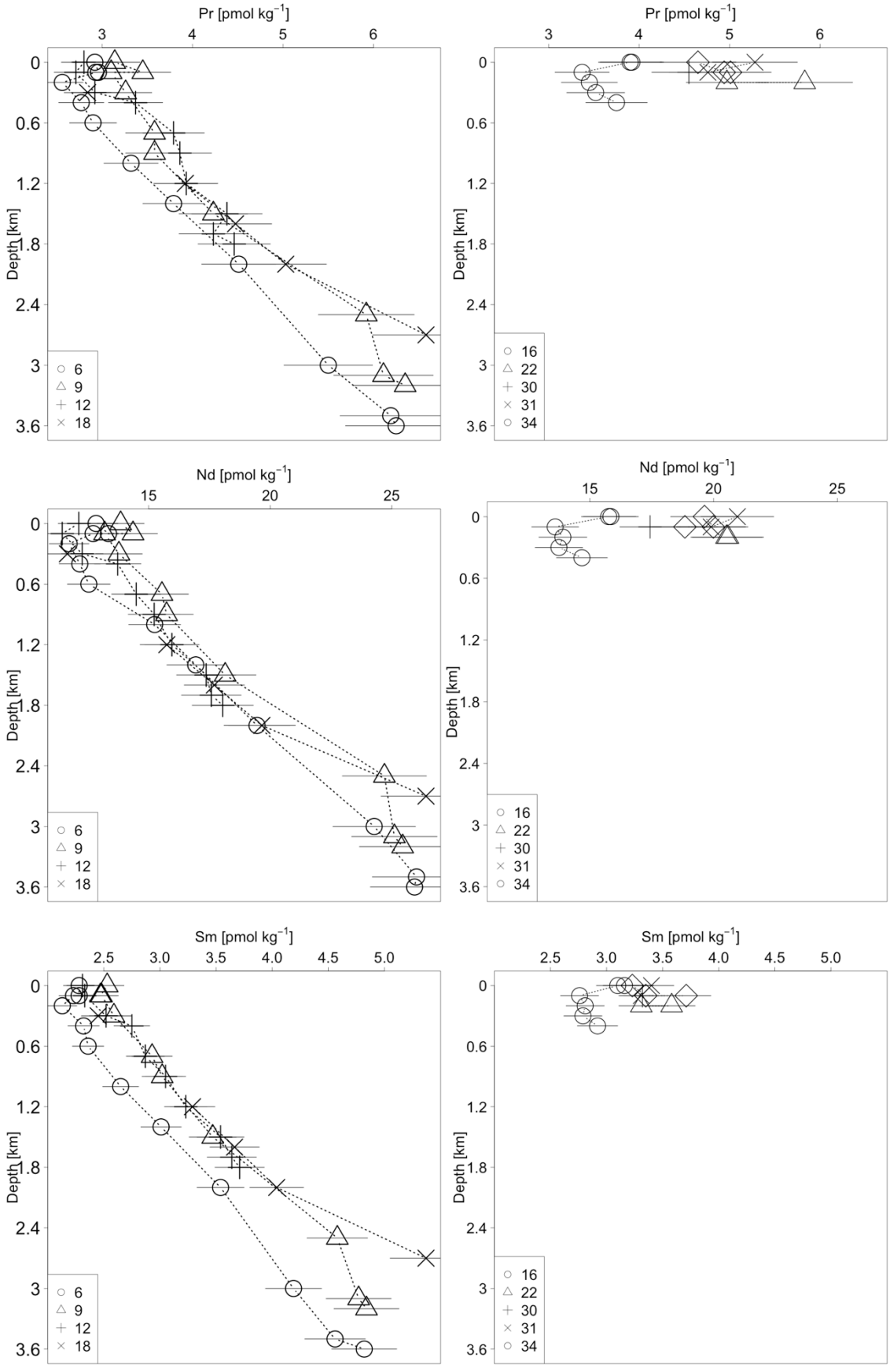
Pr [pmol kg^{-1}]
Nd [pmol kg^{-1}]
Sm [pmol kg^{-1}]
Depth [km]
6
9
12
18
16
22
30
31
34

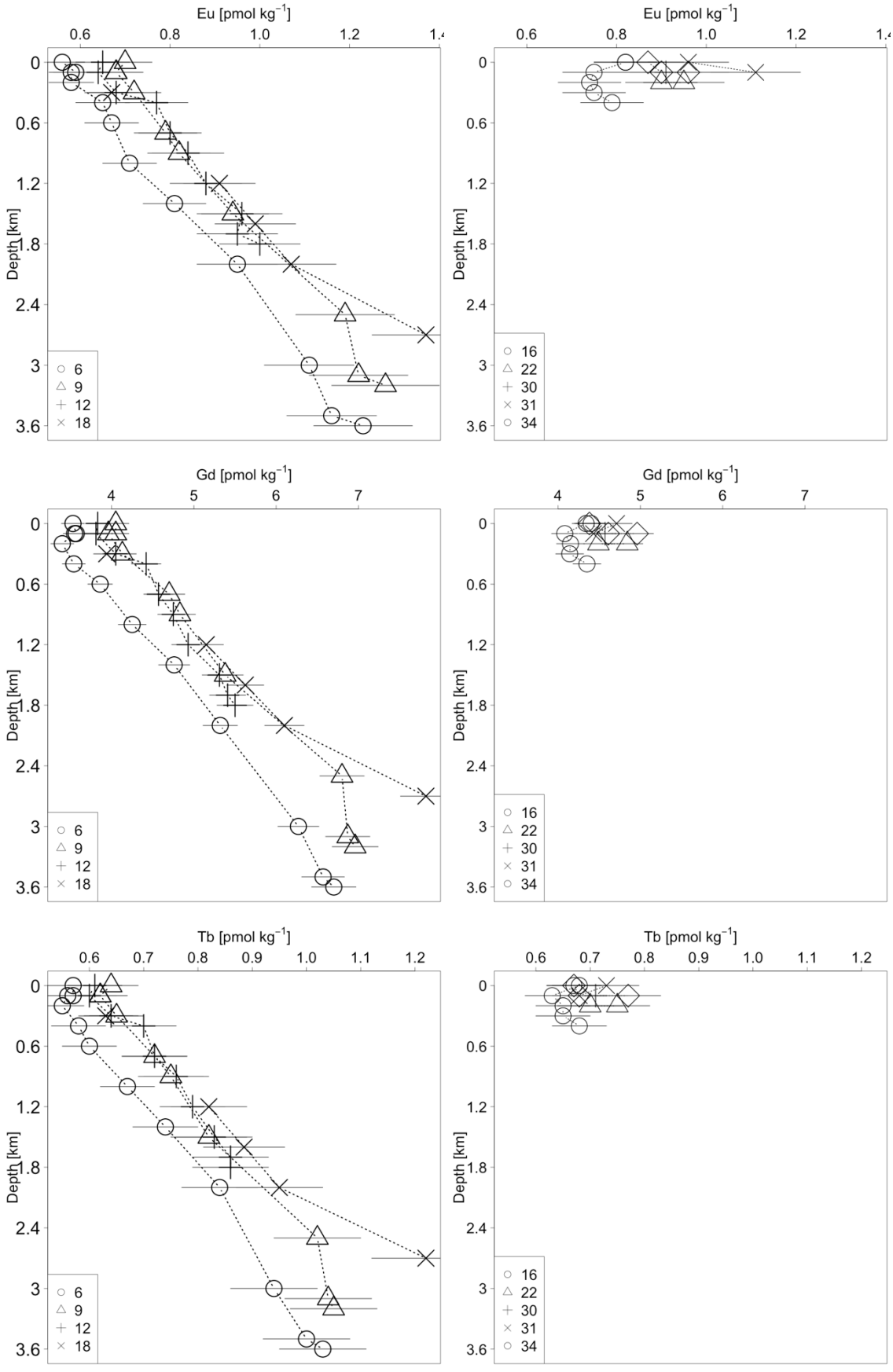
Eu [pmol kg^{-1}]
Gd [pmol kg^{-1}]
Tb [pmol kg^{-1}]
Depth [km]
6
9
12
18
16
22
30
31
34

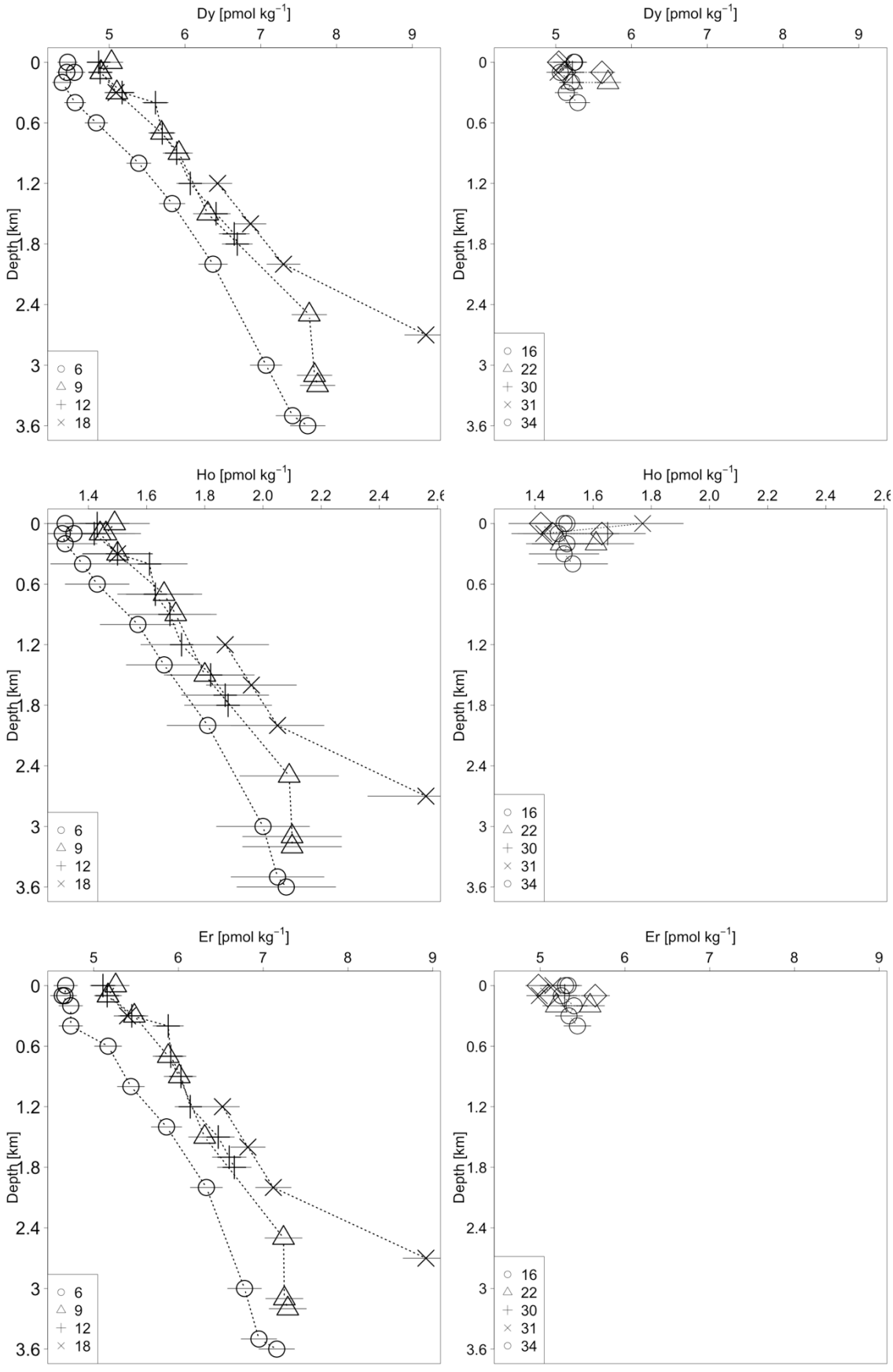
Dy [pmol kg^{-1}]
Ho [pmol kg^{-1}]
Er [pmol kg^{-1}]
Depth [km]
6
9
12
18
16
22
30
31
34

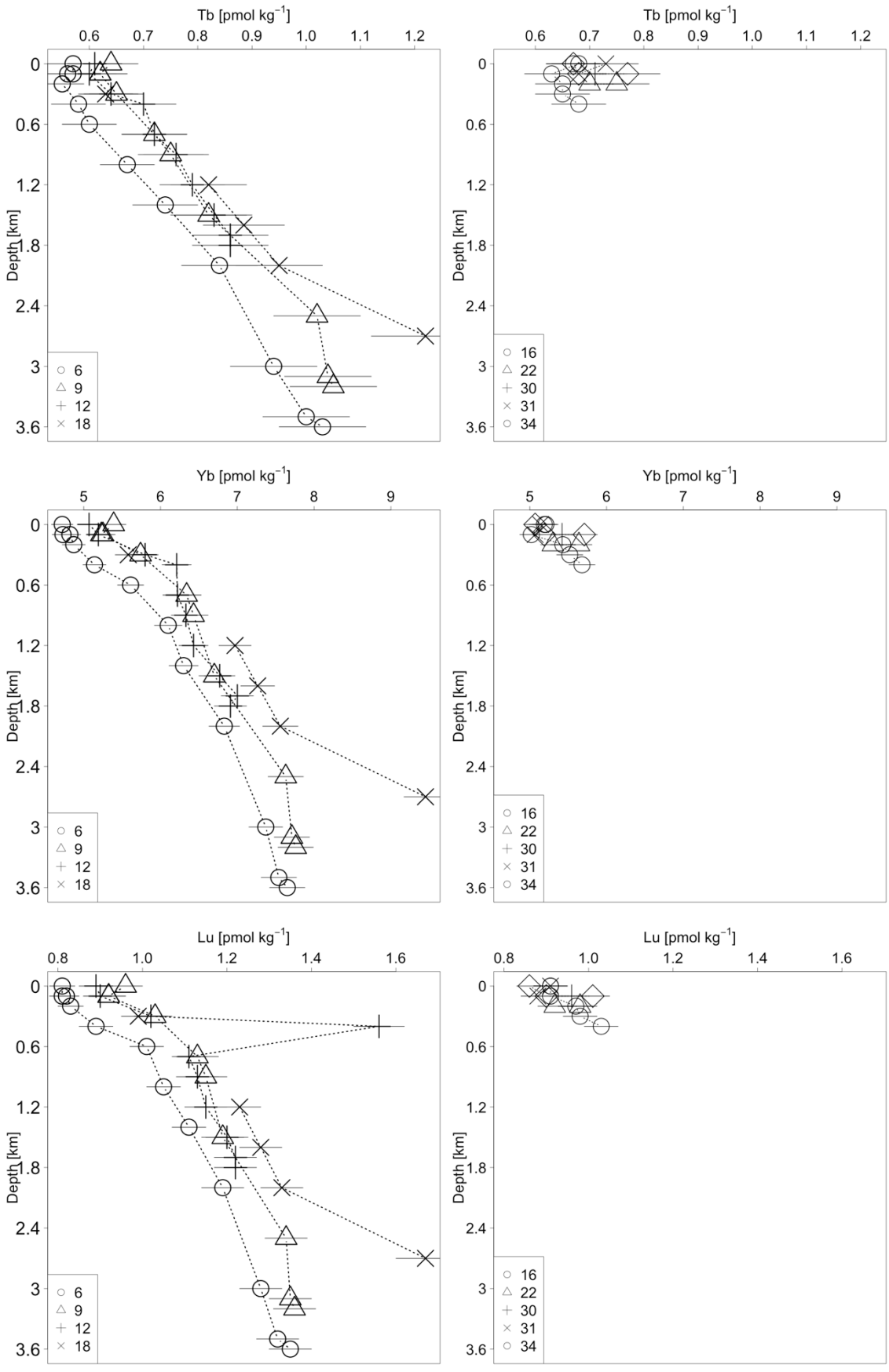
Tb [pmol kg^{-1}]
0.6 0.7 0.8 0.9 1.0 1.1 1.2
Depth [km]
0 0.6 1.2 1.8 2.4 3 3.6
6
9
12
18
16
22
30
31
34
Yb [pmol kg^{-1}]
5 6 7 8 9
Lu [pmol kg^{-1}]
0.8 1.0 1.2 1.4 1.6

Figure 4-5. REE concentration depth profiles for the HEOBI voyage. Left panels represent the concentrations found at the deep stations (6,9,12,18), and right panels show the concentrations at station 16 (central KP) and the rest of the HIMI coastal stations (22,30,31,34) to the right. La has been excluded due to blank contamination issues.

We also present the vertical distribution of Ce and Eu anomalies and the PAAS normalized $(Nd/Yb)_n$ ratio. Neodymium is considered here as a substitute for La due to previously mentioned contamination issues with La, and provides similar information to the more commonly used $(La/Yb)_n$ on the fractionation between light and heavy REE. (which gives information about the "age" of lithogenic inputs). In the following, Ce and Eu anomalies are defined as "positive" if > 1 and negative if < 1. The closer the values are to 1, the weaker the anomaly, and the strength of the anomaly increases as the value moves away from one.

All the samples from all stations present a negative Ce anomaly, which is typical of seawater (Figure 6a; Sholkovitz et al., 1994; Bolhar et al., 2004). Near-surface samples in the deep and shallow stations have a weaker negative anomaly, being weakest in the near-island stations (Figure 6b). In the deep stations the negative Ce anomaly becomes stronger with depth.

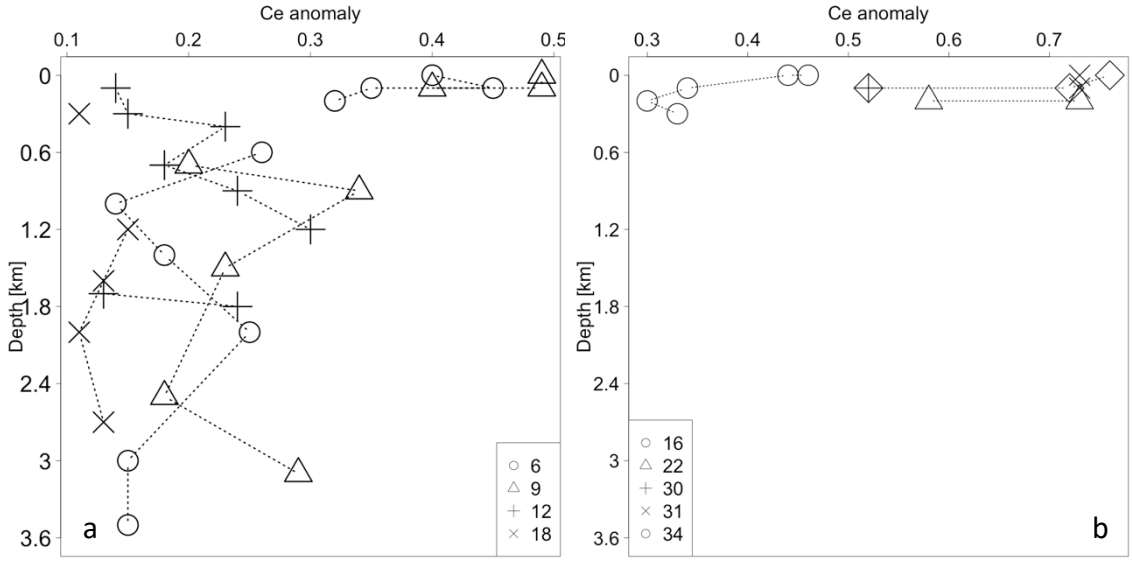

Figure 4-6. Cerium anomaly profiles in (a) deep and (b) shallow station of the HEOBI voyage.

A weakly positive Eu anomaly is evident for most of the deep stations' samples (Figure 7a) and in Station 16 located in the central part of the plateau (Figure 7b). However, the top 100 m of Station 6 present a very weak negative Eu anomaly. Coastal stations 22, 30 and 34 all present a weak positive Eu anomaly value (~1.1, Figure 7b)). Station 31, located adjacent/proximate to the front of one of the glaciers that exist on Heard Island presents the strongest Eu anomalies (1.2 and 1.4) of our dataset.

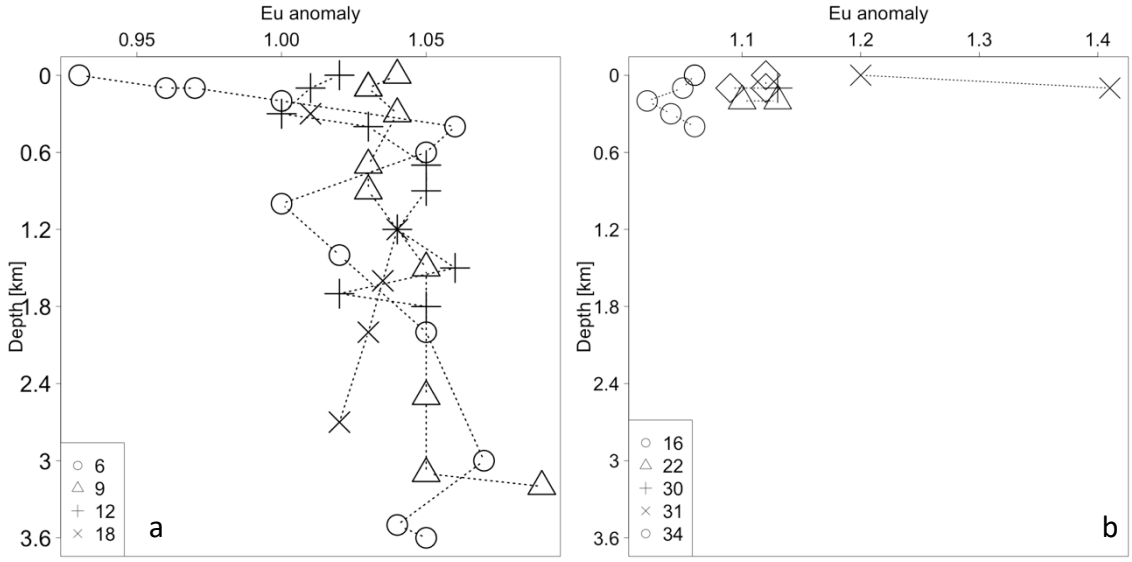

Figure 4-7. Europium anomaly profiles in (a) deep and (b) shallow station of the HEOBI voyage.

The Nd/Yb normalized ratio is an indicator of the fractionation between the lighter and heavier REE produced by the different scavenging processes and intensity that affects them (Elderfield et al., 1988). Considering surface samples, lower fractionation (higher value) can be considered as an indication of a recent lithogenic imprint on the dissolved REE concentration in seawater. All the deep stations have a subsurface maximum value that decreases until achieving a minimum value for the entire water column at ~ 600 m (Figure 8a). Below this depth the $(Nd/Yb)_n$ ratio increases gradually and achieves the maximum values with depth, very likely due to the reversible scavenging processes. As expected, the stations located near the islands present the highest values due to the recent input of dissolved REE from lithogenic material (Figure 8b).

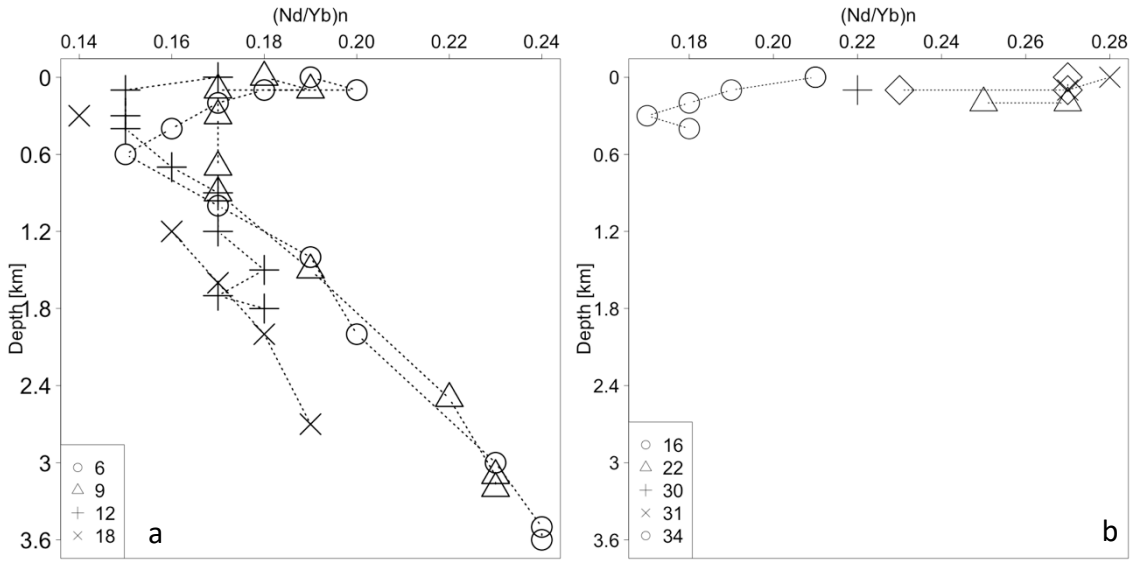

Figure 4-8. PAAS normalized $(Nd/Yb)_n$ ratio in (a) deep and (b) shallow station of the HEOBI voyage.

3.3 Neodymium isotopic composition (ε_{Nd})

The Nd isotopic composition of the top 700 m of the water column at the deep Stations 6, 12, 18 and 25 indicate a mixed isotopic composition that ranges from -7.6 to -9.4 ε_{Nd} units. At Stations 6, 9, 12 and 25 below 700 m, the ε_{Nd} signal gradually decreases towards 1,200 m depth to a value close to -10. Below 1,200 m, the ε_{Nd} remains constant (ε_{Nd} = -9.7 ± 0.4) and within the analytical uncertainty of the measurement (Figure 9a). Station 18 exhibits the same pattern, however the ε_{Nd} from 800-1,600 m is slightly more radiogenic than the previously mentioned stations (Figure 9a). In addition, the two deepest samples of Station 6 also have a slightly more radiogenic value of -8.9 and -9.0 at 3,476 and 3,576 m respectively (Figure 9).

Shallow Stations have in general more radiogenic ε_{Nd} values than deep stations (Figure 9b). However, at 15 m Station 16 has a ε_{Nd} of -9.9 ± 0.3 (Figure 9b), which is comparable with the average ε_{Nd} of the top 600 m in the deep stations (ε_{Nd} = -9.7 ± 0.4). At 40 m, the Nd isotopic composition of Station 16 quickly becomes more radiogenic (-6.7 ± 0.2). Lower in the water column, and following the trend of the deep stations, the ε_{Nd} gradually decreases to a value of -8.1 ± 0.4 and remains similar until 300 m (-8.0 ± 0.5). The stations located near the islands have the most radiogenic values of our dataset (-5.6 ± 0.5; n=6).

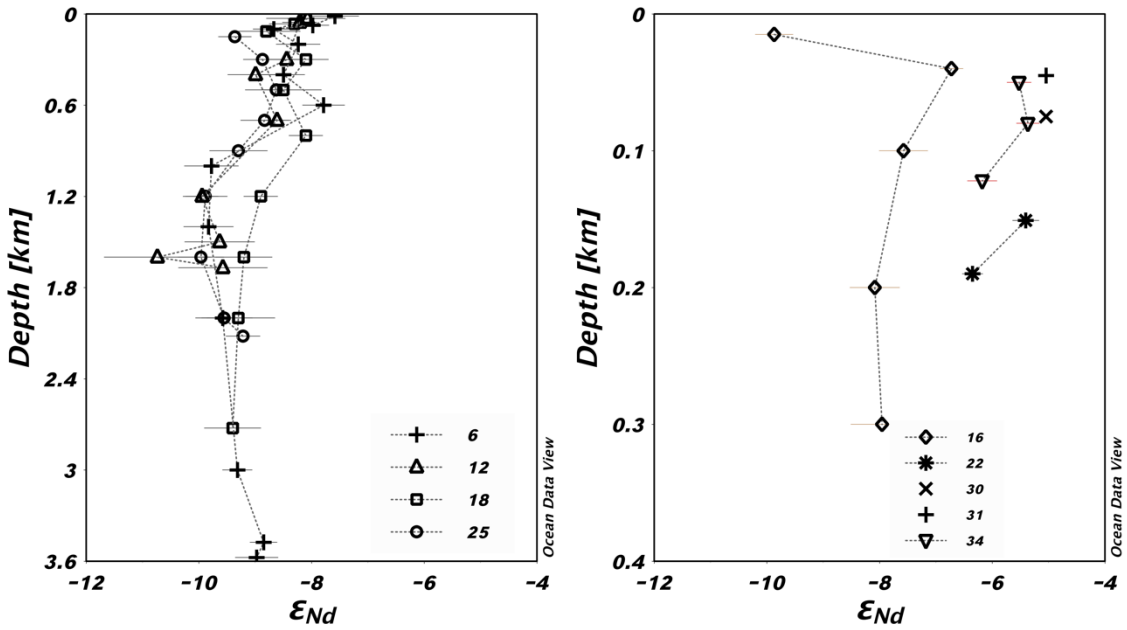

Figure 4-9. ε_{Nd} composition of the water column during the HEOBI voyage.

3.3 REE and ε_{Nd} in HEOBI sediments

The 15 sediment samples collected during the HEOBI voyage indicate quite homogenous REE concentrations. For the sake of simplicity, we present the PAAS normalized patterns averaged for samples around Heard Island, McDonald Island and South of both islands, respectively. All samples considered present an Eu enrichment relative to the PAAS content which is characteristic of the basaltic material from the Kerguelen Plateau (Barling et al., 1994; Weis et al., 2002; Doucet et al., 2005). This enrichment is very similar for Heard and McDonald Islands, however it is twice as large for the two samples located south of HIMI (Figure 10). The ε_{Nd} of the sediment samples is homogenous in the three areas with ε_{Nd} values ranging from -0.5 to 1 ($\bar{x}$ = -0.7±0.8). These values are within the range reported for recent basalts of the Kerguelen Plateau (ε_{Nd} =-2 to 1; Weis et al., 1992)

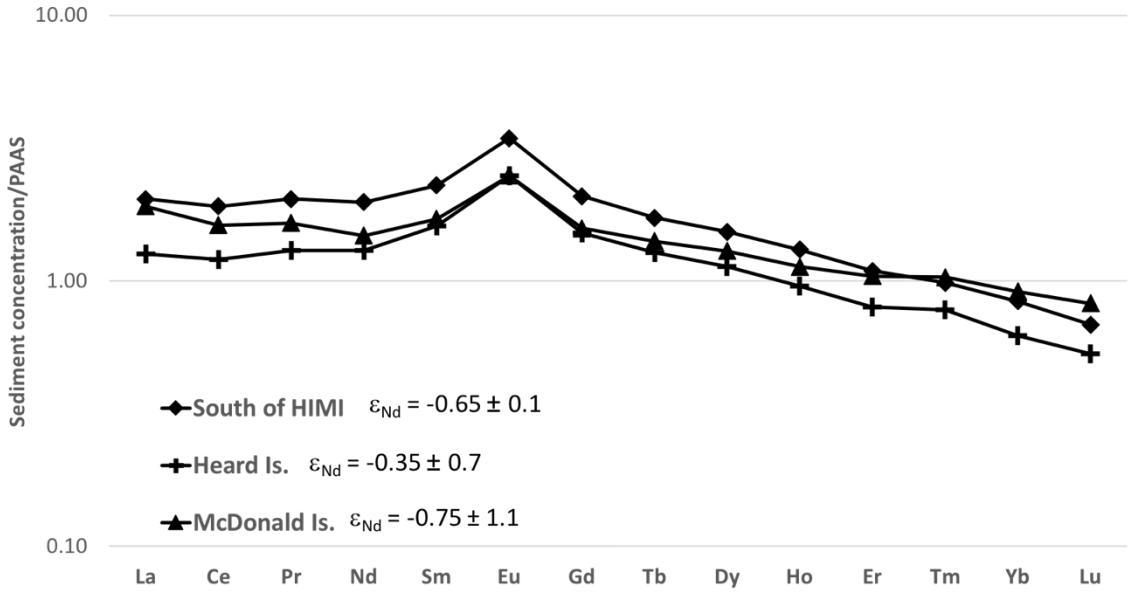

Figure 4-10. Average of PAAS normalized patterns of sediments collected South of HIMI (n=2, diamonds), around Heard (n=6, crosses) and McDonald Islands (n=7, triangles) during the HEOBI voyage.

4. Discussion

4.1 Sources of REE to the Kerguelen Plateau

The concentrations of REE indicate a enrichment of most of the REE above and on the slopes of the plateau, compared to REE concentrations found in Station 6. Almost all samples have higher REE concentrations compared to Station 6, located far to the west of the plateau (Figure 5). Additionally, more positive $(Nd/Yb)_n$ ratios (Figure 8) and weak negative Ce anomalies (Figure 6) in all coastal stations suggests a recent contact between seawater and lithogenic material sourced from the plateau. These finding are expected as it has been previously established that the KA as well as the HIMI area provide a constant supply of lithogenic particles that allow Fe-limitation in this HNLC region to be overcome (Blain et al., 2008; Bowie et al., 2015; Holmes et al., 2019; van der Merwe et al., 2019). However, the relative contribution of each group of islands is still not completely understood. Zhang et al.(2008) and Grenier et al.(2018) both highlighted the importance of REE (and Fe) around HIMI and transported northwards by the dominant circulation above the plateau (Figure 11; Park et al., 2008). This iron supplies the productivity bloom above the central part of the

plateau, south of the PF. However, the contribution of the KA to the above-mentioned region remains unclear. Radium isotope data suggested that waters that were in recent contact with the KA could potentially supply trace elements across the PF through mesoscale intrusion (Sanial et al., 2015). However, the extent/importance of this lithogenic supply mechanism is still unclear. The uncertainty in the relative importance of both lithogenic sources is in great part because of a lack of sampling resolution in the central and southern parts of the plateau. In this section we incorporate our REE and ε_{Nd} data collected around HIMI to the existing datasets produced by the KEOPS 1 (Zhang et al., 2008) and KEOPS 2 (Grenier et al., 2018) voyages in order to better constrain the sources of REE and other trace elements of the central KP waters. To better understand the possible input of each group of islands and the shallow areas that surround them, we focus on the samples located in the top 600 m of the water column.

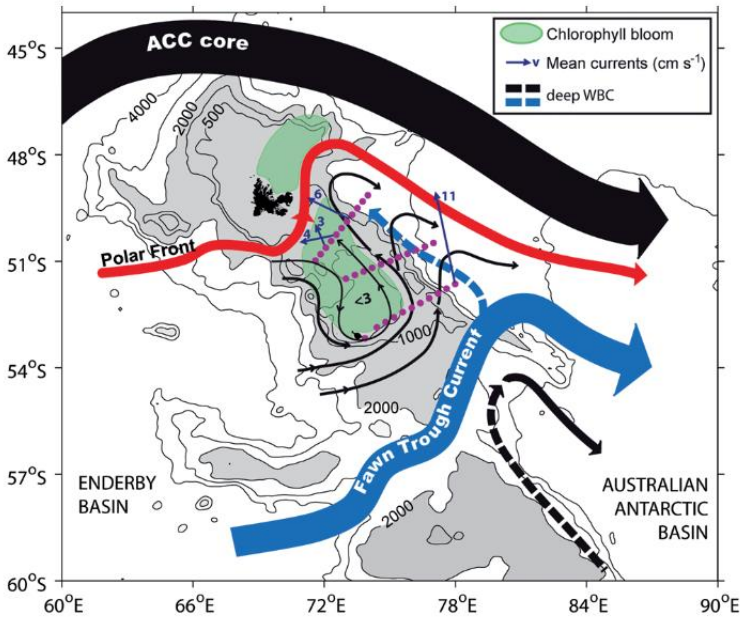

Figure 4-11. Predominant circulation pattern in the Kerguelen Plateau (taken from Park et al., 2008b). The green colour represents areas where it is historically known for the bloom to appear in the region once the sun is no longer limiting after the beginning in the austral spring. Red arrow represents the Polar Front.

The relationship between the Eu anomaly and $(Nd/Yb)_n$ in samples of the top 600 m of the water column clearly reveals the difference between the dissolved signal of Heard

Island with the one representative of the KA (Figure 12). The $(Nd/Yb)_n$ values indicate a recent input of lithogenic material in both areas. However, the samples collected around HIMI present a significant positive Eu anomaly (~1.1; Figure 12), while the samples around the KA have a negative anomaly (~0.70; Figure 12).

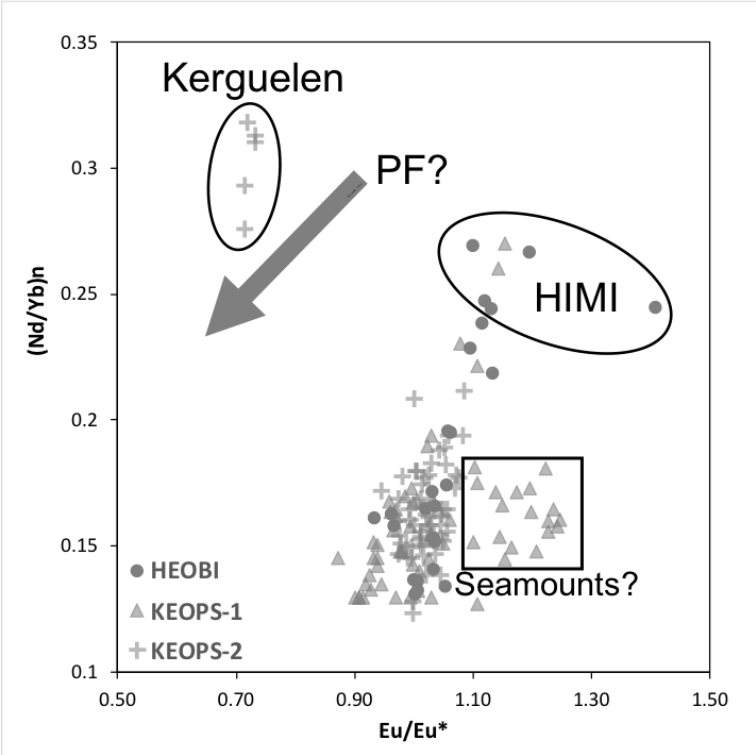

Figure 4-12. Relationship between Eu anomaly and (Nd/Yb)n values for samples above 600 m during the KEOPS 1 (triangles), KEOPS 2 (crosses) and HEOBI (circles, this study) voyages.

This difference has been explained as an enhanced leaching of trachyte and rhyolite veins present in the flood basalts from the KA (Grenier et al., 2018). These veins are characterized by a negative Eu anomaly due to a dominant glassy matrix, in contrast to the matrix alkali feldspars and plagioclases that have a positive Eu anomaly. Although the difference in the rock composition might play a role in the Eu anomaly of the seawater, the number of seawater-exposed veins of such material is not clear. Furthermore, after calculating the Eu anomaly of basalts from the KA collected in previous studies (Barling et al., 1994; Weis et al., 2002; Doucet et al., 2005), their Eu anomaly is higher (~ 2.2) than the rock samples collected near HIMI (~ 1.7). This is a surprising result and an indication that the chemical composition of the source material is not the cause of the negative Eu anomaly of the seawater close to the KA. However, this hypothesis requires further work and analysis.

Therefore, we are more inclined to believe that the positive Eu anomaly around HIMI is due to hydrothermal or glacial input. In fact, Heard Island coast is highly covered by glaciers (Figure 13) and van der Merwe et al. (2019) demonstrated that these glaciers are a source of highly labile Fe particles. Alternatively, high Fe^{2+} concentrations (Holmes et al., submitted) and ^{3}He enrichment were found around HIMI which seem to confirms the presence of hydrothermal activity, that produces an enrichment of Eu close to the source.

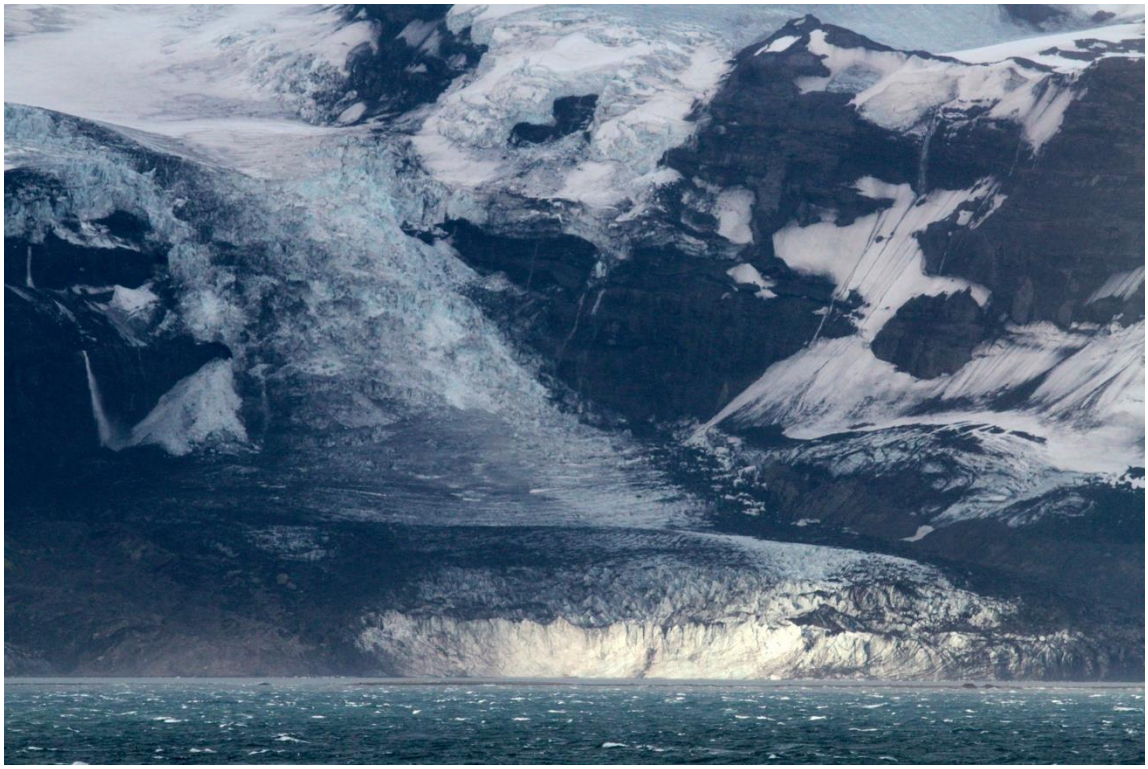

Figure 4-13. Image of one of the many existing glaciers in Heard Island. Note that the ice contains a large load of lithogenic particles and that it is in direct contact with the seawater. Additionally, streams of melt-water directly discharge into the ocean. Picture courtesy of Pete Harmsen.

The significant positive Eu anomaly found around HIMI seems to be transported and fade northwards following the predominant north-eastward circulation above the plateau (Figures 11 and 12; Park et al., 2008; Park and Vivier, 2011). All the samples from the three campaigns (excepting the ones collected next to the KA) seem to fall within this dilution pattern. Even the station sampled south of the PF during the KEOPS 2 voyage (E1, E3, E4W, E5, F-L,TEW3 and TEW7; Grenier et al., 2018) do not carry the Eu signature from the KA. Furthermore, $(Nd/Yb)_n$ ratios and Ce/Ce* values at the above mentioned stations do not

indicate any recent lithogenic input. These results confirm the findings of previous studies (Zhang et al., 2008; Grenier et al., 2018) that suggest a surface/subsurface southern source of REE transported north-eastward across the plateau all the way south of the PF, and then continues eastward parallel to the flow path of the PF (see next section). The contribution of the KA -derived material to the area south of the polar front as suggested by Sanial et al.(2015) and Grenier et al.(2018) seems less likely, or at least does not seem to be strong enough to modify the REE signature of the central part of the KP, as none of the samples collected close to the PF seem to carry the signal from the Kerguelen Islands (Figure 12).

At this stage it was tempting to discard the eddy-derived intrusions of KA material through the PF as a potential source of dissolved REE (and probably Fe according to other studies). However, strong lateral mixing can also produce the negative Eu anomaly preventing detection of this signature in the stations to the east. To further explore this, we now incorporate ε_{Nd} data available for samples collected from the top 600 m of the KEOPS 2 voyage and from this study (leaving out any sample with an analytical error > 0.5 ε_{Nd} units), in order to see if this quasi-conservative tracer can provide more information about all the coastal and plateau-originated sources of lithogenic material and trace elements to the waters above and around the KP.

It has been previously established that the seawater from the KA has a more radiogenic dissolved signal (ε_{Nd} = -3.4 to -2.6; Grenier et al., 2018) while our data collected around HIMI indicates a less radiogenic seawater signal (Figure 14; ε_{Nd} = -5.0 to -6.4). Therefore, if strong mixing was responsible for the negative Eu anomaly, then the ε_{Nd} would still carry the signal of the KA as the intensity of the mixing should not affect the Nd isotopic composition. Therefore, we would expect to see a dilution of the more radiogenic signal of the KA seawater.

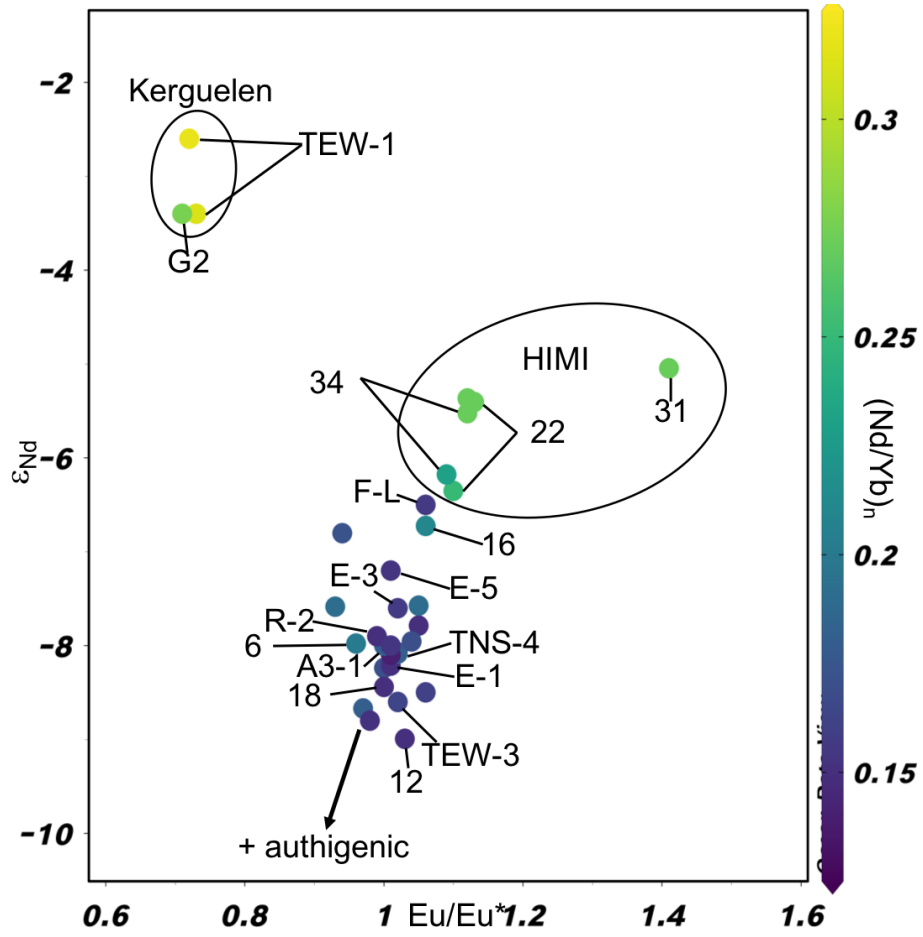

Figure 4-14. Eu/Eu* (x-axis), ε_{Nd} (y-axis) and (Nd/Yb)n (color axis) of samples from the top 600 m of the water column during the KEOPS 2 (Grenier et al., 2018) and HEOBI (this study) voyages .

The ε_{Nd} signal of most of the samples from our study and the KEOPS 2 voyage follow a mixing pattern that starts in HIMI (Figure 14). It is clear that the ε_{Nd} signal of HIMI (-5 to -6.4) dilutes with the northward flow of the circulation. As the flow approaches the PF, Stations E1, E3, E5, TNS4 and TEW6 have an average ε_{Nd} signal of -8 ± 0.6. Moreover, station TEW3, located on the northern part of the PF and just a few tens of km east of the Kerguelen Island, presents a ε_{Nd} value of -8.6 ± 0.2. Such ε_{Nd} values can be found in the surface of the Atlantic sector of the SO (Stichel et al., 2012; Garcia-Solsona et al., 2014). They likely reflect SO surface water transported along the Polar Front that has not interacted with sediments derived from the KA.

The only stations that seems to indicate some KA signal are Stations F-L (KEOPS 2) and 6 (this study), with ε_{Nd} surface values of -6.8 and -7.6, respectively. These stations are located in an area where the Polar Front converges with the surface circulation observed over the plateau, meaning that the more radiogenic value could very well be the result of the more radiogenic seawater signal from the KA, transported here by the PF. This theory is supported by slightly negative Eu (0.94 at Station F-L and 0.93 at Station 6) anomalies at the surface of both stations, and Ce anomalies and Nd/Yb ratios that do not indicate any recent particle/seawater interaction that could produce such radiogenic ε_{Nd} levels.

So far, Eu anomaly, ε_{Nd} and the (Nd/Yb)n data indicate that HIMI region is the main source of REE to the central KP. The data also suggests that the PF acts as an effective barrier for the material supplied in the vicinity of the KA, because its flow dilutes the signal due to the advection, and it is not until Station F-L and 6 that is possible to detect the signal from the Kerguelen Archipelago (Figure 12 & 14).

Additionally, another source of REEs seems to be present at station A-3 during the KEOPS 1 voyage (Figure 12, samples inside the black square). Zhang et al.(2008) suggested this potential source to be from the Kerguelen Islands - however, data from KEOPS 2 and from our study does not support this theory. We do not know the exact source of this signal, but considering the intensity of the Eu anomaly (~ 1.2) we can only hypothesize that it could originate from: the interaction of upwelling water with seamounts located north of HIMI, which is subsequently transported laterally to Station A-3; or by the effect of hydrothermal activity in the region. In addition, REE concentrations in Zhang et al. (2008) were measured without the use of a desolvating nebulizer, therefore there might be an overestimation of the Eu concentration due to barium oxide formation. Based on current measurements we cannot rule out any of these options. A more detailed sampling of the area between HIMI and the PF, especially in the western flank of the plateau, will provide more insight about this potential additional source of material.

4.2 Transport pathways above the plateau

In the previous section we demonstrated that HIMI and the Kerguelen archipelago have different Eu/Eu* and ε_{Nd} dissolved signals, which indicate two possible sources of lithogenic material to the plateau. It was evident, through (Nd/Yb)n sample ratios, that these

signals are diluted as the water travels north towards the polar front (Figure 12 and 14). This transport is in accordance with the surface circulation that has been observed above the central and northern parts of the KP (Figure 11; Park et al., 2008; Zhang et al., 2008; Zhou et al., 2014; Park et al., 2014).

Under normal seawater redox conditions Ce is present in the less soluble 4+ oxidation state. This causes Ce to rapidly precipitate after it is added by dissolution of lithogenic material to the dissolved REE pool. Therefore, seawater normally has a strong negative Ce anomaly (Elderfield and Greaves, 1981). However, in our study, samples located close to lithogenic sources only show a weak negative Ce anomaly (Figure 15). Here, the input of lithogenic material is so constant that it allows for some Ce to still be detected in the dissolved fraction of seawater. As it is carried away from the source, authigenic processes become dominant and the Ce anomaly becomes increasingly negative, hence producing the typical depletion-pattern in seawater.

To provide a better understanding of the paths that REE follow over the plateau, the Ce anomaly was plotted for the surface samples from the three different sampling campaigns (Figure 1). It is surprising that, although the data presented in Figure 15 were not collected in the same year, it is possible to see a gradient with weak negative Ce anomalies close to HIMI, which gains strength as the circulation transports these coastal waters northwards.

Around HIM, the southeastward surface/subsurface circulation, labeled with a strongly authigenic signal (Station 18; Ce/Ce*=0.1), turns northeastwards as it encounters the front associated with the trough south of HIMI (Park et al., 2008). This circulation pattern transports northwards REE originated here, and then, authigenic processes immediately come into play. This quickly causes the negative Ce anomaly to gain strength and by Stations 16 (this study), B1 and B5 (KEOPS 1; Ce/Ce* = ~0.4). In addition to the HIMI-sourced REE, vertical mixing and interaction with plateau sediments might contribute with “new” REE, and attenuate to some extent the authigenic processes. As the waters reach Station G1 (KEOPS 2) the Ce anomaly has reached a value of 0.27 and the lithogenic contribution is almost insignificant. Close to the PF, in the core of the meander stations from the KEOPS 2 voyage stations (E5, E3, TNS4; Grenier et al., 2018) the negative Ce anomaly reaches a maximum strength (Ce/Ce*=0.24 ± 0.01). On the southern edge of the PF stream, the strength of the negative Ce anomaly decreases slightly (Ce/Ce* = 0.30,) very likely due to the effect of the Kerguelen archipelago. This signal remains as the circulation flows eastwards and parallel to

the flow of the PF (Station TEW7 & F-L). It is not until Station 6, where both systems converge, that a less authigenic REE signal (Ce/Ce*=0.40) was observed. However, we cannot determine if this lithogenic imprint to Station 6 is due to material originating from the central part of the plateau, which is laterally advected east across the subsurface component of the deep western boundary current (DWBC), or if it is a result of the KA signal transported here by the PF, or even caused by upwelling of REE dissolved from sediments deposited on the eastern slope of the plateau.

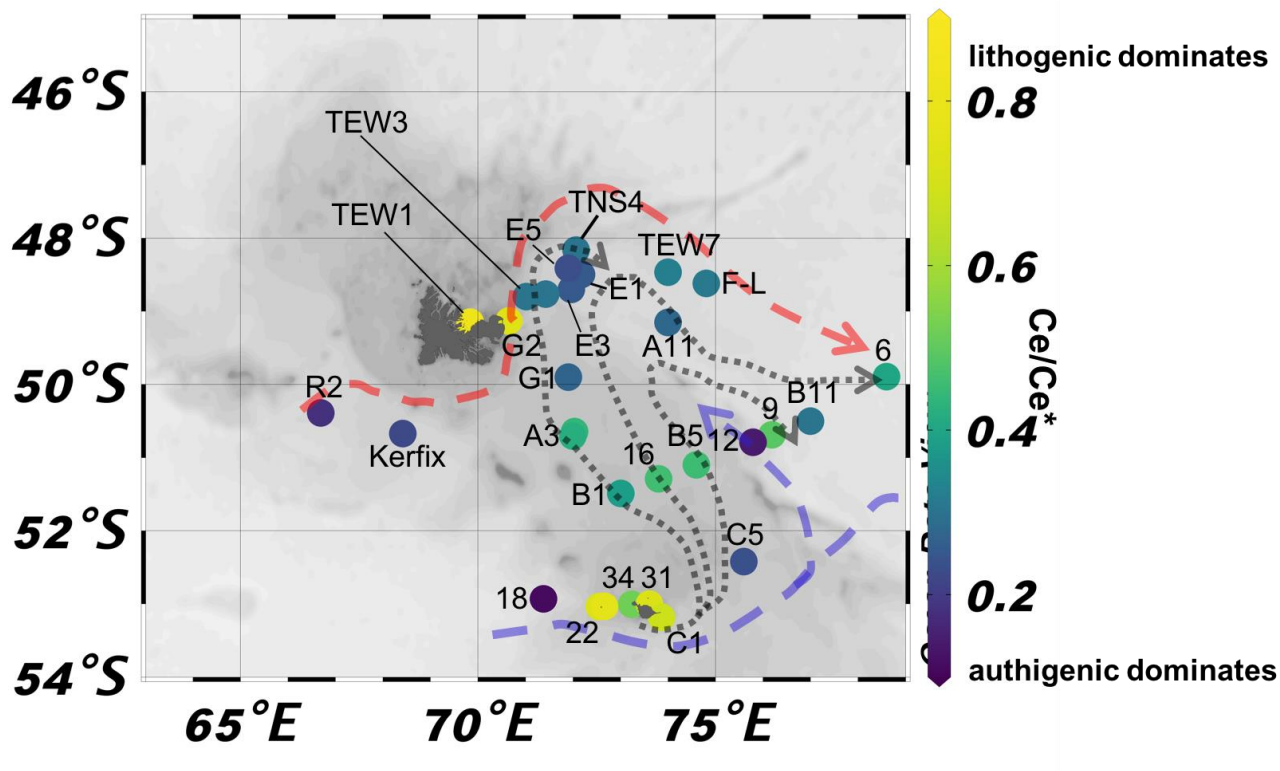

Figure 4-15. Spatial distribution of the superficial Ce anomalies of samples from the KEOPS 1, KEOPS 2 and HEOBI voyages.

The lack of enough sampling resolution in the eastern flank of the plateau prevents us from identifying the effect of the DWBC. However, a very significant Ce anomaly in Station 12 at 150 m is a strong indicator of the passage here of older waters transported to the plateau, probably by the Fawn Trough current, and then transported northwestwards by the western boundary current. In the western flank of the plateau, reference stations KERFIX and R2 as well as Station 18 exhibit a very authigenic signal (very strong Ce anomaly) and ε_{Nd} (Figure 13) typical of the surface of the Southern Ocean (German et al., 1995; Stichel et al., 2012; Garcia-Solsona et al., 2014). This is expected here as the waters have not had any significant contact with lithogenic material from the plateau.

Ce data from the three oceanographic campaigns confirm the northwards circulation above the central part of the plateau towards the polar front of lithogenic material and trace elements originating from HIMI. It reinforces our findings from the previous section that the KA signal has very little, if any, impact to the supply of REE and trace elements to the bloom south of the Polar Front.

5. Conclusions

In this chapter we have confirmed that it is possible to modify the pre-concentration technique using the Nobias resin to measure REE concentrations from 60 mL seawater samples. The Nobias resin presented a REE recovery above 93%, which enabled concentration analysis using only external calibration. With the exception of La, which presented a systematic contamination issue during the analysis of our samples, REE were determined with accuracy and precision and with blank contributions comparable to other studies.

The REE concentration data from this study, together with existing data from the literature, confirms the main role of HIMI in the natural fertilization of the waters above the central part of the plateau. Eu, Ce and Nd/Yb anomalies, together with ε_{Nd} values, indicate that REE originating in HIMI are transported northwards by the dominant circulation pattern. Our results also indicate that the PF acts as an active barrier for the material sourced in the KA, preventing exchange between sediment and seawater as observed by the ε_{Nd} and Eu content of the waters south of the PF.

Although our data has increased the knowledge on the sources of lithogenic material to the plateau, it becomes evident that some other regions, in particular the seamounts located to the north of the HIMI might also contribute to the natural fertilization observed over the plateau. However, a lack of samples sourced from that region prevents a full understanding of their influence and effect. A similar case holds for the eastern flank of the plateau where the effect of vertical advection of REE (and probably iron) is also not fully understood.

References

Anderson R. F., Fleisher M. Q., Robinson L. F., Edwards R. L., Hoff J. A., Moran S. B., van der Loeff M. R., Thomas A. L., Roy-Barman M. and Francois R. (2012) GEOTRACES

intercalibration of 230Th, 232Th, 231Pa, and prospects for 10Be. *Limnol. Oceanogr. Methods* **10**, 179–213. Available at: http://doi.wiley.com/10.4319/lom.2012.10.179.
Arsouze T., Dutay J., Lacan F. and Jeandel C. (2007) Modeling the neodymium isotopic composition with a global ocean circulation model. *Chem. Geol.* **239**, 165–177. Available at: https://linkinghub.elsevier.com/retrieve/pii/S0009254106005353.
De Baar H. J. W., Bacon M. P., Brewer P. G. and Bruland K. W. (1985) Rare earth elements in the Pacific and Atlantic Oceans. *Geochim. Cosmochim. Acta* **49**, 1943–1959. Available at: https://linkinghub.elsevier.com/retrieve/pii/0016703785900894.
de Baar H. J. W., Bathmannt U., Smetacek V., Löscher B. M. and Veth C. (1995) Importance of iron for plankton blooms and carbon dioxide drawdown in the Southern Ocean. *Nature* **373**, 412–415.
Barling J., Goldstein S. L. and Nicholls I. A. (1994) Geochemistry of Heard Island (Southern Indian Ocean): Characterization of an Enriched Mantle Component and Implications for Enrichment of the Sub-Indian Ocean Mantle. *J. Petrol.* **35**, 1017–1053. Available at: https://academic.oup.com/petrology/article-lookup/doi/10.1093/petrology/35.4.1017.
Barroux G., Sonke J. E., Boaventura G., Viers J., Godderis Y., Bonnet M.-P., Sondag F., Gardoll S., Lagane C. and Seyler P. (2006) Seasonal dissolved rare earth element dynamics of the Amazon River main stem, its tributaries, and the Curuaí floodplain. *Geochemistry, Geophys. Geosystems* **7**, n/a-n/a. Available at: http://doi.wiley.com/10.1029/2006GC001244.
Bau M., Koschinsky A., Dulski P. and Hein J. R. (1996) Comparison of the partitioning behaviours of yttrium, rare earth elements, and titanium between hydrogenetic marine ferromanganese crusts and seawater. *Geochim. Cosmochim. Acta* **60**, 1709–1725. Available at: https://linkinghub.elsevier.com/retrieve/pii/0016703796000634.
Behrens M. K., Muratli J., Pradoux C., Wu Y., Böning P., Brumsack H. J., Goldstein S. L., Haley B., Jeandel C., Paffrath R., Pena L. D., Schnetger B. and Pahnke K. (2016) Rapid and precise analysis of rare earth elements in small volumes of seawater - Method and intercomparison. *Mar. Chem.* **186**, 110–120. Available at: http://dx.doi.org/10.1016/j.marchem.2016.08.006.
Behrens M. K., Pahnke K., Schnetger B. and Brumsack H.-J. (2018) Sources and processes affecting the distribution of dissolved Nd isotopes and concentrations in the West Pacific. *Geochim. Cosmochim. Acta* **222**, 508–534. Available at: https://linkinghub.elsevier.com/retrieve/pii/S0016703717307214.
Blain S., Sarthou G. and Laan P. (2008) Distribution of dissolved iron during the natural iron-fertilization experiment KEOPS (Kerguelen Plateau, Southern Ocean). *Deep Sea Res. Part II Top. Stud. Oceanogr.* **55**, 594–605. Available at: http://www.sciencedirect.com/science/article/pii/S096706450800012X.
Blain S., Tréguer P., Belviso S., Bucciarelli E., Denis M., Desabre S., Fiala M., Martin Jézéquel V., Le Fèvre J., Mayzaud P., Marty J.-C. and Razouls S. (2001) A biogeochemical study of the island mass effect in the context of the iron hypothesis: Kerguelen Islands, Southern Ocean. *Deep Sea Res. Part I Oceanogr. Res. Pap.* **48**, 163–187. Available at: http://www.sciencedirect.com/science/article/pii/S0967063700000479.
Bolhar R., Kamber B. S., Moorbath S., Fedo C. M. and Whitehouse M. J. (2004) Characterisation of early Archaean chemical sediments by trace element signatures. *Earth Planet. Sci. Lett.* **222**, 43–60. Available at: https://linkinghub.elsevier.com/retrieve/pii/S0012821X04001347.
Bowie A. R., van der Merwe P., Quéroué F., Trull T., Fourquez M., Planchon F., Sarthou G.,

Chever F., Townsend A. T., Obernosterer I., Sallée J.-B. and Blain S. (2015) Iron budgets for three distinct biogeochemical sites around the Kerguelen Archipelago (Southern Ocean) during the natural fertilisation study, KEOPS-2. *Biogeosciences* **12**, 4421–4445. Available at: https://www.biogeosciences.net/12/4421/2015/.

Boyd P. W., Jickells T., Law C. S., Blain S., Boyle E. A., Buesseler K. O., Coale K. H., Cullen J. J., de Baar H. J. W., Follows M., Harvey M., Lancelot C., Levasseur M., Owens N. P. J., Pollard R., Rivkin R. B., Sarmiento J., Schoemann V., Smetacek V., Takeda S., Tsuda A., Turner S. and Watson A. J. (2007) Mesoscale Iron Enrichment Experiments 1993-2005: Synthesis and Future Directions. *Science (80-.).* **315**, 612–617. Available at: http://www.sciencemag.org/cgi/doi/10.1126/science.1131669.

Cantrell K. J. and Byrne R. H. (1987) Rare earth element complexation by carbonate and oxalate ions. *Geochim. Cosmochim. Acta* **51**, 597–605. Available at: https://linkinghub.elsevier.com/retrieve/pii/001670378790072X.

Coale K. H., Fitzwater S. E., Gordon R. M., Johnson K. S. and Barber R. T. (1996) Control of community growth and export production by upwelled iron in the equatorial Pacific Ocean. *Nature* **379**, 621.

Crocket K. C., Lambelet M., van de Flierdt T., Rehkämper M. and Robinson L. F. (2014) Measurement of fossil deep-sea coral Nd isotopic compositions and concentrations by TIMS as NdO+, with evaluation of cleaning protocols. *Chem. Geol.* **374**–**375**, 128–140. Available at: http://dx.doi.org/10.1016/j.chemgeo.2014.03.011.

Cutter G., Andersson P., Codispoti L., Croot P., François R., Lohan M. C., Obata H. and Rutgers v. d. Loeff M. (2010) Sampling and Sample-handling Protocols for GEOTRACES Cruises. Available at: http://epic.awi.de/34484/1/Cookbook.pdf.

DePaolo D. J. and Wasserburg G. J. (1976) Nd isotopic variations and petrogenetic models. *Geophys. Res. Lett.* **3**, 249–252. Available at: http://doi.wiley.com/10.1029/GL003i005p00249.

Dickin A. P. (2018) *Radiogenic isotope geology*., Cambridge university press.

Doucet S., Scoates J. S., Weis D. and Giret A. (2005) Constraining the components of the Kerguelen mantle plume: A Hf-Pb-Sr-Nd isotopic study of picrites and high-MgO basalts from the Kerguelen Archipelago. *Geochemistry, Geophys. Geosystems* **6**, n/a-n/a. Available at: http://doi.wiley.com/10.1029/2004GC000806.

Durand A., Chase Z., Townsend A. T., Noble T., Panietz E. and Goemann K. (2016) Improved methodology for the microwave digestion of carbonate-rich environmental samples. *Int. J. Environ. Anal. Chem.* **96**, 119–136. Available at: http://dx.doi.org/10.1080/03067319.2015.1137904.

Elderfield H. and Greaves M. J. (1981) Negative cerium anomalies in the rare earth element patterns of oceanic ferromanganese nodules. *Earth Planet. Sci. Lett.* **55**, 163–170. Available at: https://linkinghub.elsevier.com/retrieve/pii/0012821X81900959.

Elderfield H. and Greaves M. J. (1982) The rare earth elements in seawater. *Nature* **296**, 214–219. Available at: http://www.nature.com/articles/296214a0.

Elderfield H., Whitfield M., Burton J. D., Bacon M. P. and Liss P. S. (1988) The Oceanic Chemistry of the Rare-Earth Elements. *Philos. Trans. R. Soc. A Math. Phys. Eng. Sci.* **325**, 105–126. Available at: http://rsta.royalsocietypublishing.org/cgi/doi/10.1098/rsta.1988.0046.

van de Flierdt T., Pahnke K., Amakawa H., Andersson P., Basak C., Coles B., Colin C., Crocket K., Frank M., Frank N., Goldstein S. L., Goswami V., Haley B. A., Hathorne E. C., Hemming S. R., Henderson G. M., Jeandel C., Jones K., Kreissig K., Lacan F., Lambelet

M., Martin E. E., Newkirk D. R., Obata H., Pena L., Piotrowski A. M., Pradoux C., Scher H. D., Schöberg H., Singh S. K., Stichel T., Tazoe H., Vance D. and Yang J. (2012) GEOTRACES intercalibration of neodymium isotopes and rare earth element concentrations in seawater and suspended particles. Part 1: reproducibility of results for the international intercomparison. *Limnol. Oceanogr. Methods* **10**, 234–251. Available at: http://onlinelibrary.wiley.com/doi/10.4319/lom.2012.10.234/full.

Garcia-Solsona E., Jeandel C., Labatut M., Lacan F., Vance D., Chavagnac V. and Pradoux C. (2014) Rare earth elements and Nd isotopes tracing water mass mixing and particle-seawater interactions in the SE Atlantic. *Geochim. Cosmochim. Acta* **125**, 351–372. Available at: http://dx.doi.org/10.1016/j.gca.2013.10.009.

Gault-Ringold M. and Stirling C. H. (2012) Anomalous isotopic shifts associated with organic resin residues during cadmium isotopic analysis by double spike MC-ICPMS. *J. Anal. At. Spectrom.* **27**, 449. Available at: http://xlink.rsc.org/?DOI=c2ja10360e.

German C. R., Masuzawa T., Greaves M. J., Elderfield H. and Edmond J. M. (1995) Dissolved rare earth elements in the Southern Ocean: Cerium oxidation and the influence of hydrography. *Geochim. Cosmochim. Acta* **59**, 1551–1558. Available at: https://linkinghub.elsevier.com/retrieve/pii/0016703795000614.

Goldstein S. L. and Hemming S. R. (2003) Long-lived Isotopic Tracers in Oceanography, Paleoceanography, and Ice-sheet Dynamics. In *Treatise on Geochemistry* Elsevier. pp. 453–489. Available at: https://linkinghub.elsevier.com/retrieve/pii/B008043751606179X.

Grenier M., Garcia-Solsona E., Lemaitre N., Trull T. W., Bouvier V., Nonnotte P., van Beek P., Souhaut M., Lacan F. and Jeandel C. (2018) Differentiating Lithogenic Supplies, Water Mass Transport, and Biological Processes On and Off the Kerguelen Plateau Using Rare Earth Element Concentrations and Neodymium Isotopic Compositions. *Front. Mar. Sci.* **5**. Available at: https://www.frontiersin.org/article/10.3389/fmars.2018.00426/full.

Hathorne E. C., Stichel T., Brück B. and Frank M. (2014) Rare earth element distribution in the Atlantic sector of the Southern Ocean: The balance between particle scavenging and vertical supply. *Mar. Chem.* **177**, 157–171. Available at: http://dx.doi.org/10.1016/j.marchem.2015.03.011.

Hatje V., Bruland K. W. and Flegal a. R. (2014) Determination of rare earth elements after pre-concentration using NOBIAS-chelate PA-1® resin: Method development and application in the San Francisco Bay. *Mar. Chem.* **160**, 34–41. Available at: http://dx.doi.org/10.1016/j.marchem.2014.01.006.

Holmes T. M., Wuttig K., Chase Z., van der Merwe P., Townsend A. T., Schallenberg C., Tonnard M. and Bowie A. R. (2019) Iron availability influences nutrient drawdown in the Heard and McDonald Islands region, Southern Ocean. *Mar. Chem.* **211**, 1–14. Available at: https://doi.org/10.1016/j.marchem.2019.03.002.

Jacobsen S. B. and Wasserburg G. J. (1980) Sm-Nd isotopic evolution of chondrites. *Earth Planet. Sci. Lett.* **50**, 139–155. Available at: https://linkinghub.elsevier.com/retrieve/pii/0012821X80901259.

Jeandel C., Thouron D. and Fieux M. (1998) Concentrations and isotopic compositions of neodymium in the eastern Indian Ocean and Indonesian straits. *Geochim. Cosmochim. Acta* **62**, 2597–2607. Available at: http://www.sciencedirect.com/science/article/pii/S0016703798001690.

Jickells T. D. (2005) Global Iron Connections Between Desert Dust, Ocean Biogeochemistry, and Climate. *Science (80-.).* **308**, 67–71. Available at:

http://www.sciencemag.org/cgi/doi/10.1126/science.1105959.
Kulaksız S. and Bau M. (2007) Contrasting behaviour of anthropogenic gadolinium and natural rare earth elements in estuaries and the gadolinium input into the North Sea. *Earth Planet. Sci. Lett.* **260**, 361–371. Available at: https://linkinghub.elsevier.com/retrieve/pii/S0012821X07003809.
Lacan F. and Jeandel C. (2005) Neodymium isotopes as a new tool for quantifying exchange fluxes at the continent–ocean interface. *Earth Planet. Sci. Lett.* **232**, 245–257. Available at: http://www.sciencedirect.com/science/article/pii/S0012821X05000233.
Lugmair G. W. (1974) Sm-Nd ages: a new dating method. *Meteoritics* **9**, 369.
Martin John H. (1990) Glacial-interglacial CO 2 change: The Iron Hypothesis. *Paleoceanography* **5**, 1–13. Available at: http://doi.wiley.com/10.1029/PA005i001p00001.
Martin J. H. (1990) Glacial-interglacial CO 2 change: The Iron Hypothesis. *Paleoceanography* **5**, 1–13. Available at: http://doi.wiley.com/10.1029/PA005i001p00001.
van der Merwe P., Wuttig K., Holmes T., Trull T. W., Chase Z., Townsend A. T., Goemann K. and Bowie A. R. (2019) High Lability Fe Particles Sourced From Glacial Erosion Can Meet Previously Unaccounted Biological Demand: Heard Island, Southern Ocean. *Front. Mar. Sci.* **6**, 1–20. Available at: https://www.frontiersin.org/article/10.3389/fmars.2019.00332/full.
Michard A., Albarède F., Michard G., Minster J. F. and Charlou J. L. (1983) Rare-earth elements and uranium in high-temperature solutions from East Pacific Rise hydrothermal vent field (13 °N). *Nature* **303**, 795–797. Available at: http://www.nature.com/articles/303795a0.
Olivarez A. M. and Owen R. M. (1991) The europium anomaly of seawater: implications for fluvial versus hydrothermal REE inputs to the oceans. *Chem. Geol.* **92**, 317–328. Available at: https://linkinghub.elsevier.com/retrieve/pii/0009254191900764.
Park Y.-H., Durand I., Kestenare E., Rougier G., Zhou M., D'Ovidio F., Cotté C. and Lee J.-H. (2014) Polar Front around the Kerguelen Islands: An up-to-date determination and associated circulation of surface/subsurface waters. *J. Geophys. Res. Ocean.* **119**, 6575–6592. Available at: http://doi.wiley.com/10.1002/2014JC010061.
Park Y.-H., Roquet F., Durand I. and Fuda J.-L. (2008) Large-scale circulation over and around the Northern Kerguelen Plateau. *Deep Sea Res. Part II Top. Stud. Oceanogr.* **55**, 566–581. Available at: http://www.sciencedirect.com/science/article/pii/S0967064508000106.
Park Y. and Vivier F. (2011) Circulation and hydrography over the Kerguelen Plateau. *Kerguelen Plateau Mar. Ecosyst. Fish.*, 43–55.
Pérez-Tribouillier H., Noble T. L., Townsend A. T., Bowie A. R. and Chase Z. (2019) Pre-concentration of thorium and neodymium isotopes using Nobias chelating resin: Method development and application to chromatographic separation. *Talanta* **202**, 600–609. Available at: https://doi.org/10.1016/j.talanta.2019.03.086.
Piepgras D. J., Wasserburg G. J. and Dasch E. J. (1979) The isotopic composition of Nd in different ocean masses. *Earth Planet. Sci. Lett.* **45**, 223–236. Available at: https://linkinghub.elsevier.com/retrieve/pii/0012821X79901250.
Pin C. and Zalduegui J. S. (1997) Sequential separation of light rare-earth elements, thorium and uranium by miniaturized extraction chromatography: Application to isotopic analyses of silicate rocks. *Anal. Chim. Acta* **339**, 79–89. Available at: https://linkinghub.elsevier.com/retrieve/pii/S0003267096004990.

Pourmand A., Marcantonio F. and Schulz H. (2004) Variations in productivity and eolian fluxes in the northeastern Arabian Sea during the past 110 ka. *Earth Planet. Sci. Lett.* **221**, 39–54. Available at: https://linkinghub.elsevier.com/retrieve/pii/S0012821X04001098.

Robinson P., Townsend A. T., Yu Z. and Münker C. (1999) Determination of Scandium, Yttrium and Rare Earth Elements in Rocks by High Resolution Inductively Coupled Plasma-Mass Spectrometry. *Geostand. Geoanalytical Res.* **23**, 31–46. Available at: http://doi.wiley.com/10.1111/j.1751-908X.1999.tb00557.x.

Sanial V., van Beek P., Lansard B., Souhaut M., Kestenare E., D'Ovidio F., Zhou M. and Blain S. (2015) Use of Ra isotopes to deduce rapid transfer of sediment-derived inputs off Kerguelen. *Biogeosciences* **12**, 1415–1430. Available at: https://www.biogeosciences.net/12/1415/2015/.

Sholkovitz E. ., Elderfield H., Szymczak R. and Casey K. (1999) Island weathering: river sources of rare earth elements to the Western Pacific Ocean. *Mar. Chem.* **68**, 39–57. Available at: https://linkinghub.elsevier.com/retrieve/pii/S030442039900064X.

Sholkovitz E. R., Landing W. M. and Lewis B. L. (1994) Ocean particle chemistry: The fractionation of rare earth elements between suspended particles and seawater. *Geochim. Cosmochim. Acta* **58**, 1567–1579. Available at: https://linkinghub.elsevier.com/retrieve/pii/0016703794905592.

Stichel T., Frank M., Rickli J. and Haley B. A. (2012) The hafnium and neodymium isotope composition of seawater in the Atlantic sector of the Southern Ocean. *Earth Planet. Sci. Lett.* **317**–**318**, 282–294. Available at: http://dx.doi.org/10.1016/j.epsl.2011.11.025.

Struve T., van de Flierdt T., Robinson L. F., Bradtmiller L. I., Hines S. K., Adkins J. F., Lambelet M., Crocket K. C., Kreissig K., Coles B. and Auro M. E. (2016) Neodymium isotope analyses after combined extraction of actinide and lanthanide elements from seawater and deep-sea coral aragonite. *Geochemistry, Geophys. Geosystems* **17**, 232–240. Available at: http://doi.wiley.com/10.1002/2015GC006130.

Tachikawa K., Jeandel C., Vangriesheim A. and Dupré B. (1999) Distribution of rare earth elements and neodymium isotopes in suspended particles of the tropical Atlantic Ocean (EUMELI site). *Deep Sea Res. Part I Oceanogr. Res. Pap.* **46**, 733–755. Available at: https://linkinghub.elsevier.com/retrieve/pii/S0967063798000892.

Tagliabue A., Sallée J.-B., Bowie A. R., Lévy M., Swart S. and Boyd P. W. (2014) Surface-water iron supplies in the Southern Ocean sustained by deep winter mixing. *Nat. Geosci.* **7**, 314–320. Available at: http://www.nature.com/articles/ngeo2101.

Tanaka T., Togashi S., Kamioka H., Amakawa H., Kagami H., Hamamoto T., Yuhara M., Orihashi Y., Yoneda S., Shimizu H., Kunimaru T., Takahashi K., Yanagi T., Nakano T., Fujimaki H., Shinjo R., Asahara Y., Tanimizu M. and Dragusanu C. (2000) JNdi-1: a neodymium isotopic reference in consistency with LaJolla neodymium. *Chem. Geol.* **168**, 279–281. Available at: https://linkinghub.elsevier.com/retrieve/pii/S0009254100001984.

Taylor S. R. and McLennan S. M. (1985) The continental crust: its composition and evolution.

Turekian K. K. (1977) The fate of metals in the oceans. *Geochim. Cosmochim. Acta* **41**, 1139–1144. Available at: https://linkinghub.elsevier.com/retrieve/pii/0016703777901090.

Wasserburg G. J., Jacobsen S., DePaolo D. J., McCulloch M. T. and Wen T. (1981) Precise determination of ratios Sm and Nd isotopic abundances in standard solutions. *Geochim. Cosmochim. Acta* **45**, 2311–2323. Available at: papers2://publication/uuid/9687D48D-6F02-4C2C-8E61-16031CC2907B.

Weis D., Frey F. A., Schlich R., Schaming M., Montigny R., Damasceno D., Mattielli N., Nicolaysen K. E. and Scoates J. S. (2002) Trace of the Kerguelen mantle plume: Evidence from seamounts between the Kerguelen Archipelago and Heard Island, Indian Ocean. *Geochemistry, Geophys. Geosystems* **3**, 1–27. Available at: http://doi.wiley.com/10.1029/2001GC000251.

Weis D., White W. M., Frey F. A., Duncan R. A., Fisk M. R., Dehn J., Ludden J., Saunders A. and Storey M. (2013) The Influence of Mantle Plumes in Generation of Indian Oceanic Crust. In *Geophysical Monograph* pp. 57–89. Available at: http://doi.wiley.com/10.1029/GM070p0057.

Zhang Y., Lacan F. and Jeandel C. (2008) Dissolved rare earth elements tracing lithogenic inputs over the Kerguelen Plateau (Southern Ocean). *Deep Sea Res. Part II Top. Stud. Oceanogr.* **55**, 638–652. Available at: http://www.sciencedirect.com/science/article/pii/S0967064508000167.

Zheng X.-Y., Yang J. and Henderson G. M. (2015) A Robust Procedure for High-Precision Determination of Rare Earth Element Concentrations in Seawater. *Geostand. Geoanalytical Res.* **39**, 277–292. Available at: http://doi.wiley.com/10.1111/j.1751-908X.2014.00307.x.

Zhou M., Zhu Y., D'Ovidio F., Park Y.-H., Durand I., Kestenare E., Sanial V., Van-Beek P., Queguiner B., Carlotti F. and Blain S. (2014) Surface currents and upwelling in Kerguelen Plateau regions. *Biogeosciences Discuss.* **11**, 6845–6876. Available at: https://www.biogeosciences-discuss.net/11/6845/2014/.

Chapter 5 - General conclusions, remarks and prospects for the future

This thesis deals with the use of thorium and rare earth elements as tracers of the lithogenic supply that allows the development of primary productivity in the Kerguelen Plateau waters. These elements can be used to trace the sources and fate of the bio-limiting trace element iron (Fe) in the ocean. Iron is known to be crucial to overcome the HNLC conditions that prevail in the Southern Ocean (Boyd et al., 2007). When the surface waters of the Southern Ocean receive this element by the input from islands, iceberg or glacial melt and the resuspension of sediments and dust, blooms of enhanced primary productivity are sustained (Tyrrell et al., 2005). Such blooms absorb atmospheric CO_2, which can then be potentially transported into deeper layers of the ocean (Boyd and Ellwood, 2010), alleviating the increasing levels of CO_2 in the atmosphere.

The Kerguelen Plateau region, located in the Indian Sector of the Southern Ocean, hosts the largest bloom of the SO, extending for thousands of square kilometers. Previous studies have demonstrated the importance of Heard and McDonald Islands and the Kerguelen Archipelago to the supply of lithogenic trace elements that naturally fertilize the waters of the plateau (Blain et al., 2001; Blain et al., 2007; van Beek et al., 2008; Zhang et al., 2008; Grenier et al., 2018; Holmes et al., 2019; van der Merwe et al., 2019). However, the relative importance and contribution of each group of islands was not well constrained prior to this study, mainly due to the lack of sampling in the area around and north of Heard and McDonald Islands. The Heard and McDonald Earth-Ocean-Biosphere Interactions study (HEOBI), conducted during January and February of 2016, provided a more detailed sampling of this region. All the results and discussion presented in the previous three chapters are based on the following research questions:

1) Is it possible to develop a new technique to simultaneously pre-concentrate Th and Nd isotopes (ε_{Nd}) using the Nobias chelating resin? and is it possible to couple this technique with the existing chromatographic separation procedures?

2) Can the long-lived ^{232}Th and ^{230}Th isotopes be used to quantify the flux of lithogenic material and trace elements resulting from the Kerguelen Plateau and its interaction with the flow of the ACC?

3) Is it possible to further constrain the different sources and pathways of lithogenic material in the Kerguelen Plateau using ε_{Nd} and REEs?

4) Can the newly developed technique to pre-concentrate Th and Nd isotopes be adapted to measure REE concentration following a previously established protocol?

5.1 Summary of main findings of this research

The Nobias resin can effectively be used to pre-concentrate Th and Nd isotopes as well as to determine REE concentrations. Results from the analysis of these elements suggest that the area surrounding HIMI is the main contributor to the natural fertilization above the plateau. In the following paragraphs I summarize the main finding of each of the scientific chapters.

Chapter 2. Pre-concentration of thorium and neodymium isotopes using Nobias chelating resin: Method development and application to chromatographic separation.

Despite the advances in the instrumentation to measure small amounts of Th and Nd, the sampling processing techniques have remained unchanged during the last 40 years, and they involve a pre-concentration using Fe oxy-hydroxides and chromatographic separation (Anderson et al., 2012). Development of an alternative option for the pre-concentration step that saved time and sample handling represented the main motivation for the development of the second chapter. I demonstrated that it was possible to pre-concentrate Th and Nd isotopes using the proposed method and then couple it to existing separation techniques.

Analysis of 5-10 L samples with very good accuracy and precision is possible, and with low blank levels that are similar or even less than other studies. However, developing this technique was not a straightforward process and more than 18 months were required just to start producing reproducible results. During this time, we encountered several problems mainly related to the "sticky" nature of Th isotopes, the blank contribution coming from the chromatographic resins and also organic compounds leaching from these resins. This technique was successfully used to analyze 57 samples collected in the central Kerguelen Plateau area with an average Th yield of 82 ± 7%.

Chapter 3. Quantifying lithogenic fluxes to the Kerguelen Plateau using long-lived thorium isotopes

The surface waters of the Kerguelen Plateau present enrichments in the content of ^{232}Th caused by the supply of lithogenic material from the different sources that exist in the Kerguelen Plateau. Using the ^{232}Th-^{230}Th system has the advantage that, while the disequilibrium of ^{230}Th from its soluble parent ^{234}U provides a "chronometer" of the time it takes for Th to be removed from solution, the ^{232}Th provides a link with the lithogenic sources to the ocean. With additional knowledge about Th solubility and content from the source material, the fluxes of trace elements can be estimated (Hsieh et al., 2011; Hayes et al., 2013). In Chapter 3, this approach was applied for the first time to a continental-margin zone like the Kerguelen Plateau. It was found that dissolved thorium data can be used to obtain fluxes of lithogenic material and trace elements derived from the different sources that exist in the Plateau. Our estimated fluxes are within the range of the fluxes obtained from of sediment traps in the Kerguelen Plateau (Bowie et al., 2015) and other areas of the Southern Ocean, increasing confidence in both estimates.

Chapter 4. Sourcing lithogenic inputs to the Kerguelen Plateau using rare earth element concentrations and Nd isotopic composition

In the fourth chapter we were able to adapt a previously published technique (Hatje et al., 2014) to measure REE concentration in the HEOBI samples using a similar setup as the one described in Chapter 2. Except for lanthanum, this technique can determine REE concentration in an accurate and precise way and with a reasonable blank contribution. It is necessary to state that this method was developed in the last months of this PhD and therefore it was not possible to invest time to solve the blank problems that La presented. To further constrain the sources and path of REE over the plateau, we used our new data collected around HIMI and coupled it with previous REE and ε_{Nd} data produced from the KEOPS 1 (Zhang et al., 2008) and KEOPS 2 (Grenier et al., 2018) expeditions. These datasets confirm the different Eu anomaly and ε_{Nd} signals of HIMI and the Kerguelen Archipelago. The signal from HIMI dilutes northwards through its advection to the southern border of the Polar Front. The signal from the Kerguelen archipelago on the other hand is not possible to be observed anywhere in the central part of the plateau. These statements are supported by the spatial distribution of the Ce anomaly over the plateau that indicates a very lithogenic signal next to HIMI that then turns into a highly authigenic signal as the current approaches the Polar Front.

5.2 Implications of this thesis

5.2.1 Determination of Th and Nd isotopic composition in seawater.

The method to pre-concentrate Th and Nd developed in the second chapter (Pérez-Tribouillier et al., 2019) is a promising alternative for the study of these elements in seawater. First of all, using a chelating resin implies that there is no need to add any Fe carrier solution to the sample, which reduces the blank and the need to remove excess Fe during chromatographic separation. It also reduces the sample processing time, from a week-long

Fe precipitation (Anderson et al., 2012; Auro et al., 2012) to an overnight chelating resin preconcentration. The sample-handling is also reduced, as after the pre-concentration, the only necessary thing to do is to elute the sample from the Nobias cartridge. With practice this process takes less than 15 minutes to perform for 6 samples. Afterwards the solution only needs to be dried down and it is ready for the chromatographic procedure. In comparison, the Fe method requires the precipitate to be centrifuged and then also digested with strong acids, adding more processing time. The main disadvantages of the Nobias method is that it is not possible to analyze total content of Th and Nd in unfiltered samples and that the resin is quite expensive. However, the cartridges can be re-used for many samples without comprising the elemental yield.

5.2.2 Kerguelen Plateau

The REE data together with the ε_{Nd} agree with what was suggested by previous studies regarding the importance of HIMI to the natural fertilization of the central part of the plateau (Zhang et al., 2008; Grenier et al., 2018; Holmes et al., 2019; van der Merwe et al., 2019). The new data reported from the coastal HIMI area, when processed together with previous oceanographic campaigns closer to the Kerguelen Archipelago, allow us to confirm that the main source of material to the central plateau is the Heard and McDonald Islands, and the shallow plateau to the north. The data allow us to reject the hypothesis presented by Sanial et al., 2015 that the material from the Kerguelen archipelago can cross the polar front and contribute to the natural fertilization of the waters of the central plateau. Furthermore, we can conclude that the Polar Front acts as an effective barrier for the material originating in the Kerguelen Archipelago and that this material only contributes to the fertilization of the bloom that occurs north of the polar front.

The use of long-lived thorium isotopes was introduced for the first time with the objective of estimating lithogenic fluxes produced by the dissolution of mineral dust to the open ocean. In Chapter 3, I have confirmed that this approach can also be applied to more coastal environment as the data agrees with sediment trap data around the Southern Ocean. Using Th isotopes for this purpose represents a viable alternative when the deployment of sediment traps is not possible.

5.3 Future work

The simplicity of the pre-concentration of Th and Nd using the Nobias resin has the potential of being applied on-board research vessels. Although not tried yet, this would imply more than a 99% reduction in the sample volume that needs to be brought back to land and a reduction in the logistics for the transport and storage of those samples. Furthermore, there is an interest in the possibility of reducing the volume required to determine Th and Nd isotopic composition to 1 or 2 liters, which will make its on-board application even more viable. Including protactinium as an element that can be determined with the proposed method is also projected as a future work; some tests have been already performed and indicate that it is possible. Regarding the method adapted in Chapter 4 to measure REE with the Nobias resin, it is planned to include the determination of ^{232}Th under this approach. This will help to have an estimated amount of ^{232}Th in order to produce a better isotopic dilution mix for the determination of larger volume samples as described in Chapter 2.

Since the first KEOPS I voyage in 2005, the knowledge of the factors that drive the phytoplankton bloom in this region have greatly increased. However, there are still some areas of the plateau that remain unexplored and that appear as potential sources of trace elements. In particular, the REE data suggest that the seamounts that exist north of HIMI might be an additional source of lithogenic material. The positive Eu anomaly around HIMI

and close to the above-mentioned seamounts might additionally be indicative of the presence of hydrothermal activity. Although the HEOBI expedition was intended to locate hydrothermal plumes in the central plateau, it was not possible to locate any. Only acoustic flares of unknown composition were found. However, the positive Eu anomaly and the high Fe(II) concentrations found around HIMI are a clear evidence of hydrothermal activity. Therefore, a more meticulous sampling campaign that includes the use of underwater automatic vehicles and Th and REE sampling would be very useful to definitively confirm the hydrothermal contribution, if any.

Arising from the third chapter it becomes evident that the "solubility" of Th isotopes in lithogenic particles is a largely unconstrained parameter, as well as the effect of particle-size into the Th speciation. Although we are planning to realize some experiments in that regard with the sediments and particles collected during the HEOBI voyage, we support the claims of previous authors that more systematic and collaborative studies of the previously mentioned issues are required (Anderson et al., 2016), not only to further calibrate the use of thorium isotopes to estimate lithogenic fluxes, but also to better understand the processes that occur after lithogenic material enters the ocean and which amount of this material could potentially become available for the primary producers.

References

Anderson R. F., Cheng H., Edwards R. L., Fleisher M. Q., Hayes C. T., Huang K.-F., Kadko D., Lam P. J., Landing W. M., Lao Y., Lu Y., Measures C. I., Moran S. B., Morton P. L., Ohnemus D. C., Robinson L. F. and Shelley R. U. (2016) How well can we quantify dust deposition to the ocean? *Philos. Trans. R. Soc. A Math. Phys. Eng. Sci.* **374**, 20150285. Available at: https://royalsocietypublishing.org/doi/10.1098/rsta.2015.0285.

Anderson R. F., Fleisher M. Q., Robinson L. F., Edwards R. L., Hoff J. A., Moran S. B., van der

Loeff M. R., Thomas A. L., Roy-Barman M. and Francois R. (2012) GEOTRACES intercalibration of 230Th, 232Th, 231Pa, and prospects for 10Be. *Limnol. Oceanogr. Methods* **10**, 179–213. Available at: http://doi.wiley.com/10.4319/lom.2012.10.179.

Auro M. E., Robinson L. F., Burke A., Bradtmiller L. I., Fleisher M. Q. and Anderson R. F. (2012) Improvements to 232-thorium, 230-thorium, and 231-protactinium analysis in seawater arising from GEOTRACES intercalibration. *Limnol. Oceanogr. Methods* **10**, 464–474. Available at: http://doi.wiley.com/10.4319/lom.2012.10.464.

van Beek P., Bourquin M., Reyss J.-L., Souhaut M., Charette M. A. and Jeandel C. (2008) Radium isotopes to investigate the water mass pathways on the Kerguelen Plateau (Southern Ocean). *Deep Sea Res. Part II Top. Stud. Oceanogr.* **55**, 622–637. Available at: http://www.sciencedirect.com/science/article/pii/S0967064508000155.

Blain S., Quéguiner B., Armand L., Belviso S., Bombled B., Bopp L., Bowie A., Brunet C., Brussaard C., Carlotti F., Christaki U., Corbière A., Durand I., Ebersbach F., Fuda J.-L., Garcia N., Gerringa L., Griffiths B., Guigue C., Guillerm C., Jacquet S., Jeandel C., Laan P., Lefèvre D., Lo Monaco C., Malits A., Mosseri J., Obernosterer I., Park Y.-H., Picheral M., Pondaven P., Remenyi T., Sandroni V., Sarthou G., Savoye N., Scouarnec L., Souhaut M., Thuiller D., Timmermans K., Trull T., Uitz J., van Beek P., Veldhuis M., Vincent D., Viollier E., Vong L. and Wagener T. (2007) Effect of natural iron fertilization on carbon sequestration in the Southern Ocean. *Nature* **446**, 1070–1074. Available at: http://www.nature.com/articles/nature05700.

Blain S., Tréguer P., Belviso S., Bucciarelli E., Denis M., Desabre S., Fiala M., Martin Jézéquel V., Le Fèvre J., Mayzaud P., Marty J.-C. and Razouls S. (2001) A biogeochemical study of the island mass effect in the context of the iron hypothesis: Kerguelen Islands, Southern Ocean. *Deep Sea Res. Part I Oceanogr. Res. Pap.* **48**, 163–187. Available at:

http://www.sciencedirect.com/science/article/pii/S0967063700000479.

Bowie A. R., van der Merwe P., Quéroué F., Trull T., Fourquez M., Planchon F., Sarthou G., Chever F., Townsend A. T., Obernosterer I., Sallée J.-B. and Blain S. (2015) Iron budgets for three distinct biogeochemical sites around the Kerguelen Archipelago (Southern Ocean) during the natural fertilisation study, KEOPS-2. *Biogeosciences* **12**, 4421–4445. Available at: https://www.biogeosciences.net/12/4421/2015/.

Boyd P. W. and Ellwood M. J. (2010) The biogeochemical cycle of iron in the ocean. *Nat. Geosci.* **3**, 675–682. Available at: http://dx.doi.org/10.1038/ngeo964.

Boyd P. W., Jickells T., Law C. S., Blain S., Boyle E. A., Buesseler K. O., Coale K. H., Cullen J. J., de Baar H. J. W., Follows M., Harvey M., Lancelot C., Levasseur M., Owens N. P. J., Pollard R., Rivkin R. B., Sarmiento J., Schoemann V., Smetacek V., Takeda S., Tsuda A., Turner S. and Watson A. J. (2007) Mesoscale Iron Enrichment Experiments 1993-2005: Synthesis and Future Directions. *Science (80-.).* **315**, 612–617. Available at: http://www.sciencemag.org/cgi/doi/10.1126/science.1131669.

Grenier M., Garcia-Solsona E., Lemaitre N., Trull T. W., Bouvier V., Nonnotte P., van Beek P., Souhaut M., Lacan F. and Jeandel C. (2018) Differentiating Lithogenic Supplies, Water Mass Transport, and Biological Processes On and Off the Kerguelen Plateau Using Rare Earth Element Concentrations and Neodymium Isotopic Compositions. *Front. Mar. Sci.* **5**. Available at: https://www.frontiersin.org/article/10.3389/fmars.2018.00426/full.

Hatje V., Bruland K. W. and Flegal a. R. (2014) Determination of rare earth elements after pre-concentration using NOBIAS-chelate PA-1® resin: Method development and application in the San Francisco Bay. *Mar. Chem.* **160**, 34–41. Available at: http://dx.doi.org/10.1016/j.marchem.2014.01.006.

Hayes C. T., Anderson R. F., Fleisher M. Q., Serno S., Winckler G. and Gersonde R. (2013)

Quantifying lithogenic inputs to the North Pacific Ocean using the long-lived thorium isotopes. *Earth Planet. Sci. Lett.* **383**, 16–25. Available at: http://dx.doi.org/10.1016/j.epsl.2013.09.025.

Holmes T. M., Wuttig K., Chase Z., van der Merwe P., Townsend A. T., Schallenberg C., Tonnard M. and Bowie A. R. (2019) Iron availability influences nutrient drawdown in the Heard and McDonald Islands region, Southern Ocean. *Mar. Chem.* **211**, 1–14. Available at: https://doi.org/10.1016/j.marchem.2019.03.002.

Hsieh Y., Henderson G. M. and Thomas A. L. (2011) Combining seawater232Th and230Th concentrations to determine dust fluxes to the surface ocean. *Earth Planet. Sci. Lett.* **312**, 280–290. Available at: http://dx.doi.org/10.1016/j.epsl.2011.10.022.

van der Merwe P., Wuttig K., Holmes T., Trull T. W., Chase Z., Townsend A. T., Goemann K. and Bowie A. R. (2019) High Lability Fe Particles Sourced From Glacial Erosion Can Meet Previously Unaccounted Biological Demand: Heard Island, Southern Ocean. *Front. Mar. Sci.* **6**, 1–20. Available at: https://www.frontiersin.org/article/10.3389/fmars.2019.00332/full.

Pérez-Tribouillier H., Noble T. L., Townsend A. T., Bowie A. R. and Chase Z. (2019) Pre-concentration of thorium and neodymium isotopes using Nobias chelating resin: Method development and application to chromatographic separation. *Talanta* **202**, 600–609. Available at: https://doi.org/10.1016/j.talanta.2019.03.086.

Sanial V., van Beek P., Lansard B., Souhaut M., Kestenare E., D'Ovidio F., Zhou M. and Blain S. (2015) Use of Ra isotopes to deduce rapid transfer of sediment-derived inputs off Kerguelen. *Biogeosciences* **12**, 1415–1430. Available at: https://www.biogeosciences.net/12/1415/2015/.

Tyrrell T., Merico A., Waniek J. J., Wong C. S., Metzl N. and Whitney F. (2005) Effect of

seafloor depth on phytoplankton blooms in high-nitrate, low-chlorophyll (HNLC) regions. *J. Geophys. Res. Biogeosciences* **110**, n/a-n/a. Available at: http://doi.wiley.com/10.1029/2005JG000041.

Zhang Y., Lacan F. and Jeandel C. (2008) Dissolved rare earth elements tracing lithogenic inputs over the Kerguelen Plateau (Southern Ocean). *Deep Sea Res. Part II Top. Stud. Oceanogr.* **55**, 638–652. Available at: http://www.sciencedirect.com/science/article/pii/S0967064508000167.

Appendix. ^{230}Th, ^{232}Th, ε_{Nd}, and REE concentrations from the HEOBI samples

Table 1. Geographic location, depth and geochemical data of the samples reported in this thesis (Rare Earth Element concentrations are given in pmol kg^{-1}).

Station	Latitude	Longitude	depth (m)	^{232}Th [pg kg^{-1}]	S.E.	^{230}Th [fg kg^{-1}]	S.E.	ε_{Nd}	S.E.	Ce	S.E.	Pr	S.E.	Nd	S.E.
6	-49.89	-281.4	16	18.3	0.8	2.5	0.7	-7.6	0.4	8.7	1.7	2.9	0.3	12.8	0.9
6	-49.89	-281.4	75	32.5	0.7	2.6	0.7	-8	0.3	9.6	1.9	3	0.3	13.4	0.9
6	-49.89	-281.4	100	46.6	0.8	3.2	0.6	-8.7	0.4	7.7	1.5	2.9	0.3	12.7	0.9
6	-49.89	-281.4	200	34.6	0.8	3.9	0.5	-8.2	0.4	5.8	1.2	2.6	0.2	11.7	0.8
6	-49.89	-281.4	400	40.2	0.4	6.5	0.4	-8.5	0.4	5.8	1.2	2.8	0.3	12.2	0.9
6	-49.89	-281.4	601	39.5	0.5	8	0.3	-7.8	0.4	5.8	1.2	2.9	0.3	12.5	0.9
6	-49.89	-281.4	997	40.5	0.5	8.2	0.3	-9.8	0.5	3.3	0.7	3.3	0.3	15.3	1.1
6	-49.89	-281.4	1400	31.2	0.5	10.9	0.2	-9.8	0.4	5	1	3.8	0.3	16.9	1.2
6	-49.89	-281.4	2000	58.4	0.4	14.9	0.1	-9.6	0.3	8.7	1.8	4.5	0.4	19.5	1.4
6	-49.89	-281.4	3001	64.8	0.6	16.6	0.1	-9.3	0.3	6.2	1.2	5.5	0.5	24.3	1.7
6	-49.89	-281.4	3478	56.9	0.4	19.3	0.1	-8.9	0.2	7.3	1.5	6.2	0.6	26	1.8
6	-49.89	-281.4	3579	64.2	0.2	19.5	0.1	-9	0.4	C	C	6.3	0.6	25.9	1.8
9	-50.69	-283.81	29	14.6	0.6	3	0.3	P	P	11.4	2.3	3.1	0.3	13.9	1
9	-50.69	-283.81	70	10.8	0.4	2	0.2	P	P	13.6	2.7	3.5	0.3	14.4	1
9	-50.69	-283.81	121	23.7	0.5	2.6	0.2	P	P	9.8	2	3.1	0.3	13.2	0.9
9	-50.69	-283.81	300	55.5	1.1	6.9	0.2	P	P	7.6	1.5	3.3	0.3	13.8	1
9	-50.69	-283.81	500	26.8	0.5	9.3	0.3	P	P	NA	NA	NA	NA	NA	NA
9	-50.69	-283.81	700	NA	NA	12.2	1.2	P	P	5.4	1.1	3.6	0.3	15.6	1.1
9	-50.69	-283.81	900	30.2	0.6	11.9	0.4	P	P	9.2	1.8	3.6	0.3	15.7	1.1
9	-50.69	-283.81	1500	50.1	1	15	0.5	P	P	7.6	1.5	4.2	0.4	18.2	1.3
9	-50.69	-283.81	2501	40	0.8	15	0.5	P	P	8.4	1.7	5.9	0.5	24.7	1.7
9	-50.69	-283.81	3055	59.9	1.2	18.1	0.6	P	P	14.3	2.9	6.1	0.6	25.1	1.8
9	-50.69	-283.81	3156	59.1	1.2	18.6	0.6	P	P	C	C	6.4	0.6	25.5	1.8
12	-50.79	-284.21	31	6.9	0.2	2.6	0.2	-8.1	0.4	C	C	2.8	0.3	12.1	0.9
12	-50.79	-284.21	55	12.5	0.3	2.7	0.2	-8.2	0.3	3	0.6	2.7	0.2	11.5	0.8
12	-50.79	-284.21	301	15.1	0.2	6.3	0.5	-8.4	0.3	3.5	0.7	2.9	0.3	12.3	0.9

Table 1. Continuation of previous page.

Sm	S.E.	Eu	S.E.	Gd	S.E.	Tb	S.E.	Dy	S.E.	Ho	S.E.	Er	S.E.	Tm	S.E.	Yb	S.E.	Lu	S.E.	Ce/Ce*	Eu/Eu*	$(Nd/Yb)_n$
2.3	0.1	0.6	0.1	3.5	0.1	0.6	0.1	4.5	0.1	1.3	0.1	4.7	0.1	0.7	0	4.7	0.1	0.8	0	0.4	0.93	0.19
2.3	0.1	0.6	0.1	3.6	0.1	0.6	0.1	4.5	0.1	1.4	0.1	4.7	0.1	0.7	0	4.7	0.1	0.8	0	0.45	0.96	0.2
2.2	0.1	0.6	0.1	3.6	0.1	0.6	0.1	4.4	0.1	1.3	0.1	4.6	0.1	0.7	0	4.8	0.1	0.8	0	0.35	0.97	0.18
2.1	0.1	0.6	0.1	3.4	0.1	0.6	0	4.4	0.1	1.3	0.1	4.7	0.1	0.7	0	4.9	0.2	0.8	0	0.32	1	0.17
2.3	0.1	0.7	0.1	3.5	0.1	0.6	0.1	4.6	0.1	1.4	0.1	4.7	0.1	0.8	0	5.1	0.2	0.9	0	NA	1.06	0.16
2.4	0.1	0.7	0.1	3.9	0.2	0.6	0.1	4.8	0.2	1.4	0.1	5.2	0.2	0.8	0	5.6	0.2	1	0	0.26	1.05	0.15
2.7	0.2	0.7	0.1	4.3	0.2	0.7	0.1	5.4	0.2	1.6	0.1	5.4	0.2	0.9	0	6.1	0.2	1.1	0	0.14	1	0.17
3	0.2	0.8	0.1	4.8	0.2	0.7	0.1	5.8	0.2	1.7	0.1	5.9	0.2	0.9	0.1	6.3	0.2	1.1	0	0.18	1.02	0.19
3.5	0.2	1	0.1	5.3	0.2	0.8	0.1	6.4	0.2	1.8	0.1	6.3	0.2	1	0.1	6.8	0.2	1.2	0.1	0.25	1.05	0.2
4.2	0.3	1.1	0.1	6.3	0.3	0.9	0.1	7.1	0.2	2	0.2	6.8	0.2	1.1	0.1	7.4	0.2	1.3	0.1	0.15	1.07	0.23
4.6	0.3	1.2	0.1	6.6	0.3	1	0.1	7.4	0.2	2.1	0.2	7	0.2	1.1	0.1	7.5	0.2	1.3	0.1	0.15	1.04	0.24
4.8	0.3	1.2	0.1	6.7	0.3	1	0.1	7.6	0.2	2.1	0.2	7.2	0.2	1.1	0.1	7.7	0.2	1.4	0.1	NA	1.05	0.24
2.5	0.2	0.7	0.1	4.1	0.2	0.6	0.1	5	0.2	1.5	0.1	5.3	0.2	0.8	0	5.4	0.2	1	0	0.49	1.04	0.18
2.5	0.2	0.7	0.1	4.1	0.2	0.6	0.1	4.9	0.2	1.5	0.1	5.2	0.2	0.8	0	5.2	0.2	0.9	0	0.49	1.03	0.19
2.5	0.2	0.7	0.1	4	0.2	0.6	0.1	4.9	0.2	1.4	0.1	5.2	0.2	0.8	0	5.3	0.2	0.9	0	0.4	1.03	0.17
2.6	0.2	0.7	0.1	4.1	0.2	0.7	0.1	5.1	0.2	1.5	0.1	5.5	0.2	0.8	0	5.7	0.2	1	0	NA	1.04	0.17
NA	NA	NA	NA	NA	NA	NA	NA	NA	NA	NA	NA	NA	NA	NA	NA	NA	NA	NA	NA	NA	NA	NA
2.9	0.2	0.8	0.1	4.7	0.2	0.7	0.1	5.7	0.2	1.7	0.1	5.9	0.2	0.9	0.1	6.3	0.2	1.1	0.1	0.2	1.03	0.17
3	0.2	0.8	0.1	4.8	0.2	0.8	0.1	5.9	0.2	1.7	0.1	6	0.2	0.9	0.1	6.4	0.2	1.2	0.1	0.34	1.03	0.17
3.5	0.2	0.9	0.1	5.4	0.2	0.8	0.1	6.3	0.2	1.8	0.1	6.3	0.2	1	0.1	6.7	0.2	1.2	0.1	0.23	1.05	0.19
4.6	0.3	1.2	0.1	6.8	0.3	1	0.1	7.6	0.2	2.1	0.2	7.2	0.2	1.1	0.1	7.6	0.2	1.3	0.1	0.18	1.05	0.22
4.8	0.3	1.2	0.1	6.9	0.3	1	0.1	7.7	0.2	2.1	0.2	7.3	0.2	1.1	0.1	7.7	0.2	1.4	0.1	0.29	1.05	0.23
4.8	0.3	1.3	0.1	7	0.3	1.1	0.1	7.8	0.2	2.1	0.2	7.3	0.2	1.1	0.1	7.8	0.2	1.4	0.1	NA	1.09	0.23
2.3	0.1	0.7	0.1	3.8	0.2	0.6	0.1	4.9	0.2	1.4	0.1	5.1	0.2	0.8	0	5.1	0.2	0.9	0	NA	1.02	0.17
2.3	0.1	0.6	0.1	3.8	0.2	0.6	0.1	4.9	0.2	1.4	0.1	5.2	0.2	0.8	0	5.2	0.2	0.9	0	0.14	1.01	0.15

2.5	0.2	0.7	0.1	4.1	0.2	0.6	0.1	5.2	0.2	1.5	0.1	5.5	0.2	0.8	0	5.8	0.2	1	0	0.15	1	0.15

Table 1. Geographic location, depth and geochemical data of the samples reported in this thesis (Rare Earth Element concentrations are given in pmol kg^{-1}).

Station	Latitude	Longitude	depth (m)	^{232}Th [pg kg^{-1}]	S.E.	^{230}Th [fg kg^{-1}]	S.E. [fg kg^{-1}]	ε_{Nd}	S.E.	Ce	S.E.	Pr	S.E.	Nd	S.E.
12	-50.79	-284.21	400	19.1	0.2	7.4	0.6	-9	0.5	6.5	1.3	3.4	0.3	13.7	1
12	-50.79	-284.21	701	20	0.3	9.9	0.8	-8.6	0.2	6.1	1.2	3.8	0.3	14.5	1
12	-50.79	-284.21	900	69.4	0.9	10.8	0.4	SL	SL	8	1.6	3.9	0.4	15.2	1.1
12	-50.79	-284.21	1203	50.1	0.6	11.8	0.4	-9.9	0.3	9.8	2	3.9	0.4	16	1.1
12	-50.79	-284.21	1503	39.8	0.5	12.9	0.5	-9.6	0.6	7.1	1.4	4.4	0.4	17.4	1.2
12	-50.79	-284.21	1671	41.7	0.5	13.9	0.5	-10.7	0.9	4.4	0.9	4.2	0.4	17.6	1.2
12	-50.79	-284.21	1777	38.4	0.5	14	0.5	-9.6	0.8	9.1	1.8	4.5	0.4	18.1	1.3
16	-51.29	-286.2	14	20.8	0.4	2	0.2	-9.9	0.3	15.2	3	3.9	0.4	15.9	1.1
16	-51.29	-286.2	41	19.9	0.3	2.1	0.2	-6.7	0.2	14.3	2.9	3.9	0.4	15.8	1.1
16	-51.29	-286.2	101	17.1	0.3	2.7	0.3	-7.6	0.4	9.5	1.9	3.4	0.3	13.6	1
16	-51.29	-286.2	201	37.1	0.6	4.3	0.4	-8.1	0.4	8.7	1.7	3.5	0.3	13.9	1
16	-51.29	-286.2	300	62.1	1.1	4.6	0.4	-8	0.6	10.1	2	3.5	0.3	13.8	1
16	-51.29	-286.2	439	31	0.5	4.7	0.4	AV	AV	C	C	3.8	0.3	14.7	1
18	-52.93	-288.62	30	7.7	0.2	1.9	0.1	-8.1	0.7	NS	NS	NS	NS	NS	NS
18	-52.93	-288.62	65	8.6	0.2	1.8	0.1	-8.3	0.45	NS	NS	NS	NS	NS	NS
18	-52.93	-288.62	115	6.8	0.1	2	0.2	-8.8	0.6	NS	NS	NS	NS	NS	NS
18	-52.93	-288.62	301	10.4	0.1	3.7	0.3	-8.1	0.4	2.7	0.5	2.8	0.3	11.7	0.8
18	-52.93	-288.62	500	20.8	0.3	6.1	0.5	-8.5	0.675	NS	NS	NS	NS	NS	NS
18	-52.93	-288.62	800	20.9	0.3	8.5	0.7	-8.1	0.3	NS	NS	NS	NS	NS	NS
18	-52.93	-288.62	1200	NA	NA	NA	NA	-8.9	0.3	4.9	1	3.9	0.4	15.8	1.1
18	-52.93	-288.62	1600	22.1	0.3	12.5	0.4	-9.2	0.5	4.9	1	4.5	0.4	17.7	1.2
18	-52.93	-288.62	1999	23.1	0.3	14.4	0.5	-9.3	0.65	5	1	5	0.5	19.7	1.4
18	-52.93	-288.62	2726	26.1	0.4	15	0.5	-9.4	0.5	7	1.4	6.6	0.6	26.4	1.9
22	-53.04	-287.45	152	100.8	2	3.7	0.2	-5.4	0.2	29.5	5.9	5	0.5	20.5	1.4
22	-53.04	-287.45	192	96.8	1.9	3.9	0.2	-6.3	0.2	32.5	6.5	5.8	0.5	20.6	1.4

25	-54.17	-286.33	150	31.6	0.5	3.7	0.4	-9.4	0.3	NS	NS	NS	NS	NS	NS							

Table 1. Continuation of previous page.

Sm	S.E.	Eu	S.E.	Gd	S.E.	Tb	S.E.	Dy	S.E.	Ho	S.E.	Er	S.E.	Tm	S.E.	Yb	S.E.	Lu	S.E.	Ce/Ce*	Eu/Eu*	$(Nd/Yb)_n$
2.8	0.2	0.8	0.1	4.4	0.2	0.7	0.1	5.6	0.2	1.6	0.1	5.9	0.2	0.9	0.1	6.2	0.2	1.6	0.1	0.23	1.03	0.15
2.9	0.2	0.8	0.1	4.6	0.2	0.7	0.1	5.7	0.2	1.6	0.1	5.9	0.2	0.9	0.1	6.2	0.2	1.1	0	0.18	1.05	0.16
3.1	0.2	0.8	0.1	4.8	0.2	0.8	0.1	5.9	0.2	1.7	0.1	6	0.2	0.9	0.1	6.3	0.2	1.1	0.1	0.24	1.05	0.17
3.2	0.2	0.9	0.1	4.9	0.2	0.8	0.1	6.1	0.2	1.7	0.1	6.1	0.2	1	0.1	6.4	0.2	1.2	0.1	NA	1.04	0.17
3.5	0.2	1	0.1	5.3	0.2	0.8	0.1	6.4	0.2	1.8	0.2	6.5	0.2	1	0.1	6.8	0.2	1.2	0.1	NA	1.06	0.18
3.6	0.2	1	0.1	5.4	0.2	0.9	0.1	6.7	0.2	1.9	0.2	6.6	0.2	1	0.1	7	0.2	1.2	0.1	0.13	1.02	0.17
3.7	0.2	1	0.1	5.5	0.2	0.9	0.1	6.7	0.2	1.9	0.2	6.7	0.2	1	0.1	6.9	0.2	1.2	0.1	0.24	1.05	0.18
3.2	0.2	0.8	0.1	4.4	0.2	0.7	0.1	5.3	0.2	1.5	0.1	5.3	0.2	0.8	0	5.2	0.2	0.9	0	0.46	1.06	0.21
3.1	0.2	0.8	0.1	4.3	0.2	0.7	0.1	5.2	0.2	1.5	0.1	5.3	0.2	0.8	0	5.2	0.2	0.9	0	0.44	1.06	0.21
2.8	0.2	0.8	0.1	4.1	0.2	0.6	0.1	5.1	0.2	1.5	0.1	5.3	0.2	0.8	0	5	0.2	0.9	0	0.34	1.05	0.19
2.8	0.2	0.7	0.1	4.2	0.2	0.7	0.1	5.2	0.2	1.5	0.1	5.4	0.2	0.8	0	5.4	0.2	1	0	0.3	1.02	0.18
2.8	0.2	0.8	0.1	4.1	0.2	0.7	0.1	5.1	0.2	1.5	0.1	5.3	0.2	0.8	0	5.5	0.2	1	0	0.33	1.04	0.17
2.9	0.2	0.8	0.1	4.4	0.2	0.7	0.1	5.3	0.2	1.5	0.1	5.4	0.2	0.8	0	5.7	0.2	1	0	NA	1.06	0.18
NS	NS	NS	NS	NS	NS	NS	NS	NS	NS	NS	NS	NS	NS	NS	NS	NS	NS	NS	NS	NA	NA	NA
NS	NS	NS	NS	NS	NS	NS	NS	NS	NS	NS	NS	NS	NS	NS	NS	NS	NS	NS	NS	NA	NA	NA
NS	NS	NS	NS	NS	NS	NS	NS	NS	NS	NS	NS	NS	NS	NS	NS	NS	NS	NS	NS	NA	NA	NA
2.5	0.2	0.7	0.1	3.9	0.2	0.6	0.1	5.1	0.2	1.5	0.1	5.4	0.2	0.8	0	5.6	0.2	1	0	0.11	1.01	0.14
NS	NS	NS	NS	NS	NS	NS	NS	NS	NS	NS	NS	NS	NS	NS	NS	NS	NS	NS	NS	NA	NA	NA
NS	NS	NS	NS	NS	NS	NS	NS	NS	NS	NS	NS	NS	NS	NS	NS	NS	NS	NS	NS	NA	NA	NA
3.3	0.2	0.9	0.1	5.2	0.2	0.8	0.1	6.4	0.2	1.9	0.2	6.5	0.2	1	0.1	7	0.2	1.2	0.1	0.15	1.04	0.16
3.7	0.2	1	0.1	5.6	0.2	0.9	0.1	6.9	0.2	2	0.2	6.8	0.2	1.1	0.1	7.3	0.2	1.3	0.1	0.13	1.035	0.17
4	0.2	1.1	0.1	6.1	0.2	1	0.1	7.3	0.2	2.1	0.2	7.1	0.2	1.1	0.1	7.6	0.2	1.3	0.1	0.11	1.03	0.18
5.4	0.3	1.4	0.1	7.8	0.3	1.2	0.1	9.2	0.3	2.6	0.2	8.9	0.3	1.4	0.1	9.5	0.3	1.7	0.1	0.13	1.02	0.19
3.3	0.2	0.9	0.1	4.5	0.2	0.7	0.1	5.2	0.2	1.5	0.1	5.2	0.2	0.8	0	5.3	0.2	0.9	0	0.73	1.13	0.27

3.6	0.2	1	0.1	4.8	0.2	0.8	0.1	5.7	0.2	1.6	0.1	5.6	0.2	0.9	0	5.6	0.2	1	0	0.58	1.1	0.25
NS	NS	NS	NS	NS	NS	NS	NS	NS	NS	NS	NS	NS	NS	NS	NS	NS	NS	NS	NS	NA	NA	NA

Table 1. Geographic location, depth and geochemical data of the samples reported in this thesis (Rare Earth Element concentrations are given in pmol kg^{-1}).

Station	Latitude	Longitude	depth (m)	^{232}Th [pg kg^{-1}]	S.E.	^{230}Th [fg kg^{-1}]	S.E.	ε_{Nd}	S.E.	Ce	S.E.	Pr	S.E.	Nd	S.E.
25	-54.17	-286.33	301	28.5	0.4	5.4	0.7	-8.9	0.3	NS	NS	NS	NS	NS	NS
25	-54.17	-286.33	500	30.2	0.5	9.1	0.7	-8.6	0.2	NS	NS	NS	NS	NS	NS
25	-54.17	-286.33	702	87.2	1.3	9.8	0.8	-8.8	0.4	NS	NS	NS	NS	NS	NS
25	-54.17	-286.33	901	48.7	0.7	12.5	0.5	-9.3	0.5	NS	NS	NS	NS	NS	NS
25	-54.17	-286.33	1201	22.7	0.3	14.1	0.6	-9.9	0.4	NS	NS	NS	NS	NS	NS
25	-54.17	-286.33	1601	32.5	0.5	13.5	0.5	-10	0.4	NS	NS	NS	NS	NS	NS
25	-54.17	-286.33	2001	15.7	0.5	15.2	0.6	-9.6	0.5	NS	NS	NS	NS	NS	NS
25	-54.17	-286.33	2100	101.6	1	13.9	0.6	-9.2	0.3	NS	NS	NS	NS	NS	NS
30	-53	-286.39	75	59.8	1.2	3.7	0.2	-5	0.2	28	5.6	4.8	0.4	19.9	1.4
30	-53.01	-286.76	76	88.8	1.8	8.4	0.4	P	P	21.2	4.2	4.6	0.4	17.4	1.2
31	-53	-286.39	48	81.3	1.6	4.8	0.2	P	P	32.9	6.6	5.3	0.5	21	1.5
34	-53.03	-287.34	50	96.6	1.9	4.2	0.2	-5.5	0.2	28.1	5.6	4.7	0.4	19.6	1.4
34	-53.03	-287.34	80	94.3	1.9	5.5	0.3	-5.4	0.2	29.6	5.9	4.9	0.4	20	1.4
34	-53.03	-287.34	122	81.5	1.6	5.2	0.3	-6.2	0.3	23.5	4.7	5	0.5	18.8	1.3

Table 1. Continuation of previous page.

Sm	S.E.	Eu	S.E.	Gd	S.E.	Tb	S.E.	Dy	S.E.	Ho	S.E.	Er	S.E.	Tm	S.E.	Yb	S.E.	Lu	S.E.	Ce/Ce*	Eu/Eu*	$(Nd/Yb)_n$
NS	NS	NS	NS	NS	NS	NS	NS	NS	NS	NS	NS	NS	NS	NS	NS	NS	NS	NS	NS	NA	NA	NA
NS	NS	NS	NS	NS	NS	NS	NS	NS	NS	NS	NS	NS	NS	NS	NS	NS	NS	NS	NS	NA	NA	NA
NS	NS	NS	NS	NS	NS	NS	NS	NS	NS	NS	NS	NS	NS	NS	NS	NS	NS	NS	NS	NA	NA	NA
NS	NS	NS	NS	NS	NS	NS	NS	NS	NS	NS	NS	NS	NS	NS	NS	NS	NS	NS	NS	NA	NA	NA
NS	NS	NS	NS	NS	NS	NS	NS	NS	NS	NS	NS	NS	NS	NS	NS	NS	NS	NS	NS	NA	NA	NA
NS	NS	NS	NS	NS	NS	NS	NS	NS	NS	NS	NS	NS	NS	NS	NS	NS	NS	NS	NS	NA	NA	NA
NS	NS	NS	NS	NS	NS	NS	NS	NS	NS	NS	NS	NS	NS	NS	NS	NS	NS	NS	NS	NA	NA	NA
NS	NS	NS	NS	NS	NS	NS	NS	NS	NS	NS	NS	NS	NS	NS	NS	NS	NS	NS	NS	NA	NA	NA
3.3	0.2	1.1	0.1	4.4	0.2	0.7	0.1	5	0.2	1.4	0.1	5	0.2	0.8	0	5.1	0.2	0.9	0	0.73	1.41	0.27
3.3	0.2	0.9	0.1	4.6	0.2	0.7	0.1	5.2	0.2	1.7	0.1	5.3	0.2	0.8	0	5.4	0.2	1	0	0.52	1.13	0.22
3.4	0.2	1	0.1	4.7	0.2	0.7	0.1	5.1	0.2	1.8	0.1	5.2	0.2	0.8	0	5.1	0.2	0.9	0	0.73	1.2	0.28
3.2	0.2	0.9	0.1	4.4	0.2	0.7	0.1	5	0.2	1.4	0.1	5	0.2	0.8	0	5.1	0.2	0.9	0	0.76	1.12	0.27
3.4	0.2	0.9	0.1	4.6	0.2	0.7	0.1	5.1	0.2	1.5	0.1	5.1	0.2	0.8	0	5.2	0.2	0.9	0	0.72	1.12	0.27
3.7	0.2	1	0.1	5	0.2	0.8	0.1	5.6	0.2	1.6	0.1	5.7	0.2	0.9	0	5.7	0.2	1	0	0.52	1.09	0.23

C = Contaminated sample; P = Determination pending; AV = Abnormal value; NS = Not sampled; NA = Not applies due to contaminated or not collected sample.

That's all folks